The manufacture of bioscaffolds by printing.

Soo, Woan Yi

Swansea University
Prifysgol Abertawe

The Manufacture of Bioscaffolds by Printing

By

Woan Yi SOO

B.Eng. (Hons)

Thesis submitted to the University of Wales Swansea in fulfilment of the requirements for the degree of Doctor of Philosophy.

Swansea University

2010

Summary

Printing technology is mainly used for graphic arts and packaging applications, but also is a potential technology for the micro manufacture of electronic devices, biosensors and tissue engineering scaffolds. The main goal of this research is to print fine lines of biopolymer by means of volume printing processes. To assess the feasibility of printing fine features for bioscaffolds using conventional printing technology, an experimental investigation into the rheological behaviour of biopolymer inks was conducted. This is because the rheological characteristics of the biopolymers have a significant influence on the performance of different printing processes. The biopolymers undergo significant phase transition which affects the printed products. The rheological tests focus on ink viscosity, viscoelastic and gelation properties. Gelatine appeared to be more favourable than collagen for scaffolds fabrication by printing technologies. Thus this study was mainly focused on aqueous gelatine solution as printing ink. All inks display shear-thinning and thixotropic behaviours which are important for good printing. The temperature ramp and multi-frequency sweep tests yield information on gelation temperature and gel point. The rate of ordering and gel formation of biopolymer inks was found to be strongly concentration-, temperature- and time-dependent. An increase in gelatine concentrations caused a reduction in the dynamic surface tension of the inks. Printing conditions that are compatible with printing biopolymer inks were being optimised in terms of operation temperature interval to accommodate phase transition.

Three printing processes inkjet printing, flexography and screen printing were evaluated for printing fine features of biopolymers. Surfactants were used to lower the ink surface tension to below 30 mN/m, so that the ink could be jetted onto substrate. These printing methods are aimed to produce cost effective bioscaffolds in mass production. The quality of printed lines was examined in terms of width and film thickness to establish the best printing method for gelatine printing. Fine lines printed by inkjet and flexographic printing processes were mostly broken. Screen printing process looks more promising because the printed gelatine fine lines showed the best quality. The line width and line film thickness measured were more consistent and closer to the desired dimensions.

A laboratory screen printing trial was conducted using L_{16} orthogonal array technique to investigate the effect of process parameters on the reproduction of the screen printed fine gelatine lines in terms of line width and film thickness. Six parameters studied were ink type, mesh type, squeegee hardness, snap-off gap, squeegee speed and squeegee pressure. The most significant parameter was the ink type, followed by snap-off gap and mesh type. The effect of squeegee parameters (squeegee type, speed and pressure) was considered insignificant. The orientation has an effect on line width but insignificant effect on line film thickness. Most process parameters had interactions with one another which complicated the optimisation of the process parameters.

Declaration

This work has not previously been accepted in substance for any degree and is not being concurrently submitted in candidature for any degree.

Signed ..... (Candidate)

Date 18th MAY 2010

Statement 1

This thesis is a result of my own investigations, except where otherwise stated.

Other sources are acknowledged giving explicit references. A bibliography is appended at the end of each chapter in the thesis.

Signed ..... (Candidate)

Date 18th MAY 2010

Statement 2

I hereby give consent for my thesis, if accepted, to be available for photocopying and for inter-library loan, and for the title and summary to be made available to outside organisations.

Signed ..... (Candidate)

Date 18th MAY 2010

Certificate of Originality

The thesis is submitted to the Swansea University, Swansea, under the supervision of Prof. Tim Claypole in the Welsh Center of Printing and Coating, School of Engineering, Swansea University, Swansea, in candidature for the degree of Philosophy Doctor. The material in this thesis is the original work of the author except where acknowledgement to other authors is expressly made.

Signed,

.....

Woan Yi SOO

(Candidate)

Signed,

Prof. Tim Claypole

(Supervisor)

Date: 18th May 2010

Dedication

To my beloved parents, sister and brothers

Life has always been an exploratory journey of ups and downs

But the reflection of the light at the end of the tunnel

Motivates the memorable battle to reach and obtain the glowing beacon

A PhD

I love you all from the bottom of my heart

Acknowledgements

I would like to express my utmost gratitude to Professor Tim Claypole, my supervisor, for his unvarying encouragement, guidance and most importantly the financial support throughout the academic period of this study. I am particularly thankful for his caring temperament and incessant compassion that got me through the difficult hurdles for the past four years, and for providing an appropriate incentive to complete the thesis in time.

It is with greatest appreciation that I would like to convey my thankfulness to Dr. Tatyana Korochkina for the invaluable encouragement and supervision she provided throughout the entire course. Despite the unfamiliarity with the topic of my research, she was willing to learn and explore the answers to any issues. It was such pleasant support that made solutions and results successfully obtained.

I would like to express my thanks to Dr. Chris Wright, through whom I was introduced to Professor Tim. He has guided me through the toughest initial year of my programme. There is also Dr. Karl Hawkins who has kindly assisted me in the FTMS tests with his excellent skill that is second to none.

To my dear friend, Tiffany Chan, I am so thankful that she is always there for me over the good times and the bad. Thanks for listening to my complaints and frustrations and for believing in my ability to go through this hurdle in life, and for making something bitter, sweet.

Last but definitely not the least, I would like to convey my thankfulness to my entire family who have always been supportive in spite of the sufferance of geographical distance between us. I treasure their thoughtfulness that has always been vital to me. Also to my dearest cousin Kiat Wei who kindly offered me his help in reading and correcting my grammatical errors.

This acknowledgement is not, in any way, exhaustive as I would like to thank everyone who has helped me along the way. In particular, I would like to thank all my friends and colleagues at the University who have kindly and selflessly helped me along the way all these years.

Contents

Chapter 2.0: Literature Review

Chapter 3.0: Methodologies

List of Figures

List of Tables

Abbreviations

The abbreviations are divided into the relevant data for each Chapter for convenience.

Chapter 1

3D	Three-dimensional
PLA	Polylactic acid
PGA	Polyglycolic acid
PLGA	Poly(DL-lactic-co-glycolic acid)
PCL	Polycaprolactone
HA	Hydroxyapatite
β-TCP	β-tricalcium phosphate
SFF	Solid freeform fabrication
SLA	Stereolithography
FDM	Fused deposition modelling
3DP	Three-dimensional printing
DOD	Drop on demand
PVC	Polyvinyl chloride

Chapter 2

ECM	Extracellular matrice
Gly	Glycine
Pro	Proline
Hypro	Hydroxyproline
FDA	Food and Drug Administration
DHT	Dehydrothermal

UV	Ultraviolet
GTA	Glutaraldehyde
EDAC	Carbodiimides
BSE	Bovine spongiform encephalopathy
pI	Isoelectric point
pH	Potential hydrogen
CJD	Creutzfeldt-Jakob disease
PLLA	Poly(L-lactic acid)
CO_2	Cardon dioxide
CAD	Computer aided design
CPP	Calcium polyphosphate
poly(CL/TMC)	Poly(ε-caprolactone-co-trimethylene carbonate
PEG	Poly(ethylene glycol)
TMG	Trimethylene glycol
PEG-DMA	Poly(ethylene glycol)-dimethacrylate
PEO	Poly(ethylene oxide)
CaP	Calcium phosphate
PED	Precision extruding deposition
SLS	Selective laser sintering
IR	Infrared
PEEK	Poly(etheretherketone)
PVA	Poly(vinyl alcohol)
HCs	Hepatocytes
MSCs	Mesenchymal stem cells
ppm	Parts per million
SMCs	Smooth muscle cells

DMSO	Dimethyl sulfoxide
lpi	Lines per inch
bcm	Billion cubic microns
ANOVA	Analysis of variance
PDMS	Polydimethylsiloxane
PU	Polyurethanes
HPG	Hydroxypropylguar
FTMS	Fourier transform mechanical spectroscopy
TEOS	Tetraethylorthosilane
VTES	Vinyltriethoxysilane

Chapter 3

CCD	Charged couple device
PSI	Phase-shifting interferometry
VSI	Vertical scanning interferometry
WLI	White light interferometer

1.0 Introduction

1.1 Tissue engineering

Despite technological advances, there is a severe shortage of donor organs or tissues available for transplantations. On average, thousands of people die each year while waiting for an organ transplant. Several methods have been developed as a cure, by replacing the function of failing organs mechanically (dialysis and heart-lung bypass machines), or through implantation of synthetic replacements (blood vessel and joint replacements). However, these methods are only temporary solutions and do not allow the patients to resume normal activities completely [1]. As a result, research regarding tissue engineering has been vigorously pursued throughout the world as means of producing artificial tissues or organs with bioengineering techniques and biological materials to repair or replace defective organs. It is expected to be one of the more promising approaches to resolve this problem.

Tissue engineering is commonly defined as an emerging multidisciplinary field which involves the application of principles of engineering, biology and chemistry towards the development of biological substitutes that restore, maintain or improve the functionality of damaged tissue or organ [2][3]. It has the potential to create viable artificial tissues or organs that can grow upon implantation in human body. Tissue engineering is different from standard therapies in that the engineered tissues become integrated within the patient, leading to a potentially permanent specific cure of the disease, injury or impairment. This method would also have a lower risk of infection

and immune rejection comparing to conventional treatments based on organ transplantation as the cultured cells can be harvested from patient's own body.

One of the common approaches in tissue engineering often involves the seeding of tissue-specific cells onto a three-dimensional (3D) porous matrices, known as scaffold, which is then cultivated in a suitable bioreactor before implanted into the human body when a mature matrix is formed, as illustrated in Figure 1.1. Therefore, the scaffold is an important component in tissue engineering.

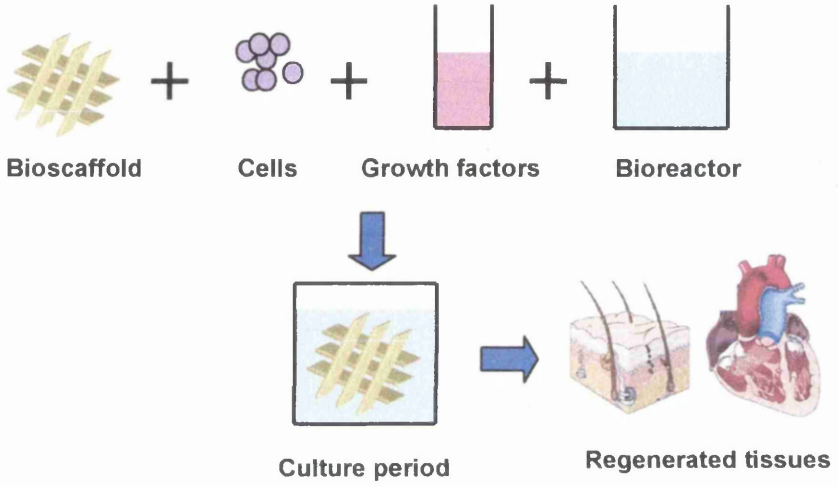

Figure 1.1: Tissue engineering approach [4]

Bioscaffolding also has potential applications in regenerative medicine where they can be used *in vivo* to support body structures while the natural healing process takes places, for example, in cases of major trauma. Printing offers the potential to mass produce scaffolding. This thesis presents research into the printing of biopolymers as a necessary precursor to the creation of three-dimensional scaffolding by printing which could eventually lead to a method for volume manufacturing. The remainder of this chapter will look at the background to bioscaffolding and possible printing processes for fabrication of scaffolding. The general structure of the thesis will then be described.

1.2 Tissue engineered bioscaffold

A scaffold is critical, both in vitro and in vivo, in recapitulating the tissue development process and allowing cells to formulate their own microenvironments. It serves as a temporary physical support structure on which the cells can adhere, proliferate, differentiate and migrate. This leads to the formation of a functional tissue with a desired shape.

The choice of suitable scaffolding material is crucial to the success of the technique in tissue engineering. Most primary organ cells are anchorage dependent and their growth is affected by the substrates onto which they are attached in tissue culture. The scaffolding materials need to exhibit good biocompatibility and biodegradability. The materials must not provoke any unwanted tissue response to the implant and also possess the right surface chemistry to encourage cell attachment and function. At the site of implantation, the materials will gradually resorb and degrade into non-toxic by-products, leaving behind a matrix of living connective tissue and cells with appropriate structural and mechanical properties. The materials need to have sufficient mechanical properties to support the desired structure, and also be easily sterilised before introducing cell cultures to prevent infection.

Three main materials types which have been successfully investigated for use in formulating scaffolds are:

(i) natural polymers such as collagen [5][6][7][8], gelatine [9][10][11], alginate [12][13][14], hyaluronan (also called hyaluronic acid) [15][16], glycosaminoglycan (GAGs), starch, chitin [17], and chitosan [18].

(ii) Synthetic polymers [19] such as polylactic acid (PLA), polyglycolic acid (PGA) and their co-polymers such as poly(DL-lactic-co-glycolic acid) (PLGA), and polycaprolactone (PCL), and

(iii) Ceramics such as hydroxyapatite (HA) [20][21] and β-tricalcium phosphate (β-TCP) [22].

Naturally derived biomaterials can mimic the natural extracellular matrix of tissues more closely, offering better biocompatibility and environment for tissue culture. However, they tend to have large batch-to-batch variations in quality due to extraction from different sources as well as their poor mechanical performance. The concern about the feasibility of finding enough materials needed for clinical applications has prompted research into the use of synthetic polymers.

Many synthetic polymers have been developed and used in biomedical field with established clinical success. Synthetic polymers are advantageous in their stronger mechanical properties and greater flexibility where their properties can be tailored for specific applications. They can also be easily mass-produced with reproducible properties, maintaining better consistency in quality of scaffolds. However, the degradation of these synthetic polymers produces acidic by-products [23], for example lactic acid is released by PLA. Although these degradation products are present in the human body and are removed by natural metabolic pathway [24], the pH of the microenvironment is reduced and thus may cause an immunological response. Such acidic environment can cause autocatalysis which further accelerating the degradation rate of the polymers [25]. In addition, synthetic polymers lack biocompatibility [26] which is a concern for clinical use.

Bioactive ceramics (inorganic, non metallic materials) have also been used as a candidate scaffolding material, popularly in the field of orthopedics, dentistry and plastic surgery. These ceramics have high biocompatibility and osteoconductive properties, and resemble the natural inorganic component of bone and teeth [27][28]. The limitations of ceramics are their brittleness with insufficient rigidity and slow biodegradability which is not beneficial in tissue engineering applications. Therefore, polymer/ceramic composites have been developed where biodegradable polymers such as gelatine, collagen or PLA are used as matrices for ceramic particles, where the mechanical, degradation and biological properties can be tailored for specific applications [29].

Apart from the substrate materials, the structure and properties of the scaffolds are also important for their application in tissue engineering [30][31]. In general, the scaffolds have to be three-dimensional and highly porous with a good interconnected

network to increase the surface area for cell attachment and facilitate the transport of nutrients as well as removal of waste products. The optimal pore size is depended on the specific cell type where it has to be large enough for cell migration and formation of extracellular matrix. The scaffolds should have high biocompatibility and low antigenicity, and need to be made from biodegradable materials with controllable degradation and resorption rate so that tissue will gradually replace the scaffold. Scaffolds should also possess adequate mechanical properties to match those of tissue at the site of implantation; suitable surface chemistry and wettability to favour cell attachment, differentiation and proliferation. Furthermore, these scaffolds should be easily processed into a variety of shapes and sizes.

Several techniques have been developed to fabricate bioscaffolds. These include fibre bonding [32][33] to provide large surface area for cell interaction and growth, solvent casting and particulate leaching [34][35] to create large variations in pore size, gas foaming [36] to eliminate the need for organic solvents in the pore-making process and requires no leaching step, melt moulding [37][38] to increase the uniformity of scaffold surface, phase separation[39][40][41], solution casting [42][43] and freeze drying [43] to fabricate highly porous polymer scaffolds. However, current chemical scaffold fabrication techniques cannot control the architecture of scaffolds precisely such as pore size, pore interconnectivity and spatial distribution of pores.

The limitations of conventional chemical techniques have prompted the development of solid freeform fabrication (SFF) technology that was adapted to custom fabricate biological scaffolds with precise control over the matrix microstructure [45][46]. These can create three-dimensional scaffolds with customised size and shape that can be tailored to individual needs of the patients [47]. SFF is an additive method where thin layers of biomaterials are deposited on top of each other repeatedly, layer-by-layer, to build the desired scaffolds. There are several SFF approaches such as stereolithography (SLA) [48][49], fused deposition modelling (FDM) [50][51], selective laser sintering (SLS) [52][53], three-dimensional printing (3DP) [54][55][56] and 3D plotting [57][58].

However, the limitation of these processes considered to date is their production speed. They are not compatible with the rate of production required for applications

such as wound healing. Printing affords the potential for volume production of bioscaffolding for research and regeneration.

1.3 Conventional printing technologies

Printing, in its many forms, is a process in which the printing ink is applied to various substrates in order to reproduce the required two-dimensional or three-dimensional images in a repeatable form using an image carrier [59]. Generally, the printing plate or image carrier is an information carrying medium which has an image area and a non-image area. The image area will receive and transfer the ink to the materials being printed, whereas the non-image area does not allow ink transfer to the substrate.

Offset printing, commonly used for newsprint and commercial printing is capable of high production rates, but subjects the ink to high shear and pressure, which would probably damage the efficacy of the biopolymers. It also gives a thin deposit, less than 1 – 2 μm, which would require multiple hits to produce a thick enough layer. Therefore, offset printing was not used in this project.

Gravure printing is noted for its ability to reproduce thin lines and a highly repeatable thin deposit. It is an intaglio process with an engraved line but requires structure in the engraving to enable it to hold ink in large areas. It also lays down a thinner deposit than offset. Therefore, it would also require multiple hits to build up sufficient height for the scaffold structure. It does, however, offer advantages in terms of the longevity of the image carrier compared to that of flexography. In terms of assessment of the potential of gravure for making scaffolding, flexography could be considered as a form of offset gravure and results obtained with flexography could be used to indirectly assess the potential for gravure printing.

This leaves three prime candidates of established volume printing processes for printing biomaterials. These are:

- Inkjet
- Flexography

- Screen printing

Inkjet has the ability to produce discrete custom prints by depositing ink droplets precisely onto the desired positions on the substrate with a low volume production rate. On the other hand, flexography is a high volume printing process which gives medium ink deposit. Screen printing is a highly versatile process of slow printing speed where the ink is subjected to low shear and produces thick ink deposit. A description of each of those three printing processes is presented in the following sections.

1.3.1 Inkjet Printing

Inkjet printing can be used to seed scaffolds as they are constructed. Direct inkjet printing can deposit any material that can be delivered in liquid form or as a suspension in liquid. It also can print mixed materials using one inkjet dispenser per material. Inkjet printing is now a mature technology developed about 30 years ago. It is widely used in graphic arts, product marking, microdosing, and rapid prototyping.

Inkjet printing can be split into two main categories depending on the method by which the droplet of ink is formed and directed towards the target substrate, namely continuous inkjet and drop on demand (DOD) inkjet. Continuous inkjet printing uses a continuous stream of charged droplets and deflects those which are to be used for printing. A schematic of this type of inkjet printing system is shown in Figure 1.2. The fluid under pressure is forced through an orifice, typically 50 – 80 μm in diameter, and breaks up into uniform drops to form a liquid jet in the presence of an electrostatic field, referred to as the charging field. The charged droplets are directed to the desired location on the substrate or into the catcher by the deflection field (electrostatic field). The trajectories of the droplets are varied by the amount of charge applied. The sizes of the droplet produced are typically 150 μm (approximately twice the orifice diameter) but can be as small as 20 μm. Commercially available continuous mode inkjet printers are usually operating at a droplet generation rates of 80 – 100 kHz [60].

DOD inkjet printing differs from continuous inkjet by virtue that the production of the droplets is controlled digitally. The printing head is moved towards the position where printing is to occur before depositing a droplet which is created by a transducer only when needed. There are two basic processes available in DOD inkjet printing: thermal and piezoelectric. They work on one simple principle – when the control mechanism wants to fire a droplet of ink onto a substrate it sends a signal to the inkjet head: one signal results in one droplet. Both rely on strategically placing drops of ink onto the substrate. Figure 1.3 illustrates a schematic of DOD inkjet printing system which is conceptually less complex than continuous inkjet system. Thermal DOD inkjet printing works by locally heating the ink to a high temperature using a high speed digitally controlled micro heater at the rear of the chamber, causing the ink to expand and form a vapour bubble. This vapour bubble displaces the ink in the chamber and forces the droplet out through the nozzle onto the substrate. As the thermal heater cools, a vacuum is created which draws a fresh supply of ink from the reservoir into the ink chamber. Piezoelectric technology, as opposed to thermal inkjet where the droplet is generated by raising the temperature, uses an electrical charge which is applied to the piezoelectric transducer located inside a printing chamber connected to ink reservoir. Opening of the printing chamber acts as a capillary valve and droplet is ejected when the local pressure pulse exceeds a critical value. Then the voltage is removed, the piezo crystal resumes its original shape and a new portion of ink comes in. The droplet sizes are approximately equal to the orifice diameter [61], up to 120 μm. Typical DOD printers operate at 4 – 12 kHz.

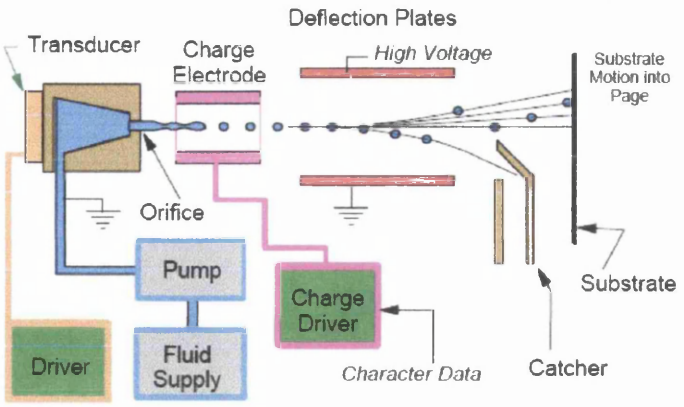

Figure 1.2: Schematic of a continuous type inkjet printing system [60]

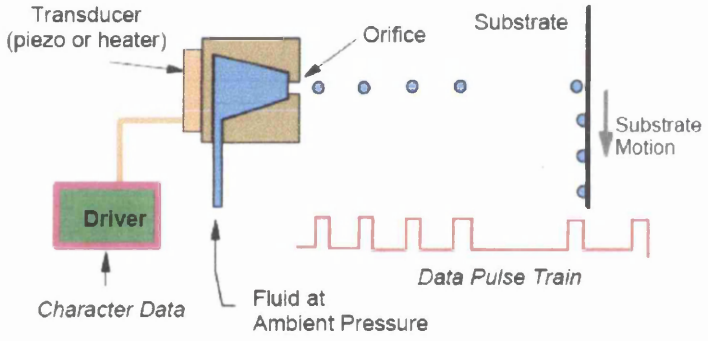

Figure 1.3: Schematic of a drop-on-demand ink-jet printing system [60]

1.3.2 Flexographic Printing

Flexography printing is an inexpensive technique generally used for packaging and labelling products. The image is raised above the cylinder surface. Figure 1.4 shows a schematic of a typical single flexographic printing unit which is used to print an ink or a single colour onto the substrate. Multiple print units can be used to print multiple colours for a complete run. In its simplest form, the system consists of three basic parts: an ink delivery system, a plate cylinder and an impression cylinder.

The inking system transfers ink from an ink chamber to an anilox roll which is engraved with a series of cells to meter the ink and the surface wiped clean by a doctor blade, supplying a controlled volume of ink to the printing plate. The printing plate is normally made by rubber or elastic photopolymers on which the image areas are above the non-image area of the plate. The printing plate is mounted to the plate cylinder where the raised image areas collect ink from the anilox roll and carry it to the printing nip between the plate and impression cylinder, transferring the ink to the substrate. The impression cylinder is used to apply pressure so that the plate cylinder is in contact with the substrate for printing.

Flexographic printing process is capable to print inks of medium viscosity range between 0.1 and 10 Pa.s with film thickness varying from 4 to 10 μm [59]. Flexography is the major printing process used in the high speed, web fed (reel-to-reel) packaging industry, however variations can be made to cover most printing requirements.

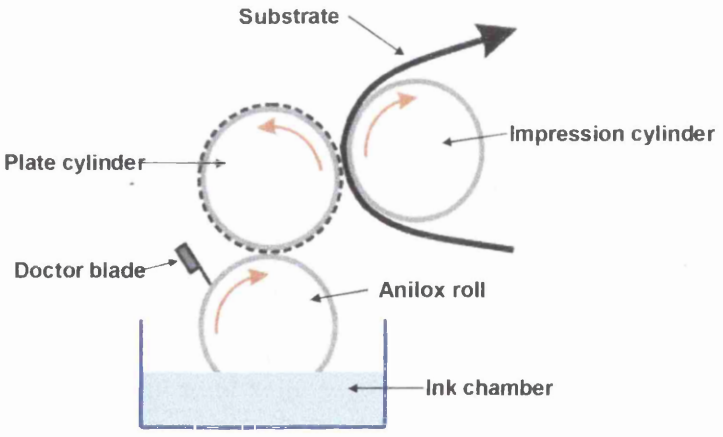

Figure 1.4: Schematic of flexographic printing process [62]

1.3.3 Screen Printing

Screen printing is one of the older forms of printing [62]. It is based on stencil printing where a pattern is cut into a sheet of material, such as paper, to produce a stencil. The stencil is placed onto the substrate and ink is spread over the top of it. A positive of the image is then produced on the substrate. Screen printing is a modern development of this process that utilises a mesh to hold the stencil which allows more complicated patterns. A screen comprises the mesh and stencil which is an element that carries the image to be printed. The mesh is made of a piece of finely woven porous fabric such as polyester, which is pre-tensioned and glued to a rectangular frame of aluminium. The non-image areas of the screen are blocked off with a non-permeable photosensitive material to form a stencil, which is the positive of the image to be printed. The open spaces (holes) between the mesh fibres allow the ink to flow through the mesh and transfer onto the substrate.

Figure 1.5 illustrates a detailed schematic diagram of the screen printing process. Before a print cycle begins, an adequate amount of ink is held on the upper surface of screen. A flowcoater is used to fill the mesh openings with ink without contact with the substrate. The flowcoater moves across the screen at a small height above it, distributing an even layer of ink spread over the whole image area of the print. The linear movement of the squeegee then pushes down, forcing the mesh onto the substrate. It is drawn across the screen until it reaches the end of the print length. The ink in the mesh opening is transferred through the screen onto the substrate. This reproduces a positive of the image on the substrate. The tension of the screen pulls the stencil off the substrate behind the squeegee. Excess ink builds up ahead of the squeegee. The squeegee is released and the press returned to the original position.

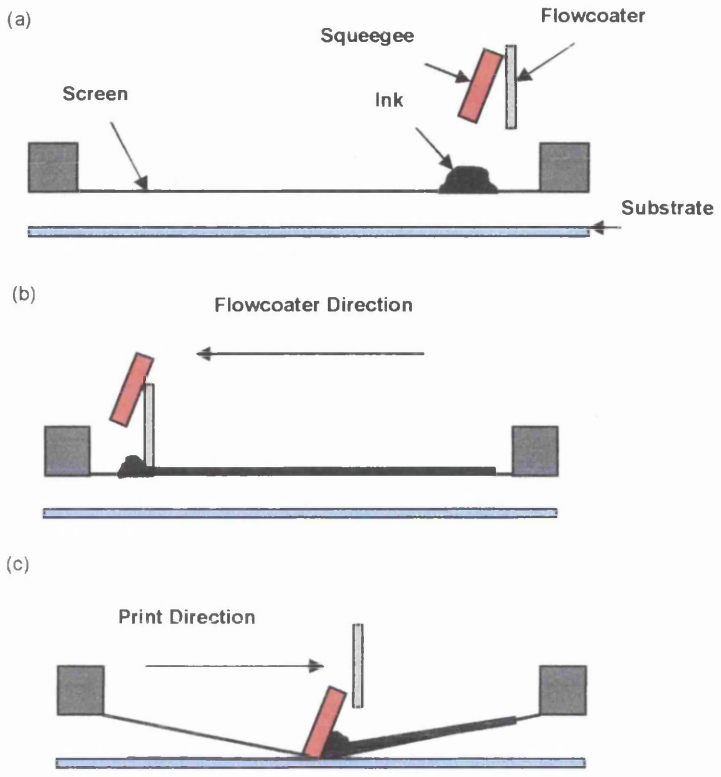

Figure 1.5: A schematic cross section of the screen printing process [63]

Screen printing has several important advantages over other printing processes in terms of ink deposit and process flexibility. It can print a wide variety of inks onto most substrates with simple contours and flat inflexible surfaces such as glass where the ink viscosity can be ranging from 0.1 to 40 Pa.s. It is capable of printing a wide range of ink film thicknesses between 10 to 60 μm which is the thickest ink deposits of all the printing processes. Its ability to lay down thicker ink film, print low viscosity inks and to print on rigid substrates makes it one of the options to construct biopolymer scaffolds. However, the major disadvantages of screen printing process are its relatively slow printing speeds compared to flexo. There are a vast number of process parameters that affect this process, making it a very difficult process to set-up and maintain to produce consistent prints.

1.4 The objectives of the investigation

In order to be able to construct a 3D tissue engineering scaffold, it is essential to understand the printing of fine lines. The main goal of this research is to print fine lines of biopolymer by means of volume printing processes. Lines of biopolymer will be printed in a sense of different thicknesses and different line rulings on a suitable substrate such as polystyrene, glass slides, polyvinyl chloride (PVC), polyester, cellulose acetate and etc. The desired resolution of printed fine lines, as shown in Figure 1.6, is ranging from 100 – 300 microns with same range for line spacing with each other (see Chapter 3).

The rheological characteristics of potential biopolymers will have a significant influence on the performance of the different printing processes. The biopolymers also undergo significant changes of state as they solidify which affect the printed products. Therefore, rheological tests were performed to characterise the rheological behaviour of the scaffolding biopolymers. Three printing processes inkjet printing, flexography and screen printing (as described previously) were evaluated for the printing of the biopolymers. These printing methods are aimed to produce cost effective bioscaffolds in mass production. The process parameters have to be optimised in order to achieve good quality fine lines. The effect of each process parameters on printed lines in terms of width and thickness was studied and evaluated.

Figure 1.6: Fine line of biopolymer

1.5 Structure of the thesis

The thesis is split into seven chapters and their content is outlined below.

Chapter 1 An introduction into tissue engineering and tissue engineered bioscaffolds. The conventional printing processes: inkjet, flexography and screen printing are described. The aim of the research is also highlighted here.

Chapter 2 A review of relevant literature of previous works carried out with a focus on the biomaterials (collagen and gelatine) and methods used to fabricate bioscaffolds. The effect of process parameters on image quality by different printing processes is also reviewed.

Chapter 3 Description of the experimental programme conducted and the measurement techniques to characterise the width and thickness of printed fine lines, including the instrumentation used, and also the details of orthogonal array method.

Chapter 4 The rheological characterisation of biopolymer inks is conducted. The viscous flow behaviour of both inks is compared and gelatine is chosen as the model ink for further investigation in its viscoelastic and gelation properties. An appropriate printing process is identified for each ink.

Chapter 5 Preliminary investigation into the feasibility of printing fine features of gelatine by three printing processes: inkjet, flexography and screen printing in order to establish the best method in printing gelatine.

Chapter 6 A laboratory screen print trial is designed using orthogonal array method, and conducted to investigate the effect of process parameters on the quality of printed fine lines in terms of width and film thickness.

Chapter 7 Conclusions drawn from the research and recommendations suggested for further investigation.

1.6 References

[1] Thomson R. C., Wake M. C., Yaszemski M. J., Mikos A. G. (1995) Biodegradable polymer scaffolds to regenerate organs. Advances in Polymer Science 122: 245- 274.

[2] Langer R., Vacanti J. P. (1993) Tissue engineering. Science 260 (5110): 920-926.

[3] PTEI. Tissue Engineering: An Introduction. Vol. 2006. PTEI: Pittsburg.

[4] Habermehl J. (2005) Development and validation of a collagen based scaffold for vascular tissue engineering. M. Sc. Thesis Laval University, France.

[5] Wakitani S., Goto T., Pineda S. J., Young R. G., Mansour J. M., Caplan A. I., Goldberg V. M. (1994) Mesenchymal cell-based repair of large, full-thickness defects of articular cartilage. Journal of Bone and Joint Surgery 76-A: 579-592.

[6] Caplan A. I., Elyaderani M., Mochizuki Y., Wakitani S., Goldberg V. M. (1997) Principles of cartilage repair and regeneration. Clinical Orthopaedics and Related Research 342: 254-269.

[7] Grande D. A., Halberstadt C., Naughton G., Schwartz R., Manji R. (1997) Evaluation of matrix scaffolds for tissue engineering of articular cartilage grafts. Journal of Biomedical Materials Research 34: 211-220.

[8] Weinberg C. B., Bell E. (1986) A blood vessel model constructed from collagen and cultured vascular cells. Science 231: 397-400.

[9] Ponticiello M. S., Schinagl R. M., Kadiyala S., Barry F. P. (2000) Gelatine-based resorbable sponge as a carrier matrix for human mesenchymal stem cells in cartilage regeneration therapy. J. Biomed. Mater. Res. 52: 246-255.

[10] Choi Y. S., Hong S. R., Lee Y. M., Song K. W., Park M. H., Nam Y. S. (1999) Studies on gelatine-containing artificial skin: Ii. Preparation and characterization of cross-linked gelatine-hyaluronate sponge. J. Biomed. Mater. Res. 48: 631-639.

[11] Kang H. W., Tabata Y., Ikada Y. (1999) Fabrication of porous gelatine scaffolds for tissue engineering. Biomaterials 20 (14): 1339-1344.

[12] Marijnissen W. J., van Osch G. J., Aigner J., van der Veen S. W., Hollander A. P., Verwoerd-Verhoef H. L., Verhaar J. A. (2002) Alginate as a chondrocyte-delivery substance in combination with a non-woven scaffold for cartilage tissue engineering. Biomaterials 23: 1511-1517.

[13] Yang J., Goto M., Ise H., Cho C. S., Akaike T. (2002) Galactosylated alginate as a scaffold for hepatocytes entrapment. Biomaterials 23: 471-479.

[14] Bettinger D., Gore D., Humphries Y. (1995) Evaluation of calcium alginate for skin graft donor sites. J. Burn Care Rehabil. 16: 59-61.

[15] Solchaga L. A., Dennis J. E., Goldberg V. M., Caplan A. I. (1999). Hyaluronic acid-based polymers as cell carriers for tissue-engineered repair of bone and cartilage. Journal of Orthopaedic Research 17: 205-213.

[16] Drury J. L., Mooney D. J. (2003) Hydrogels for tissue engineering: Scaffold design variables and applications. Biomaterials 24: 4337-4351.

[17] Tsioptsias C., Tsivintzelis I., Papadopoulou L., Panayiotou C. (2009) A novel method for producing tissue engineering scaffolds from chitin, chitin-hydroxyapatite, and cellulose. Mater. Sci. Eng. 29 (1): 159-164.

[18] Mao C., Zhu J. J., Hu Y. F., Ma Q. Q., Qiu Y. Z., Zhu A. P., Zhao W. B., Shen J. (2004) Surface modification using photocrosslinkable chitosan for improving hemocompatibility. Colloids Surf. B. Biointerf. 38: 47-53.

[19] Freed L. E., Vunjak-Novakovic G. (1998) Culture of organized cell communities. Adv. Drug Deliver. Rev. 33: 15-30.

[20] Wahl D. A., Czernuszka J. T. (2006) Collagen-hydroxyapatite composites for hard tissue repair. Eur. Cell Mater. 11: 43-56.

[21] Burg K. J. L., Porter S., Kellam J. F. (2000) Biomaterial developments for bone tissue engineering. Biomaterials 21: 2347-2359.

[22] Miranda P., Saiz E., Gryn K., Tomsia A. P. (2006) Sintering and robocasting of β-tricalcium phosphate scaffolds for orthopaedic applications. Acta Biomaterialia 2 (4): 457-466.

[23] Lin A. S. P., Barrows T. H., Cartmell S. H., Guldberg R. E. (2003) Microarchitectural and mechanical characterization of oriented porous polymer scaffolds. Biomaterials 24: 481-489.

[24] Sachlos E.,Czernuszka J. T. (2003) Making tissue engineering scaffolds work. Review on the application of solid freeform fabrication technology to the production of tissue engineering scaffolds. Eur. Cell Mater. 5: 29-40.

[25] Vert M., Mauduit J., Li S. (1994) Biodegradation of PLA/GA polymers: increasing complexity. Biomaterials 15: 1209-1213.

[26] Gunatillake P. A., Adhikari R. (2003) Biodegradable synthetic polymers for tissue engineering. Eur. Cell Mater. 5: 1-16.

[27] Chu T. M. G., Orton D. G., Hollister S. J., Feinberg S. E., Halloran J. W. (2002) Mechanical and in vivo performance of Hydroxyapatite implants with controlled architectures. Biomaterials 23: 1283-1293.

[28] Habraken W. J. E. M., Wolke J. G. C., Jansen J. A. (2007) Ceramic composites as matrices and scaffolds for drug delivery in tissue engineering. Advanced drug delivery reviews 59: 234-248.

[29] Laurencin C. T., Lu H. H. (2000) Polymer-ceramic composites for bone-tissue engineering. In Bone Engineering. J. E. Davies (Ed.): 462-472.

[30] Hutmacher D. W. (2001) Scaffolds in tissue engineering bone and cartilage. Biomaterials 21 (24): 2529-2543.

[31] Hutmacher D. W. (2001) Scaffold design and fabrication technologies for engineering tissues-state of the art and future perspectives. J. Biomater. Sci. Polym. Ed. 12 (1): 107-124.

[32] Freed L. E., Marquis J. C., Nohria A., Emmanual J., Mikos A. G., Langer R. (1993) Neocartilage formation in vitro and in vivo using cells cultured on synthetic biodegradable polymers. J. Biomed. Mater. Res. 27: 11-23.

[33] Mooney D. J., Mazzoni C. L., Breuer C., McNamara K., Hern D., Vacanti J. P. (1996b) Stabilized polyglycolic acid fibre-based tubes for tissue engineering. Biomaterials 17: 115-124.

[34] Mikos A. G., Thorsen A. J., Czerwonka L. A., Bao Y., Langer R., Winslow D. N., Vacanti J. P (1994) Preparation and characterization of poly(L-lactic acid) foams. Polymer 35: 1068-1077.

[35] Mikos A. G., Sarakinos G., Leite S. M., Vacanti J. P., Langer R. (1993b) Laminated three-dimensional biodegradable foams for use in tissue engineering. Biomaterials 14: 323-330.

[36] Mooney D. J., Baldwin D. F., Suh N. P., Vacanti J. P., Langer R. (1996) Novel approach to fabricate porous sponges of poly(D,L-lactic co-glycolic acid) without the use of organic solvents. Biomaterials 17: 1417-1422.

[37] Thomson R. C., Yaszemski M. J., Powers J. M., Mikos A. G. (1998) Hydroxyapatite fiber reinforced poly(a-hydroxy ester) foams for bone regeneration. Biomaterials 19: 1935-1943.

[38] Goldstein A. S., Zhu G., Morris G. E. Meszlenyi R. K., Mikos A. G. (1999) Effect of Osteoblastic Culture conditions on the structure of poly(DL-lactic-co-glycolic acid) foam scaffolds. Tissue Engineering 5: 421-433.

[39] Lo H., Ponticiello M. S. and Leong K. W. (1995) Fabrication of controlled release biodegradable foams by phase separation. Tissue Engineering 1: 15-28.

[40] Nam Y. S., Park T. G. (1999a) Biodegradable polymeric microcellular foams by modified thermally induced phase separation method. Biomaterials 20: 1783-1790.

[41] Nam Y. S., Park T. G. (1999b) Porous biodegradable polymeric scaffolds prepared by thermally induced phase separation. J. Biomedic. Mater. Res. 47: 8-17.

[42] Schmitz J. P., Hollinger J. O. (1988) A preliminary study of the osteogenic potential of a biodegradable alloplasticosteoinductive alloimplant. Clin. Orthop. 237: 245-255.

[43] Heckman J. D., Boyan B. D., Aufdemorte T. B., Abbott J. T. (1991) The use of bone morphogenetic protein in the treatment of non-union in a canine model. J. Bone Joint Surg. Am. 73: 750-764.

[44] Hsu Y. Y., Gresser J. D., Trantolo D. J., Lyons C. M., Gangadharam P. R. J., Wise D. L. (1997) Effect of polymer foam morphology and density on kinetics of in vitro controlled release of isoniazid from compressed foam matrices. J. Biomed. Mater. Sci. 35: 107-116.

[45] Matsuda T., Mizutani M. (2002) Liquid acrylateendcapped biodegradable poly(e-caprolactone-*co*-trimethylene carbonate). II. Computer-aided stereolithographic microarchitectural surface photoconstructs. J. Biomed. Mater. Res. 62: 395-403.

[46] Yang S. F., Leong K. F., Du Z. H., Chua C. K. (2002) The Design of Scaffolds for Use in Tissue Engineering. Part II. Rapid Prototyping Techniques Tissue Engineering 8 (1): 1-11.

[47] Boland T., Xu T., Damon B., Cui X. (2006) Application of inkjet printing to tissue engineering. Biotechnol. J. 1 (9): 910-917.

[48] Hull C. (1990) Method for production of three-dimensional objects by stereolithography. US Patent 4929402.

[49] Dhariwala B., Hunt E., Boland T. (2004) Rapid prototyping of tissue-engineering constructs, using photopolymerizable hydrogels and stereolithography. Tissue Engineering 10 (9-10): 1316-1322.

[50] Hutmacher D. W., Schantz T., Zein I., Ng K. W., Teoh S. H., Tan K. C. (2001) Mechanical properties and cell cultural response of polycaprolactone scaffolds designed and fabricated via fused deposition modelling. J. Biomed. Mater. Res. 55 (2): 203-216.

[51] Zein I., Hutmacher D. W., Tan K. C., Teoh S. H. (2002) Fused deposition modeling of novel scaffold architectures for tissue engineering applications. Biomaterials 23: (4): 1169-1185.

[52] Tan K. H., Chua C. K., Leong K. F., Cheah C. M., Gui W. S., Tan W. S., Wiria F. E. (2005) Selective laser sintering of biocompatible polymers for applications in tissue engineering. Biomed. Mater. Eng. 15 (1-2): 113-124.

[53] Williams J. M., Adewunmi A., Schek R. M., Flanagan C. L., Krebsbach P. H., Feinberg S. E., Hollister S. J., Das S. (2005) Bone tissue engineering using polycaprolactone scaffolds fabricated via selective laser sintering. Biomaterials 26 (23): 4817-4827.

[54] Sachs E., Cima M., Williams P., Brancazio D., Cornie J. (1992) Three Dimensional Printing: Rapid Tooling and Prototypes Directly from a CAD Model. J. Eng. Ind. 144: 481-488.

[55] Giordano R. A., Wu B. M., Borland S. W., Cima L. G., Sachs E. M., Cima M. J. (1996) Mechanical properties of dense polylactic acid structures fabricated by three dimensional printing. J. Biomater. Sci. Polym. Edn. 8(1): 63-75.

[56] Kim S. S., Utsunomiya H., Koski J. A., Wu B. M., Cima M. J., Sohn J., Mukai M., Griffith L. G., Vacanti J. P. (1998) Survival and function of hepatocytes on a novel three-dimensional synthetic biodegradable polymer scaffold with an intrinsic network of channels. Ann. Surg. 228: 8-13.

[57] Landers R., Mulhaupt R. (2000) Desktop manufacturing of complex objects, prototypes and biomedical scaffolds by means of computer-assisted design combined with computer-guided 3D plotting of polymers and reactive oligomers. Macromol. Mater. Eng. 282: 17-21.

[58] Yousefi A. M., Gauvin C., Sun L., DiRaddo R. W., Fernandes J. (2007) Design and fabrication of 3D-plotted polymeric scaffolds in functional tissue engineering. Polym. Eng. Sci. 47 (5): 608-618.

[59] Kipphan H. (2001) Handbook of print media: technologies and production methods. Springer-Verlag Berlin Heidelberg, New York.

[60] Cooley P., Wallace D., Antohe B. (2001) Applications of ink-jet printing technology to BioMEMs and microfluidic systems. Proceedings, SPIE Conference on Microfluidics and BioMEMS, MicroFab Technologies, Inc.

[61] Wallace D. B. (1989) A method of characteristics model of a Drop-On-Demand ink-jet device using an Integral Method Drop Formation Model. ASME publication 89-WA/FE-4.

[62] MSc in printing and coating technology modules notes, Printing Technology, WCPC.

[63] Barden T. J. (2007) The application of the three-dimensional profiling to the measurement and characterisation of screen printed fine lines. Phd Thesis University of Wales Swansea 2007.

2.0 Literature Review

2.1 Introduction to the literature review

This chapter describes and discusses the literature on fabrication of bioscaffolds for tissue engineering applications. This is used to assess the feasibility of conventional printing technologies in constructing bioscaffolds.

The literature is described in three sections; the materials and methods used to fabricate bioscaffolds, and also the methods of characterising scaffolding materials and bioscaffolds. Previous work performed to investigate the effect of variables in printing processes on the print quality is also reviewed.

2.2 Materials used to fabricate bioscaffolds

There have been several reviews on biomaterials used to fabricate tissue engineered scaffolds: biopolymers (natural and synthetic), bioactive ceramics as well as composite materials [1][2]. Although it is well known that human tissue contain a considerable amount of water, the major emphasis of scaffold fabrication technologies was placed upon melt and powder processing of biocompatible polymers in the absence of water. Therefore printing of water based bioactive systems such as hydrogels (water-based biopolymers), growth factors and cells would offer new opportunities in tissue engineering.

Generally, naturally occurring materials have the potential advantage of biocompatibility. Natural hydrogels such as gelatine or swollen collagen are advantageous due to their chemical similarity to the extracellular matrix, flexibility and rapid diffusion of hydrophilic nutrients and metabolites. Moreover, their low content of dry mass causes hydrogels contain only 1 up to 20 wt% of dry polymer mass. The natural hydrogels are degraded readily because the entire polymer backbone is exposed to water soluble enzymes.

In this section, collagen and gelatine are further reviewed below in terms of its structure and properties, also their feasibility in constructing a bioscaffold. The advantages and disadvantages of scaffolds fabricated from these natural biomaterials are summarised.

2.2.1 Collagen

Extracellular matrices (ECMs) are the defining feature of connective tissues of multicellular organisms which are composed of cells surrounded by complex microenvironments. ECMs consist of various glycoproteins, proteoglycans and hyaluronic acid where collagen is the most abundant natural protein, making up about one third of the total. Collagen is the essential structural component of all connective tissues such as tendons and ligaments, which serve a mechanical function, skin, and the organic substance of teeth and bones in animals. At least twenty types of collagen molecules have been identified to date [3][4] where Type I, II, and III are the most abundant and form fibrils of similar structure. The structure of Type I collagen fibrils is shown in the schematic diagram in Figure 2.1. It is a rod-like triple helical protein, called tropocollagen, of 300 nm long and 1.5 nm in diameter. It consists of three left-handed polypeptide α-chains, which are twisted around each other to form a right-handed superhelix, also known as triple helices, a cooperative quaternary structure stabilised by intra- and inter-molecular hydrogen bonds. These collagen molecules align along the helix axis and associate to form fibrils and fibril bundles of about 50 nm diameter. The tropocollagen molecules are packed in a characteristic D-band

structure where the adjacent molecules are displaced longitudinally by approximately 67 nm, 1/4 of their length to form a cylindrical fibril [5].

The amino acid composition of collagen is unusual and distinctive. The most abundant amino acids are glycine (Gly), proline (Pro) and hydroxyproline (Hypro) as shown in Figure 2.2. The regular arrangement of amino acids in each of the three chains of these collagen subunits often follows the pattern Gly-X-Y, where X is usually proline and Y is usually hydroxyproline. The repetition of glycine in every third position is the most essential factor determining collagens triple helical structure. Different types of collagen have different chemical structure and organisation that are adjusted to function at a specific site of the body.

Collagen is tough and inextensible with great tensile strength due to its innate structure, a triple helical structure that forms fibrils. Therefore, it has been extensively used in biomedical applications that require structural integrity, for example, the construction of biomedical devices such as bone substitutes and artificial blood vessels and valves. Collagen has also been popular in drug delivery applications. It is a versatile biomaterial with a lot of advantageous properties. First of all, collagen is a naturally derived material, so it is not likely to induce inflammatory and antigenic responses at the site of implant [5]. This has been approved by the United States Food and Drug Administration (FDA) for various types of medical applications including artificial skin and wound dressing [6]. Collagen is biodegradable and bio-reabsorbable. The in vivo resorption rate is determined by the density of the implant and the degree of intermolecular cross-linking. Collagen matrix of lower density gives greater interstitial space and generally has larger pore sizes, allowing an increase in cell infiltration that leads to a higher rate of implant degradation [7]. Collagen implants degrade via a sequential attack by lysosomal enzymes. Hence, the degradation rate can be reduced by making the collagen molecules less susceptible to enzymatic attack with the presence of intermolecular cross-linking. Collagen is easily modifiable and can be combined with several biological or synthetic polymers to produce a variety of medical devices and drug delivery systems.

Scaffolds made from collagen have been widely used in biomedical applications. However, collagen scaffolds in their pure form have several drawbacks. In many

cases, collagen scaffolds degrade very fast in vivo and this occurs before the implant could complete its function. Also, cells are prone to interact with collagen so easily that they can alter and reorganize the collagen fibres, causing the scaffolds to lose their shape if they are not strong enough. Therefore, physical or chemical cross-linking techniques are introduced to enhance the mechanical strength of collagen scaffolds by introducing intra- and intermolecular linkages. Physical cross-linking methods include dehydrothermal (DHT) treatments [8][9], ultraviolet (UV) irradiation [10], whilst chemical cross-linking methods involve the use of cross-linking agents such as glutaraldehyde (GTA) [11], hexamethylene diisocynate [12], formaldehyde [13] and carbodiimides (EDAC) [8][14]. The toxicity of the cross-linking agents has to be taken into serious consideration in developing bioscaffolds for surgical and orthopedic operations.

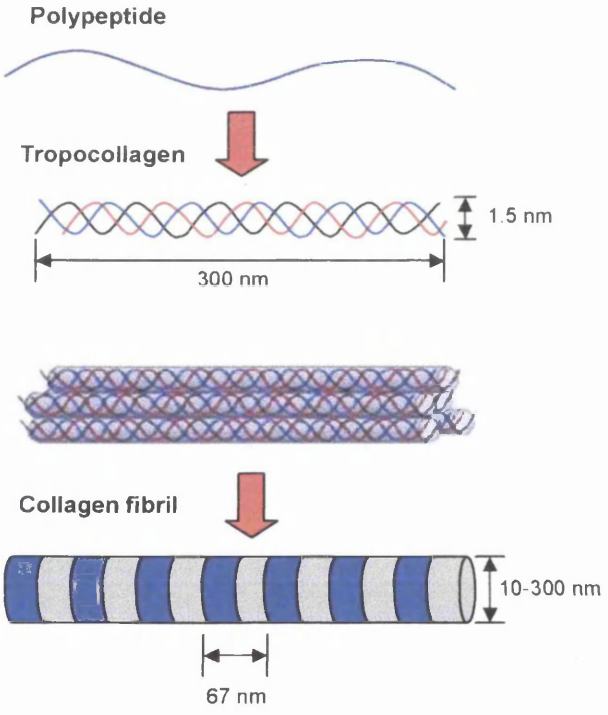

Figure 2.1: Type I collagen fibril structure. Helical collagen molecules form from three polypeptide chains, and these associate laterally to form collagen fibrils with a characteristic banded structure (adapted from Azonanotechnology article)

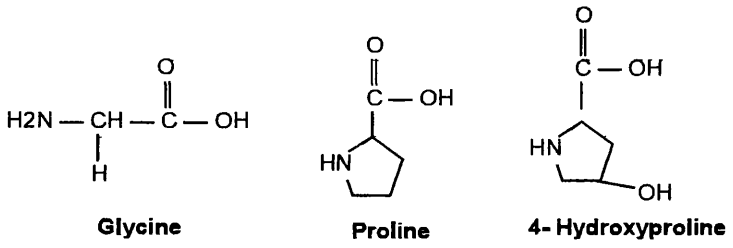

Figure 2.2: The main constituents of collagen [15]

2.2.2 Gelatine

Gelatine is an important biopolymer with a wide range of industrial applications. It is a translucent, colourless, brittle and tasteless solid substance, derived from the insoluble fibrous protein, collagen via partial hydrolysis process which involves the unravelling of the collagen triple helix into individual random chains. Gelatine is composed of polypeptide chains that consist of 18 different amino acids arranged in a unique sequence as shown in Figure 2.3. Figure 2.4 displays the amino acid composition of gelatine. Most commercial gelatines are obtained from mammalian sources such as pigskin and cowhide, but alternative substitutes, particularly from marine sources, have gained considerably increasing importance, especially since the food safety issues over BSE (bovine spongiform encephalopathy).

There are two types of gelatine dependent upon the type of pre-treatment used in the manufacturing processes. The acid pre-treatment produces Type A gelatine and the alkaline pre-treatment yields Type B gelatine. The ionisable groups of several amino acids in gelatine determine the specific net charge of the gelatine depending on the gelatine type and pH of the solution. This net charge affects the molecular interactions which results in the difference between properties of each gelatine type, Table 2.1. Isoelectric point (pI) is the pH at which the net charge on the gelatine molecule is zero with an equal number of positive and negative charges. Type B gelatine has lower pI value than that of type A gelatine because it contains a larger amount of free carboxyl groups than type A due to its alkaline processing, causing a greater degree of deamidation of the asparagine and glutamine amino acids than acid hydrolysis [15].

Gelatine is also categorised according to its bloom value, a measure of the gel strength.

Properties	Type A	Type B
pH	3.8 – 5.5	5.0 – 7.5
Isoelectric point, pI	6.3 – 9.5	4.5 – 5.2
Gel strength (Bloom)	50 – 300	50 - 300

Table 2.1: Typical properties of gelatine

Gelatine is one of the more versatile food substances, which is readily usable and easily digestible. It has been extensively used in the food processing, pharmaceuticals, photography and paper production. Its wide range of applications is mainly based on its unique functional properties used to gel, thicken, stabilise, emulsify, bound, firm and aerate. The chemical composition of gelatine is closely similar to that of its parent collagen in many respects. It produces a solution of high viscosity in water which sets to gel upon cooling where the gelatine chains associate with one another forming triple helical structures, and melt when the temperature is raised where the chains dissociate again into a more amorphous form. Being a protein, gelatine is also a very useful nutritive component.

The gelation of gelatine will take place by two mechanisms which are chemical gelation and physical gelation. Chemical gelation is caused by carrying out a cross-linking reaction on the gelatine in solution by using a cross-linking reagent. This leads to the formation of permanent covalent bonds between functional groups of monomers and thus, chemical gels are thermo-irreversible. They may only be degraded by the breaking of bonds and structure and are called thermosetting. Unlike chemical gels, physical gels are thermo-reversible. The physical gelation arises through a change of temperature when the intermolecular forces of interaction such as hydrophobic and electrostatic interaction, stereocomplex formation, hydrogen bonding, Coulombic, dipole-dipole or Van der Waals forces, bind the monomers.

These physical junctions are constantly created and destroyed at very low rates such that the gel networks appear to be permanently connected. This gelation may be removed by changing the temperature which causes the gel to melt and reform the solution [17].

Gelatine is basically a partial denatured form of collagen that retains common properties as collagen [18]. Even though collagen is a major component of skin, bones and connective tissue, it is often difficult to obtain collagen in industrial scale or high concentration from same natural source of collagen [18]. Thus, there are big variations in the properties of collagen from batch to batch lots according to the tissue sources, tissue maturation and collagen modification, aging and cross-linkings in collagen [19][20]. These differences complicate the application of collagen from natural sources which lead to difficulty in reproducing or maintaining the quality of the product. Gelatine, unlike collagen, does not exhibit any antigenicity in physiological condition [20][22]. The major antigenic determinant of collagen molecules is the amino-terminal telopeptides which can be enzymatically or chemically removed or can be masked by performing cross-linking reactions to minimise the charged groups [5]. Even though collagen exhibits a low degree of antigenicity, adverse immune reactions (formation of antibodies) to implanted collagen may be induced in patient's body. It has been reported that about 3% of the population are allergic to bovine collagen [23]. It has been reported that bovine and porcine collagen raised some epidemic concerns on the application of animal tissues where animal diseases such as Creutzfeldt-Jakob disease (CJD) was transmitted to human and caused at least 100 deaths after the transplantation of collagen [24]. Gelatine also shows non-cytotoxic and non-immunogenic behaviours [25]. Hence, gelatine is known to have wide biomedical applications where it has been used as wound dressings, adhesive and absorbent pad for surgical use [26]. It is a popular scaffolding material to fabricate porous scaffolds reinforced with hydroxyapatite particles which are highly effective in bone tissue engineering [27].

Ratanavaraporn et al. [28] have studied and compared the physical, chemical and biological properties of both gelatine and collagen scaffolds, including the cross-linking degree, morphology, swelling ratio, mechanical strength, degradation rate, as

well as cell attachment and proliferation. Gelatine scaffolds was found to possess comparable properties, especially the cell proliferation, to those of collagen scaffold. However, the rapid degradation rate and poor mechanical performances of gelatine scaffolds are drawbacks for tissue engineering purposes. However, gelatine scaffolds can be modified by increasing the crosslink densities to improve its mechanical properties and reduce the degradation rate by making the fabricated scaffold less susceptible to enzymatic degradation. Here, gelatine was cross-linked by dehydrothermal (DHT) treatment at 140°C for 24 and 48 hours in a vacuum.

Cross-linking by either physical or chemical techniques that have been performed on gelatine are the same methods that have been applied on collagen as mentioned earlier. Different cross-linking techniques used for hydrogels were summarised and discussed in the previous work done by Hennink and van Nostrum [29]. Physical cross-linking by DHT treatment [8] and short wave length ultraviolet (UV) irradiation (254 nm) [9] have been performed on gelatine films, giving lower degree of cross-linking. Weadock and co-workers [30][31] have compared the effects of both methods on the mechanical properties, molecular integrity and durability of collagen fibres. They demonstrated that these methods gave rise to partial denaturation of collagen which may influence the cell growth. These physical methods have increased the Young modulus, the swelling resistance and resistance to enzymatic digestion. The UV-cross-linked collagen fibres remained intact for a longer period of time and thus should exhibit greater resistance to proteases in vivo whilst DHT-cross-linked fibres were not suitable for load-bearing implants. Scaffolds can be further cross-linked by carrying out chemical cross-linking reactions through formation of permanent chemical bonds using a number of cross-linking agents such as glutaraldehyde [11], diisocynates [12], formaldehyde [13], diepoxy compounds [32] and water-soluble carbodiimide [14]. These chemical methods efficiently improve the mechanical stability of the structure and also allow a better control over the rate and extend of biodegradation in vivo. However, the cross-linkers used are often cytotoxic to the cells which give unwanted response at the implantation site [33].

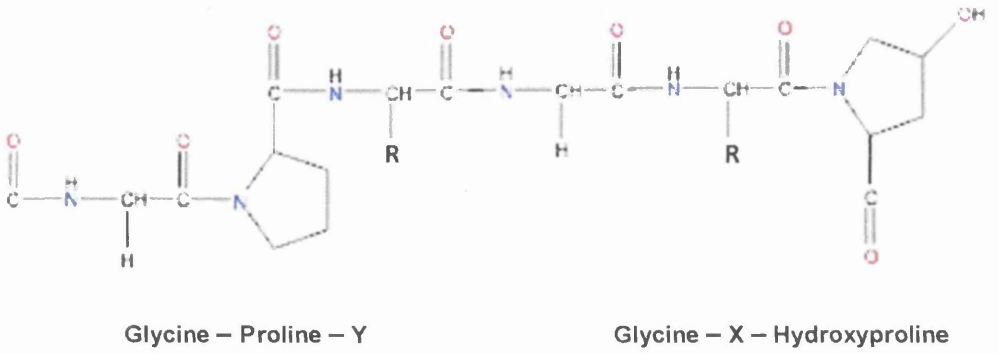

Figure 2.3: The structure of gelatine [34]

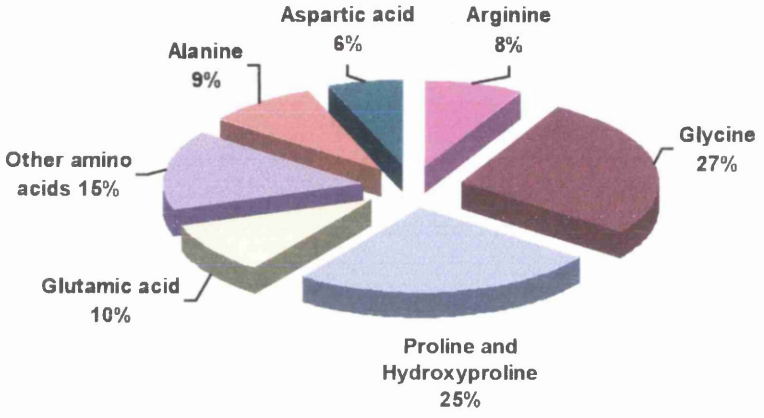

Figure 2.4: The main compositions of gelatine with high content of amino acids [35]

2.3 Methods to fabricate Bioscaffolds

This section describes and discusses the methods of bioscaffolds fabrication, including the development and revolution of conventional chemical techniques, solid freeform fabrication techniques and conventional printing techniques. The advantages and limitations of each technique are presented.

2.3.1 Conventional chemical techniques

Several conventional techniques have been developed to fabricate porous scaffolds, such as fibre bonding, solvent casting and particulate leaching, gas foaming, phase separation, melt moulding and freeze drying. All these methods aim to produce highly porous scaffolds with large surface areas to support the adhesion and growth of cells. An adequate pore size and a uniformly distributed and interconnected pore structure are crucial, allowing an easy distribution of cells throughout the scaffold structure. A description of the different techniques follows.

Fibre bonding is a technique that develops scaffolds from a mesh of polymer fibres which were some of the earliest constructs proposed in tissue engineering [36][37]. Polyglycolic acid (PGA) nonwoven meshes are produced by extruding PGA into fibres of 13 micron diameter, which are subsequently stretched and relaxed at high temperatures, crimped and cut, carded into a lofty web, and finally needled to form a nonwoven mesh. The lack of structural stability of these nonwoven scaffolds led to the development of a method to bond PGA fibres by Mikos et al. [38]. A composite material was formed by dissolving poly(L-lactic acid) (PLLA) in methylene chloride solution and casting over a nonwoven PGA fibre mesh. The nonbonded PGA/PLLA composite is heated above the melting temperature of both polymers to bond the PGA fibres at the cross-points forming highly porous foams. Once the foams are quenched, the PLLA is removed by dissolving the composite structure in methylene chloride again. The bonded scaffolds have high porosity of about 81% and pore sizes up to 500 μm in diameter.

Mooney et al. [39] described spray casting method where PLLA or poly(DL-lactic-co-glycolic acid) (PLGA) is dissolved in chloroform and sprayed over the surface of PGA fibre mesh using a dental atomizer, forming hollow tubes. The solvent was then evaporated, leaving the PGA fibres bonded at cross-points with PLLA or PLGA. The mechanical properties of the scaffold are dictated by PGA fibre mesh while the surface properties are determined by PLLA or PLGA. These scaffolds have interconnected pore structure with pore sizes similar to those of the techniques mentioned earlier, as large as 500 μm. PLLA bonded tubes degrade much slower and have greater resistance to compressive force than PLGA bonded tubes. When PLLA

bonded tubes were implanted in rats for 17 days, fibrovascular tissue ingrowth was observed. A tubular tissue also formed when smooth muscle cells and endothelial cells were seeded onto the devices in vitro. This indicates the potential of these scaffolds in encouraging the formation of specific tissues.

Scaffolds formed by fibre bonding technique give high porosities and high interconnectivity pores, resulting in large surface area to volume ratio for cell attachment and a rapid diffusion of nutrients that are suitable for tissue generation. There are some disadvantages that pore sizes are difficult to be controlled accurately and the use of solvents in both methods are potentially toxic to cells. It is also not possible to incorporate cells or bioactive materials such as growth factors into the scaffolds during processing due to the high temperature and toxic chemicals involved.

Solvent casting and particulate leaching technique involves producing a solution of PLLA in methylene chloride. Water-soluble porogens (salt particles) are added to the solution to produce a uniform suspension [40]. The solvent was allowed to evaporate and a solid polymer-porogen construct formed. The salt particles were then leached out to produce a highly porous and crystalline structure with interconnecting interior channels for cell cultivation. The porosity of scaffolds can be controlled by the amount of salt particles added while the pore sizes are dependent on the size of salt particles. High interconnectivity pores can be created with salt particles of 70 percent weight and above. A lamination technique was proposed by Mikos et al. [41] to shape these scaffolds into three-dimensional structure using chloroform as the solvent.

The technique has been modified by Thomson et al. [42] and Goldstein et al. [43] by adding a melt (heating and compression) moulding process before the leaching of salt particles in water. A composite material consisting of gelatine microspheres and hydroxyapatite short fibres embedded in a PLGA matrix was formed by casting the mixture into a Teflon mould which was then set by applying heat above the glass transition temperature of PLGA and pressure [42]. After the gelatine component has been leached out by immersing in water, an open-cell composite foam remains which has a pore size and morphology defined by the porogens. These scaffolds have pores of 500 μm in diameter and greater porosity of over 90% with an increase in the uniformity of scaffold surface. Waxy hydrocarbons were also used as porogens by

Shastri et al. [44] where scaffolds with porosity up to 87%, pores of over 100 μm diameter and thickness up to 2.5 cm were constructed. These scaffolds of PLLA were seeded with bovine chondrocytes and cultured in vitro for two weeks, a structurally stable cartilage-like tissue-polymer composite was formed, showing their biocompatibility.

Scaffolds constructed by this technology have been extensively used with various types of cells. No adverse effects were shown on the tissue formation [36][41][43]. However, the organic solvents involved in the method preclude the addition of pharmacological agents to the scaffold during fabrication. The leaching step is also time consuming and increases the time of preparing a scaffold significantly.

In order to eliminate the use of organic solvent, a gas foaming technique has been introduced by Mooney et al. [45]. Solid discs of PGA, PLLA or PLGA were formed by compression moulding which were saturated with carbon dioxide (CO_2) at high pressure for three days. The solubility of the gas in the polymer was rapidly decreased by bringing the CO_2 gas pressure to atmospheric level, resulting in nucleation and growth of bubbles or cells. Scaffolds with porosities up to 93% and pore sizes approximately 100 μm could be fabricated with this technique, but the pores were largely unconnected. This made it difficult for the cell to attach and migrate within the structure. High temperature during disc formation also hinders the incorporation of cells or bioactive molecules, same as that in fibre bonding technique.

Nam et al. [46] developed another approach which involved both gas foaming and particulate leaching methods where ammonium bicarbonate particulates were used as a gas foaming agent as well as a salt leaching porogen. PLLA polymer was dissolved in methylene chloride or chloroform, and ammonium bicarbonate added to the solution and mixed vigorously. The polymer/salt/solvent mixture was then cast into a mould. The solvent was evaporated and the composite either vacuum dried or immersed into hot water to leach out the salt particles while generating gaseous ammonia and CO_2. The resultant scaffolds had a well interconnected macroporous structure of pore sizes ranging from 100 – 500 μm. Primary rat hepatocytes were seeded into the scaffolds and exhibited over 90% cell seeding efficiency and up to 40% viability at one day in culture. This suggested that scaffolds constructed in this

manner were biocompatible and had efficient transport of oxygen and nutrients to the cells.

Liquid-liquid phase separation technique is based on the principle that a two phase homogeneous solution of polymers can become thermodynamically unstable by altering the temperature, inducing phase changes [47][48][49][50]. Synthetic polymer (PLLA or PLGA) was dissolved in naphthalene or molten phenol. The temperature was reduced to produce a liquid-liquid phase separation via a nucleation and growth mechanism, and quenched to form a two-phase solid via spinodal decomposition that produces more interconnected pores within the matrix [49][51]. The solvent was then removed by sublimation yielding a porous scaffold of up to 91% porosity with pore diameter ranging from 10 – 300 μm [51]. The pore size could be enlarged by annealing process [49][50]. Although the use of organic solvents is a disadvantage, the pore sizes and distribution can be tailored for specific applications via manipulating the processing conditions.

Another technique based on the concepts of phase separation is emulsification freeze drying. PLGA was dissolved in methylene chloride and ultrapure water added to form a water-in-oil emulsion [52]. The mixture was then cast into a mould and quenched in liquid nitrogen. After quenching, the scaffolds were freeze-dried at -55°C to remove the dispersed water and polymer solvents and produce a porous structure. These scaffolds had high porosities up to 95%, but with small pore sizes of only 13 – 35 μm in diameter. These properties were dependent on process parameters such as the ratio of polymer solution to water and viscosity of the emulsion. It was thought to be possible to increase the pore size by tuning the process parameters. This technique does not require an extra leaching step, but the use of organic solvents and the small pores obtained limit its application in tissue engineering.

Solution casting technique involves solubilising PLGA in chloroform and precipitating it by adding methanol or ethanol to the solution [53][54]. It can be mixed with the demineralised freeze-dried bone powder. The composite was then moulded into the required shape and heated to 45 – 48°C for one day to create the scaffold. The porous scaffolds fabricated using this technique, had as high as 80% porosity.

Freeze drying (also called lyophilisation) technique is commonly used to construct scaffolds from both natural and synthetic biopolymers. Synthetic polymers, such as PLGA, are dissolved in glacial acetic acid or benzene, the solution is then frozen and freeze-dried to form a low density porous structure. The morphology of these scaffolds is dependent on the polymer and the solvent used in the fabrication process[55]. Freeze-dried collagen scaffolds [56][57] were prepared by freezing an aqueous collagen dispersion that results in the formation of ice crystals which aggregate the collagen molecules into the interstitial spaces. The resultant construct was then freeze-dried to remove the ice crystals, giving a highly porous scaffold with small pore sizes of under 100 μm. The pore structure of the freeze-dried scaffolds could be controlled by altering the dispersion pH and viscosity, freezing temperature and freezing rate. Collagen dispersion of lower viscosity and higher pH gave larger pores. Also, the pore sizes could be increased by increasing freezing temperature and at slower freezing rate. This was explained on the basis of ice crystal growth after freezing [58][59].

In order to manufacture a collagen scaffold with an adjustable and homogenous three-dimensional pore structure, unidirectional solidification has been applied during the freezing process where the whole sample was solidified under thermally constant freezing conditions [60][61]. Cross-linking, by either physical or chemical methods was employed to the collagen scaffolds to improve the mechanical properties and decrease the solubility, antigenicity and degradation rate [8]. Apart from collagen, other natural biopolymers such as silk fibroin [62][63][64], chitosan [65][66], gelatine [67][68] and alginate [69][70], as well as a blend of these polymers [71][72][73][74] have also been fashioned into scaffolds via freeze-drying technique.

Table 2.2 summarises the advantages and limitations of conventional scaffold processing techniques. All chemical scaffold fabrication techniques are able to produce scaffolds with porosity that promotes cell attachment and growth. Most techniques can create large and interconnected pores to facilitate cell proliferation and nutrient transport, except both emulsification freeze drying and freeze drying methods which are limited to small pore sizes of up to 50 μm. Scaffolds fabricated by fibre bonding, solvent casting/particulate leaching and gas foaming methods have been

reported to exhibit good biocompatibility, making these approaches promising for tissue engineering purposes. However, a drawback of these chemical techniques is the lack of precise control over the scaffold specifications such as pore size, pore geometry, pore network and interconnectivity, spatial distribution of pores, and the final scaffold shape. The use of organic solvents such as methylene chloride and chloroform in most techniques, can lead to the presence of residual solvents that can exert toxic and carcinogenic effects to cell growth and differentiation. Thus, the complete removal of these solvents is essential yet will be extremely difficult even with a long processing time. Some of the techniques such as fibre bonding and melt moulding involve the application of elevated processing temperature that precludes the incorporation of cells or bioactive materials (growth factor) into the scaffolds.

Process	Advantages	Disadvantages
Fibre bonding	Highly porous structure (Porosity ≈ 81%) Pore sizes up to 500 μm High pore interconnectivity	Limited range of polymers Residual organic solvents High processing temperature Poor mechanical strength
Solvent casting and particulate leaching	Highly porous structure (Porosity < 87%) Large range of pore sizes Independent control of porosity and pore size	Limited membrane thickness ≈ 3mm. Limited interconnectivity Poor control over internal architecture Residual porogens
Melt moulding	Independent control of porosity and pore size (Porosity > 90%) Pore size range: 100 – 500 μm Increased uniformity of scaffold surface	High processing temperature
Gas foaming	Highly porous structure (Porosity < 93%) No organic solvents Good biocompatibility	Poor pore interconnectivity Limited to small pore size ≈100 μm High processing temperature
Liquid-liquid phase separation	Highly porous structure (Porosity < 91%) Pore size range: 10 – 300 μm Allows incorporation of bioactive materials	Poor control over internal architecture Residual organic solvents
Emulsification freeze drying	Highly porous structure (Porosity < 95%) No extra leaching process	Limited range of small pore sizes: 13 – 35 μm Residual organic solvents
Freeze drying	Highly porous structure (Porosity > 90%) High pore interconnectivity	Limited to small pore sizes < 100 μm

Table 2.2: Summary of conventional scaffold fabrication techniques [75][76]

2.3.2 Solid Freeform Fabrication (SFF) Techniques

It is important to create optimal pore size, and structure that favours cell attachment and migration throughout the scaffold. Recent developments in SFF techniques could overcome those limitations of conventional chemical process. SFF methods [78] involve building 3D object via layer-by-layer process based on a computer-generated model. Corresponding to each cross section, the SFF machine lays down the first layer of material starting from the bottom and building layers up (one layer at a time) to create the physical structure where each new layer formed is adhered on top of the previous layer. Post processing such as cleaning, curing and finishing is often required to remove the temporary support structures, yielding the final product [7]. SFF technology appears to be of a great advantage to tissue engineering world in such that it is able to construct three-dimensional porous scaffolds with customised external shape, predefined and reproducible internal microstructures and compositional variation across the entire structure. These techniques provide excellent computer control over pore size, porosity, pore interconnectivity, pore distribution, as well as an artificial vascular system which is responsible to supply sufficient transport of oxygen and nutrients to the cells, and remove the waste products from the cells via natural metabolism. It is also possible to incorporate cell seeding into the scaffold fabrication process that facilitates cell infiltration into the interior of scaffold.

SFF should make it possible to design and manufacture tailor-made tissue engineering scaffolds [77]. SSF techniques can be integrated with 3D medical scans of the patient's defect site to design a customised model in order to create a scaffold with not only the desired overall external size and shape but also appropriate mechanical properties which is a perfect fit to the damaged tissue site. There are several SFF approaches such as stereolithography [79][80], fused deposition modelling [81][82], selective laser sintering [83][84], three-dimensional printing [85][86][87] and 3D plotting [88].

Stereolithography (SLA) [79] utilises an ultraviolet (UV) laser beam to polymerise material from a vat of photocurable solution selectively in a layer-by-layer process. The CAD cross-sectional data guide the UV beam onto the liquid monomer surface within x-y plane. After the first layer is built, the elevator platform is descended vertically (z-plane) by a single layer thickness, typically 50 – 150 μm into the vat to

enable the liquid photopolymer monomer to cover the surface. This is followed by surface flattening with a 'wiper arm' sweeping over the liquid. On this new liquid surface, the subsequent layer pattern is traced and adhered to the previous layer. This procedure is repeated until a complete 3D model is constructed and post processed. This system requires the use of support structures to attach the model to the elevator platform so that the 2D cross-sections are held accurately in place to resist the lateral pressure from the wiper, and also to prevent the model from deflecting due to gravity. After completion, the supports are removed from the finished product manually.

SLA was first used by Griffith et al. [89] to create 3D ceramic green bodies by curing the suspension of ceramic particles (silica, alumina and silicon nitride) dispersed within a UV-photocurable solution, layer by layer. The binder was subsequently removed by pyrolisis resulted in sintered ceramic parts. SLA has also been used to fabricate ceramic scaffolds from HA [90] and calcium polyphosphate (CPP) [91] that are only limited to bone engineering purposes. Matsudas et al. [78] have developed biodegradable liquid acrylate-endcapped poly(ε-caprolactone-co-trimethylene carbonate), poly(CL/TMC) by using hydrogels of poly(ethylene glycol) (PEG) or trimethylene glycol (TMG) as an initiator and a photoactive acrylate group for terminal capping, which was used as photocurable copolymer to produce microarchitectured photoconstructs. Rapid degradation of the copolymers within the structure was observed both in vitro and in vivo and anti-inflammatory drug, indomethacin was added to the structure surfaces to minimise the inflammatory reactions. Besides, the incorporation of photocurable hydrogels such as poly(ethylene glycol)-dimethacrylate (PEG-DMA) and poly(ethylene oxide) (PEO) with cell encapsulation appears feasible to fabricate complex bioactive 3D scaffolds using SLA technique [80][92]. These scaffolds show high cell viability and can be used for various tissue engineering applications.

Fused deposition modeling (FDM) works on an "additive" principle by laying down material in layers [81][82]. This method uses a moving nozzle that extrudes a polymeric fibre in the horizontal plane. After the first layer is deposited, the plane is lowered and the procedure is repeated until the complete physical model is built layer-by layer. Bioresorbable poly-ε-caprolactone (PCL) scaffolds with honey-comb like pattern are

fabricated by optimising the process parameters for the extrusion of PCL filaments [81]. These PCL scaffolds have pore sizes ranging from 160 microns (vertically) to 700 microns (horizontally) and filament diameters up to 370 microns. The porosity obtained is varied from 48% to 77%, depending on the diameter of the extruder tip [82]. Human fibroblasts were cultured in PCL scaffolds and formed a cell-to-cell and cell-to-ECM interconnected structure throughout the entire matrix. PCL scaffolds have been integrated with ceramics such as calcium phosphate (CaP) [93] and HA [94] for the purposes of bone tissue engineering. The PCL/CaP scaffolds have higher degradation if compared to PCL scaffolds [93]. No significant difference in structural and mechanical properties was found between PCL and PCL/HA scaffolds. Both types of scaffolds exhibited superior mechanical strength and mineralization with increased tissue growth after 14 weeks in vivo [94]. FDM is advantageous in its high degree of precision in directing the nozzle on location in x-y plane. It does not require toxic organic solvents, but the high temperatures involved preclude the incorporation of biological molecules into the process. The extrusion process also limits the types of materials that can be processed and thus has limited the application of FDM only to synthetic thermoplastic polymers.

Wang et al. [95] used precision extruding deposition technique (PED) to fabricate PCL scaffolds. PED is very similar to FDM, except that PED directly extrudes the scaffolding materials in the form of granules or pellets which are deposited in fibre form without the need of precursor filament as in FDM process. PED offers good control over the designed internal architecture and the scaffolds fabricated have a controlled pore size at about 250 microns scale.

Selective laser sintering (SLS) is operationally similar to SLA that involves selectively sinters small particles of polymers [83][84], ceramics [83] or composites of polymers and hydroxyapatite [96][97][98] from a powder bed by using a computer-directed high power laser beam such as CO_2 laser and infrared (IR) laser, into a desired 3D complex scaffold with pre-defined macro- and microstructures. The laser beam scans across the surface and increases the local temperature to the glass transition temperature of the powder that causes the powdered particles to fuse to each other in a preprogrammed pattern for each layer. Upon completion, the powder bed is

lowered to deposit a new layer of powder on top and the process is repeated. Tan et al. [83] have used SLS in manufacturing highly porous scaffolds from biocompatible polymers such as poly(etheretherketone) (PEEK), poly(vinyl alcohol) (PVA), PCL and PLLA, and also bioceramic HA. PCL porous scaffolds fabricated using SLS exhibit sufficient biological and mechanical properties for bone tissue engineering applications [84]. The use of biocomposites such as PVA and HA [97] and PCL and HA [98] for scaffold fabrication via SLS showed favourable potential for tissue engineering applications.

SLS technique provides control over the microstructures of scaffolds by varying the laser processing parameters [96] such as laser power and scan speed to control the degree of particle fusion and porosity. The scaffolds produced were highly porous due to the low compaction forces during fabrication in SLS. Unlike other SFF techniques, SLS does not require support structures because the model is always surrounded by unfused powdered particles throughout the whole process. However, additional post processes are required for debinding the polymer binder and sintering the ceramic structure which in turn, increase the processing time and cost required in scaffold manufacture [97]. The high processing temperature involved is also a drawback that eliminates the possibility of including bioactive molecules and cells into scaffold fabrication.

Three dimensional printing (3DP) [85][86][87] involves ink-jet printing of a chemical binder from a jet head onto a powder surface, one layer at a time. The jet head moves in accordance to the CAD cross-sectional data to dispense the binder which selectively dissolves and joins the adjacent powder particles. Then, the piston chamber is lowered to have a new layer of powder and the process is repeated. Support structures are not required in this method as the unbound powder serves as a support for any overhanging or unconnected features. After completion, the unbound powder is removed manually. Synthetic biodegradable polymers such as PLLA [86] and PLGA [87] have been used to produce scaffolds by using chloroform as a binder. The printed scaffold can be post processed by cold isostatic pressing to enhance its mechanical properties [86]. Additionally, successful attachment and survival of hepatocytes (HCs) co-cultured with nonparenchymal cells on 3D PLGA scaffolds

fabricated using 3DP demonstrated its potential for use in treatment of liver disease [87]. These scaffolds were built in a cylindrical shape, consisting of interconnected longitudinal and radial channels of 800 μm in diameter running through the length of the scaffold. Salt leaching process was used to remove the sodium chloride particles loaded within PLGA polymer to create scaffolds with micropores of various diameters up to 150 μm and a microporosity of 60% was obtained. Koegler et al. [99] modified the surface chemistries of PLGA scaffolds with addition of PEO which resulted in a reduction in adhesion, growth rates and migration of osteoblasts. 3D-printed porous scaffolds made of β-TCP can be combined with mesenchymal stem cells (MSCs) suspended in hydrogels to form bone tissue in vitro [100].

Scaffolds can be fabricated from a wide range of biological materials using 3DP given that an appropriate chemical binder is selected. The resolution of 3D-printed objects varies upon the complexity of the object. One significant drawback in 3DP method is the use of cytotoxic organic solvents such as chloroform or methylene chloride as the chemical binder. Post processing such as vacuum drying is not completely effective in removal of the residual solvent. It was found that there still remained 0.5 %wt (5000 ppm) chloroform on samples after one week of drying [86] which is well exceeded the amount of residual chloroform permitted in pharmaceutical products, as described by US Pharmacopoeia which is only 60 ppm [101]. This level of chloroform can be significantly reduced below 50 ppm via high pressure liquid CO_2 extraction with minimal changes in scaffold architecture [102]. The duration of drying is predicted by a simple Fickian diffusion model and depended on the thickness of printed scaffolds. Starch-based polymer scaffolds were fabricated from a unique blend of cornstarch, dextran and gelatine using 3DP with water acting as a binder [103]. Post processing was also necessary to improve the mechanical and chemical properties of the scaffolds. Although 3DP is a helpful technique in fabricating scaffolds, the requirements of organic solvent as a liquid binder, time-consuming post processes, custom 3DP machines and experienced operator restrict its application in tissue engineering.

3D plotting [88][105] has been developed at Freiburger Materialforschungszentrum. This system uses a moving extruder head to force out strands of various plotting materials continuously by compressed air into a liquid medium with matching density, building up a complex 3D model with customised internal structures layer by layer without the use of any binder. The material solidifies once touching the substrate or adhering to the previous layer to form each new layer. The 3D scaffold constructed is then cured by means of either physical phase transition or chemical reaction. The 3D plotter is capable of dispensing a wide variety of biomaterials prepared in various forms such as hotmelts, solutions, pastes and dispersions of polymers as well as monomers and reactive oligomers [88]. The extruder head can be heated to the required temperature to prevent the plotting medium from solidification upon dispensing. 3D plotting system has been used to create scaffolds from biodegradable polymers such as PLLA [104] and PCL [105]. These scaffolds have completely interconnecting pores for cell growth and a porosity ranging from 30% to 70% throughout the whole structure, facilitating mass transport of oxygen and nutrient not only at the surface but also in the core. It was reported that the scaffold architecture influences the cell response in terms of seeding efficiency and proliferation [104].

3D plotter also allows the processing of low viscosity hydrogel materials such as gelatine, agar and alginic acid solutions [106][107]. Different types of hydrogel formation including thermoreversible gelation, complex formation or enzymatic gelation have been used. Thermoreversible hydrogel scaffolds were created by dispensing the warm agar solution (70°C) into a cold aqueous gelatine solution (20°C) to form layers of stable gel due to gelation process [107]. The agar scaffolds were then coated with hyaluronic acid and alginic acid to enhance the cellular attachment of fibroblasts and osteosarcoma cells. Besides, fibrinogen has been added to the alginic acid solution (plotting material) and dispensed into a solution of thrombin and calcium chloride (liquid medium) to form hydrogels via precipitation reaction. Thrombin acts as an enzyme which catalyses the polymerisation of fibrinogen to fibrin. Furthermore, the relative mild operation condition of 3D plotting system allows the incorporation of living cells [108] and bioactive molecules such as peptides and growth factors into the process that improve the cell attachment and promote ingrowth of tissues. These

hydrogel scaffolds are promising approaches for a variety of soft tissue engineering applications.

Among the available fabrication techniques, 3D plotting has shown a great potential in manufacturing reproducible design-based complex scaffolds with controlled mechanical properties and pore structures for mimicking human organs. However, the strand surfaces of the 3D plotted scaffolds were too smooth and unfavourable during cell seeding [108]. Thus, a new 3D plotting method assisted by piezoelectric vibration system has been developed to fabricate scaffolds with hierarchical surface structures [109]. These scaffolds have greater surface roughness that improves the initial cell attachment and proliferation.

SFF techniques have successfully manufactured synthetic and natural biodegradable polymer, bioceramic and hydrogel scaffolds. However, concerns arise from the limitations such as difficulty in removal of support powdered particles, the use of toxic organic binders, high processing temperature preclude the use of biological molecules and lack of mechanical strength. The requirements of scaffolds for tissue engineering are complex and tissue specific, regarding to the structure and function. Hence, optimising the scaffolds is essential to make them work in replacing or repairing damaged human tissues.

2.4 Conventional printing technologies

Living cells require a continuous supply of growth factors and removal of waste products. This can be achieved by circulation of culture medium around the cells or by diffusion through the surrounding material. Although hydrogels offer a high diffusion rate of hydrophilic substances, effective diffusion is limited to the micrometer scale and does not yet permit fabrication of cm scale scaffolds. This is why scaffolds for tissue engineering require a porous internal structure to host most cell types. To provide sufficient internal surface area the pore size has to be in the region of 200 – 400 μm to accommodate cell sizes of 10 – 30 μm [110]. This lies within the capability of most conventional printing technologies.

Although conventional printing technologies are mainly used for graphic arts and packaging applications, recently there have been significant developments in the use of conventional inkjet printing for applications in biomaterials and biosensors to directly print proteins, enzymes and living cells [111]. It is a powerful tool for precision patterning and volume manufacture. These developments offer promising possibilities for tissue engineering application. It is surprising that apart from inkjet printing technology, there is no successful attempts of other conventional printing technology are found in the literature, neither flexographic nor screen printing processes. The literatures on application of commercial inkjet printing technology in printing biopolymers to form tissue construct and the effect of process parameters on inkjet droplet formation, deposition and its behaviour on substrate are described.

This section also reviews the previous works in flexographic printing and screen printing regarding the ink transfer during printing. In graphic printing industry, ink transfer is measured by using optical methods. The two common parameters used are tone gain and solid ink density. Tone gain is a measure of the increase of ink laid down compared to the amount required whilst solid ink density is a numerical measure of how much complementary light is absorbed (darkness) by a printed solid region. Nevertheless, the ink film thickness (height) is also used as a physical measurement of ink transfer. A more detailed review on screen printing is presented to determine the most appropriate process parameters to investigate in the laboratory screen print trial. An understanding of the screen printing process is required to explain the trends of the results obtained in Chapter 6. This is mainly focused on the effect of process parameters on ink transfer and on fine line reproduction.

2.4.1 Inkjet printing in tissue engineering

Inkjet printing, initially used in the field of electronics and mechanics, has been extended to bioengineering applications. Drop-on-demand (DOD) inkjet printers have been adopted for tissue engineering purposes due to their precise material deposition on a substrate and its capability of patterning aqueous solutions of biomaterials with or without cells into complex 3D structures of varying shape and

thickness [112][113][114][115]. It is a non-contact and non impact process thus eliminating the concern of cross-contamination on surfaces. The inkjet nozzles can fire an ink droplet in a very short time of less than 20 μs, onto a substrate with relatively high accuracy of about 20 – 30 μm. Due to the short time required, cells were shown to survive and remain physiologically and functionally normal after being ejected through the printhead nozzles [115].

The commercial available inkjet printers have been modified to suit the demand of biomaterials, allowing printing of biomaterials onto target substrates with minimal reduction of their bioactivities. Roth et al. [112] have modified a Canon Bubble Jet (BJC-21000) according to the modifications described in previous work [116]. The ink cartridge was purged and rinsed thoroughly with double distilled water and ethanol prior refilling it with acidic collagen solutions. The solutions were maintained at 4°C, above which the gelling occurs, prior to printing onto the substrates to form the cellular patterns. Figure 2.5 shows optical microscope images of printed collagen patterns prior to cell seeding, where the crystallised patterns were formed by the residual salt in the solvent. These patterns were rehydrated and seeded with smooth muscle cells (SMCs). They demonstrated that the modified inkjet printer could be used for depositing protein solutions in order to create features in the size range of 300 – 400 μm. For the application of thermal inkjet printer, there are concerns of damaging the functions of protein as the ink was heated to a high temperature of 200 – 300°C for a few microseconds for firing. However, the results showed that the cells could still attach, proliferate and remain viable in the printed collagen patterns, Figure 2.6. This concluded that the elevated temperature caused limited denaturisation of proteins.

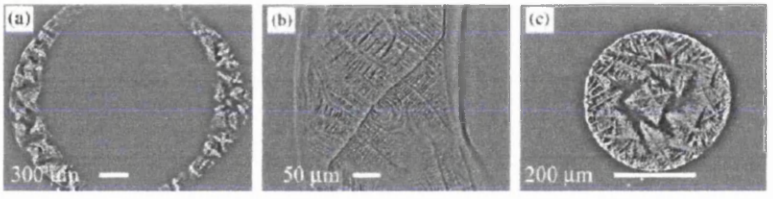

Figure 2.5: Light microscopy images of a ring pattern after seeding with SMCs at a density of 30,000 cells 4 days into culture (a) 200x image, (b) 40x image, (c) printed ring pattern after 4 h of high-density seeding (75,000 cells) with SMCs [112]

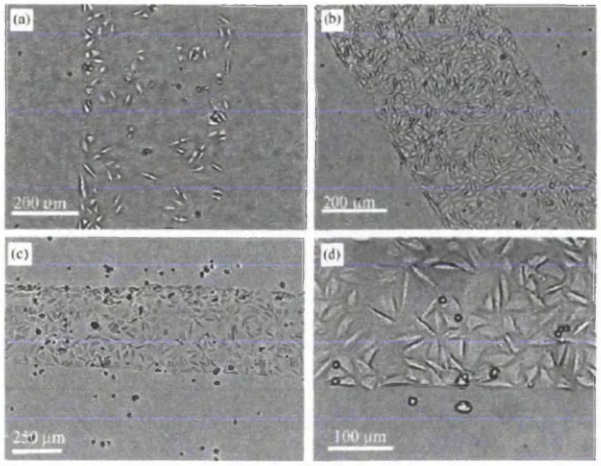

Figure 2.6: 40x magnification optical microscope images of a printed collagen line pattern seeded with SMC's after culture times of (a) 1 day, and (b) 4 days and (c) a 500 μm wide line 4 h after high-density seeding, but prior media rinse to remove unattached cells. The morphology of the patterned SMCs is demonstrated by (d) which is a 200x image of the line shown in (c) [112]

Xu et al. [113] successfully printed two different kinds of mammalian cells with good viability (>90%) using a modified Hewlett Packard (HP 550C) printer onto biopapers (soy agar and collagen hydrogels coated substrates) under low power conditions. However, there were potential limitations in this approach. Most cells, particularly neurons are relatively delicate and more sensitive to heat and mechanical stress. They are not likely to survive through the harsh nozzle firing at very high temperature of above 300°C and shear force. Besides, the diameter of nozzle is not much bigger than a typical cell size of 20 – 30 μm. This may result in a high incidence of nozzle clogging during printing.

Boland et al. [117] added a z-axis module into the previous modified printer which was electronically controlled by an elevator chamber using a stepper motor, Figure 2.7. The chamber was filled with uncross-linked hydrogels (2% agarose solution with alginate solution on top), whereas the cartridge was filled with 0.25 M calcium chloride used as a cross-linker. This cross-link was printed layer-by-layer onto the liquid alginate/gelatine solutions, causing instantaneous gelling of the alginate

solutions to form 3D scaffolds. The calcium ions cross-linked negatively charged alginic acid chains. After each printed layer, the elevator rod was lowered and the uncrosslinked hydrogel would cover the printed areas. This process was repeated until the rod reached the bottom of the chamber where a printed hydrogel structure was found on the stage. Boland et al. suggested that many layers of cells and hydrogels can be printed into 3D structures using a fast gelling hydrogel system. Several acellular structures, including tubes, branched tubes, hollow cones and capillaries were printed. The droplets printed were hollow with no hydrogel material. This might be due to the surface gelling mechanism where the surface of the drop gelled very fast, thus forming a capsule or shell. Endothelial cells were shown to survive during printing and attach to the inside of printed hydrogel pores.

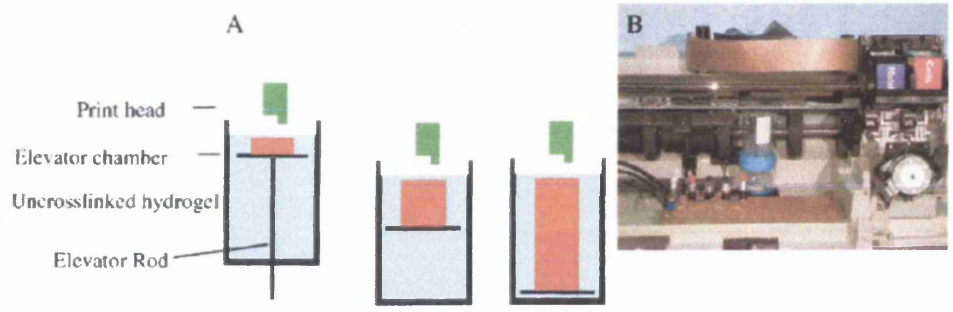

Figure 2.7: (A) Schematic view of the moving platform inside the chamber. (B) Photograph of the chamber under a modified HP DeskJet. The chamber is removable and can be installed under many different printers [117]

Piezoelectric inkjet printers were also modified for biomaterial and cell printing due to their wide applications in ceramics and polymer printing. Commercial piezo-printers use a more viscous ink which prevents the ink from backflowing. However, this requires more power (20 – 100 W) and higher vibration frequencies (up to 30 kHz) that can break and damage the cell membranes [118]. Saunders et al. [119] studied the cell behaviour when exposed to mechanical and fluid stresses during piezoelectric inkjet printing suspensions of human fibroblast cells. The stresses applied on the cells

could be altered by manipulating the amplitude and rise time of the electrical pulse. When the pulse amplitude increased from 40 V to 80 V, the cell survival rates dropped from 98% to 94%, indicating an insignificant influence. The rise time of the pulse had no influence on cell survivability. However, the cell suspensions were unstable after about 20 minute printing where some cells started to agglomerate or sediment, and thus affecting the printing performance. In their previous works [120], they showed that increasing the droplet velocity would cause a reduction in the cell survival and proliferation rates but both primary mammalian cells grew to confluence after printing.

2.4.2 Inkjet: Drop formation, deposition and behaviours on substrates

The characteristic of the inkjet printing process is to print uniform dots, but for printing 3D bioscaffolds which require good porosity and interconnectivity, lines with good dot-to-dot continuity are necessary to build the 3D shape and size. The literature points out some important challenges faced in inkjet applications on polymer deposition in terms of ink formulation, the design of the printhead and printer, substrate choice and preparation, and also control of solvent evaporation [121][122]. In addition, de Gans et al. [123] have discussed about the potential and limitations of inkjet printing polymer regarding the molecular weight and concentration of polymer and the solvent properties. The results showed that many common solvents could be used as the carrier liquid, but the solvent volatility was a concern. Increasing the polymer molecular weight and concentration decreased the printability significantly due to the elastic stresses imposed in the elongational flow in the micropipette nozzle of 70 μm in diameter. This was also affected by the solvent shear viscosity and elasticity, particularly at high molecular weights. They suggested a linear relation between the voltage pulse amplitude and ink viscosity which was a mixture of glycerol and water. Linear relations between voltage and droplet velocity and droplet velocity and viscosity were shown in earlier papers [124][125].

Tekin et al. [126] studied the optimisation of inkjet process parameters to reproduce homogenous polymer films (polystyrene in various solvents) and improve the quality

of printed films, mainly focused on the solvent mass ratio, printhead velocity, dot spacing and printing methodology. First of all, choosing an appropriate combination of solvent and substrate is important to the success of inkjet printing of polymer films. A small contact angle is more favourable in printing structures of length scale greater than the droplet diameter and vice versa, otherwise dewetting may occur when curing and resulting in an inhomogeneous film. 2% polystyrene solutions were printed at voltages of 95 – 120 V and pulse widths of 45 – 67 μs, with dot spacing between 60 – 140 μm. The films printed based on one single solvent suffered from ring formation, also called the Marangoni effect, due to the pinning of the droplet contact line and the increased evaporation at the edges. Deegan et al. explained this effect in their previous works [127][128]. Marangoni effect occurs after evaporation of a printed solution droplet where most of the solute is deposited as a ring that marks the original contact line. This could be reduced by using either a lower vapour pressure solvent or solvent mixtures consisting of a low- and a high-boiling solvent. Also, the film quality was decreased when the printhead velocity increased [126].

In a recent study of Yun et al. [129], the construction of three-dimensional micropatterned polymer structures with good shape definition was shown feasible by using a piezoelectric, DOD inkjet printer. The polymer used was PVA (polyvinly alcohol) with water and DMSO (dimethyl sulfoxide) as the ink solvent. A variety of polymer inkjet variables were studied and optimised, including firing voltage, temperature, solvent composition, viscosity and surface tension. The appropriate range of PVA ink concentrations for inkjet printing was between 3 – 5 g/dL. The optimal parameter settings of the printer were jetting voltage of 20 – 30 V and firing frequency of 3 kHz. As shown in Figure 2.8, the Marangoni effect was observed in the printed dots where the dot (45 – 50 μm in diameter) had a shape like volcano. However, this effect was insignificant in the printed fine lines of width and height of 160 – 200 μm and 0.25 – 0.30 μm respectively.

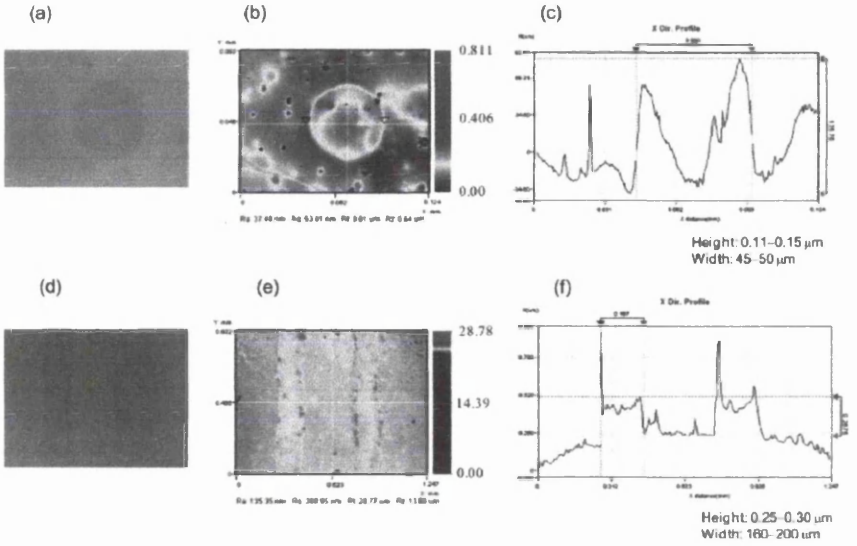

Figure 2.8: Optical photographs and cross-sectional profiles of an inkjet printed droplet (a-c) and inkjet printed lines (d-f) under inkjet conditions: PVA concentration 3 g/dL in water/DMSO mixture (4/1 v/v), firing voltage 22 V, temperature 32°C [129]

The characteristics of the ejected droplet (i.e. shape and size) are crucial in forming 3D structures as it affects printing resolution, precision, and accuracy. Droplet splash must be avoided. The jetting frequency must be coordinated with the print-head sweep velocity. During the formation of ink droplet, the liquid experiences high shear strain rate (usually of the order of about 10^4 s^{-1}), similar to that occurs during droplet impact on a surface. This would subject the polymer chains to high stresses especially at the middle of the chain that ruptured the chains with a reduction of the average size of the molecular chains [130]. This effect is known as chain scissioning. Thus, the viscosity of the polymer solution would decrease and so reduce the droplet size. Droplet size is a function of molecular weight and the polymer viscosity. For cells in suspension subject to high stresses, the deformation and response of cells is still unclear. The UMIST researchers reported that droplets should not be smaller than 10 µm in diameter which is about 1 picolitre in volume; else their behaviour after ejection from the nozzle is not predictable enough for reliable printing. To summarise, the factors affecting the quality of the final pattern are divided into three groups: ink, printer and substrate as tabulated in Table 2.3.

Ink	Printer	Substrate
Viscosity	Nozzle size	Surface energy
Concentration	Droplet dimensions	Porosity
Molecular weight	Dot spacing	Absorbency
Composition	Printhead lateral resolution	Hydrophilicity
Surface tension	Firing frequency	
Temperature	Firing voltage amplitude	
	Temperature	

Table 2.3: Factors affecting quality of piezo-inkjet printing patterns

2.4.3 Flexographic printing: Ink transfer

Ink transfer in the flexographic printing process can be seen as a three stage process, inking chamber to anilox, anilox to plate and plate to substrate. There are three main parameters in choosing the appropriate anilox rolls: screen ruling, volume and depth-to-open ratio. The screen ruling is the number of available cells per roll length with a unit of lpi (lines per inch). The higher the resolution of an anilox roll, the smaller and closer the cells packed. For fine line work, high screen rulings are preferred where as low screen rulings are used in solids to maximise the ink deposit. The cell volume is quantified in bcm (billion cubic microns per square inch of anilox area) and determines the ink quantity carried by the cells. The depth-to-open ratio (also known as cell ratio) is a measure of the release characteristics of the cell. Insufficient inking will occur if the cell is not deep enough, whereas if the cell is too deep, the ink will dry at the bottom.

Lindholm and Ström [131] assessed the transfer of water-based inks on a flexographic printing press using an infrared camera. Three cyan inks were used at viscosities 39, 34 and 49 seconds with Zahn 4 printed on an uncoated paper. The print speed was varied between 1.3 and 3.3 ms^{-1}. A banded anilox was used with a screen ruling of

80l/cm with various depths and volumes, 25 μm 8 cm^3/m^2, 35 μm 10 cm^3/m^2 and 45 μm 12 cm^3/m^2 respectively. The results showed that when the ink viscosity increased, the ink transfer from anilox to plate decreased. In comparison, the ink viscosity had less effect on the ink transfer from plate to substrate, particularly at low anilox volume. Approximately 70 – 80% of the ink was transferred from the plate to the substrate. The volume of the anilox was determined to have significant effect on the amount of ink on the plate, with a non-linear relationship of increasing ink transfer with increasing anilox volume. The variation in print speed had no effect on the transfer from the anilox to the plate.

The relationship between anilox rollers and print quality was studied by Castellanos and Haak [132] using four anilox rollers of screen rulings 400, 700, 900 and 1600 lpi and volumes of 4.76, 2.5, 1.48 and 1.84 bcm on a production press. The dot gain was decreased when using an anilox roll with high screen ruling and low volume, so was the solid ink density. Increasing the anilox screen ruling also improved the definition in other printed images such as lines, text, image highlights and shadows which were examined visually.

Besides, the effect of printing pressures on the printed ink film in terms of uniformity was assessed by Laksin and Parris [133] using IGT F1 printability tester. Cationic UV ink was printed on both coated paperboard and film. The printing pressures between anilox and plate (anilox force) and between plate and substrate (print force) were varied at three levels from 100 to 500 N. An increase in the anilox force had a small effect on the optical density, gloss or ink lay for the film substrate. However, increasing the printing pressure caused a strong negative effect on the uniformity of the printed image. Bohan et al. [134] demonstrated that the solid ink density decreased with increasing anilox force. The effect of increasing the pressure between plate and impression cylinder was negligible in the solid ink density but the tone gain was increased due to the plate deformation during printing. Similar trend was shown by Galton and Rosenberger [135].

Bould et al. [136] concluded that increasing printing pressures had a greater effect on dot gain at low engagements. For higher printing pressures, the dot gain was not further increased as there was a finite volume of ink carried on the plate. In the study

of Walker and Fetsko [137], the ink transfer from plate to substrate increased when the print pressure was increased. The increase was not proportional to the increase in pressure where the rate of change in ink transfer with pressure was found to be lower at high pressures. Besides, the variation in printing speed and ink viscosity also affected the ink transfer. An increase in ink transfer was observed when print speed was decreased because the increased contact or dwell time between the plate and substrate allowed increased absorption and longer spreading time [137][138]. Overall, the effect of printing speed is relatively small comparing to other variables [139]. Lower ink viscosity increased the ink transfer and more ink was required for full ink coverage.

This section evaluates previous experimental investigations carried out on the flexographic printing process, especially the effect of variables such as properties of anilox roll, printing pressures, printing speed and ink viscosity on the ink release and transfer from anilox to plate and plate to substrate. This could be related to the variations in the line width and film thickness observed by manipulating the printing pressures in the preliminary printing trial presented in Chapter 5. Overall, it could be summarised that:

- An increase in the anilox volume gives greater ink transfer and the relationship between ink transfer and anilox volume is non-linear.
- The ink released from the anilox roll decreased when the ink viscosity decreased.
- Both printing pressures and speeds affect the ink transfer from the plate to the substrate

2.4.4 Screen printing: Ink transfer and fine line reproduction

Many parameters affect the screen printing process, Table 2.4. The work presented here concentrates on the experiments conducted in graphic screen printing industry to show the effect of process parameters on ink transfer and fine line reproduction in screen printing.

Printing Process	**Substrate**	**Screen**	**Squeegee**	**Ink**
Squeegee pressure	Cleanliness	Mesh count	Squeegee material	Viscosity
Squeegee angle	Surface energy	Thread diameter	Shape of edge	Solid content
Print speed	Surface roughness	Mesh opening	Squeegee backing or stiffening	Particle size
Snap-off distance	Planarity	Mesh height		Shear strength
Print stroke length	Geometry size	Mesh material		Homogeneity
Paste quantity on screen		Emulsion thickness		Adhesion
Flowcoater height		Stencil roughness		Stability and consistency
Flowcoater speed		Stencil type		Surface tension
		Screen tension		

Table 2.4: Parameter settings in screen printing process

The mesh has the most significant parameter affect on ink film thickness [140]. Changing the size of mesh opening affects the ink transfer as the larger mesh opening carries more ink and thus increases the ink transfer. A mesh with thicker threads and

larger open area gives a greater ink film thickness. An increase in the stencil thickness also increases the ink film thickness.

An investigation into ink film thickness was conducted by Holh and Hunt [141] using a UV-cured ink and nine meshes of various mesh counts. The results showed a decrease in ink film thickness with increasing mesh counts up to 250 threads per inch. Above that, the ink film thickness decreased insignificantly. The variations in mesh counts up to 250 threads per inch largely changed the thread diameter of the meshes, whereas there was only a small change in the thread diameter at higher mesh counts. The effect of mesh volume or height on ink film thickness was not studied which would give a better analysis of the results.

Jewell et al. [142] used an orthogonal array to examine the effect of flat bed screen printing parameters on ink film thickness using a constant mesh ruling. The parameters studied were ink type, stencil type, mesh tension, squeegee type, snap-off gap, squeegee angle, squeegee speed and squeegee pressure. Seven types of substrates were printed. Of all the parameters the ink type was the most influential in determining the ink film thickness, the conventional UV ink produced about 12 μm and water based UV ink produced around 6 μm. The effect of squeegee angle was shown to be the dominant on press parameter, the ink film thickness increased when squeegee was brought closer to the horizontal. Other parameters that had a relatively small effect on ink film thickness were:-

- Stencil type: Increasing stencil thickness increased the ink film thickness, and the capillary film produced the thickest ink film.
- Mesh tension: Increasing mesh tension increased the ink deposit and thus the ink film thickness.
- Squeegee type: Increasing squeegee hardness from soft to hard decreased the solid density which resulted in a decrease in ink film thickness. However, medium squeegee produced the thickest ink film. This might be due to the difference between the squeegee tip profiles or interactions between the squeegee parameters.
- Snap-off gap: Increasing the snap-off gap increased the ink deposit as the screen tension force was higher at larger gap.

- Squeegee speed: Increasing the squeegee speed increased the ink transfer on smoother substrates.

For some measurements, the edge of the ink film showed a raised area which was known as 'crowning'. This was attributed to the ink release mechanism from the screen supported by the ink transfer theory postulated by Messerschmitt (reviewed by Fox) [143]. Another feature observed was mesh marking where the ink film was rippled.

Barden [144] carried out an experimental investigation to study the effect of screen printing parameters on ink film thickness and fine line reproduction. There were eight process parameters involved: ink type, stencil type, mesh tension, squeegee hardness, snap-off gap, squeegee angle, squeegee speed and squeegee pressure. This study determined that again the ink type was the most significant parameter, followed by squeegee angle, squeegee type and the least effect was squeegee speed and squeegee pressure. The results showed similar trend as those of Jewell et al. [142] where more ink transfer was observed when:

- the squeegee angles were closer to the horizontal plane,
- the soft squeegees were used when compared to those hard ones, and
- both squeegee speed and squeegee pressure were increased but the ink transfer was less significant than changing the angle.

Barden et al. [145] also conducted a full factorial experiment to further examine the effect of three squeegee parameters on fine line reproduction, namely squeegee type, pressure and angle. The difference between two line measurement methods was examined; an image processing based system and a surface profiling based system. A solvent based ink was used and each parameter was examined at three levels. The width of the printed lines was measured. The squeegee angle and type were found to have the greatest effect, producing wider lines when squeegee angles closer to the horizontal and softer squeegees were used. The effect of squeegee type was more significant on the line film thickness comparing to line width. When the squeegee pressure increased, there was a small increase in the average line width. This was

caused by the transfer of insufficient ink when the printing pressure was not enough to create a good contact between the screen and substrate, resulting in lines of poor quality. At printing pressure of 2.5 bar, the printed lines were found to be incomplete whilst the lines printed at 4.5 bar had good edge characteristics. The results were in line with previous works [142][143]. All measured lines were narrower than lines on the film. Both analysis tools gave the same pattern of results. The interactions between parameters were insignificant, apart from the squeegee angle had a small effect on the effect of pressure.

Pan [146] studied the effect of four press parameters which were snap-off gap, squeegee hardness, squeegee speed and squeegee pressure on the screen printing process using orthogonal array techniques. The test image consisted of parallel lines of equal width and spacing: 0.125, 0.2 and 0.25 mm, with two line directions: parallel and perpendicular to the print direction. The lines were examined in terms of space width, the distance between two adjacent lines. This study showed that different line orientations affected the line quality which could not be quantified. There were many connections between lines when printed perpendicular to squeegee direction. Analysis of variance (ANOVA) was used to determine the statistically significant parameters. Squeegee hardness and squeegee speed were found to have significant effect with a 95% confidence level. Squeegee hardness had the most significant effect where hard squeegees were considered the best for fine pitch printing. Increasing the squeegee speed increased the space width deviation, especially for lines parallel to the print direction. Snap-off gap and squeegee pressure had no significant effect.

Bertrams et al. [147] examined and discussed the influence of several parameters: ink, printer and printer settings, substrate surface conditions, screen and dry and sinter conditions on the achievable line resolution (in terms of line width). The results concluded that the ink and screen affected the line definition more significant than the press settings. The influence of ink was studied from the start of the squeegee movement to the drying of ink on the substrate. During a print stoke, the movement of squeegee forces the ink through the meshes onto the substrate. In order to ensure the inks fill and flow into and through the mesh, the ink viscosity has to be low at shear rates between 100 – 1000 s^{-1}, preferably 50 – 70 Pa.s at a shear rate of 100 s^{-1}. This

also enables a good separation of the ink from the mesh. During the ink transfer, the adhesive forces between the ink and screen, the cohesive forces within the ink, and the adhesive forces between the ink and substrate primarily dictate the amount of ink deposited on the substrate. After the ink transfer, the surface tension and gravity influence the ink causing ink spreading (low shear rates of about 0.1 s^{-1}) which affects the film thickness and width of printed lines. Betrams et al. used spreading coefficient, S to explain the phenomenon of ink spreading on the substrate after printing. This expression defines the work required to separate the liquid from the substrate and is given as:

$$S = \gamma_S - \gamma_L - \gamma_{SL} \tag{2.1}$$

where γ_L is the liquid surface tension, γ_S is the surface tension of substrate and γ_{SL} is the interfacial tension between substrate and liquid.

Liang et al. [148] studied the effect of surface energies on line resolution of screen printing, using 3 types of inks printed on 6 types of substrates. The test image comprised of a series of line groups of equal line width and gap ranging from 100 μm to 250 μm. The ability of ink to wet the substrate is important in screen printing. The ink has to flow to cover the gaps caused by the mesh so that mesh marks will not occur, and also to remove the surface imperfections. However, the ink should not run too freely as the line will spread increasing the line width. The excessive line expansion will cause connections between two parallel lines printed with small spacing, and thus decreasing the line resolution. The wettability effect of ink on substrate was decreased by reducing the surface energies of substrates. The reduction in wettability minimised the spreading of inks and improved the printable line resolution. This means that a liquid of low surface energy will wet a substrate of a high surface energy. For high surface energy substrates where wetting occurs readily, the line resolution can be improved by using high thixotropic inks. On the other hand, the effect of wettability is dominant on resolution of screen printing for low surface energy polymer substrates. High line resolutions can still be achieved with low viscosity inks, only if the critical surface tension of a substrate is lower than the surface energy of ink.

2.5 Methods to characterise Bioscaffolding materials

This section reviews the previous experimental works performed to characterise the rheological properties of gelatine and different approaches used to accurately locate the gel point of polymers. The gel point determined for gelatine was used to compare with the gel points obtained in the results presented in Chapter 4.

2.5.1 Rheological Characterisation of Gelatine

Rheology, especially the viscosity measurements and determination of gel point, is a very important criterion in the processing of network-forming polymers. Appropriate rheological properties are required for successful printing. These are related to their chemical characteristics. The gel strength, viscosity, setting behaviour and melting point of gelatine depends on their molecular weight distribution and the amino acid composition [149]. As gelatine is the denatured form of collagen, the source and type of the collagen will influence the properties of the resultant gelatines. This is because of the variations in the amino acid contents and the sequence for different sources.

The viscosity of gelatine is critical in process control to ensure proper handling in the industrial processes. Wulansari et al. [150] have studied the flow behaviour of the gelatine solutions at a temperature of 50°C using the approach frequently applied to polysaccharides. The viscosity of the gelatine solutions is shear rate dependence over a wide range of concentrations. The gelatine solutions were practically Newtonian over the shear rate range at 50°C. Previous viscosity measurements performed by Leuenberger et al. [151] showed that gelatine solutions up to a concentration of 10% exhibited Newtonian behaviour over shear rates of 10 s^{-1} to 350 s^{-1}. It has been reported that a gelatine solution at rest with a concentration of a few percent in protein, sets when the temperature is lowered below 30°C where the coil-helix transition takes place [152][153]. Above 40°C, the gelatine chains are in a random coil conformation in the solution [154][155]. Additionally, when the solutions are sheared at high shear rates, the coils do not have time to entangle before the molecules separate in the shear field. Non-newtonian regime was observed when concentration C, is greater than the critical

concentration C* and at low shear rate [156][157]. This is typically 0.4 – 1.0% (w/w) for commercial mammalian gelatines. At higher concentration where $c \geq 1.0\%$ (w/w), the helix growth induces chain association and three-dimensional network formation [153]. Thus, the flow behaviour of gelatine solution can be described as a function of concentration and temperature, corresponding to the shear rate imposed.

Gel is defined as a class of systems which show solid-like properties in the presence of excess solvent by Lapasin and Pricl [158]. The solid-like behaviour is known as an essential characteristic of a gel [159]. Gelation is principally motivated by the formation of a three-dimensional network in the fluid which extends throughout the entire sample effectively. There have been many experimental works carried out to study the structural and mechanical behaviour of thermoreversible gels during the polymerisation from the polypeptide gelatine in both micro- and macroscopic scales [152][153][160]. Most studies have focused on the gelation process during heating or cooling in both pre-gel and post-gel regions. Different experimental approaches such as polarimetry, electron microscopy and rheology have been used to monitor and provide complementary view of the gelation mechanism, mostly based on the development of the gel network and gel structure. The review by te Nijenhuis [161] summarises much of these endeavours. Additional techniques (small angle X-ray scattering and neutron scattering, optical rotation and differential scanning calorimetry) and the combination with thermodynamics and network models have shown to further deepen the insight into the cross-linking process and the gel structure.

Gelatine dissolves in warm water above 40°C and exists as flexible random coils in solution. When the solution is cooled to below ambient temperature, the conformational coil-helix transition (gelation) occurs with reformation of the triple helical junction zones to produce a transparent physical gel, Figure 2.9. The melting and gelling temperature of gelatine have been found to correlate with the proportion of imino acids proline and hydroxyproline in the parent collagen. The proline content plays an important role in the stability of gelatine gels, since it promotes formation of the polyproline II helix. This in turn determines the form of the tropocollagen trimer. Zandi et al. [162] have studied the early stages of gelation in gelatine solution observed in the temperature range of 30 – 50°C. The results showed that the formation of a

reversible gel is affected by the intra-molecular foldings and inter-molecular interactions which are pH and temperature dependent, corresponding to the mobility of the amino acids.

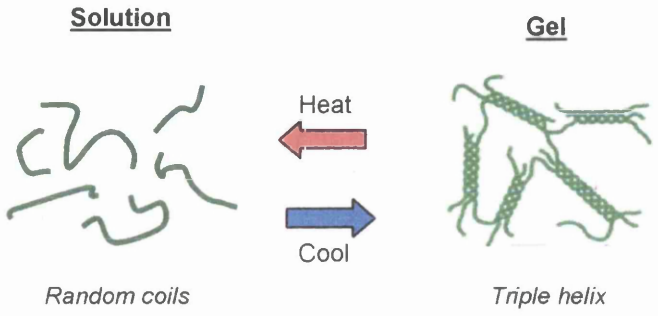

Figure 2.9: Gelation process of gelatine (adapted from www.fao.org)

2.5.2 Approaches to determine gel point

For polymer solutions, the gel point is defined as the point when the first macromolecule of infinite dimensions appears and determines the liquid to solid transition [163]. The gel point determination is important in polymer processing. For example, the polymer has to be shaped or deposited on the substrate while the polymer is still able to flow. However, it is not a simple procedure to determine the exact point at which the bulk behaviour of a material passes from that of a liquid to a gel.

The classical theory of gelation was developed by Flory [164][165] and Stockmayer [166] where the critical degree of cross-linking, p_c was predicted as a function of cross-link functionality and stoichiometric ratio. This suggested that the gel point can be detected by monitoring the degree of cross-linking until the theoretical value of p_c is achieved. This physical method, based on the extrapolation, can only be used to 'estimate' the gel point due to the errors arise in measurements of the degree of cross-linking. Rheological methods have been developed later to determine the gel point accurately.

The simplest rheological method to determine gel point is by measuring the diverging steady shear viscosity when the gel point is approached. This method has some significant disadvantages that result in inaccuracies. When approaching the gel point, the sample behaviour is shear thinning with increasing viscosity and the eventual destruction of the fragile network structure by shear causes a delay in gelation. Errors have been introduced in the extrapolation to infinite viscosity. Additionally, the infinite viscosity can also occur due to other phenomena such as glass transition and phase separation.

Another method proposed by Tung and Dynes [148] suggested that the gel point occurs at the point of crossover of the storage modulus (G') and loss modulus (G'') in small-amplitude oscillatory shear experiments. Winter [168] noted that this definition is not universal and is only valid for stoichiometrically balanced systems or those with excess cross-linkers. Moreover, the crossover of G' and G'' can be readily observed in the liquid phase of many polymer fluids not containing an extended network [169] and also in uncross-linked polymers due to the presence of entanglements [170].

Winter and Chambon [171] have developed a more general rheological method which allows precise detection of gel point from dynamic oscillatory measurements at several frequencies. At the instant a polymer gels, the G' and G'' should display the same frequency dependence. The gel point is thus identified at the point when the loss tangent, tan δ is independent of frequency and is given by:

$$\tan\delta(\omega) = \frac{G'(\omega)}{G''(\omega)} \tag{2.2}$$

and δ can be represented by equation below

$$\delta = \frac{\alpha\pi}{2} \tag{2.3}$$

where α is defined as the stress relaxation exponent, $0 \leq \alpha \leq 1$.

For an ideal system, the cross-linking occurs only at the ends of the polymer molecules, the initial molecular weight of the polymer is such that the entanglement

are excluded, only intermolecular cross-linking occurs, and the cross-links formed are permanent. Also, the temperature at which the experiments are performed should be below the glass transition temperature; otherwise, vitrification may occur.

This gel point criterion developed by Winter and Chambon has been applied to various types of polymer gels. Scanlon and Winter [172] investigated the end-linked polydimethylsiloxane (PDMS) polymers with various stoichiometry, chain length and concentration. The values of relaxation exponent were found to fall in the range between 0.19 and 0.92. A prepolymer of low molecular weight produced critical gels with α values range between 0.4 and 0.7, while lower α values ranging between 0.2 and 0.4 for high molecular weight prepolymer (above the entanglement molecular weight), both depending on the stoichiometry.

Chambon et al. [173] have studied the cross-linking process of polyurethanes (PU) by an end-linking reaction at a constant temperature of 30°C by monitoring the evolution of G' and G'' moduli. They suggested that for stoichiometrically balanced end-linking polymers with different molecular weight between cross-link points, the relaxation exponent is equal to 0.5 at gel point. However, the work done by Winter et al. [174] on the same PU system but with imbalanced stoichiometry showed that the relaxation exponent was greater than 0.5 where $\alpha \approx 0.67$. Similarly to the PU system, rheological measurements were performed on PDMS gels. The stoichiometrically balanced PDMS exhibited an exponent value of $\alpha = 0.5$ whereas a higher exponent value, $\alpha > 0.5$ was measured on PDMS with imbalanced stoichiometry (cross-linker deficiency) [175].

In the work of Michon et al. [176], the gelling behaviour of thermoreversible gelatine gels was studied at various concentrations. A limited frequency range of 0.5 to 2.5 rad/s was applied to the system. The polymer formed a network structure through low-energy physical interactions between polymer segments without any cross-linking agents. The values of exponent obtained were generally varied from 0.60 to 0.72 but could be as low as 0.20 – 0.30 in some experimental conditions. Power and Rodd [177] investigated a physical gel prepared from borate cross-linked hydroxypropylguar (HPG). The frequency independent relaxation exponents were determined in the range between 0.14 and 0.5, depending on the concentration of both

the HPG and borate ions. At the gel transition, a maximum in the loss modulus was observed.

However, this technique has limitations which are mainly related to the total experimental time required for performing the viscoelastic measurements of the gelling system over a reasonable range of frequencies, particularly at low frequencies. Therefore, a more reliable new technique using Fourier transform mechanical spectroscopy (FTMS) has been developed by Holly et al. [178] to monitor the changes of the viscoelastic properties simultaneously at several frequencies instead of consecutively as in a frequency sweep. This method has effectively reduced the experimental time required for the rheological measurements where the gel point can be detected with just one multiwave frequency sweep test using FTMS. It is advantageous particularly for testing polymers with transient structure that requires speedy testing because its structure may change during the test. In addition, the data obtained from the FTMS method agree well with conventional measurements on stable polymeric materials, but with increased accuracies. FTMS technique is further described in Chapter 3.

In and Prudhomme [179] have used FTMS method to characterise the gelation behaviour of zirconium alkoxide ceramic gels. The gelation times were varied from minutes to months and were controlled by varying the concentrations of zirconium propoxide and acetylacetone, and hydrolysis with water. Kim et al. [180] have conducted experiments using FTMS technique to study the gelling of tetraethylorthosilane (TEOS) solution in the presence of silane coupling agent vinyltriethoxysilane (VTES) with various molar ratios at different temperatures up to 65°C. At relatively high temperatures, the gel point was scattered due to the low frequency noise caused by thermal fluctuations. In this case, a statistical method was used to predict the gel point unambiguously, which was shown to reduce significantly with temperature. The gel exponent was ranged from 0.561 to 0.771, depending on the TSEO/VTES composition.

Nevertheless, the gelling behaviour of gelatine (bovine) was studied by Karl et al. [181] based on FTMS method to identify the gel point. Results showed that the gelation time obtained in the range ca. $10^2 - 10^4$ s, depending on both gelatine concentrations

and temperature. The values of the relaxation exponent were found to be independent of temperature and concentration, with a value of $\alpha \approx 0.69$. They suggested that the appearance of low α values was attributable to the inappropriate rheometrical procedures (rapid gelling conditions).

The self assembly of type I collagen has been studied extensively both in vivo [182] and in vitro [183] which was focused on kinetic or structural details with little attempt to analyse the self-assembly process using concepts from physics of polymers. Forgacs et al. [184] studied and analysed the mechanism of gelation in the process of type I collagen self-assembly in terms of percolation theory [185]. Percolation theory was used to predict the power law behaviour for the macroscopic physical properties such as the elastic modulus or viscosity in the vicinity of the gel point. The viscoelastic properties (G' and G'') were measured as a function of time using rotating disk rheometer. Five frequencies were applied, ranging from 0.2 – 6.9 rad/s. They demonstrated that the gelation of type I collagen was a second order phase transition with the critical exponent $\alpha = 0.7$ and a frequency independent critical loss tangent at gel point, as predicted by percolation theory. The gel point of collagen (C = 1.7 mg/ml) occurred at a gelation time of 605 s. The gelation process of collagen was observed to be temperature dependence where a small temperature decrease of 2°C (from 12 to 10°C) caused a delay in gelation of about 5 minutes. This was half of the gelation time required when the temperature was 12°C. The results shown in this study agree well with earlier studies [186].

2.6 Closure

This chapter reviewed previous experimental work on characteristic of biopolymers (collagen and gelatine) and techniques used to fabricate bioscaffolds for tissue engineering purposes. Biomaterials offer significant advantages over chemical techniques for scaffolds in terms of reduced post processing and the better compatibility with live cells. The chemical residues which are difficult to remove can be poisonous to living cells (such as traces of chloroform). It could be said that cells survive on chemical scaffold, whereas they grow on biopolymer scaffold. Both gelatine and collagen are lead candidates in bioscaffolding, however gelatine appears to be a better choice of biopolymer over collagen for volume production of bioscaffolds by conventional printing processes. This is due to the consistency of the properties of gelatine. Collagen suffers from inconsistency according to the different source of material and it is only available in low concentrations where higher concentration of material is required in this investigation. Also, collagen carries animal diseases such as CJD which would transmit to human and cause deaths. Thus, it could be concluded in this literature review that gelatine is more suitable in industrial production of bioscaffolds.

The application of conventional printing technologies on bioscaffolding for regenerative medicines opens a new direction in tissue engineering offering the potential for volume manufacture of biopolymer scaffolds. There is a gap in the literature review where there is no publications on printing biopolymers using neither flexographic nor screen printing technologies, although some researchers had inkjet printed bioscaffolds. This requires further research and development which is the main thrust of this thesis. The effect of process parameters in printing processes on ink transfer and fine line reproduction was presented. Previous work on rheological characterisation of gelatine and approaches of gel point determination were described.

The main conclusions from this review were

- In order to be able to volume manufacture the bioscaffolds, the properties of the scaffolding material has to be consistent and reproducible. Thus, gelatine appears to be a better choice of biopolymer over collagen for volume production of

scaffolds using conventional printing processes. The rheological properties of the biopolymers that required investigation were the viscosity, viscoelasticity, gelation temperature and gel point.

- The review into conventional printing process in bioscaffold fabrication showed its potential in tissue engineering applications. Thus, it is necessary to carry out preliminary printing trials (inkjet, flexography and screen printing) to print biopolymer inks (aqueous gelatine solutions) in order to establish the best suited printing process that produces good quality lines for further investigation by conducting a laboratory print trial.
- The screen printing process parameters that required investigation were the squeegee parameters, the ink and the screen, as these were the most significant process parameters. Due to the fact that the biopolymer inks used are temperature sensitive, the temperature of the surroundings is an important factor too.
- The review into ink transfer of screen printing process showed that there were three stages involved: ink flow and fill into the screen, ink is forced out of the screen by the squeegee and ink spreading after the ink was deposited onto the substrate.

2.7 References

[1] Cheung H. Y., Lau K. T., Lu T. P., Hui D. (2007) A critical review on polymer-based bio-engineered materials for scaffold development. Composites Part B: Engineering 38 (3): 291-300.

[2] Frenkel S. R., Di Cesare P. E. (2004) Scaffolds for Articular Cartilage Repair. Ann. Biomed. Eng. 32 (1): 26-34.

[3] Yasumitsu M., Akira O. (1998) Diversity and function of collagen molecules. J. Connect Tissue 30 (4): 301-305.

[4] Gelse K., Poschl E., Aigner T. (2003) Collagens – structure, function, and biosynthesis. Advanced Drug Delivery Rev. 55 (12): 1531-1546.

[5] Pachence J. M. (1996) Collagen based devices for soft tissue repair. J. Biomed. Mater. Res. 33: 35-40.

[6] Kim B. S., Baez C. E., Atala A. (2000) Biomaterials for tissue engineering. World J. Urol. 18: 2-9.

[7] Yarlagadda P. K., Chandrasekharan M., Shyan J. Y. (2005) Recent advances and current developments in tissue scaffolding. Biomed. Mater. Eng. 15 (3): 159-177.

[8] Weadock K., Olsen R. M., Silver F. H. (1983-84) Evaluation of collagen cross-linking techniques. Biomater. Med. Dev. Art. Org. 11(4): 293-318.

[9] Thompson J. I., Czernuszka J. T. (1995) The effect of two types of cross-linking on some mechanical properties of collagen. Biomed. Mater. Eng. 5: 37-48.

[10] Miyata T., Sohde T., Rubin A. L., Stenzel K. H. (1971) Effects of ultraviolet irradiation on native and telopeptidepoor collagen. Biochem. Biophy. Acta 229: 672-680.

[11] Olde Damink L. H. H., Dijkstra P. J., Van Luyn M. J. A., Van Wachem P. B., Nieuwenhuis P., Feijen J. (1995) Glutaraldehyde as a cross-linking agent for collagen-based biomaterials. J. Mater. Sci. Mater. Med. 6 (8): 460-472.

[12] Olde Damink L. H. H., Dijkstra P. J., Van Luyn M. J. A. , Van Wachem P. B., Nieuwenhuis P., Feijen J. (1995) Cross-linking of dermal sheep collagen using hexamethylene diisocyanate. J. Mat. Sci. Mater. Med. 6 (7): 429-434.

[13] Barker H., Oliver R., Grant R., Stephen L. (1980) Formaldehyde as a pre-treatment for dermal collagen heterografts. Biochem. Biophys. Acta. 632 (4): 589-597.

[14] Sheehan J. C., Hlavka J. J. (1957) The Cross-linking of Gelatine Using a Water-soluble Carbodiimide . Am. Chem. Soc. 79 (16): 4528-4529.

[15] Heinau V., Kirste B.(1994) http://www.chemie.fu-berlin.de/chemistry/bio/amino-acids_en.html.

[16] Gennadios A. (2002) Protein-based films and coatings. CRC Press Inc., USA.

[17] Daniel C., Dammer C., Guenet J. M. (1994) On the definition of thermoreversible gels – The case of syndiotactic polystyrene. Polymers 35 (19): 4243-4246.

[18] Baeuerlein E., Behrens P., Epple M., Mann S. (2009) Handbook of Biomineralization : Biomimetic and Bioinspired Chemistry. Wiley-VCG 2009; ISBN 3527318054, 9783527318056.

[19] Lee K. Y., Mooney D. J. (2001) Hydrogels for tissue engineering. Chem. Rev. 101 (7): 1869-1880.

[20] Baez J., Olsen D., Polarek, J.W. (2005) Recombinant microbial systems for the production of human collagen and gelatine. Appl. Microbiol. Biotechnol. 69: 245-52.

[21] Chvapil M. (1977) Collagen sponge, theory and practice of medical application. J. Biomed. Mater. Res. 11: 721-741.

[22] Sela M., Armpm R. (1960) Studies on the chemical basis of the antigenicity of proteins. 1. Antigenicity of polypeptidyl gelatines. Biochem. J. 75: 91-102.

[23] Cretel E., Richard M. A., Jean R., Durand J. M. (2001) Still's-like disease, breast prosthesis, and collagen implants. Theumatol. Int. 20: 129-131.

[24] Heath C.A., Barker R. A., Esmonde T. F. G., Harvey P., Roberts R., Trend P., Head M. W., Smith C., Bell J. E., Ironside J. W., Will R. G., Knight R. S. G. (2006) Dura mater-associated Creutzfeldt-Jakob disease: experience from surveillance in the UK. J. Neurol. Neurosurg. Psychiatry 77: 880-882.

[25] Vaz C. M., de Graaf L. A., Reis R. L., Cunha A. M. (2003) Effect of cross-linking, thermal treatment and UV irradiation on the mechanical properties and in vitro degradation behaviour of several natural proteins aimed to be used in the biomedical field. J. Mater. Sci.: Mater. Medic. 14: 789-796.

[26] Tomihata K., Burczak K., Shiraki K., Ikada Y. (1994) Cross-linking and biodegradation of native and denatured collagen. American Chemical Society Symposium Series 540.

[27] Narbat M. K., Orang F., Hashtjin M. S., Goudarzi A. (2006) Fabrication of porous hydroxyapatite-gelatine composite scaffolds for bone tissue engineering. Iran. Biomed. J. 10 (4): 215-223.

[28] Ratanavaraporn J., Damrongsakkul S., Sanchavanakit N., Banaprasert T., Kanokpanont S. (2006) Comparison of Gelatine and Collagen Scaffolds for Fibroblast Cell Culture. J. Metals, Materials and Minerals 16 (1): 31-36.

[29] Hennink W. E., van Nostrum C. F. (2002) Novel cross-linking methods to design hydrogels. Adv. Drug Deliv. Rev. 54 (1): 13-36.

[30] Weadock K. S., Miller E. J., Keuffel E. L., Dun M. G. (1995) Effect of physical cross-linking methods on collagen-fiber durability in proteolytic solutions. J. Biomed. Mater. Res. A 32 (2): 221-226.

[31] Weadock K. S., Miller E. J., Bellincampi L. D., Zawadsky J. P., Dun M. G. (2004) Physical cross-linking of collagen fibers: Comparison of ultraviolet irradiation and dehydothermal treatment. J. Biomed. Mater. Res. 29 (11): 1373-1379.

[32] Sung H. W., Hsu H. L., Shih C. C., Lin D. S. (1996) Cross- linking characteristics of biological tissues fixed with monofunctional or multifunctional epoxy compounds. Biomaterials 17 (14): 1405-1410.

[33] Friess W. (1998) Collagen – biomaterial for drug delivery. Eur. J. Pharm. Biopharm. 45: 113-136.

[34] Image adapted from http://www.niroinc.com/food_chemical/spray_drying_gelatin.asp.

[35] Leiner-Davis (2000) http://www.gelatin.com.

[36] Freed L. E., Marquis J. C., Nohria A., Emmanual J., Mikos A. G., Langer R. (1993) Neocartilage formation in vitro and in vivo using cells cultured on synthetic biodegradable polymers. J. Biomed. Mater. Res. 27: 11-23.

[37] Cima L. G., Vacanti J. P., Vacanti C., Ingber D., Mooney D., Langer R. (1991) Tissue engineering by cell transplantation using degradable polymer substrates. J. Biomech. Eng. 113 (2): 143-151.

[38] Mikos A. G., Bao Y., Cima L. G., Ingber D. E., Vacanti J. P., Langer R. (1993a) Preparation of poly(glycolic acid) bonded fiber structures for cell attachment and transplantation. J. Biomed. Mater. Res. 27 (2): 183-189.

[39] Mooney D. J., Mazzoni C. L., Breuer C., McNamara K., Hern D., Vacanti J. P. (1996b) Stabilized polyglycolic acid fibre-based tubes for tissue engineering. Biomaterials 17: 115-124.

[40] Mikos A. G., Thorsen A. J., Czerwonka L. A., Bao Y., Langer R., Winslow D. N., Vacanti J. P. (1994) Preparation and characterization of poly(L-lactic acid) foams. Polymer 35: 1068-1077.

[41] Mikos A. G., Sarakinos G., Leite S. M., Vacanti J. P., Langer R. (1993b) Laminated three-dimensional biodegradable foams for use in tissue engineering. Biomaterials 14: 323-330.

[42] Thomson R. C., Yaszemski M. J., Powers J. M., Mikos A. G. (1998) Hydroxyapatite fiber reinforced poly(a-hydroxy ester) foams for bone regeneration. Biomaterials 19: 1935-1943.

[43] Goldstein A. S., Zhu G., Morris G. E., Meszlenyi R. K., Mikos A. G. (1999) Effect of Osteoblastic Culture conditions on the structure of poly(DL-lactic-co-glycolic acid) foam scaffolds. Tissue Engineering 5: 421-433.

[44] Shastri V. P., Martin I., Langer R. (2000) Macroporous polymer foams by hydrocarbon templating. Proceedings of the National Academy of Sciences USA 97: 1970-1975.

[45] Mooney D. J., Baldwin D. F., Suh N. P., Vacanti J. P., Langer R. (1996) Novel approach to fabricate porous sponges of poly(D,L-lactic co-glycolic acid) without the use of organic solvents. Biomaterials 17: 1417-1422.

[46] Nam Y. S., Yoon J. J., Park T. G. (2000) A novel fabrication method of macroporous biodegradable polymer scaffolds using gas foaming salt as a porogen additive. J. Biomed. Mater. Res. (Appl. Biomater.) 53: 1-7.

[47] Lo H., Ponticiello M. S., Leong K. W. (1995) Fabrication of controlled release biodegradable foams by phase separation. Tissue Engineering 1: 15-28.

[48] Schugens C., Maquet V., Grandfils C., Jerome R., Teyssie P. (1996) Polylactide macroporous biodegradable implants for cell transplantation II. Preparation of polylactide foams for liquid-liquid phase separation. J. Biomed. Mater. Res. 30: 449-461.

[49] Nam Y. S., Park T. G. (1999a) Biodegradable polymeric microcellular foams by modified thermally induced phase separation method. Biomaterials 20: 1783-1790.

[50] Nam Y. S., Park T. G. (1999b) Porous biodegradable polymeric scaffolds prepared by thermally induced phase separation. J. Biomed. Mater. Res. 47: 8-17.

[51] Schugens C., Maquet V., Grandfils C., Jerome R., Teyssie P. (1996) Polylactide macroporous biodegradable implants for cell transplantation. II. Preparation of polylactide foams by liquid–liquid phase separation. J. Biomed. Mater. Res. 30: 449-461.

[52] Whang K., Thomas C. H., Healy K. E., Nuber G. (1995) A novel method to fabricate bioabsorbable scaffolds. Polymer 36: 837-842.

[53] Schmitz J. P., Hollinger J. O. (1988) A preliminary study of the osteogenic potential of a biodegradable alloplasticosteoinductive alloimplant. Clin. Orthop. 237: 245-255.

[54] Heckman J. D., Boyan B. D., Aufdemorte T. B., Abbott J. T. (1991) The use of bone morphogenetic protein in the treatment of non-union in a canine model. J. Bone Joint Surg. Am. 73: 750-764.

[55] Hsu Y. Y., Gresser J. D., Trantolo D. J., Lyons C. M., Gangadharam P. R. J., Wise D. L. (1997) Effect of polymer foam morphology and density on kinetics of in vitro

controlled release of isoniazid from compressed foam matrices. J. Biomed. Mater. Sci. 35: 107-116.

[56] Yannas I. V., Burke J. F., Gordon P. L., Huang C., Rubenstein R. H. (1980) Design of an artificial skin. Part II. Control of chemical composition. Biomaterials 14: 107-131.

[57] Von Heimburg D., Zachariah S., Heschel I., Kühling H., Schoof H., Hafemann B., Pallua N. (2001) Human preadipocytes seeded on freeze-dried collagen scaffolds investigated in vitro and in vivo. Biomaterials 22 (5): 429-438.

[58] Dagalakis N., Flink J., Stasikelis P., Burke J. F., Yannas I. V. (1980) Design of an artificial skin. Part III. Control of pore structure. Biomaterials 14: 511-528.

[59] Doillon C. J., Whyne C. F., Brandwein S., Silver F. H. (1986) Collagen-based wound dressings: Control of the pore structure and morphology. J. Biomed. Mater. Res. 20: 1219-1228.

[60] Schoof H., Burns L., Fisher A., Heschel I., Rau G. (2000) Dendritic ice morphology in unidirectionally solidified collagen suspensions. J. Cryst. Growth 209: 122-129.

[61] Schoof H., Apel J., Heschel I., Rau G. (2001) Control of pore structure and size in freeze-dried collagen sponges. J. Biomed. Mater. Res. 58 (4): 352-357.

[62] Nazarov R., Jin H. J., Kaplan D. L. (2004) Porous 3-D scaffolds fom regenerated silk fibroin. Biomaterials 5 (3): 718-726.

[63] Zhan J. L., Sun X. D., Cui F. Z., Kong X. D. (2007) Preparation of 3-D porous fibroin scaffolds by freeze drying with treatment of methanol solutions. Chinese Science Bulletin 52 (13): 1791-1795.

[64] Mandal B. B., Kundu S. C. (2009) Cell proliferation and migration in silk fibroin 3D scaffolds. Biomaterials 10 (15): 2956-2965.

[65] Madihally S. V., Matthew H. W. T. (1999) Porous chitosan scaffolds for tissue engineering. Biomaterials 20: 1133-1142.

[66] Kim S. E., Park J. H., Cho Y. W., Chung H., Jeong S. Y., Lee E. B., Kwon I. C. (2003) Porous chitosan scaffold containing microspheres loaded with transforming growth factor-β1: Implications for cartilage tissue engineering. J. Controlled Release 91 (3): 365-374.

[67] Kang H. W., Tabata Y., Ikada Y. (1999) Fabrication of porous gelatine scaffolds for tissue engineering. Biomaterials 20 (14): 1339-1344.

[68] Lee S. B., Kim Y. H., Chong M. S., Hong S. H., Lee Y. M. (2005) Study of gelatine-containing artificial skin V: fabrication of gelatine scaffolds using a salt-leaching method. Biomaterials 26 (14) 1961-1968.

[69] Glicklis R., Shapiro L., Agbaria R., Merchuk J.C., Cohen S. (2000) Hepatocyte behavior within three-dimensional porous alginate scaffolds. Biotechnol Bioeng 67 (3): 344-353.

[70] Zmora S., Glicklis R., Cohen S. (2002) Tailoring the pore architecture in 3-D alginate scaffolds by controlling the freezing regime during fabrication. Biomaterials 23 (20): 783-793.

[71] Chung T. W., Yang J., Akaike T., Cho K. Y., Nah J. W., Kim S. I., Cho C. S. (2002) Preparation of alginate/galactosylated chitosan scaffold for hepatocyte attachment. Biomaterials 23 (14): 2827-2834.

[72] Mao J. S., Zhao L. G., Yin Y. J., Yao K. D. (2003) Structure and properties of bilayer chitosan–gelatine scaffolds. Biomaterials 24 (6): 1067-1074.

[73] Zhang Y. F., Cheng X. R., Chen Y., Shi B., Chen X. H. (2007) Three-dimensional Nanohydroxyapatite/Chitosan Scaffolds as Potential Tissue Engineered Periodontal Tissue. J. Biomater. Appl. 21 (4): 333-349.

[74] She Z. D., Jin C. R., Huang Z., Zhang B. F., Feng Q. L., Xu Y. X. (2008) Silk fibroin/chitosan scaffold: preparation, characterization, and culture with HepG2 cell. J. Mater. Sci. Mater. Med. 19 (12): 3545-3553.

[75] Leong K. F., Cheah C. M., Chua C. K. (2003) Solid freeform fabrication of three-dimensional scaffolds for engineering replacement tissues and organs. Biomaterials 24: 2363-2378.

[76] Yang S., Leong K. F., Du Z., Chua C. K. (2001) The design of scaffolds for use in tissue engineering. Part I. Traditional factors. Tissue Eng. 7: 679-689.

[77] Yang S., Leong K. F., Du Z. H., Chua C. K. (2002) The Design of Scaffolds for Use in Tissue Engineering. Part II. Rapid Prototyping Techniques. Tissue Eng. 8 (1): 1-11.

[78] Matsuda T., Mizutani M. (2002) Liquid acrylateendcapped biodegradable poly(e-caprolactone-*co*-trimethylene carbonate). II. Computer-aided stereolithographic microarchitectural surface photoconstructs. J. Biomed. Mater. Res. 62: 395-403.

[79] Hull C. (1990) Method for production of three-dimensional objects by stereolithography. US Patent 4929402.

[80] Dhariwala B., Hunt E., Boland T. (2004) Rapid prototyping of tissue-engineering constructs, using photopolymerizable hydrogels and stereolithography. Tissue Engineering 10 (9-10): 1316-1322.

[81] Hutmacher D. W., Schantz T., Zein I., Ng K. W., Teoh S. H., Tan K. C. (2001) Mechanical properties and cell cultural response of polycaprolactone scaffolds designed and fabricated via fused deposition modelling. J. Biomed. Mater. Res. 55 (2): 203-216.

[82] Zein I., Hutmacher D. W., Tan K. C., Teoh S. H. (2002) Fused deposition modeling of novel scaffold architectures for tissue engineering applications. Biomaterials 23: (4): 1169-1185.

[83] Tan K. H., Chua C. K., Leong K. F., Cheah C. M., Gui W. S., Tan W. S., Wiria F. E. (2005) Selective laser sintering of biocompatible polymers for applications in tissue engineering. Biomed. Mater. Eng. 15 (1-2): 113-124.

[84] Williams J. M., Adewunmi A., Schek R. M., Flanagan C. L., Krebsbach P. H., Feinberg S. E., Hollister S. J., Das S. (2005) Bone tissue engineering using polycaprolactone scaffolds fabricated via selective laser sintering. Biomaterials 26 (23): 4817-4827.

[85] Sachs E., Cima M., Williams P., Brancazio D., Cornie J. (1992) Three Dimensional Printing: Rapid Tooling and Prototypes Directly from a CAD Model. J. Eng. Ind. 144: 481-488.

[86] Giordano R. A., Wu B. M., Borland S. W., Cima L. G., Sachs E. M., Cima M. J. (1996) Mechanical properties of dense polylactic acid structures fabricated by three dimensional printing. J. Biomater. Sci. Polym. Edn. 8(1): 63-75.

[87] Kim S. S., Utsunomiya H., Koski J. A., Wu B. M., Cima M. J., Sohn J., Mukai M., Griffith L. G., Vacanti J. P. (1998) Survival and function of hepatocytes on a novel three-dimensional synthetic biodegradable polymer scaffold with an intrinsic network of channels. Ann. Surg. 228: 8-13.

[88] Landers R, Mulhaupt R (2000) Desktop manufacturing of complex objects, prototypes and biomedical scaffolds by means of computer-assisted design combined with computer-guided 3D plotting of polymers and reactive oligomers. Macromol. Mater. Eng. 282: 17-21.

[89] Griffith M. L., Halloran J. W. (1996) Freeform fabrication of ceramics via stereolithography. J. Am. Ceram. Soc. 79: 2601-2608.

[90] Levy R. A., Chu T. G. M., Halloran J. W., Feinberg S. E., Hollister S. (1997) CT-generated porous hydroxyapatite orbital floor prosthesis as a prototype bioimplant. Am. J. Neuroradiol. 18: 1522-1525.

[91] Peter N. L., Pilliar R. M., Grynpas M. D. (2001) Fabrication of porous calcium polyphosphate implants by solid freeform fabrication: A study of processing and in vitro degradation characteristics. J. Biomed. Mat. Res. 56: 504-515.

[92] Arcaute K., Mann B. K.,Wicker R. B. (2006) Stereolithography of three-dimensional bioactive poly(ethylene glycol) constructs with encapsulated cells. Ann. Biomed. Eng. 34 (9): 1429-1441.

[93] Schantz J. T., Brandwood A., Hutmacher D. W., Khor H. L., Bittner K. (2005) Osteogenic differentiation of mesenchymal progenitor cells in computer designed fibrin-polymer-ceramic scaffolds manufactured by fused deposition modelling. J. Mater. Sci. Mater. Med. 16 (9): 807-819.

[94] Chim H., Hutmacher D. W., Chou A. M., Oliveira A. L., Reis R. L., Lim T. C., Schantz J. T. (2006) A comparative analysis of scaffold material modifications for load-bearing applications in bone tissue engineering. Int. J. Oral Maxillofac. Surg. 35 (10): 928-934.

[95] Wang F., Shor L., Darling A., Khalil S., Sun W., Guceri S., Lau A. (2004) Precision extruding deposition and characterization of cellular poly-ε-caprolactone tissue scaffolds. Rapid Prototyping J. 10 (1): 42-49.

[96] Tan K. H., Chua C. K., Leong K. F., Cheah C. M., Cheang P., Abu Bakar M. S., Cha S. W. (2003) Scaffold development using selective laser sintering of polyetheretherketone-hydroxyapatite biocomposite blends . Biomaterials 24 (8): 3115-3123.

[97] Chua C. K., Leong K. F., Tan K. H., Wiria F. E., Cheah C. M. (2004) Development of tissue scaffolds using selective laser sintering of polyvinyl alcohol/hydroxyapatite biocomposite for craniofacial and joint defects. J. Mater. Sci. Mater. Med. 15 (10): 1113-1121.

[98] Wiria F. E., Leong K. F., Chua C. K., Liu Y. (2007) Poly-epsilon-caprolactone/hydroxyapatite for tissue engineering scaffold fabrication via selective laser sintering. Acta Biomater. 3 (1): 1-12.

[99] Koegler W. S., Griffith L. G. (2004) Osteoblast response to PLGA tissue engineering scaffolds with PEO modified surface chemistries and demonstration of patterned cell response Biomaterials 25 (14): 2819-2830.

[100] Weinand C., Pomerantseva I., Neville C. M., Gupta R., Weinberg E., Madisch I., Shapiro F., Abukawa H., Troulis M. J., Vacanti J. P. (2004) Hydrogel-β-TCP scaffolds and stem cells for tissue engineering bone. Bone 38 (4): 555-563.

[101] Federal Register (1997) ICH Q3C Impurities: Guideline for Residual Solvents. US Department of Health and Human Services: Food and Drug Administration. Federal Register 62: 67377-67388.

[102] Koegler W. S., Patrick C., Cima M. J., Griffith L. G. (2002) Carbon dioxide extraction of residual chloroform from biodegradable polymers. J. Biomed. Mater. Res. 63: 567-576.

[103] Lam E. X. F., Mo X. M., Teoh S. H., Hutmacher D. W. (2002) Scaffold development using 3D printing with a starch-based polymer. Mater. Sci. Eng. C20: 49-56.

[104] Yousefi A. M., Gauvin C., Sun L., Di Raddo R. W., Fernandes J. (2007) Design and fabrication of 3D-plotted polymeric scaffolds in functional tissue engineering. Polym. Eng. Sci. 47 (5): 608-618.

[105] Yilgor P., Sousa R. A., Reis R. L., Hasirci N., Hasirci V. (2008) 3D Plotted PCL Scaffolds for Stem Cell Based Bone Tissue Engineering. Macromol. Symp. 269: 92–99.

[106] Landers R., Hübner U., Schmelzeisen R., Mülhaupt R. (2002) Rapid prototyping of scaffolds derived from thermoreversible hydrogels and tailored for applications in tissue engineering. Biomaterials 23 (23): 4437-4447.

[107] Landers R., Pfister A., Hubner U., John H., Schmelzeisen R., Mulhaupt R. (2002) Fabrication of soft tissue engineering scaffolds by means of rapid prototyping techniques. J. Mater. Sci. 37 (15): 3107-3116.

[108] Kim G. H., Son J. G. (2009) 3D polycarprolactone (PCL) scaffold with hierarchical structure fabricated by a piezoelectric transducer (PZT)-assisted bioplotter. Appl. Phys. A Mater. Sci. Proc. 94 (4): 781-785.

[109] Boland T., Xu T., Damon B., Cui X. (2006) Application of inkjet printing to tissue engineering. Biotechnol. J. 1 (9): 910-917.

[110] Lu L., Mikos A. G. (1996) The importance of new processing techniques in tissue engineering. MRS Bull 21: 28-32.

[111] Derby B. (2008) Bioprinting: inkjet printing proteins and hybrid cell-containing materials and structures. J. Mater. Chem. 18 (47): 5717-5721.

[112] Roth E. A., Xu T., Das M., Gregory C., Hickman J. J., Boland T. (2004) Inkjet printing for high-throughput cell patterning. Biomaterials 25: 3707-3715.

[113] Xu T., Jin J., Gregory C., Hickman J. J., Boland T. (2005) Inkjet printing of viable mammalian cells. Biomaterials 26: 93-99.

[114] Xu T., Petridou S., Lee E. H., Roth E. A., Vyavahare N. R., Hickman J. J., Boland T. (2004) Construction of high-density bacterial colony arrays and patterns by the ink-jet method. Biotechnol. Bioeng. 85: 29-33.

[115] Xu T., Gregory C. A., Molnar P., Cui X., Jalota S., Bhaduri S. B., Boland T. (2006) Viability and electrophysiology of neural cell structures generated by the inkjet printing method. Biomaterials 27: 3580-3588.

[116] Pardo L., Wilson W. C., Boland T. (2003) Characterization of patterned self-assembled monolayers and protein arrays generated by the ink-jet method. Langmuir 19 (5): 1462-1466.

[117] Boland T., Xu T., Damon B. J., Manley B., Kesari P., Jalota S., Bhaduri S. (2007) Drop-on-demand printing of cells and materials for designer tissue constructs. Mater. Sci. Eng. C 27: 372-326.

[118] Simons K. R., Morton R. J., Mosier D. A., Fulton R. W., Confer A. W. (1989) Comparison of the Pasteurella haemolytica A1 envelope proteinsobtained by two cell disruption methods. J. Clin. Microbiol. 27(4): 664–667.

[119] Saunders R. E., Gough J. E., Derby B. (2008) Delivery of human fibroblast cells by piezoelectric drop-on-demand inkjet printing. Biomaterials 29 (2): 193-203.

[120] Saunders R., Gough J., Derby B. (2005) Inkjet printing of mammalian primary cells for tissue engineering applications. Materials Research Society Symposium Proceedings.

[121] Creagh L. T., Mc Donald M. (2003) Design and performance of inkjet print heads for non-graphic arts applications. MRS Bull. 28: 807-811.

[122] Shimoda T., Morii K., Seki S., Kiguchi H. (2003) Inkjet Printing of Light-Emitting Polymer Displays. MRS Bull. 28: 821-827.

[123] De Gans B. J., Kazancioglu E., Meyer W., Schubert S. (2004) Inkjet Printing Polymers and Plymer Libraries Using Micropipettes. Macromol. Rapid Commun. 25: 292-296.

[124] W. Meyer, M. Döring (2000) Liquid handling in the pico- and nanoliter range. In Microreaction Technology: Industrial Prospects – IMRET3: Proceedings of the 3rd International Conference on Microreactor Technology, W. Ehrfeld, Ed. Springer Berlin: 145.

[125] Dijksman J. F. (1984) Hydrodynamics of small tubular pumps. J. Fluid Mech. 139: 173-191.

[126] Tekin E., de Gans B. J., Schubert U. S. (2004) Ink-jet printing of polymers- from single dots to thin film libraries. J. Mater. Chem. 14: 2627-2632.

[127] Deegan R. D., Bakajin O., Dupont T. F., Huber G., Nagel S. R., Witten T. A. (1997) Capillary flow as the cause of ring stains from dried liquid drops. Nature 389: 827-829.

[128] Deegan R. D. (2000) Pattern formation in drying drops. Phys. Rev. E: Stat. Phys., Plasmas, Fluids, Relat. Interdiscip. Top. 61(1): 475-485.

[129] Yun Y. H., Kim J. D., Lee B. K., Cho Y. W. (2009) Polymer inkjet printing: Construction of three-dimensional structures at micro-scale by repeated lamination. Macromolecular Res. 17 (3): 197-202.

[130] Christanti Y., Walker L. M. (2001) Surface tension driven jet break up of strainhardening polymer solutions. J. Non-Newtonian Fluid Mech. 100: 9-26.

[131] Lindholm G., Ström G. (1995) On-line measurements of ink film thickness in a flexo press. Proc. 23rd IARIGAI Conference of Printing Research Institutes, Paris, France: 337-353.

[132] Castellanos A., Haak P. (2000) Characterization of anilox rollers. Proc. 52nd Annual TAGA Conference, Pike's Peak, Colorada Springs, USA: 788-800.

[133] Laksin P., Parris J. (1997) Optimisation of ink lay in UV flexographic printing. Proc. 49th Annual TAGA Conference, Quebec City, Canada: 861-871.

[134] Bohan M. F. J., Townsend P., Hamblyn S. M., Claypole T. C., Gethin D. T. (2003) Evaluation of pressures in flexographic printing. 55th Annual TAGA Tech. Conference.

[135] Galton D., Rosenberger R. (2006) A novel solution to the evaluation of flexographic print quality. TAGA J.: 355-372.

[136] Bould D. C., Claypole T. C., Bohan M. F. J. (2003) An experimental investigation into flexographic printing plates. TAGA J. Graphic Technology 1 (3): 1-8.

[137] Fetsko J. M., Walker W. C. (1955) Measurements of ink transfer on coated paper. American Ink Maker.

[138] De Grace J. H., Mangin P. J. (1984) A mechanistic approach to ink transfer Part 1: Effect of substrate properties and press conditions. Advances in Printing Science and Technology 17: 312-332.

[139] Lavelle J. S., Quinn J. A., Gallagher J. E., Micale F. J. (1996) Measurement of flexographic ink transfer on a modified Prufbau. Proc. TAPPI International printing and graphic arts conference, Atlanta, GA, USA: 199-222.

[140] Goodridge M. (1995) Selecting the right mesh. Screen Play Magazine, June 1995.

[141] Holh D. M., Hunt D. D. (1991) Polyester mesh capability study with UV inks. Screen Printing Technical Foundation.

[142] Jewell E. H., Barden T., Claypole T. (2000) The effect of flat bed screen printing parameters on ink film thickness. Screen Printing Technology Group, January 2000.

[143] Fox I. (1999) A review of ink flow through screens. Screen Printing Technology Group, January 1999.

[144] Barden T. (2000) The effect of process parameters on ink film thickness and fine line reproduction in the flat bed screen printing process. University of Wales Swansea, December 2000.

[145] Barden T., Jewell E. H., Claypole T. (2001) The effect of squeegee parameters on fine line reproduction. Screen Printing Technology Group, November 2001.

[146] Pan J., Tonkey G. L., Quintero A. (1999) Screen printing process design of experiments for fine line printing of thick film ceramic substrates. J. Electronics Manufacturing September 1999.

[147] Bertrams P. J., Keuper W., Koch G., van Mourik J. H. C. (1983) Guidelines for finer lines in thick film circuitry. Electrocomponent Science and Technology 10: 237-245.

[148] Liang T. X., Sun W. Z., Wang L. D., Wang Y. H., Li H. D. (1996) Effect of surface energies on screen printing resolution. IEE Transactions on components, Packaging and Manufacturing Technology B, 19 (2): 423-426.

[149] Johnston-Banks F. A. (1990) Gelatine. In P. Harris (Ed.) Food gels: 233-289. London: Elsevier Applied Science Publishers.

[150] Wulansari R., Mitchell J. R. and et al. (1998) Why are gelatine solutions Newtonian? Food Hydrocolloids 12: 245-249.

[151] Leuenberger B. H. (1991) Investigation of viscosity and gelatine properties of different mammalian and fish gelatines. Food Hydrocolloids 5 (4): 353-361.

[152] Djabourov M. (1988) Architecture of gelatine gels. Contemp. Phys. 29 (3): 273-297.

[153] Djabourov M., Leblond J., Papon P. (1988) Gelation of aqueous gelatine solutions. I. Structural investigation. J. Phys. France 49: 319-332.

[154] Prystupa D. A., Donald A. M. (1996) Infrared study of gelatine conformations in gel and sol states. Polymer Gels and Networks 4 (2): 87-110.

[155] Guo L., Colby R. H., Lusignan C. P., Whitesides T. H. (2003) Kinetics of triple helix formation in semidilute gelatine solutions. Macromolecules 36 (26): 9999-10008.

[156] Clark A. H., Ross-Murphy S. B. (1987) Structural and mechanical properties of biopolymer gels. Adv. Polym. Sci. 83: 56-192.

[157] de Carvalho W., Djabourov M. (1997) Physical gelation under shear for gelation gels. Rheologica Acta 36: 591–609.

[158] Lapasin R., Pricl S. (1995) Rheology of industrial polysaccharides: Theory and applications. Blackie Academic & Professional, London.

[159] Flory P. J. (1974) Introductory lecture to a general discussion on gels and gelling processes. Faraday Discuss. Chem. Soc. 57: 7-18.

[160] Ross-Murphy S. B. (1992) Structure and rheology of gelatine gels: recent progress. Polymer 33 (12): 2622-2627.

[161] te Nijenhuis K. (1997) Thermoreversible networks. Viscoelastic properties and structure of gels. Adv. Polym. Sci. 130: 160–193.

[162] Zandi M., Mirzadeh H., Mayer C. (2007) Effects of concentration, temperature, and pH on chain mobility of gelatine during early stages of gelation. Iranian Polym. J. 16 (12): 861-870.

[163] Mortimer S., Ryan A. J., Stanford J. L. (2001) Rheological behaviour and gel point determination for a model levis acid-initiated chain growth epoxy resin. Macromolecules 34 (9): 2973-2980.

[164] Flory P. J. (1941) Molecular size distribution in three dimentional polymers. I. Gelation; II. Trifunctional branching units; III. Tetrafunctional branching units. J. Am. Chem. Soc. 63: 3083-3090, 3096-3100.

[165] Flory P. J. (1953) Principles of polymer chemistry. Cornell University Press. Ithaca, NY.

[166] Stockmayer W. H. (1943) Theory of molecular size distribution and gel formation in branched-chain polymers. J. Chem. Phys. 11: 45-55.

[167] Tung C. Y. M., Dynes P. J. (1982) Relationship between viscoelastic properties and gelation in thermosetting systems. J. Appl. Polym. Sci. 27: 569-574.

[168] Winter H. H. (1987) Can the Gel Point of a cross-linking polymer be detected by the G'- G'' Crossover? Polym. Sci. Tech. 27 (22): 1698-1702.

[169] Winter H. H., Morganelli P., Chambon F. (1988) Stoichiometry effects on rheology of model polyurethanes at the Gel Point, Macromolecules 21: 535-537.

[170] Muller R., Gerald E., Dugand P., Rempp P., Gnanou Y. (1991) Rheological characterization of the gel point: A new interpretation, Macromolecules 21: 1321-1326.

[171] Winter H. H., Chambon F. (1986) Analysis of linear viscoelasticity of a cross-linking polymer at the gel point. J. Rheol. 30: 367-382.

[172] Scanlan J. C., Winter H. H. (1991) Composition dependence of the viscoelasticity of end-linked poly(dimethylsiloxane) at the gel point. Macromolecules 24 (1): 47-54.

[173] Chambon F., Petrovic Z. S., MacKnight W. J., Winter H. H. (1986) Rheology of model polyurethanes at the gel point. Macromolecules 19 (8): 2146-2149.

[174] Winter H. H., Morganelli P., Chambon F. (1988) Stoichiometry effects on rheology of model polyurethanes at the gel point. Macromolecules 21 (2): 532-535.

[175] Chambon F., Winter H. H. (1987) Linear viscoelasticity at the gel-point of a cross-linking PDMS with imbalanced stoichiometry. J. Rheol. Acta 33: 683-697.

[176] Michon C., Cuvelier G., Launay B. (1993) Concentration dependence of the critical viscoelastic properties of gelatine at the gel point. Rheol. Acta 32: 94-103.

[177] Power D. J., Rodd A. B. (1998) Gel transition studies on nonideal polymer networks using small amplitude oscillatory rheometry. J. Rheol. 42 (5): 1021-1037.

[178] Holly E. E., Venkatarman S. K., Chambon F., Winter H. H. (1988) Fourier transform mechanical spectroscopy of viscoelastic materials with transient structure. J. Non-Newtonian Fluid Mech. 27: 17-26.

[179] In M., Prudhomme R. K. (1993) Fourier transform mechanical spectroscopy of the sol-gel transition in zirconium alkoxide ceramic gels. Rheol. Acta 32: 556.

[180] Kim S. Y., Choi D. G., Yang S. M. (2002) Rheological analysis of the gelation behaviour of Tetraethylorthosilane/Vinyltriethoxysilane hybrid solutions. Korean J. Chem. Eng. 19 (1): 190-196.

[181] Hawkins K., Lawrence M., Williams P. R., Williams R. L. (2007) A study of gelatine gelation by Fourier transform mechanical spectroscopy. J. Non-Newtonian Fluid Mech. doi:10.1016/j.jnnfm.2007.05.016.

[182] Birk D. E., Fitch J. M., Babiarz J. P., Linsenmayer T. F. (1988) Collagen type I and type V are present in the same fibril in the avian corneal stroma. J. Cell Biol. 106: 999-1008.

[183] Brightman A. O., Rajwa B. P., Sturgis J. E., McCallister M. E., Robinson J. P., Voytik-Harbin S. L. (2000) Time-lapse confocal reflection microscopy of collagen fibrillogenesis and extracellular matrix assembly in vitro. Biopolymers. 54: 222-234.

[184] Forgacs G., Newman S. A., Hinner B., Maier C. W., Sackmann E. (2003) Assembly of collagen matrices as a phase transition revealed by structural and rheologic studies. Biophys. J. 84 (2): 1272-1280.

[185] Durand D., Delsanti M., Adam M., Luck J. M. (1987) Frequency dependence of viscoelastic properties of branched polymers near gelation threshold. Europhys. Lett. 3: 297-301.

[186] Newman S., Cloître M., Allain C., Forgacs G., Beysens D. (1997) Viscosity and elasticity during collagen assembly in vitro: relevance to matrix-driven translocation. Biopolymers 41: 337-347.

3.0 Methodologies

3.1 Introduction

This chapter describes the methods used in this investigation. The printing presses used to examine their feasibility to print biopolymer ink and the experimental methodologies used to examine the screen printed line characteristics are described. The instrumentation involved in examining the ink characteristics, measuring and analysing the printed image is also detailed below.

3.2 Printing technologies

3.2.1 Introduction

Printing in its various forms has one main objective, which is to reproduce two-dimensional texts or images, with ink onto various substrates. Most of the printing processes are based on the concepts of high volume mass production, producing repeatable and consistent products. This section describes the processes

used to print the biopolymer ink. Three printing technologies were chosen: inkjet printing, flexographic printing and screen printing.

3.2.2 Inkjet

The inkjet printer used to print the aqueous gelatine solutions was Dimatix materials printer DMP-2800 series, Figure 3.1. This printer operates in drop-on-demand process where the printhead is controlled digitally by software to move to the desired position before jetting ink droplets. This is capable of depositing micro-droplets of functional fluids, including nanoparticle-based metallic and organic materials, for printing feature size widths as small as 50 microns on any flat substrate, utilizing a disposable piezo-inkjet cartridge. The jettable fluid viscosity range is 2 and 30 mPa.s. Ideally, the fluid should have a viscosity of 10 mPa.s and a surface tension of about 30 mN/m [1]. The particles should not aggregate or settle.

The print area of 200 x 300 mm is a maximum and with an adjustable z height can accommodate substrates up to 25 mm thick. The vacuum platen holds the substrate firmly in place and the temperature of the platen can be controlled up to 60°C. The two-dimensional pattern is determined by the editor programme. The characteristics of drop as it is jetted out from the nozzle can be optimised via manipulation of the electronic pulses to the piezo-jetting device by the waveform editor and drop-watch camera system. When a voltage is applied, the piezoelectric material changes shape, which generates a pressure pulse in the fluid forcing a droplet of ink from the nozzle.

The Dimatix printing system has a disposable cartridge-style printhead (DMC-11610) which can be filled with any type of jettable fluids and print instantly in the lab. The inkjet head cartridge can be heated up to 70°C, depending on the ink characteristics. Each cartridge reservoir has a maximum capacity of only 1.5 ml to minimise the waste of expensive fluids, while the minimum volume a cartridge can hold is about 0.2 ml. Under-filling may not allow jet priming. Each cartridge has 16 nozzles linearly spaced at 254 microns with typical drop sizes of 1 and 10 picolitres, Figure 3.1.

The combination of the piezoelectric inkjet printer with ability to alter the jet characteristic and disposable makes DMP-2800 series printer the most suitable candidate to print biopolymer ink for tissue engineering applications.

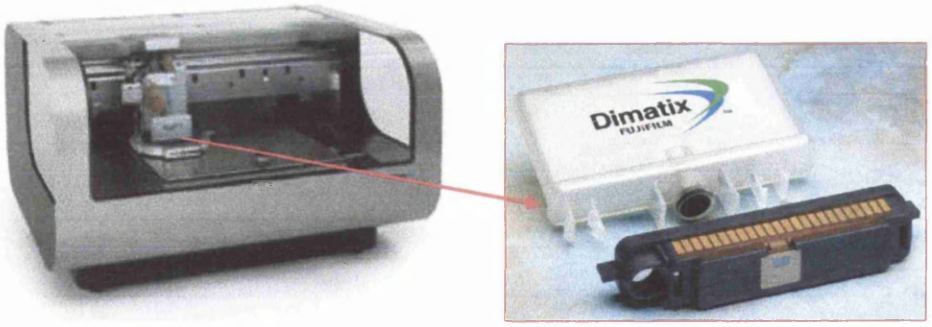

Figure 3.1: Dimatix materials printer (DMP-2800 series) and cartridge-style printhead [2]

3.2.3 Flexography

The IGT F1 printability tester, Figure 3.2 is designed to simulate the flexographic printing process. It was used in this investigation because only a small volume of ink is required to print images comparing to a full-scale printing press. The IGT F1 consists of a combined inking section with an anilox roll and doctor blade and a printing section with a plate cylinder and an impression cylinder. A photopolymer plate is mounted to the plate cylinder using a double-sided tape. Unlike on a press the substrate is attached to a substrate carrier using an adhesive tape at either end. The substrate carrier is rigid, but contains a layer of cushion on the side nearest to the plate onto which the substrate is attached. The substrate carrier is placed onto a substrate holder between the photopolymer plate and the impression cylinder. The maximum print width is 40 mm.

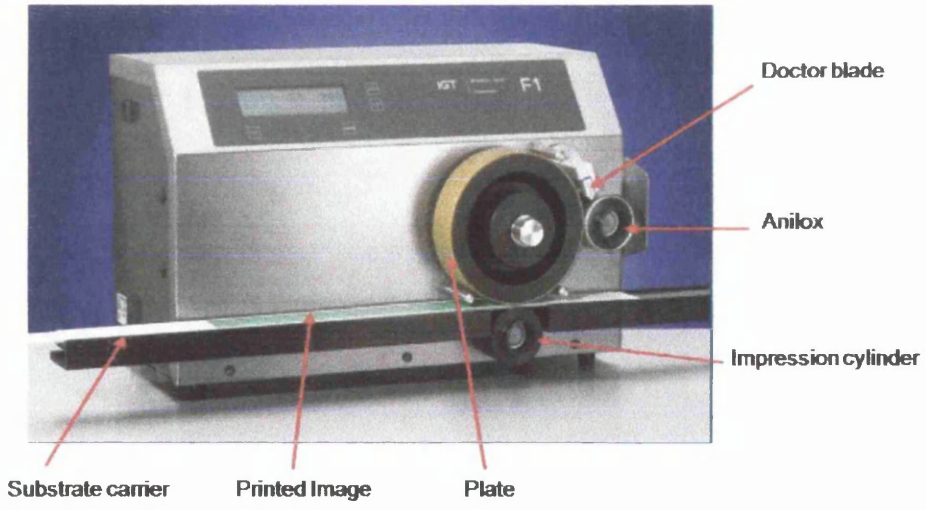

Figure 3.2: IGT F1 printability tester (adapted from www.igt.nl)

When IGT F1 is activated, the anilox and the substrate come into contact with the printing plate and the doctor blade contacts the anilox. To produce a print, 2.5 ml ink is applied to the nip between the doctor blade and the anilox using a pipette. The anilox force (between the anilox and plate) and printing force (between the plate and the substrate) are preset independently. The anilox is rotated for a set number of times in contact with the plate to ensure that the anilox cells are well filled, therefore transferring a constant amount of ink to the plate surface for each trial. The reverse angle doctor blade removes the excess ink on the anilox to prevent excess inking of the plate. Then, the impression roll is engaged with the plate, bringing the substrate in contact with the plate surface. The rotation of the plate cylinder pulls the substrate carrier along the channel through the print nip, therefore transferring the ink from the printing plate to the substrate. The impression cylinder and anilox are both driven from the rolling contact with the substrate carrier and plate respectively. Ink is continuously transferred to the plate from the anilox. At the end of the print the impression cylinder and anilox are disengaged from the plate automatically.

3.2.4 Screen press

The laboratory print trial was performed on a small format screen printing press Presco SP1. This is a manual flat bed screen press with compact design and is shown in Figure 3.3. Presco SP1 was chosen due to its simplicity and requirement of a small quantity of biopolymer ink comparing to DEK screen press or large format Svecia screen press, which were also available. Presco SP1 can accommodate a print width up to 150mm, however it is sufficient as the print width used for the trial was 85 mm.

The press also allows a convenient access for observing and correcting the printing process during operation.

When the screen press is switched on, the parameter settings are set to the desired level manually. The screen is attached to the press underneath the squeegee and flowcoater, the squeegee angle and snap-off gap are then accurately set. The position of flowcoater is just resting on the screen prior printing. The substrate is placed and held firmly on the substrate carrier with vacuum. Many parameters affect the screen printing process. The parameters that could be adjusted by this screen press are the snap-off gap and squeegee angle, the squeegee speed and squeegee force, which are pneumatically controlled. As all other parameters are set manually, great care has to be taken to avoid human errors. Further details on the choice of parameters and the test image are described in Chapter 6.

To produce a print, 8 ml of ink was deposited on the upper surface of the screen. The screen printing process was as described in Chapter 1, except that the flowcoater and squeegee move across the screen simultaneously where the spreading of ink to fill the mesh openings by flowcoater and transferring of ink from the mesh to the substrate by squeegee were performed in one direction and one stroke. This is more time effective enabling the biopolymer ink to be printed quickly, which is essential because of its tendency to gel in a short period of time at ambient temperature.

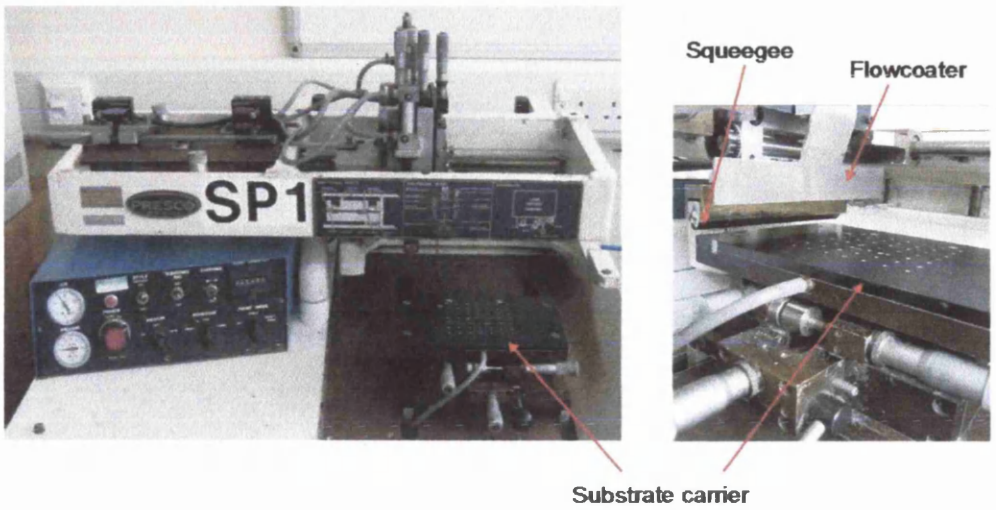

Figure 3.3: Presco SP1 screen press

3.3 Measurement of ink characteristics

3.3.1 Introduction

This section describes the instrumentation used to measure the ink characteristics. The rheological properties of the biopolymer inks were measured using rheometers and the relative surface tension of the inks was measured using a dynamic contact angle measurement instrument. These ink characteristics have previously been shown by Barden [4] to be important parameters in printing process.

3.3.2 Rheological measurements

Rheology is a branch of science dealing with the deformations and flow of all matters. It is particularly concerned with the properties of matter determining its behaviour or

reaction when a mechanical force is exerted on it. Rheology is distinguished from fluid mechanics in that it is concerned with all three of the traditional states of matter rather than only with liquids and gases. The results of rheology provide a mathematical description of the viscoelastic behaviour of matter. There are important implications of rheology in many areas of industry, involving plastics, polymer, metals and other materials, where the measurement of rheological properties is very useful. Thus, rheological instrumentation and rheological measurements have become essential tools in the analytical laboratory for characterising materials, monitoring process conditions, as well as predicting product performance and consumer acceptance.

Rheological measurements have been categorised into three main classes as follows:

(a) Materials flow steadily through a tube or between rotating surfaces.
(b) Deformation is not steady and the variation of deformation with time under the action of forces or the variation of force with time when a body is held in a deformed state.
(c) Oscillatory, usually harmonic forces are applied to a material and its response.

3.3.3 Flow characterisation

Flow characterisation test for viscometry illustrates how a material is likely to flow under an imposed constant shear rate or shear stress. It determines the viscous properties of the materials at a defined temperature and the correlations between shear rate, shear stress and time. When a shear force is applied to a fluid surface parallel to

the direction in which the material is flowing, the molecules of the fluid are displaced from their original positions and slide past each other, establishing a velocity gradient in the fluid, Figure 3.4. The shear rate produced by a given shear stress depends upon the viscosity of the fluid where the viscosity is quantitatively defined as a measure of the material's internal resistance to deformation.

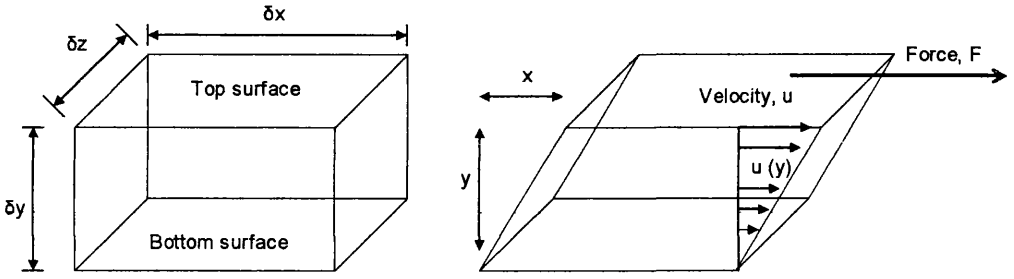

Figure 3.4: Deformation of a fluid element. (a) Undeformed block (b) Deformed block after top surface has moved a distance, x parallel to itself [3]

If the surface area of the top of the element is $A = \delta z \times \delta x$, then the shear stress τ is equal to force per unit area (Nm^{-2}) i.e.

$$\tau = \frac{F}{A} \tag{3.1}$$

If the particle at point E moves under the shear stress to point E', it has moved the distance x under time t. For a small deformation, shear strain is given by

$$\Phi = \frac{x}{y} \tag{3.2}$$

Thus, shear rate (also called shear strain rate) is

$$\dot{\gamma} = \frac{\Phi}{t} = \frac{x}{ty}$$

$$\dot{\gamma} = \frac{u}{y} \tag{3.3}$$

where $u = \frac{x}{t}$ is the velocity of the particle at E.

As the shear stress is proportional to the shear rate then

$$\tau = \text{constant} \times \frac{u}{y} \tag{3.4}$$

Shear rate is the velocity gradient (change in velocity with y) which is a measure of the rate of deformation of the fluid. It may be written in the differential form $\frac{du}{dy}$. The constant of proportionality between the force and the gradient is denoted by μ and is known as the dynamic viscosity of the fluid, giving

$$\tau = \mu \frac{du}{dy} \tag{3.5}$$

This is known as *Newton's law of viscosity*.

Since the relationship of shear stress to shear rate is strictly related to flow, the flow characteristics of a material can be directly shown by plotting a flow curve, a graph of shear stress against shear rate. Figure 3.5 shows the flow curves of the five flow patterns. Each of these curves can be represented by the equation below.

$$\tau = A + B\left(\frac{du}{dy}\right)^n \tag{3.6}$$

where A, B and n are constants.

If the fluid has a constant viscosity m passing though the origin, it obeys the Newton's law and is known as Newtonian fluid where A = 0, B = m and n = 1. For fluids in which the value of m is not constant are known as non-Newtonian fluids and are outlined briefly below.

(i) Shear thinning: Viscosity decreases as shear rate is increased.

(ii) Shear thickening: Viscosity increases as shear rate is increased.

(iii) Plastic: Viscosity appears to be infinite until a certain minimum shear stress is achieved.

(iv) Bingham plastic: As with the plastic above a minimum shear stress must be achieved, but the n value is equal to 1.

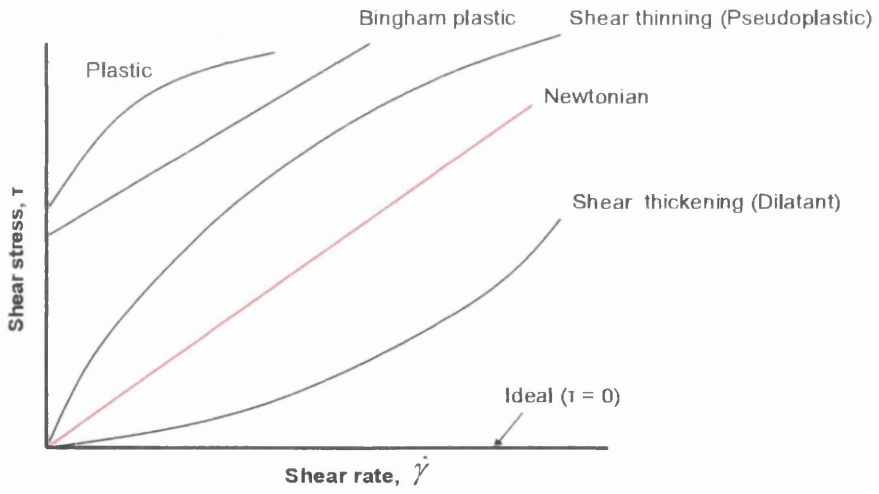

Figure 3.5: Summary of shapes of shear stress-shear rate curves [3]

3.3.4 Viscoelastic characterisation

Fluids are complex material and all structured fluids have a natural rest condition where their microstructure represents a minimum energy state. When a material is deformed there is a definite change in the materials' microstructure. When the stress is removed, the deformed material may or may not restore its original shape at rest condition. If it does the material is said to be solid-like; if it does not then flow has occurred and the material is said to be liquid-like. For some solids such as hard metals the deformation and recovery are instantaneous and are called ideally elastic. Some solids such as polymers have slow recovery (not instantaneous) and are called viscoelastic. The term viscoelastic can also be used for fluids. Viscoelastic materials behave like plastic if there is a sudden large change in shear, otherwise they are similar to Newtonian materials.

Recovery is the process by which the stored energy of the material decreases continuously throughout the microstructure by rearranging the dislocations into low energy configurations. This process exhibits time dependent behaviour. If the deformation is irreversible, this phenomenon is called rheo-malaxis or rheodestruction. Reversible change in the material structure can be split into two broad categories below.

(i) Thixotropic substances: Viscosity decreases with length of time when shear force is applied.

(ii) Rheopectic substances (negative-thixotropy): Viscosity increases with length of time when shear force is applied.

A dynamic test involves applying a stress or strain whose value is changing according to a sine wave equation with time. Thus the resulting stress or strain response follows a sine wave. It can be seen that the material can be continuously excited but never exceed a certain strain so that the material structure is not destroyed (providing steps are taken to keep the strain small enough). The measured result shows a phase difference which indicates the type of material being tested. For viscoelastic materials within the region of linear behaviour, an imposed stress of angular frequency ω would result in a harmonic strain of amplitude proportional to the stress amplitude [5].

Figure 3.6 shows an example of the shear strain lags behind the shear stress by a phase angle δ. The phase angle is a good indication of the overall viscoelastic nature of the material. The in-phase response, at $\delta = 0°$, the sample is ideal elastic material (not achievable), and the out-of-phase response, at $\delta = 90°$ the sample is ideal viscous material (Newtonian). For viscoelastic behaviour, the phase angle is $0° < \delta < 90°$.

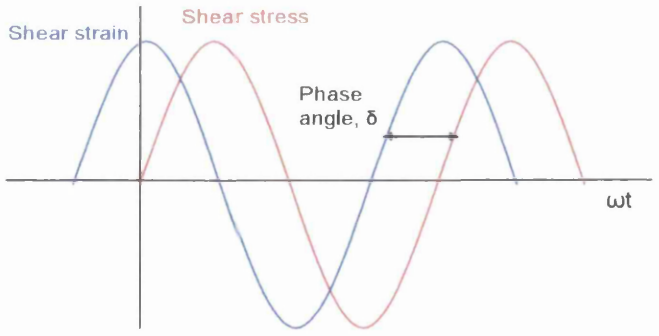

Figure 3.6: Viscoelastic fluid response in oscillatory shearing motion [5]

Most materials are made up of a combination of Hookean (analogous to a spring being extended) and Newtonian (analogous to a viscous dashpot) behaviour, Figure 3.7. The spring describes the elastic element G' (any element of the microstructure that can store energy) while the dashpot describes the viscous behaviour (the microstructure shows a loss of energy).

The simple equations that govern both these basic elements are:

Spring (Hookean solid): $\tau = G'.\gamma$ (3.7)

Dashpot (Viscous Newtonian fluid): $\tau = \eta.\dot{\gamma}$ (3.8)

where G' is elastic modulus and η is the apparent viscosity

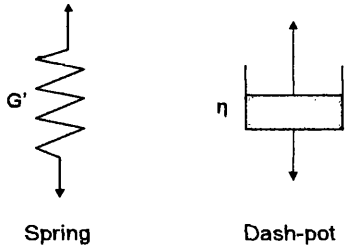

Figure 3.7: Schematic diagram of spring and dashpot model [5]

Hooke's law of elasticity is a simple linear relationship where the applied stress is in direct proportion to the measured strain as long as the stress does not exceed the elastic limit. The viscoelastic solid behaviour of a material is commonly described by Kelvin-Voight model [6] in which a dashpot is placed parallel with a spring. The

Maxwell model [6] describes the viscoelastic fluid behaviour of material in which a dashpot is connected in series with a spring.

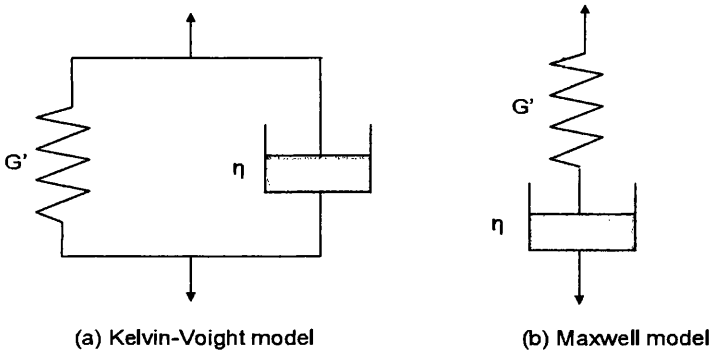

Figure 3.8: Diagram of mechanical analogs of viscoelastic behaviour [6]

The parameters representing viscoelastic behaviour can then be calculated from the measured amplitude ratio of stress to strain and phase angle. A complex shear modulus G* is the total resistance of a material to the applied stress [7] and can be defined as:

$$G^* = \frac{\tau^*}{\gamma^*} = \frac{\tau_0 e^{i(\omega t+\delta)}}{\gamma_0 e^{i\omega t}} = \frac{\tau_0}{\gamma_0} e^{i\delta} = G' + iG'' \qquad (3.9)$$

where the storage modulus G' is the in-phase (real) component and the loss modulus G'' is the out-of-phase (imaginary) component. The storage modulus G' gives information about the elastic properties of the material whilst the loss modulus G'' gives information about the viscous properties of the material.

$$G' = \frac{\tau_0}{\gamma_0} \cos\delta \qquad (3.10)$$

and $$G'' = \frac{\tau_0}{\gamma_0} \sin \delta \qquad (3.11)$$

where $$e^{i\theta} = \cos\theta + i \sin\theta, \quad i = \sqrt{-1}$$

Loss tangent is the ratio of viscous and elastic properties as shown by the equation below. With a tan δ value of 1, the elastic and viscous properties of the material are equal. The smaller the loss tangent is, the more elastic is the material.

$$\tan \delta = \frac{G''}{G'} \qquad (3.12)$$

The conditions of the oscillation tests performed on a material must fall into the region of linear strain response (also called linear viscoelastic range). This region can be determined by oscillating at a fixed frequency and slowly increasing the applied amplitude, either strain or stress. The measured values for the viscoelasticity will remain constant. Beyond this region, the induced strain starts to destroy the elastic structure of the material, causing the material to 'rupture'.

3.3.5 Bohlin Gemini HR nano Rheometer

The rheological characterisation of the inks was conducted using the Bohlin Gemini HR nano rheometer (Figure 3.9). It is a high performance, modular rheometer system designed to provide accurate rheological measurements on a wide variety of materials. Its adaptive control technology is optimised for both stress controlled and strain controlled operations in steady, dynamic and transient modes. Bohlin rheometer enables the measurement and control of nano-torque levels to probe sensitive or weak material structures, in this case the low viscosity biopolymer inks (diluted collagen

solutions and aqueous gelatine solutions), yet retains a working torque range from 3 nNm to 200 mNm. In addition, the temperature control via integrated Peltier devices affords accurate temperature measurement and control. It can be configured for testing on a full range of materials and applications including polymer melts, composites, fluids and semi-solids.

A Bohlin Gemini rheometer was used to characterise the rheological properties of biopolymer inks due to its capabilities of measuring low viscosity, low volume and weakly-structured fluids more accurately than other available rheometers such as Carri-med rheometer and Ares-G2 rheometer. The specifications of this rheometer are tabulated in Table 3.1.

Prior to tests, a small quantity of sample, about 1.9 ml, was placed between the top plate and stationary bottom plate (Figure 3.10 and Figure 3.11). The top plate was then spun at a constant speed and the torque required maintaining the speed is measured. Each measuring geometry used in the rheometer has its associated 'form factor' to convert torque to shear stress and angular velocity to shear rate which are used to quantify the viscosity.

Figure 3.9: Bohlin Gemini HR nano rheometer

Torque range	10 nNm – 200 mNm, controlled stress/rate viscometry. 3 nNm – 200 mNm, controlled stress/ strain oscillation.
Torque resolution	Better than 1 nNm
Position resolution	50 nano radians
Frequency range	1 micro Hz to 150 Hz
Controlled speed range	0.01 mili rad/sec – 600 rad/sec
Measurable speed range	10 nano rad/sec – 600 rad/sec
Normal force NI measurement range	0.001 N – 20 N
Step change in strain	< 10 ms
Temperature range	- 150°C – 550°C

Table 3.1: Malvern Bohlin Gemini rheometer specifications

Many different types of geometries can be used on the rheometer. Two common geometries used in the experiments were:-

(a) Parallel plate geometry consists of two circular flat plates situated parallel to each other, Figure 3.10. The gap between the plates can be adjusted to meet the needs of application [8][9]. Parallel plate geometries are used with test materials containing large particles. The main disadvantage of the parallel plate geometry is that the shear rate is not constant throughout the material in the gap with radial position during deformation, but varies with distance from zero at the centre to a maximum at the edge. Thus the material found at the edge of the plate will contribute most to the measurement, leading to large errors if there is any evaporation of the test material.

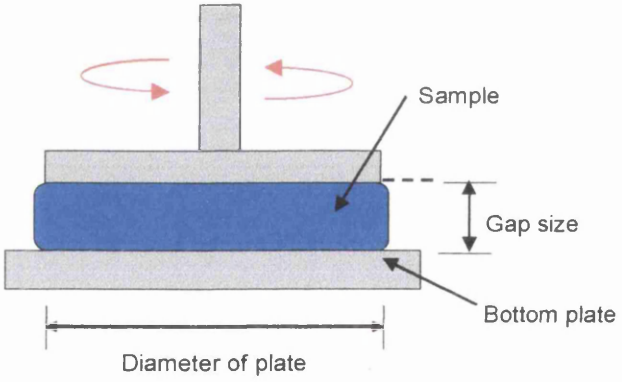

Figure 3.10: Schematic of a parallel plate geometry [8]

(b) Cone and plate geometry (Figure 3.11) consists of an upper cone and a fixed lower flat plate with a sample contained between them. The cone is truncated to ensure that there will not be any contact between two surfaces in case of any

particles in the material. The dimensions of the cone and plate geometry used are 50 mm and a cone angle of 2° with the truncation allowing a preset gap size of 70 μm. The main advantage is that a uniform shear rate will exist throughout the sample if the angle θ between the cone and plate is small (< 5°). High shear rate is possible due to the small angle cone, therefore making it well suited for the study of strongly shear thinning fluids. Also, only a small volume of sample (about 1.9 ml) is required for each loading. The disadvantage is that the materials containing large particles are not applicable due to the small gap size where the particulate materials may trap in the gap leading to noisy data. The cone and plate measuring system was chosen because the biopolymer solutions contain no large particles, so not causing any problems with the small gap size.

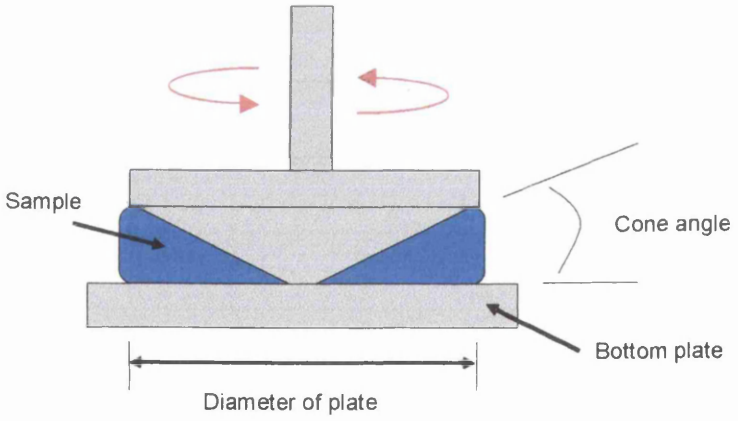

Figure 3.11: Schematic of a cone and plate geometry [8]

The associated form factors for both geometries [8] provide the basis for obtaining the non-Newtonian viscosity. It is important that the correct amount of sample is loaded

when performing a test because under filling or over filling will result in errors in experimental data. For samples where solvent evaporation or drying may happen, a solvent trap can be used with the measuring system. Alternatively, a small amount of low viscosity silicone oil can be placed around the geometry to seal the sample. It is crucial to ensure that the viscosity of the oil is much less than that of the sample being measured and the oil does not mix in with the sample during the test.

The sample was loaded carefully on the centre of the lower plate and the gap was properly filled. It is normally easier to overfill the sample and trim off any excess sample after bringing the upper and lower plates together.

3.3.6 Surface Tension measurement

The relative surface tension of the biopolymer ink was measured using a Fibro DAT 1100 (Fibro System AB, Sweden) dynamic absorption and contact angle tester at ambient temperature, Figure 3.12. The instrument consists of a syringe containing the test liquid, tubing through which the liquid is passed, a cannula through which the drop is delivered to the test chamber, a CCD camera to monitor the change in dot profile and a testing block where the drop is fallen to after measurement. A schematic of the DAT 1100 is shown in Figure 3.12.

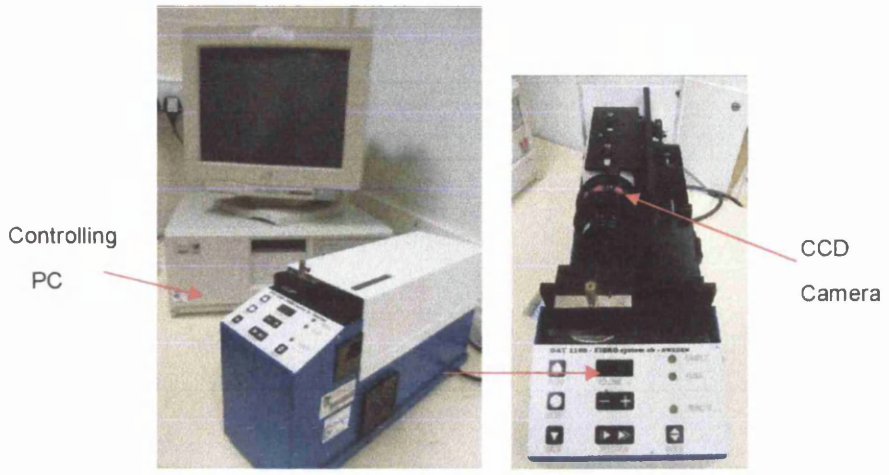

Figure 3.12: DAT 1100 tester

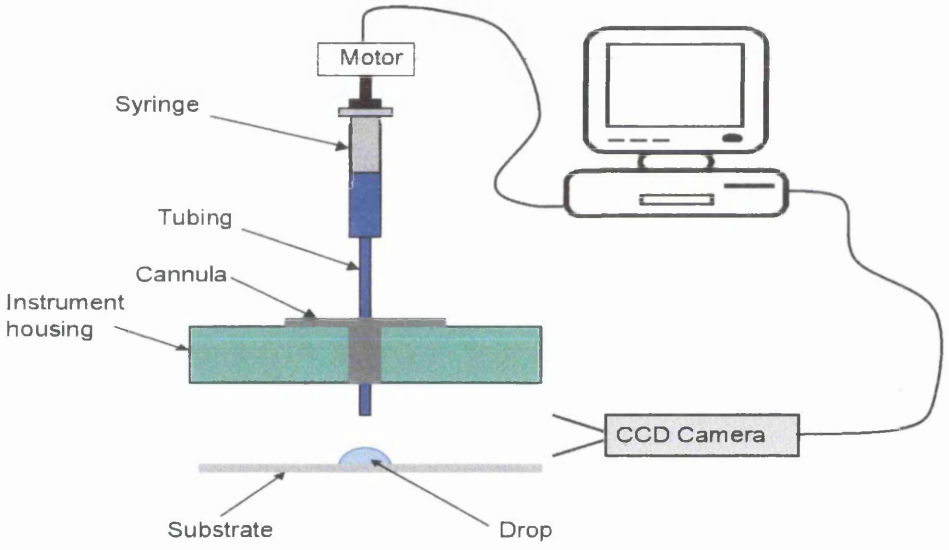

Figure 3.13: Schematic of DAT 1100 (adapted from WCPC, Swansea University)

Prior testing, the syringe and almost the whole of the tubing were filled with biopolymer ink and place in the holder. Before the tubing was connected to the

syringe, the air bubbles in the syringe have to be removed. The syringe was then driven by a motor to pump a controlled volume of ink slowly through to the tip of the tubing directly above the blanket, forming a pendant droplet (tear-drop shape) due to the gravity force hanging from the tubing as shown in Figure 3.13.

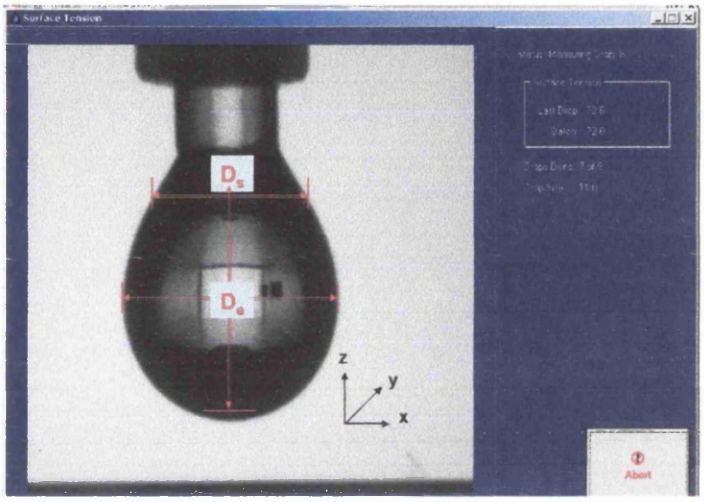

Figure 3.14: Pendant drop image of water at room temperature.

The DAT 1100 tester works on the pendant drop technique which has two principal assumptions in drop shape analysis. The drop has to be symmetric about a central vertical axis and stationary where surface tension and gravity are the only forces shaping the drop [12]. A CCD camera records an image of the drop and the surface tension is then determined by image analysis of the drop shape and the accurate density of the droplet.

Andreas et al. [13] introduced a shape factor, H, relating the surface tension to the shape of the pendant drop, Figure 3.14. This gave a convenient relationship as the following equation [14][15]:

$$\gamma = \frac{g\Delta\rho D_e^{\,2}}{H} \tag{3.13}$$

where γ is surface tension, g is the gravitational constant, $\Delta\rho$ is the difference in density between fluids at interface, D_e is the equatorial diameter of the drop and the parameter H is defined as

$$H = \beta(\frac{D_e}{b})^2 \tag{3.14}$$

The value of 1/H is a function of the ratio $S = D_s / D_e$ which is given in a numerical table in Andreas's paper [13][16] . D_s is the diameter at the distance D_s away from the vertex of the drop.

The pendant drop mode is the most widely used simple static method for measuring the interfacial tension and surface tension of a variety of fluids with established accuracy and reliability [13][16][17]. Another common method of surface tension measurement is sessile drop mode where a sitting drop is utilised instead of a hanging drop. However, pendant drop mode was used because it is often more accurate than the sessile drop mode because the assumption of axial symmetry is easier to satisfy. Sessile drop mode is normally used when the test materials are not convenient to form a pendant drop.

3.4 Measurement of image carrier and printed image

3.4.1 Introduction

Two methods were used to measure the line profile; image analysis and white light interferometry. Image analysis was used to measure the line width of printed lines. It is not possible to measure the three-dimensional characteristics of lines using image analysis. Therefore, white light interferometry was used not only to characterise the image carriers used in printing trials, but also to investigate the line profile of the printed images in terms of line width and line film thickness.

3.4.2 Image processing instrumentation

For the printed samples, a high resolution CCD monochrome Pulnix TM-865 camera was used to capture the image of printed lines in 256 greyscales through Leica MZ 2125 microscope. This microscope has a wide range of magnification from 0.8 to 10 times the internal magnification. A xenon light source was used to illuminate the image. The image acquisition system is shown in Figure 3.15. The calibration of the system was carried out by measuring circles of known diameters. An image of these circles and their diameters are shown in Appendix A. The digital image of circles was captured and the ratio of pixels to microns was calculated for each circle to determine the average pixel ratio. By changing the magnification of the image capture equipment manually, a range of image sizes could be obtained; from an image with a length of approximately 500 μm and a sampling interval of 0.72 μm to an image with a length of 6.3 mm with a sampling interval of about 9 μm.

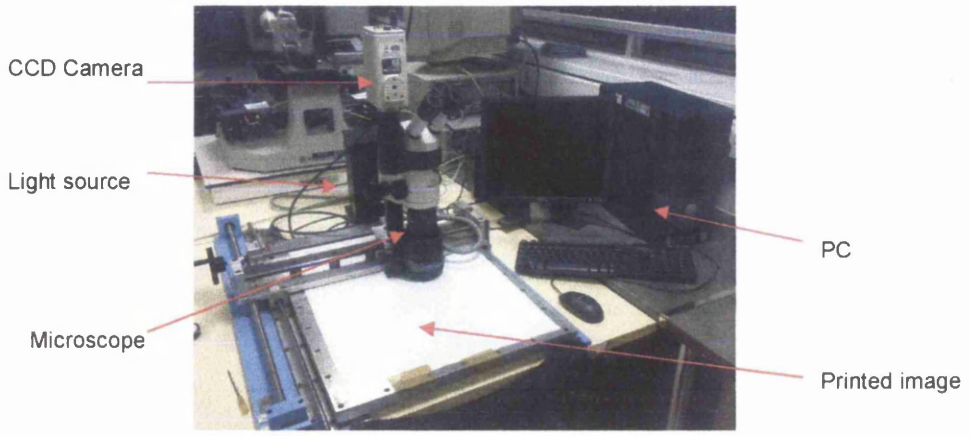

Figure 3.15: Image acquisition system

However, the image capturing device mentioned earlier (microscope and camera) was incapable of capturing printed images which had low contrast. An EPSON Perfection Photo Scanner 4990 was used to scan and convert those printed samples into digital images. This flatbed colour image scanner with the moving light source enables scanning images with high precision quality and intricate detail, due to its 4800 × 9600 dpi resolution, 48 bit colour depth and up to 4.0 Dmax. Additionally, its built-in transparency unit can accommodate film as large as 216 mm × 297 mm. The system was calibrated using the same method as mentioned previously, where circles of known physical size were scanned.

Figure 3.16: EPSON Perfection Photo Scanner 4990 (adapted from www.epson.com)

The images printed by screen printing were captured using the microscope and camera while those images printed by flexographic printing were captured using the scanner. The image capturing process of scanner is more time consuming because images of highest resolution are preferable. It was only used as an alternative image capturing device for images with low contrast level.

3.4.3 Image processing

Image processing is used to extract, characterise and interpret pictorial information [18]. There are many applications of image processing, but they can split into two main groups [19]. These are the production of images for closer and more detailed examination by humans or the collection of data for interpretation by machines.

There are five steps to image processing and analysis [19]: (i) image acquisition; (ii) pre-processing; (iii) segmentation; (iv) detection and description; and

(v) interpretation. This study only examines black and white images; therefore colour image processing is not discussed.

Image acquisition is the capturing of the image in digital form by optical scanning, either by camera and microscope or flat bed scanner. Scanning generates signals which indicate the intensity value of sampled image elements known as pixels. The brightness range is often called the greyscale.

Pre-processing is used to enhance the image. This includes optimisation of the contrast and reduction in noise to improve the quality of the image. Generally, the noise can be reduced by using averaging technique such as signal averaging [20][21] or filters.

Segmentation is one of the most important steps leading to the analysis of processed image data. Its main aim is to separate an image into parts to highlight the areas of interest from the background. Thresholding is the simplest method of image segmentation which can be used to convert a greyscale image into a binary image [22]. For example, a line is detected and segmented, as shown in Figure 3.17. Figure 3.17(a) displays the original captured image and Figure 3.17(b) displays the segmented image with the line highlighted. The selection of a consistent optimum threshold value is of crucial importance in image processing for successful threshold segmentation. A description of the global approach of thresholding techniques is presented below.

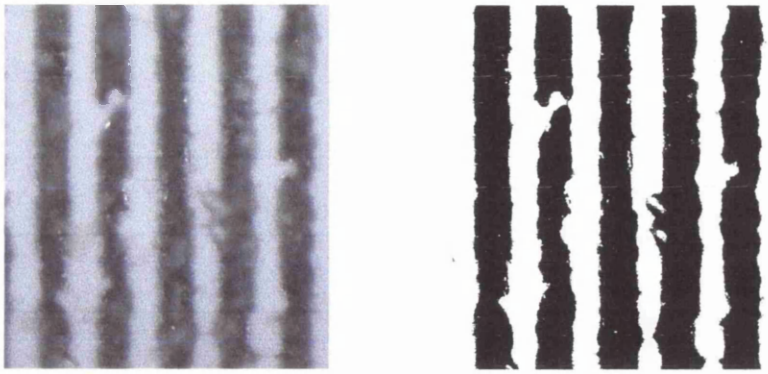

(a) Original image (b) Binary image

Figure 3.17: The original image and segmented image when the correct greyscale threshold value is applied

Histogram-based methods are very efficient, comparing to other image segmentation methods such as edge detection and region growing methods [23], because they typically require only one pass through the pixels. In this technique, a greyscale histogram is computed to show the number of pixels in an image at different intensity values. The peaks and valleys in the graph are used to locate the clusters in the image [22]. For an image of a line, the histogram will exhibit a bimodal distribution which consists of a curve with two distinct peaks and a valley, Figure 3.18. One peak represents the line as dark pixels, and one represents the substrate as light pixels.

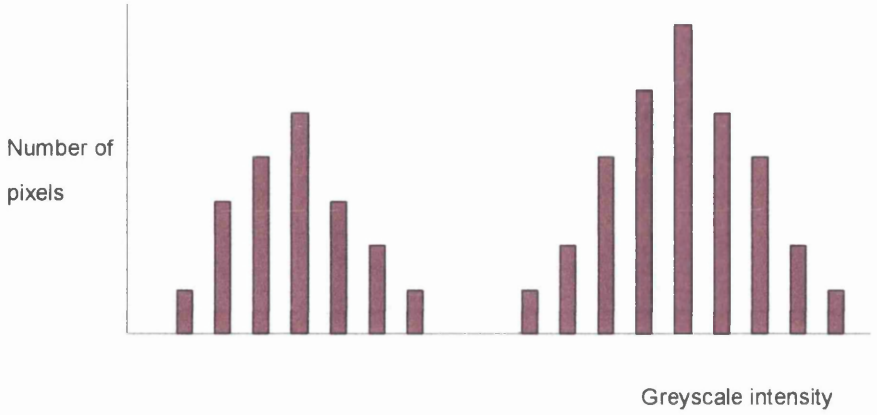

Figure 3.18: A greyscale histogram

The image can then be segmented by locating the minimum of the histogram plot, Figure 3.19. This approach has some limitations as the minimum is not always well defined. The valley might be very broad which leads to uncertainty regarding the appropriate threshold value [24].

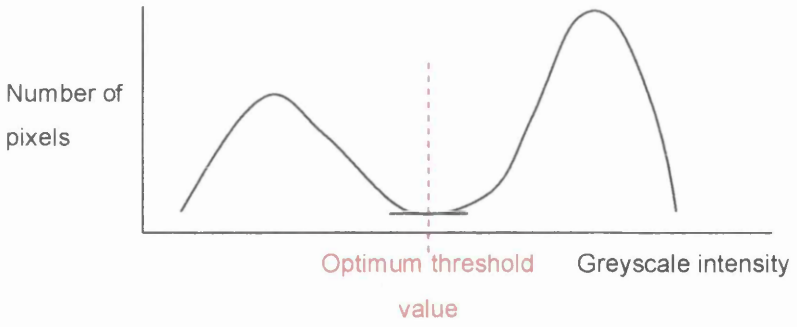

Figure 3.19: Optimum threshold level using minimum value method

As the peaks are often more distinct and better defined than the minimum point, a more repeatable approach of determining the threshold value has been developed

where the mid point between the two peaks is located [18][24], as shown in Figure 3.20. This method has been previously used to successfully examine printed images [24] and thus was adopted in this investigation.

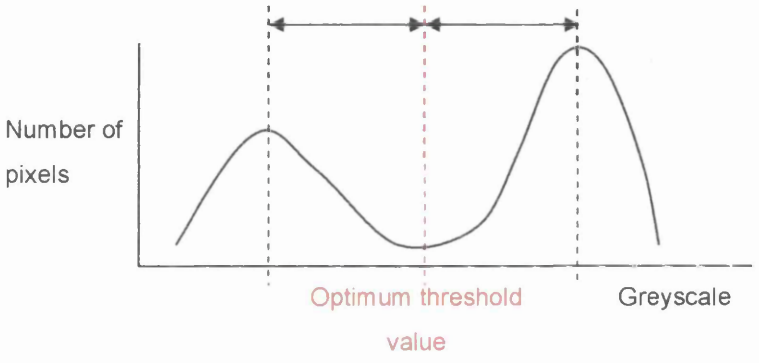

Figure 3.20: Optimum threshold level using the mid point method

Once the image is segmented, measurements may need to be taken to provide the user with information about the image, for example the average width of the line in the image in Figure 3.17. The final part is the interpretation which is the analysis of the raw data collected to gain some useful information about the image, in this case, the line that is being measured.

3.4.4 White light interferometry for three dimensional measurement

In order to measure the line film thickness, a tool needs to be able to measure a three dimensional profile of a surface. Image analysis was investigated in previous works to

study the effect of ink height on absolute greyscale by measuring three lines of known heights [4]. Although the lines had different heights, they exhibited the same minimum lightness value. Thus, it was impossible to distinguish between lines of different height using image analysis. It was also not possible to produce a three-dimensional profile of the line from its optical properties because the ink density does not change linearly with ink film height [24]. Figure 3.21 illustrates the effect of ink film thickness on ink density where the ink density tends to reach a plateau with increasing ink film thickness. This means that any optical method would have a reduction in accuracy as the height increased.

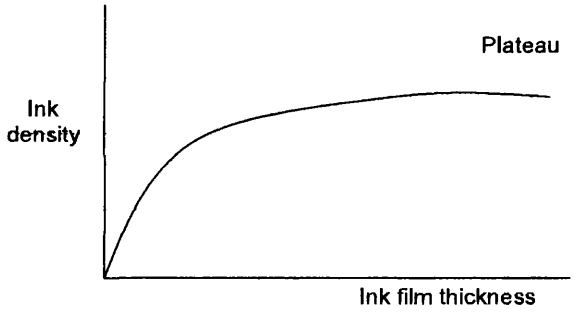

Figure 3.21: The relationship between ink film thickness and ink density [25]

White light interferometry was found to be the most suitable method and was chosen for measuring the three dimensional profile of printed lines, including line film thickness as well as line width [4]. Other methods such as scanning microscope which is only capable of measuring the sample two-dimensionally, diamond stylus that is a contact method which would damage the sample surface and atomic force microscope

(AFM) has very high resolution (nano-scale) but incapable of measuring the printed line width of 300 microns, are not that suitable. White light interferometry is a non contact method so the samples would not be damaged and could be re-measured if necessary. White light interferometry allows measurement of a large sample within a short period of time, while still maintaining a high resolution in all dimensions. Similar techniques to those used in the image analysis can be used to segment and measure the image obtained to gain a profile of line width and height.

3.4.5 The WYKO white light interferometer

The WYKO NT-2000 white light interferometer was used to produce the surface topography profiles of printed lines, Figure 3.22. It contains three objective lenses of 5x, 20x and 50x external magnifications and three internal magnifications of 0.5x, 1.0x and 2.0x, providing a large range of possible sample magnifications from 2.5x to 100x. The vertical resolution of WYKO white light interferometer is 3nm. Figure 3.23 shows a schematic diagram of a typical interferometer set up. A white light beam emitted by a high temperature stable Tungsten bulb is filtered and passed through an interferometer objective to the sample surface. The beam splitter splits the light into two separate beams, one beam is directed towards the sample surface and one beam is directed towards a reference surface. The beams reflected from the surface and the reference surface, are then recombined to form interference fringes of the surface of the sample which are then analysed by WYKO Vision 32 software to produce a graphical output display representing a contour map of a surface [26].

The WYKO NT 2000 can be operated in two scanning modes, phase-shifting interferometry (PSI) or vertical scanning interferometry (VSI). PSI is reliable for resolving surface heights when the fringe pattern is sufficiently sampled. However, it is limited to the measurement of fairly smooth and continuous surfaces as only a small measurement range is possible where the vertical range of PSI is 160 nm. To determine the profiles of rougher surfaces, vertical scanning interferometry (VSI) techniques was used. It has an operating range of approximately 500 microns, making it suitable for the measurement of image carriers and printed images in this study. The basic interferometric principle of VSI is similar to PSI, except the degree of fringe modulation, or coherence is measured instead of the phase of the interference fringes. Table 3.2 illustrates the operational difference between PSI and VSI scanning modes.

Figure 3.22: WKYKO NT-2000 white light interferometer

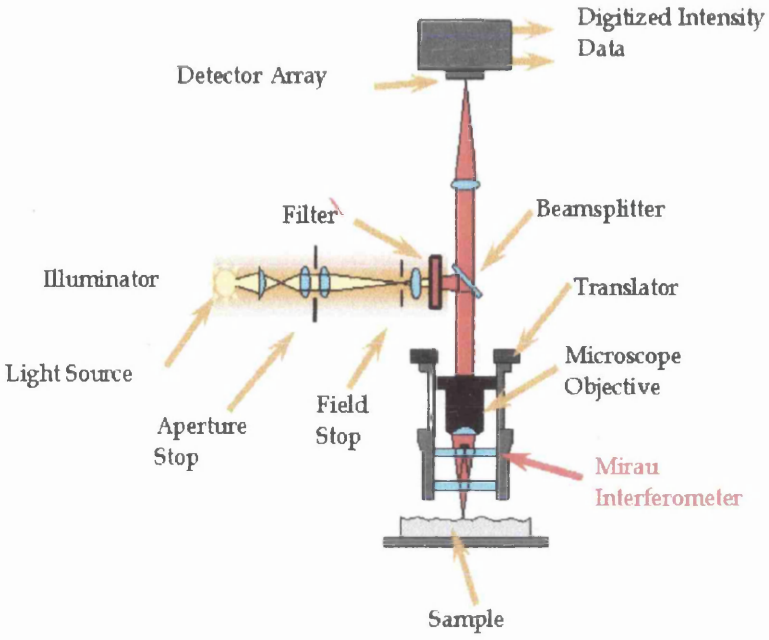

Figure 3.23: A schematic of an interferometer [25]

PSI	VSI
Narrow bandwidth filtered	Neutral density filter for white light
Phase-shift at a single focus point – the objective does not move	Vertically scans – the objective actually moves through focus
Phase data processed from the intensity signal to calculate surface heights	Fringe modulation data processed from the intensity signal to calculate surface heights
Vertical range of 160 nm	Vertical range of 500 μm
Vertical resolution of 0.3 nm	Vertical resolution of 3 nm
Shorter measurement time per image (3s)	Measurement time per image is 10s

Table 3.2: Operational differences between PSI and VSI [26]

3.4.6 Measurement of line profile

In the print trial, six prints were produced where the second and third prints of each run were measured to examine the repeatability of the process using white light interferometer (WLI). The process of choosing the suitable printed images is described in Chapter 6. Individual lines were measured in the horizontal, diagonal and vertical directions at 10.0x magnification. The resolution of WLI used is tabulated in Table 3.3.

Both width and height of the line were determined using 2-dimentional analysis where a 2-point cursor is placed across the surface of line. The line is shown in convex shape where the width was measured by taking the distance between the edges of the convex line, Figure 3.24. The line height was measured by the difference between the line top and substrate in Figure 3.25. Three images were taken for each line direction and analysed using LineWCPC code, giving approximately 1200 measurements of width and thickness per line. On average, the standard deviation obtained was as low as ± 4.5% (as presented in Chapter 6) which can be considered statistically reliable.

Parameter	**Resolution**
Maximum measurement area	614 × 470 μm
Minimum measurement area	0.01 μm^2
Lateral (X)	0.8342 μm
Lateral (Y)	0.9792 μm
Vertical (Z)	< 0.0010μm

Table 3.3: Measurement resolution of white light interferometer at 10x magnification

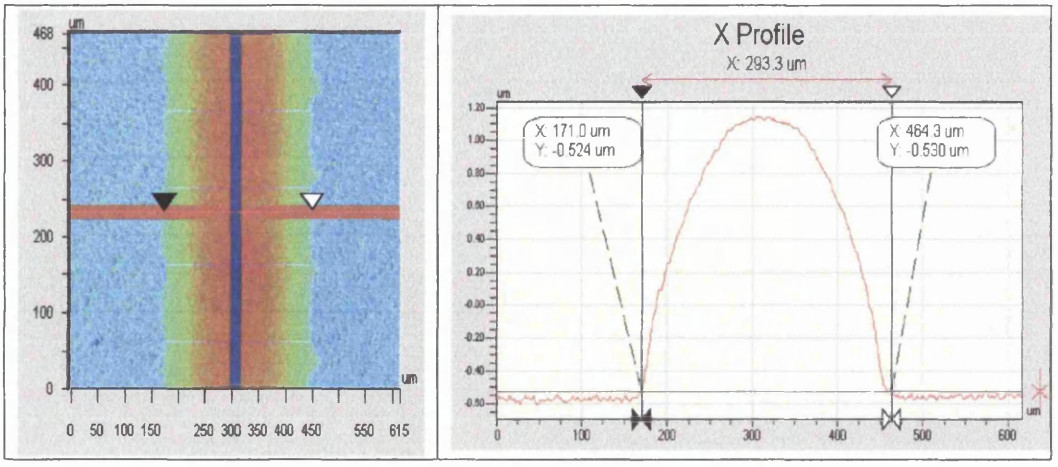

Figure 3.24: Example of line width analysis

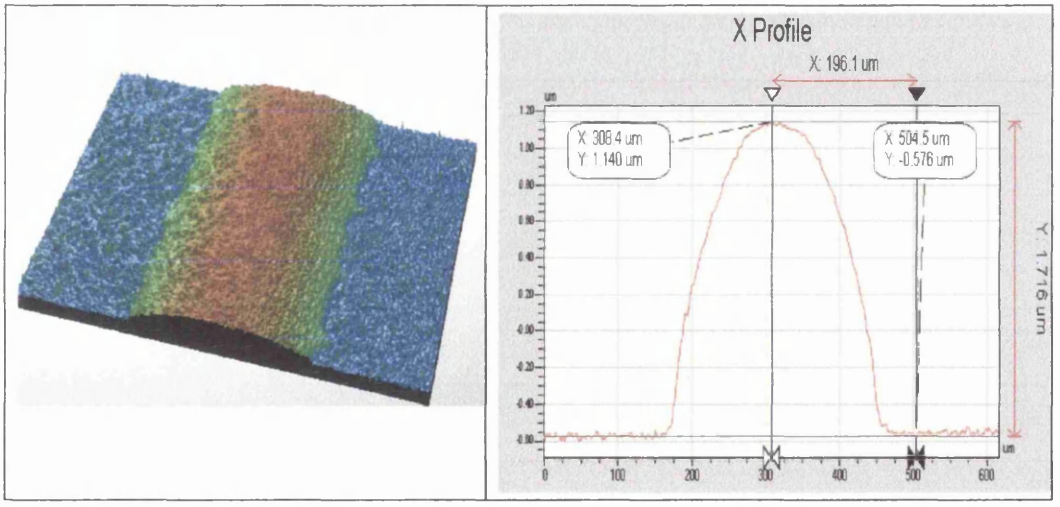

Figure 3.25: Example of film thickness analysis

3.5 Analysis methodology

3.5.1 Introduction

This section describes the background and basis of the orthogonal array (Taguchi) experimental technique which has been applied on the investigation of parameter effects on printed fine line characteristics using screen printing process.

3.5.2 Line profile analysis

A scaffold cannot be completely solid as cells need to grow within it, thus parallel lines of biopolymer ink were printed instead of in the form of sheets. After the first layer of parallel lines is laid on the substrate, the next layer of parallel lines could be laid on the previous layer but at an angle of 90°. By repeating the procedure, a 3D structure of bioscaffold is then constructed (Figure 3.26). The spacing between lines of repeated layers constitute to the pore size which is an important characteristic of bioscaffolds for tissue engineering applications. The interconnectivity between pores could be achieved by ensuring the printed lines are continuous and adhere to the previous layers. The pore size should be in the range of 5 – 10 times the size of the cells that will be seeded on it (typically 100 – 300 μm) [27], providing enough space to facilitate the transport of nutrients and removal of waste.

The pore or channel size range is depended individually on the type of tissue growth as cells making up different tissues have different shape of different dimensions. Oh et al. [28] studied the effect of pore size on cell-PCL scaffold interaction. The scaffold section with pore sizes ranging from 380 – 405 μm was favourable for

chondrocyte and osteoblast growth while the 186 – 200 micron range was better suited for fibroblast growth. Moreover, the pore size range of 290 – 310 μm was the most suitable one for new bone formation. This pore size range can change during the cell differentiation and proliferation to form new tissue. The line size can be related to the mechanical stability of the bioscaffold constructed. If the lines are too narrow, they might not be rigid enough to support the 3D structure and the construction may collapse due to the fine lines but large pores (large line spacing) required.

Fine lines of width ranging from 100 – 300 μm with the same range for line spacing were printed in printing trial, i.e. lines of 100 micron width with 100 micron spacing etc. Theoretically, the scaffolds formed by layering these lines at 90° should result in maximum porosity values of 50 – 65% [27]. These printed lines were scanned by WYKO interferometer. The images captured were saved in ascii format files which were analysed by using 3DProfileWCPC version 1.01, a software developed in Welsh Centre of Printing and Coating, Swansea University by Dr. Deganello D. [29] for the measurement of printed lines, engraved cells and plates. This software is capable of extracting profiles for line width, line height and line cross-section with many measurements taken in just 5 minutes. Assuming the line has a rectangular cross section is not a good approximation for fine lines. There is a curved section at the edges of the line profile which affects the area of the line, Figure 3.27. However, the curved section is not taken into account in this investigation as only line width and line height were involved.

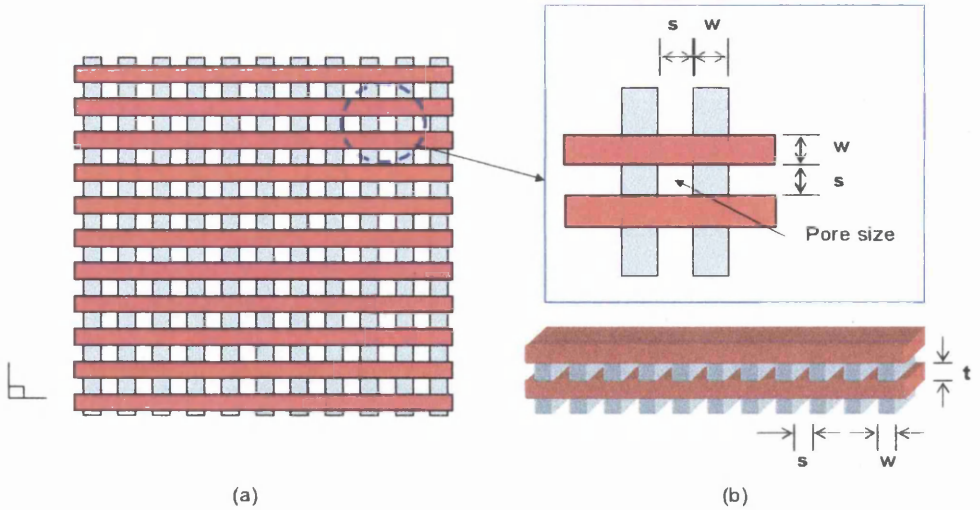

Figure 3.26: Model three-dimensional construct (bioscaffold). (a) Top view: s is line spacing and w is line width. (b) Side view: line height (thickness)

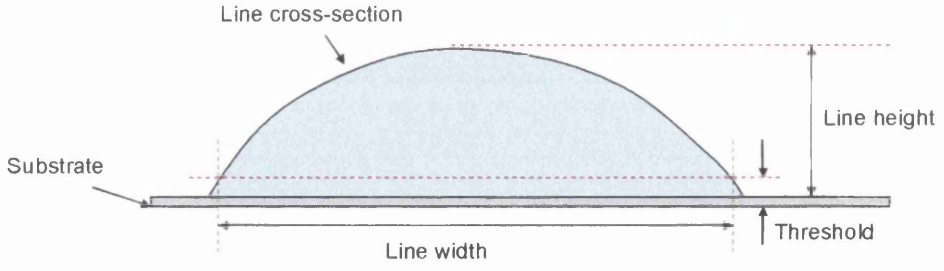

Figure 3.27: A schematic diagram of line profile

Figure 3.28 illustrates the contour plot of printed line. The 3DProfileWCPC software is capable of aligning the substrate surface for a flat substrate surface to avoid anomalies due to the tilted substrate, Figure 3.28(c). If there is a height difference from one side to the other, where height exceeds the threshold value at one side, then the program may not pick up on the end of the line, Figure 3.29. The line width

measured is thus much larger than the actual line width. An optimum threshold level has to be set, not smaller than Ra of the substrate. Ra is the arithmetic mean of the peak height of the substrate roughness. Thus a value of three times the Ra was adopted as the threshold level to ensure that the highest peak height of the substrate roughness was excluded. This value indicates the distance between a peak and valley of the roughness features [30]. If the threshold is below this level then the program may pick up on the irregularity of the substrate rather than the line, Figure 3.30. The area of interest for printed line was highlighted and sectioned into multiple horizontal lines of 1 micron thickness each from top to bottom, Figure 3.28(b). The measurements of line width and height along the printed line was taken and recorded. The data was then exported to MS Excel file. The average of both width and height of lines was calculated and their variations were obtained in terms of standard deviation.

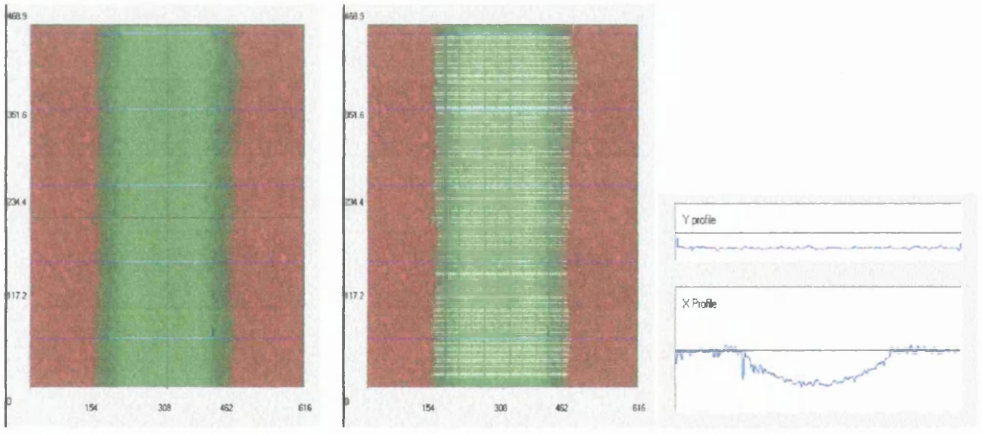

Figure 3.28: 2D contour plot of printed line where red regions represent the substrate and green region represents the line. (a) Line before segmentation (b) Line after segmentation for measurements (c) Substrate alignment on both sides

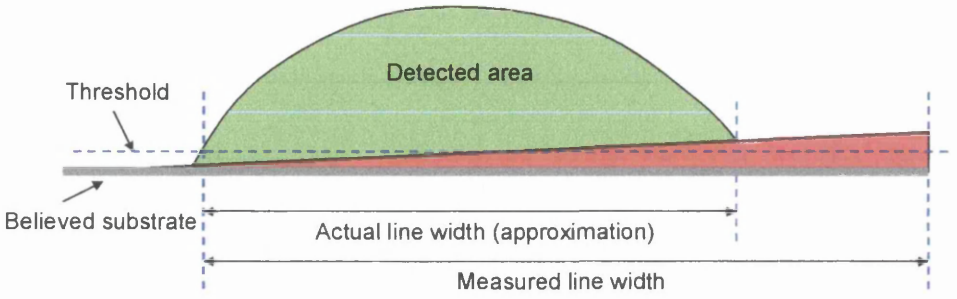

Figure 3.29: Problems of substrate not being flat

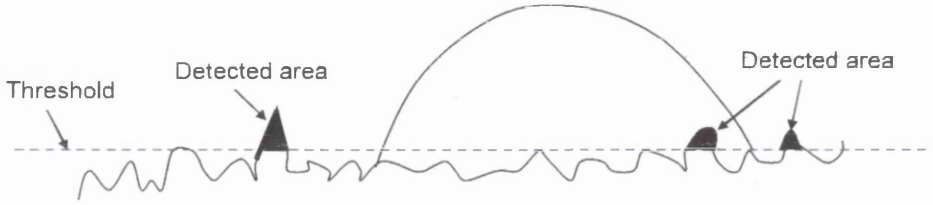

Figure 3.30: Problems of setting the threshold level too low

3.5.3 Orthogonal Array Technique

To optimise the design of a process, it is necessary to identify which factors have the greatest influence on performance, with a minimum number of experiments. The common conventional method is to perform a full factorial experiment which uses every possible combination of parameters by changing one variable at one time while keeping the rest constant. For example, if there are eight variables in a process, seven of them are set to 3 levels and one at 2 levels, and then a total of $3^7 \times 2 = 4374$ experiments are required. Although this method will give a good evaluation of the process, it is often impractical due to the number of tests required.

There are other designs of fractional factorial experiments such as elimination approach and the use of experience to dramatically reduce the parameters have both advantages and disadvantages depending on the application, but in most case these are less efficient or do not cover the full range of combinations of factors. The technique of response surface methodology was first introduced by Box and Wilson (1951) and later developed by Box and Hunter (1957) led to more versatile modelling and statistical optimisation in the 1950's. In the 1970's and 1980's, it was noted that there were limitations in the applications of conventional experimental design techniques for the use of industrial experiments. Genechi Taguchi developed the foundations of robust design [31] which adds a new dimension to conventional experimental design. The robust design method has been found valuable in virtually all engineering fields and business applications.

Orthogonal array is a design of experiment which allowed the independent assessment of each of the factors. The array is a balanced subset of the full factorial experiment where each variable setting occurs for the same number of times. Also, no two experiments are the same or even mirror images of each other. The arrays have been improved and published in a simpler tabular format which is in effect a route map by which the experiment should be performed [32][33]. The factors to be investigated are assigned to appropriate columns and the table displays the level of settings that should be used for each factor in each experiment.

Investigation of a process using orthogonal array technique in the experimental design provides several advantages over conventional methods. It significantly reduces the number of experiments required to fully evaluating a set of process parameters where the example discussed above ($3^7 \times 2$) could be reduced to 18 experiments by

performing one L18 orthogonal array experiment. It can be used to identify any interactions between the parameters studied. The interactions between factors can then be analysed and with certain elements of the arrays or the interactions can be ignored as their effects smeared across all results.

A L8 array which consists of 8 experiments is shown in Table 3.4 and a linear graph of these is shown in Figure 3.31 [31]. The linear graphs created based on the triangle tables, both developed by Taguchi aid in allocating factors and interactions in the array. Considering the two dots of 1 and 2, with the line 3 joining them would indicate that in columns 1 and 2 of the array are placed two variables and the effect of the interaction may be found in column 3. In this case, L8 array is used to investigate the effect of four parameters at two levels each in columns 1, 2, 4 and 7, with the interactions calculated in other columns. All arrays consist of setting each parameter at a number of levels which is depended on the design. Each of the eight experiments is completed, with the parameters set to the levels indicated in the array shown in Table 3.4.

To analyse the array, a result is obtained for each experiment and placed into the quantitative result column which is the way of assessing the effect of changes in the process parameters. In each column, all the results pertaining to level 1 in that column are averaged, and placed into the first row of the result table (indicated Lev1). These averaged results show the effect of level 1 setting of the variable. The results pertaining to level 2 of the column are also averaged. The difference between them is then calculated (Lev1 – Lev2). This is repeated for each column, and the difference provides a value indicating the net effect of changing the variables between the levels which is linked to the column. The interactions can be calculated from columns 3, 5

and 6 in a similar way. Knowledge of the process and possible interactions is essential in the experiment design, allowing for the possible interactions to be detected and not eliminated.

Column	1	2	3	4	5	6	7	Quantitative Result
Factor	A	B	-	C	-	-	D	
Run No.								
1	1	1	1	1	1	1	1	
2	1	1	1	2	2	2	2	
3	1	2	2	1	1	2	2	
4	1	2	2	2	2	1	1	
5	2	1	2	1	2	1	2	
6	2	1	2	2	1	2	1	
7	2	2	1	1	2	2	1	
8	2	2	1	2	1	1	2	
Lev1								
Lev2								
[Lev1-Lev2]								

Table 3.4: Taguchi L8 orthogonal array [31]

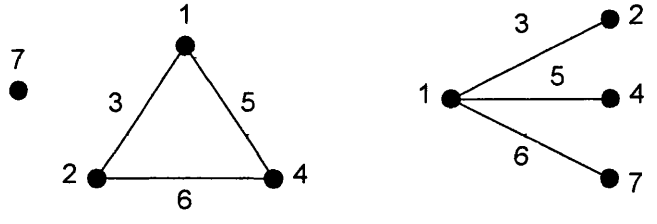

Figure 3.31: Linear graphs for L8 Taguchi array [31]

The orthogonal array technique was used to design the screen printing trial which was performed to investigate and analyse the effect of the process parameters on the printed fine line quality in terms of width and film thickness. The design of print trial used is further detailed and described in Chapter 6.

3.6 Conclusions

This chapter described the printing presses used to print fine lines of biopolymer ink. The instrumentation used to measure the ink characteristics and the printed image was also described. The theory used for rheological measurements was also presented. The software used to analyse the line quality in terms of width and height was included. A brief description of the development of Taguchi method was also presented and the orthogonal array parameter design was introduced.

3.7 Reference

[1] DMP-2800 Jettable Fluid Formulation Guidelines.

[2] Dimatix Materials Printer and Cartridges Datasheet: DMP-2831 and DMC-11601/11610.

[3] Steffe J. F. (1996) Rheological Methods in Food Process Engineering. 2nd Edition, Freeman Press, East Lansing, USA.

[4] Barden T. J. (2007) The application of the three-dimensional profiling to the measurement and characterisation of screen printed fine lines. Phd Thesis University of Wales Swansea.

[5] Ferry J. D. (1980) Viscoelastic properties of polymers. John Wiley & Sons Inc., New York.

[6] Lenk R. S. (1978) Polymer Rheology. Applied Science Publishers Ltd., London.

[7] Ferry J.D. (1980) Viscoelastic Properties of Polymers. John Wiley & Sons, First published in 1961.

[8] User Manual for Bohlin Rheometers Issue 3.0, July 2004, Part No. MAN0329-3.

[9] Van Wazer J. R., Lyons J. W., Kim K. Y., Colwell R. E. (1963) Viscosity and Flow Measurement: A Handbook of Rheology. Interscience, New York.

[10] Rosenthal A. J. (1999) Food texture: Measurement and perception; Van Vliet T. Rheological classification of foods and instrumental techniques for their study: 65-97. Aspen Publishers US.

[11] Rao M. A. (2007) Rheology of fluid and semisolid foods: Principles and applications. Second edition, Springer, New York.

[12] Roger P. W. Surface tension measurements using the drop shape method. First Ten Angstroms, Inc. Portsmouth, VA.

[13] Andreas J. M., Hauser E. A., Tucker W. B. (1938) Boundary Tension by Pendant Drops. J. Phys. Chem. 42: 1001-1019.

[14] Demarquette N. R., Kamal M. R. (1994) Interfacial tension in polymer melts. Polym. Eng. Sci. 34: 1823-1833.

[15] Anastasiadis S. H., Chen J. K., Koberstein J. T., Siegel A. F., Sohn J. E., Emerson J. A. (1987) The Determination of Interfacial Tension by Video Image Processing of Pendant Fluid Drops. J. Colloid Interface Sci. 119: 55-66.

[16] Hansen F. K., Rodsrud G. (1991). Surface Tension by Pendant. Drop. J. Colloid Interface Sci. 141: 1-9.

[17] Hayashi R., Takahashi M., Yamane H. (2000) Measurement of interfacial tension between polymer liquids: Pendant drop, improved imbedded fiber retraction and steady shear flow methods. The Society of Rheology, Japan. 28 (3): 137-142.

[18] Hussain Z. (1991) Digital Image Processing: Practical Applications of Parallel Processing Techniques. Ellis Horwood.

[19] Gonzalez R. C., Woods R. E. (1992) Digital image processing. Addison – Wesley Publishing Group 1992.

[20] Wade A., Fitzke F. (1998) A fast, robust pattern recognition asystem for low light level image registration and its application to retinal imaging. Opt. Express 3: 190-197.

[21] Goatman K. A., Manivannan A., Hipwell J. H. Sharp P. F., Lois N. , Forrester J. V. (2001) Automatic registration and averaging of ophthalmic autofluorescence images. in Medical Image Understanding and Analysis.

[22] Shapiro L. G., Stockman G. C. (2001) Computer Vision. New Jersey, Prentice-Hall: 279-325.

[23] Sezgin M., Sankur B. (2004) Survey over image thresholding techniques and quantitative performance evaluation. J. Electronic Imaging 13(1): 146–165.

[24] Davies E. R. (1990) Machine Vision: Theory, Algorithms, Practicalities. Academic Press.

[25] Kippan H. (2001) Handbook of print media – Technologies and production methods. Springer.

[26] Lamb C., Zecchino M. (1999) WYKO Surface Profilers Technical Reference Manual, Veeco Metrology Group. Version 2.2.1.

[27] Landers R., Pfister A., Hübner U., John H., Schmelzeisen R., Mülhaupt R. (2002) Fabrication of soft tissue engineering scaffolds by means of rapid prototyping techniques. J. Mater. Science 37 (15): 3107-3116.

[28] Oh S. H., Park I. K., Kim J. M., Lee J. H. (2007) In vitro and in vivo characteristics of PCL scaffolds with pore size gradient fabricated by a centrifugation method. Biomaterials 28 (9): 1664-1671.

[29] Deganello D. (2007) Study of ink release from gravure cells using Neural Networks and CFD simulations. Phd Thesis University of Wales Swansea.

[30] Maruyama O., Numata Y., Nishida M., Yamane T., Oshima I., Adachi Y., Masuzawa T. (2005) Hemolysis caused by surface roughness under shear flow. J. Artif. Organs 8: 228-236.

[31] Taguchi G., Wu Y. (1979) Introduction to off-line quality control. Central Japan Quality Control Assoc.

[32] Phadke M. S. (1989) Quality engineering using robust design. Prentice Hall Int. 1989.

[33] Groove D. M., Davies T. P. (1992) Engineering quality and experiment design. Longman Sci. and Tech.

4.0 Rheological Characterisation of Biopolymers

4.1 Introduction

Rheology is defined as the science of deformation and flow of matter[1]. In practice, rheology is principally concerned with extending the "classical" disciplines of elasticity and (Newtonian) fluid mechanics to materials whose mechanical behaviour cannot be described with the classical theories. It is also concerned with establishing predictions for mechanical behaviour (on the continuum mechanical scale) based on the micro- or nanostructure of the material, e.g. the molecular size and architecture of polymers in solution or the particle size distribution in a solid suspension.

This section sets out the results from an experimental investigation into the characteristics of biopolymer inks, in terms of rheological behaviour and surface tension. The rheological properties of a printing ink are key parameters in ink transfer for all printing processes. To assess the feasibility of using conventional printing technology for the printing of fine features for tissue engineering scaffolds, the biopolymer inks (gelatine and collagen) have been developed and characterised rheologically to identify their limits. The rheological tests focus on ink viscosity, viscoelastic and gelation properties. The aim was to screen for increases in the rate and extent of triple-helix formation, and associated gelation, of gelatine in response to

concentration and temperature change. In addition, the dynamic surface tension of the inks has been measured. The results are reported and discussed. An appropriate printing technology is identified for each ink.

4.2 Materials

In this study, collagen Type I (rat tail) stock of concentration 4.35 mg/ml, equal to 0.435 % (w/v) was used. This was supplied by Cardiff University. Rat tail tendons have been a preferred source of collagen Type I due to its high accessibility and homogeneity [2]. The average molecular weight is about 300 kDa. It was diluted with 0.001 mg/ml acetic acid (Sigma-Aldrich, Gillingham, UK) to obtain four concentrations of 0.04%, 0.07%, 0.1% and 0.2% (w/v). For gelatine, a commercial cell culture grade of Type A (acid process pigskin) gelatine with a Bloom strength of 300 (Sigma-Aldrich, Gillingham, UK) was used. The average molecular weight is about 100 kDa. The pH of gelatine solutions was adjusted to 7.0. The biopolymer inks were freshly prepared for each experiment by dispersing the desired mass of gelatine powder at room temperature in deionised water and heating at 60°C in preheated water bath for 45 minutes. Gelatine concentrations used were 1%, 3%, 5%, 7% and 10% (w/v).

4.3 Viscosity Measurements

4.3.1 Introduction

Rheological tests were carried out to identify the flow behaviour of the biopolymer inks. Flow curves were measured where the viscosity was calculated as a function of shear rate to determine whether the inks exhibit non-Newtonian behaviour. The effect of temperature and concentration was also studied. Thixotropic loop tests were

performed to investigate whether the inks were shear history and time dependent. The concentration dependency of the degree of thixotropy was also evaluated.

4.3.2 Simple Direct Stress Test

The flow curves of shear stress against shear rate were measured and the viscosity curves were formed. Both inks were subjected to a range of shear rates at steady rotation. The shear rate was gradually increased from 1 s^{-1} to 100 s^{-1}. The diluted collagen solutions were studied at five different temperatures of 4°C, 8°C, 15°C, 25°C and 35°C. The typical viscosity curves derived for an increasing shear rate for both inks are shown in Figure 4.1 at operating temperature of 35°C to prevent gelling of the sample. Gelation is rarely observed above 34°C regardless of concentration for aqueous gelatine solutions [3] while the diluted collagen solutions would gel at 37°C, hence 35°C was chosen as the operating temperature for most rheological tests. The behaviour of sample at lower temperature of 30°C was also investigated. This temperature was chosen as the sample was more prone to gelling at temperature lower than 30°C.

The aim was to test the biopolymer inks to determine what type of fluid the material is, i.e. the shape of curve in the graph of shear stress and shear rate. The effect of temperature on the material at different concentrations was also determined. Both diluted collagen and aqueous gelatine solutions were expected to show the behaviour of shear thinning fluid.

4.3.2.1 Steady Shear Viscosity

Viscosity is a measure of the resistance of a fluid to deformation under shear stress. It describes the internal resistance of a fluid to flow and may be thought of as a measure of fluid friction. A flow curve, viscosity against shear rate, shows the changes of the structure of sample when subjected to applied shear at different temperatures. The aqueous gelatine solution was observed to transform into gel form during the operation at lower temperature. The sample was then cleaned and reloaded again to minimise the repeatability errors in the results of the test. During printing, the internal structure of the ink will change when the shear rate changes which will be reflected in the change of stress or viscosity.

At a constant operating temperature of 35°C, the typical flow curves for 0.2% diluted collagen solution and 10% gelatine solution are shown in Figure 4.1. Both samples exhibited similar trend of flow behaviour where the viscosity started to decrease when the shear rate was increased from 1 s^{-1} to 100 s^{-1}. This is indicative of a shear thinning behaviour. The viscosity became almost constant in the limit of high shear rates which was above 100 s^{-1} for diluted collagen solution and was lower for aqueous gelatine solution (above 20 s^{-1}). The collagen solutions were found to have significant higher viscosity at a lower concentration with greater decrease rate than that of gelatine solution. This might be due to collagen having higher molecular weight and greater amount of triple helices in solution than that of gelatine. Collagen has an average of 300 kDa whilst 100 kDa for gelatine.

The viscosity is shear rate dependent which is important for good printing. This is because the ink must flow easily into the small mesh cells of the image area on the screen to be able to transfer onto the substrates. The rheological behaviour is strongly dependent on shear rate, which means that great care must be taken when loading the sample as the sample is always sheared, to ensure that the sample was fully recovered prior to testing.

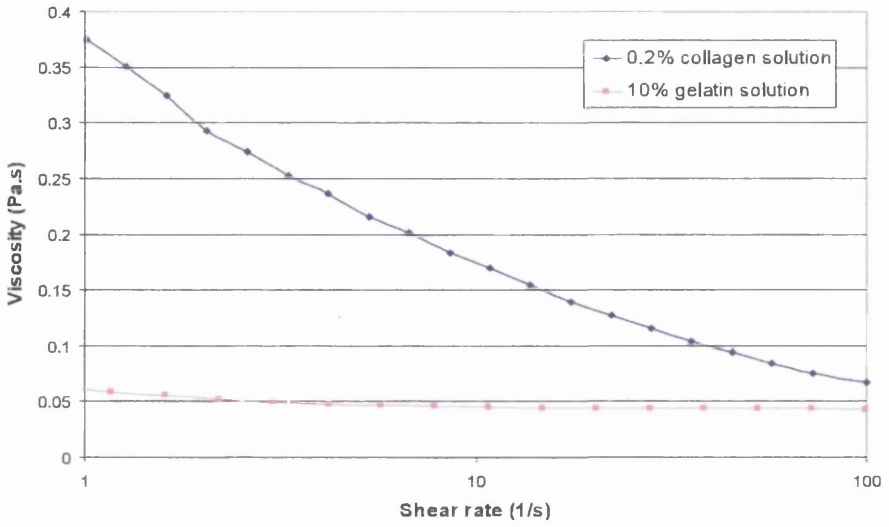

Figure 4.1: Flow curves for biopolymer inks (greatest concentration) at 35°C

4.3.2.2 Variation with Concentration

Concentration refers to the amount of solute dissolved in a solvent. In this case, the collagen stock was diluted by acetic acid whilst the gelatine powder was diluted by deionised water. The flow curves for the inks at 35°C are shown in Figure 4.2, displaying how the change in ink concentration affects the observed flow curves. Similar results occur at temperatures in the range of 35 – 40°C for gelatine concentrations up to 10% (w/v). For low concentration, 1% gelatine solution exhibits a Newtonian behaviour for all shear rates [3][4], but increasing the gelatine concentration leads to the appearance of non-Newtonian behaviour. The viscosity of the 3%, 5%, 7% and 10% w/v gelatine solutions falls as the shear rate increases. This is indicative of a shear thinning behaviour. Similar trend was observed for all diluted collagen solutions, where the viscosity increased with increasing collagen concentration, Figure 4.2(a). The viscosity of diluted collagen solution (at high shear of 100 s^{-1}) was almost doubled when the concentration increased from 0.1% to 0.2%

(doubled). The viscosity is shear rate dependent, but the shear stress versus shear rate curve becomes nearly linear at high shear so permitting an extrapolation to the stress axis. This behaviour is important for good printing, as the ink must flow easily into the small cells of the image carrier during printing.

The viscosity of the sample eventually reaches Newtonian plateau in the limit of high shear rates. Thus, flow curves for both samples show two distinctive regions, namely R1 – shear-thinning and R2 – Newtonian plateau (denoted by the red dashed line), apart from 0.2% diluted collagen solution which exhibits Newtonian plateau at very high shear rate of above 100 s^{-1}. The viscosity in R2 region can be used to identify appropriate printing process as the ink will be subjected to high shear rates during printing. The viscosity increases with an increase in concentration due to an increase in a number of triple helixes. At shear rate of 1 s^{-1}, the viscosity of 0.2% diluted collagen solution increased by about 0.32 Pas comparing to 0.04% collagen solution. The 10% gelatine solution displays about 0.04 Pas increase in viscosity in comparison to 3% gelation solution at shear rate of 1 s^{-1}. The rheological behaviour is strongly dependent on shear rate, which means that after loading, the sample must be pre-conditioned using the software on the rheometer at low shear rate for about 2 minutes.

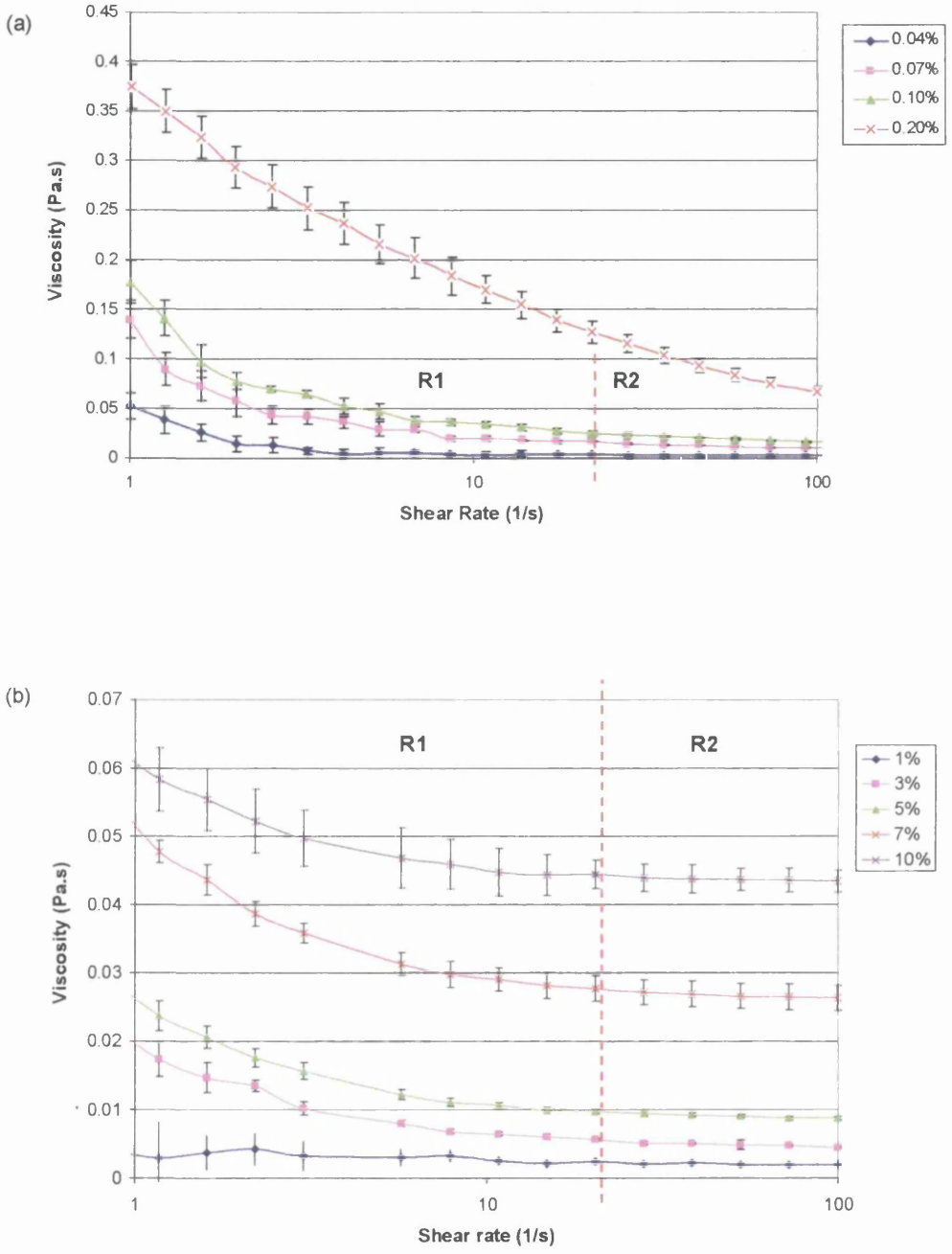

Figure 4.2: Flow curves of (a) diluted collagen solutions and (b) aqueous gelatine solutions at 35°C

The following analysis is focused on gelatine solutions because it appeared to be a better candidate for scaffold fabrication (see section 4.7). However, similar results would be expected for diluted collagen solutions. Two models were used to describe the flow behaviour of gelatine solutions, linear (Newtonian) and power law (Ostwald-de Waele). Since the viscosity of 1% aqueous solutions of gelatine did not vary much with changing shear rate, it was evaluated using a Newtonian Model:

$$\tau = \eta\dot{\gamma} \tag{4.1}$$

where τ is the shear stress, η is the viscosity and $\dot{\gamma}$ is the shear rate.

The power law model is the most widely employed model for non-Newtonian fluids, ideally for shear-thinning, and relatively mobile fluids such as weak gels and low viscosity dispersions. It is used extensively to describe the flow properties of liquids in theoretical analysis as well as in practical engineering applications [5]. This model will fit a typical shear stress against shear rate or viscosity against shear rate curve within the range of about one to a few hundred reciprocal seconds.

The power law model takes the form of:

$$\tau = \mathrm{K}\dot{\gamma}^{n} \tag{4.2}$$

$$\eta = \mathrm{K}\dot{\gamma}^{n-1} \tag{4.3}$$

where K is often known as the flow consistency coefficient. It describes the overall range of viscosities across the part of flow curve that is being modelled. The power law index value, n is known as the flow behaviour index. It can be used to categorise the power law fluids into three different types of fluids as shown below in Table 4.1.

n	Type of fluid
<1	Pseudoplastic
1	Newtonian fluid
>1	Dilatant

Table 4.1: Types of power law fluids based on index n

The concentration effect of gelatine solution of different concentrations at 35°C was examined by using the power model (equation 4.4). The power law model parameters, K and n, together with the correlation coefficient for the trends in Figure 4.2 are tabulated in Table 4.2. Correlation coefficients, R^2 above 0.99 indicate the acceptability of the data fit. For gelatine solutions at all concentrations (except 1%), flow behaviour index (n) was observed to be less than 1 which is again evident that gelatine solutions exhibit shear thinning behaviour. The values of n decrease with increasing concentration of gelatine solutions, accompanied with an increase in pseudoplasticity [5]. As expected, the consistency coefficient (K) increased with the concentration of gelatine solutions.

Sample	K (Pa.s)	n	R^2
3%	0.0191	0.5338	0.95
5%	0.0254	0.4484	0.99
7%	0.0484	0.2480	0.98
10%	0.0599	0.1703	0.99

Table 4.2: Power-law parameters for gelatine solutions at different concentrations

4.3.2.3 Errors

For each test, three to five runs were carried out dependent on the consistency of the results. Errors were calculated in terms of standard deviation because of the inconsistency of the data in runs, shown as error bars in Figure 4.2. The errors found were greater in the low shear rate region. This was probably because of the human errors when loading the sample and the changes of the internal structure of the sample at 35°C for a period of time in the water bath. In high shear rate region, the error obtained can almost be as low as almost zero which is an ideal result. The greater the concentration, the greater the error obtained at the same temperature. This is likely to be due to the greater concentration of the solutions, making it more sensitive to the surrounding temperature.

4.3.2.4 Variation with Temperature

The effect caused by the temperature on the rheological behaviour of both diluted collagen solution and gelatine solution was investigated and the typical experimental results are shown in Figure 4.3 respectively. For both samples, the viscosity decreased with increasing temperature. When the temperature was reduced from 35°C to 4°C, the viscosity of 0.2% diluted collagen solution was increased by 0.8 Pa.s. For 7% gelatine solution, the viscosity was increased by 0.04 Pa.s when temperature was reduced to 30°C. It is the similar trend for 10% gelatine solution, except it exhibits shear-thickening behaviour at lower temperature of 30°C. The strength of cross-linking in gelatine solution had overcome the applied shear rate, increasing the viscosity.

The effect of temperature on ink viscosity in R2 region is shown in Figure 4.4. The viscosity increases with a decrease in temperature for all diluted collagen solutions and gelatine solutions but 1% gelatine solution due to an increase in the number of

helixes. When the temperature increases, the distances between the molecules increases, so the molecules are easier to slip pass each other, thus decreasing the viscosity. At sufficiently low temperatures, gelatine chains undergo a conformational disorder-order transition and form thermoreversible networks by associating helices in junction zones stabilised by hydrogen bonds [7]. It is classically assumed that the cross-linking junction zones consist of triple helix structures as for native collagen (partial collagen renaturation) [8]. The rate and extent of triple-helix formation increase with an increase in concentration. This is reflected in an increase in viscosity.

The viscosity of the low concentration sample only increases slightly when the temperature was reduced. The rate of increase is more pronounced at higher concentrations. Thus, the biopolymer inks are strongly dependent on temperature. If the temperature of the inks was not carefully controlled, large errors can arise. Therefore, great care must be taken to control the operating temperature in order to ensure the print consistency. The solutions were equilibrated to a desired, predetermined temperature prior to viscosity measurements.

(a)

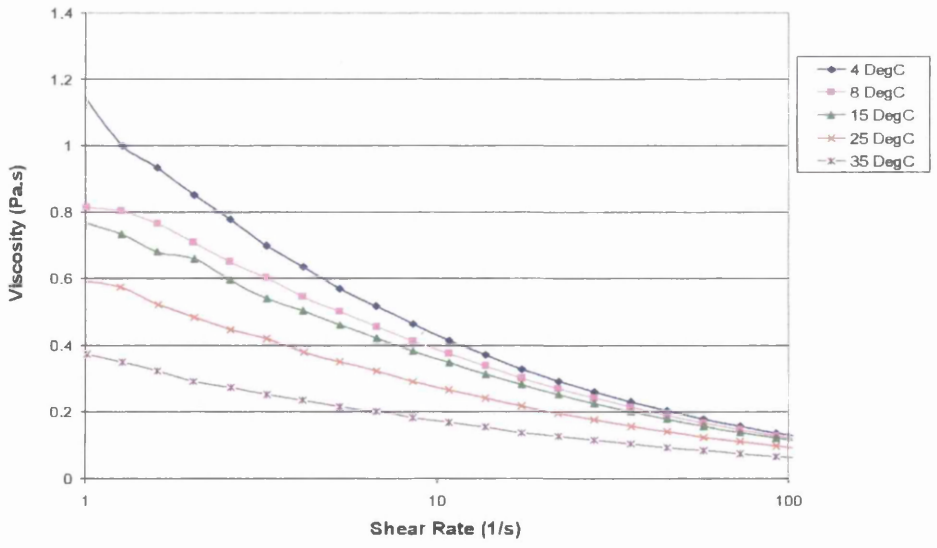

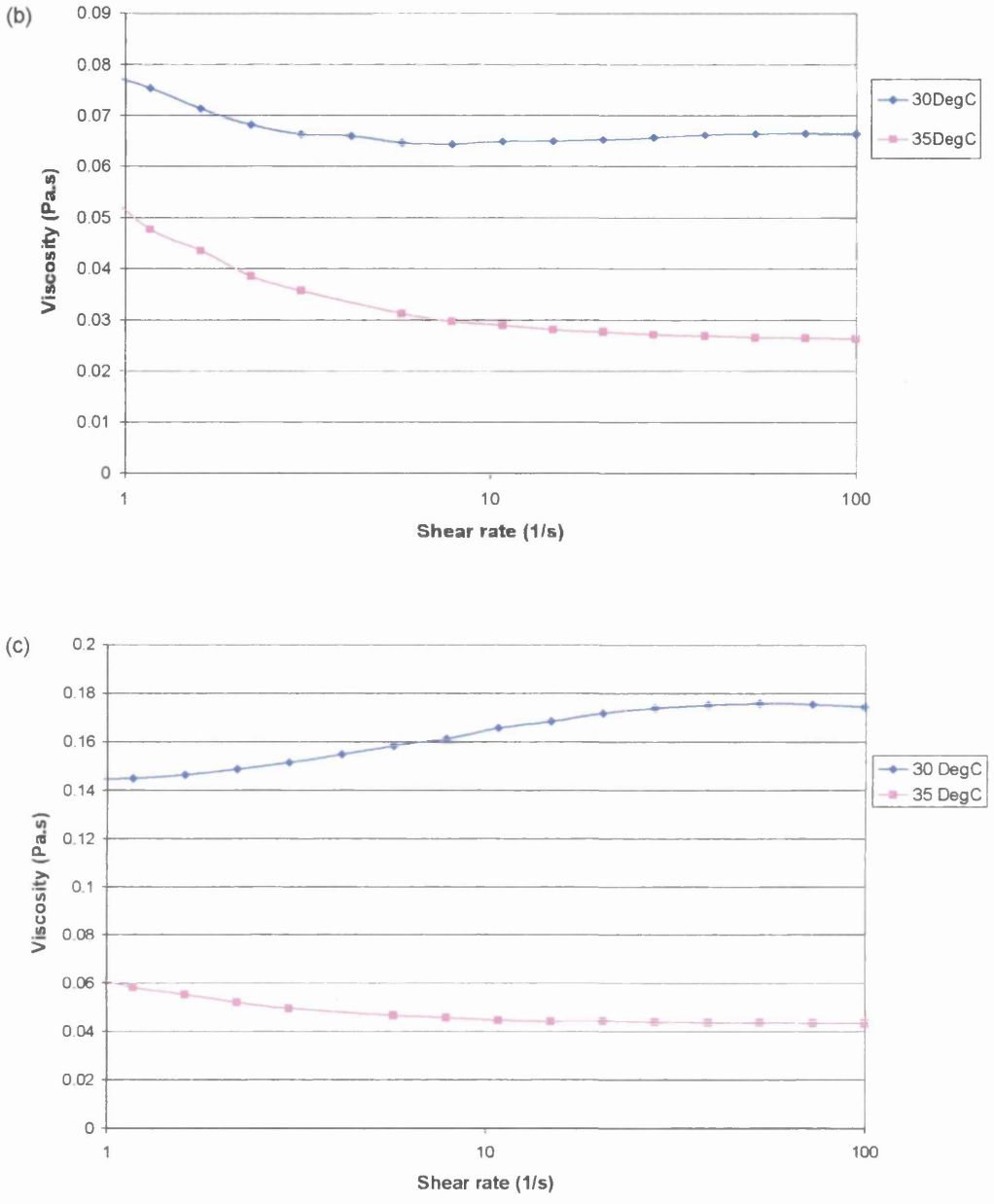

Figure 4.3: The effect of temperature on viscosity for (a) 0.2% diluted collagen solution, (b) 7% and (c) 10% aqueous gelatine solution

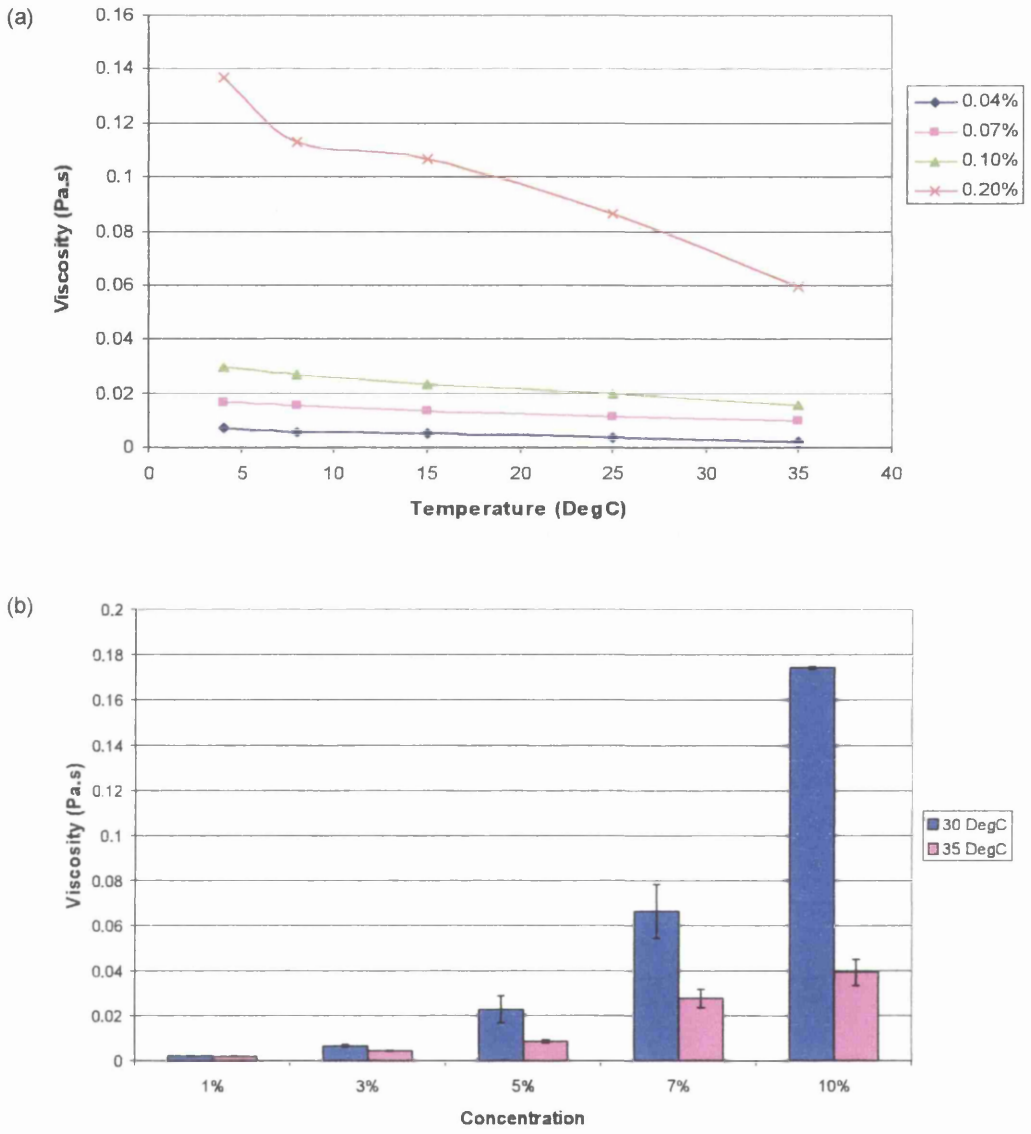

Figure 4.4: Influence of the temperature on the viscosity of the (a) diluted collagen solutions and (b) aqueous gelatine solutions at different concentrations (at a high shear of 100 s^{-1})

4.3.3 Thixotropic loop

The biopolymer inks (only gelatine solutions) were subjected to a range of shear rates. The loop test was performed allowing the increase and subsequent decrease of shear rate within the preset total test time. Firstly, the loop test was carried out in order to investigate whether the shear thinning of the ink is time dependent. Secondly, two more additional tests were performed sequentially on the same sample for a range of test times: 60 s, 120 s and 240 s.

4.3.3.1 Results and Discussions

Thixotropic behaviour describes a degradation of the ink structure during shear loading. When the shear force is applied, a decrease in viscosity with time occurs. The original structure of the ink recovers when the loading is removed. The extent of structure recovery is dependent on the duration of time allowed for the recovery. Therefore, a thixotropic ink exhibits shear thinning behaviour when a gradually increasing shear rate is applied. This is because the orientation of the molecules will change to align with the flow direction. After the external force is removed, the original structure orientation of the molecules will be restored. The break down of the ink structure and its reestablishment when the shearing stress is removed are not instantaneous. As there is a delay in time for the ink structure to recover completely, the rheogram readings were taken at increasing shearing stress differ from those where the shearing stress is being reduced.

A thixotropic (hysteresis) loop, the region between flow curves for the increasing and decreasing ramps, represents the deformation history of the sample and provides qualitative information about its time dependence. The loop area indicates how fast the ink sample structure will recover after the load is removed. The loop area is dependent on the nature of the sample and the length of time that passes after the load

is removed. This test is related to the kinetics of structural change as encountered in aggregated colloidal dispersions.

1% gelatine solution shows a Newtonian behaviour, while 3%, 5%, 7% and 10% gelatine solutions display thixotropic behaviour (see Figure 4.5). As the stress is increased, structure in the ink is reduced (the upper curve in Figure 4.5). When, after reaching the maximum value, the stress is progressively reduced, the lower curve is generated because structure recovery takes much longer. The area in the hysteresis loop may be taken as an indication of the degree of thixotropy existing in the ink. A similar trend was observed for all inks. The degree of thixotropic loop was reduced with increasing concentrations where the 10% gelatine solution has the highest degree of thixotropy followed by 7%, 5%, and 3% gelatine solutions. The rate of recovery was faster at higher concentration where shorter time was required to reach equilibrium state. Thus, the recovery of gelatine solutions is concentration dependent [9].

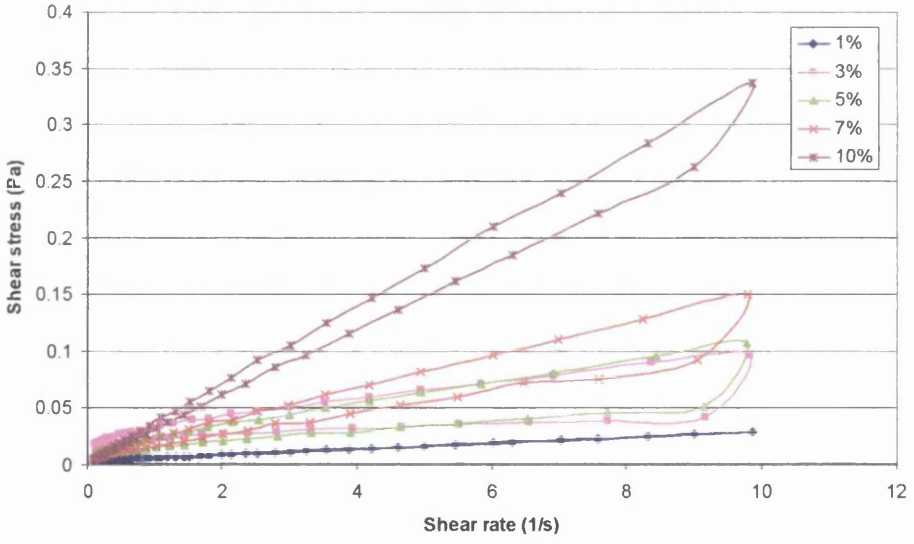

Figure 4.5: Thixotropic behaviour of biopolymer inks, depending on the concentration

To compliment the standard thixotropic loop test, additional tests were performed sequentially on the samples (3%, 5%, 7% and 10% w/v) for a range of test times: 60 s, 120 s and 240 s. A series of three thixotropic loops were generated for each sample, Figure 4.6. For 3% aqueous gelatine solution, the viscosity decreased by 0.11 Pa.s during sequence 1, by 0.007 during sequence 2 and by 0.004 during sequence 3 when being sheared at about 5 s^{-1} at 35°C, Figure 4.6(a). Similar trends are observed for other concentrations which are illustrated by Figure 4.6(b-d). The loop areas decreased in sequence where the reduction between the first and second sweeps is more significant than that of second and third sweeps. The majority of the network structure was disrupted during the first shear sequence and the recovery of the network was slow in such a short period of time. During the second and the third sweeps, the viscosity of the sample was reduced when sheared with an increase in total test time due to its thixotropy nature. The disconnected structure of sample was shown to rebuild back to the initial value more quickly upon removal of shear forces for longer period of time.

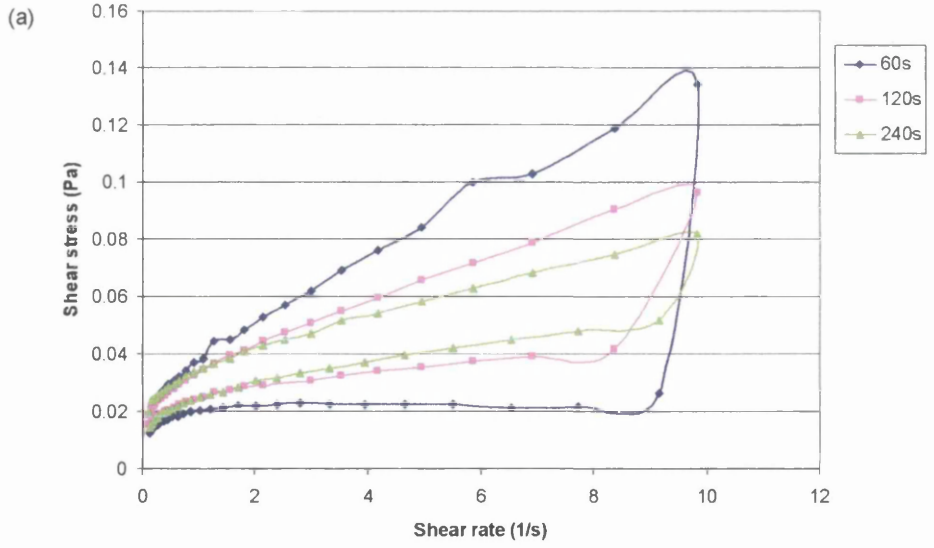

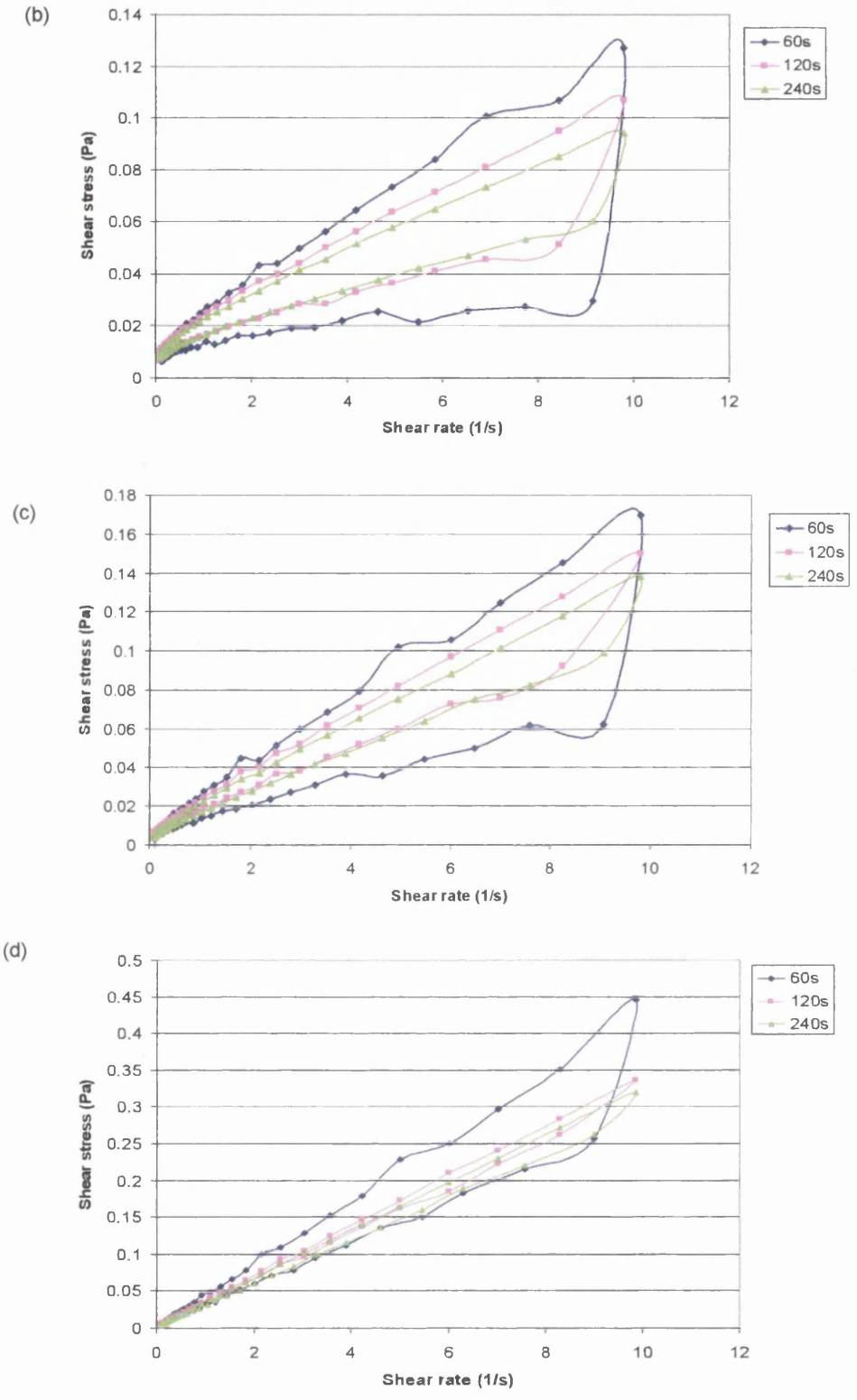

Figure 4.6: Thixotropic loops for gelatine solutions of (a) 3% (b) 5% (c) 7% (d) 10% (w/v) for test times of 60 s, 120 s and 240 s respectively at a temperature of 35°C

In general, shear thinning measures how easily the ink structure can be broken and the loop area indicates the recovery extent of that broken ink structure within a given time. The information obtained from steady tests is valuable in many situations; such as an ink formulation must have proper fluidity during preparation and printing; a certain consistency is required so that the pigment particles can be dispersed effectively in the vehicle during storage and printing or so that ink film can be formed uniformly after application. Therefore, it is important for the disturbed ink structure to rebuild at a suitable rate upon resting in order to have proper ink film formation and sedimentation resistance.

4.3.3.2 Closure

The characterisation of time-dependent rheological properties of printing inks is important to establish the relationship between the structure and flow. All aqueous gelatine solutions (3%, 5%, 7% and 10%) displayed thixotropic behaviour, a time dependent phenomenon and also shear history dependent. Shearing breaks down the loose and interconnecting network within the thixotropic biopolymer ink, resulting in the viscosity drop. Also, the degree of thixotropic loop was depended on the gelatine concentration.

Thixotropy is an important characteristic of printing ink behaviour where the ink viscosity decreases abruptly under the high shear stress during printing. For example, the relatively high viscosity screen ink thins down when being sheared by squeegee, forcing through a fine mesh screen. The reduction in ink viscosity allows the ink to flow during printing, transferring from the image area (i.e. a screen, a roller or a plate) onto a flat substrate where the printed ink dots are able to merge together into a continuous film. When the shear forces are removed, the ink becomes more viscous and gels completely before the ink can spread beyond the boundaries. It is quite

difficult to control the change in viscosity of biopolymer ink not only due to its thixotropic nature but also its gelling behaviour.

4.3.4 Discussion

Both diluted collagen solutions and aqueous gelatine solutions exhibited similar flow of shear thinning behaviour and respond in same manner to concentration and temperature. Gelatine was chosen as the scaffolding material in this investigation because only low concentration of collagen solution can be prepared from native collagen. There are big variations in properties from batch to batch of collagen solutions due to different sources. Furthermore, unlike collagen, gelatine does not exhibit any antigenicity in physiological condition. Gelatine has been widely used for biomedical applications such as wound dressings, adhesive and absorbent pad for surgical use. Hence, the rheological properties of gelatine solutions are discussed below.

When gelatine was dissolved in water, the chains entangle and interpenetrate in constant motion due to the Brownian randomising force between their segments. The flexible chains change and fold their conformations constantly. With water as the solvent, the chain in gelatine is enveloped in a sheath of water molecules that solvate its functional groups. The water molecules are hydrogen-bonded to the amide groups of polypeptides. These water molecules prevent the chain segments that are in proximity from attracting and touching one another through intermolecular interactions such as hydrogen bonds and van der waals forces. When the gelatine solution is sheared, the chains start to deform. At higher shear rate (during printing), the structure of molecules is more oriented where the free water molecules between the chains enable the chains to slip past one another and move more freely, hence lower viscosity was observed.

By increasing the gelatine concentrations, the amount of water molecules are reduced, thus lowering the hydration of dissolved macromolecules which reduce the sheath of hydration separating adjacent chains. When the hydration is low, the chains tend to attract one another via intermolecular forces which are weak and reversible. It should be noted that hydrophobic bonding is an important contribution to the interchain between polypeptide chains even in solution.

Generally, the majority of inks used in printing industry exhibit pseudoplastic (shear thinning) behaviour where the inks will flow by the high shearing force during printing. In this study, it has been shown that aqueous gelatine solutions exhibited shear-thinning behaviour, an important requirement of printing ink, at all concentrations except 1% gelatine solution due to its very low concentration. 1% gelatine solution was determined to be Newtonian fluid at 35°C because its viscosity is almost independent of the shear strain rate. This can be explained by its composition of 99% water that makes it behave more like water. The intra and intermolecular forces formed between molecules are very weak, thus the resistance to flow is very small that can be neglected. This result in the viscosity remains almost constant with shear rate.

At high shear rate (say 100 s^{-1}), the viscosity of gelatine solutions was measured. This provides useful information in choosing the suitable printing technology according to the allowable viscosity range of inks. Aqueous gelatine solutions of 1% to 5% concentrations are applicable to inkjet printing, allowing a viscosity range up to 0.1 Pa.s. At room temperature, the viscosity of gelatine solutions will increase significantly due to gelation process. The wide viscosity range of printable inks for flexographic printing (0.1 – 10 Pa.s) and screen printing (0.1 – 40 Pa.s) makes these two processes suitable to print gelatine solutions of higher concentrations: 7% and 10%.

Another important requirement of printing inks is that most practical fluids in printing and coating exhibit some degrees of thixotropy. Aqueous gelatine solutions were time and shear history dependent where the viscosity decreases with the time taken to increase the shear rate. However, the deformation of the polymer structure and its recovery upon the removing of shear stress are not instantaneous, the rheogram readings taken at increasing shearing stress differ from those where the shearing stress is being reduced. The intra and intermolecular interactions of gelatine solution were reduced when high shear rate was applied, resulting in low viscosity readings. After the maximum value was reached, the stress gradually decreased and the lower curve generated because the structure recovery takes much longer time.

The complication of thixotropy arises because this reversible, microstructural change takes time due to local spatial rearrangement of the components. This frequently found time-response of a microstructure that is itself changing with time makes thixotropic, viscoelastic behaviour one of the greatest challenges facing rheologists today, in terms of its accurate experimental characterisation and its adequate theoretical description [10].

4.3.5 Conclusion

The rheological behaviour of the biopolymer inks is strongly dependent on shear rate, temperature, time and shear history. In comparison to diluted collagen solutions, it is possible to print aqueous gelatine solutions as biopolymer inks by optimising the gelatine concentration corresponding to the operational temperature with its application to suitable printing processes. These tests are only a part of the complete rheological characterisation of the ink systems. Thus, dynamic oscillation tests were performed in the next section to reveal the microstructure and viscoelastic properties of aqueous gelatine solutions.

4.4 Monitoring Gelation Mechanism by Dynamic tests

4.4.1 Introduction

Although rotational tests give information on flow properties such as steady shear flow and recovery tests, these are only a part of the complete rheological characterisation of the ink systems. Dynamic oscillatory testing is a more robust tool to examine the structure of a viscoelastic material and is therefore more useful from a practical point of view. Oscillatory tests provide information about the structure and elasticity of the inks, and can be used to determine storage stability.

Since the bio-polymer inks are thixotropic, they are likely to show viscoelastic behaviour. Thus, dynamic oscillation measurements were performed to explore viscous and elastic behaviour of biopolymer inks over a range of shear strain rate, duration, and frequency. The effect of concentrations on viscoelastic behaviour of biopolymer inks was also being investigated.

4.4.2 Strain sweep test

A dynamic strain sweep test was utilised to establish the linear viscoelastic range of the aqueous gelatine solution for performing subsequent dynamic tests. If the viscoelastic behaviour is non-linear, the analysis of the data is very difficult because the stress and time anomalies are combined. In the dynamic strain sweep, the sample was subjected to a sinusoidal oscillation at a fixed frequency of 1 Hz over a range of strain levels. The strain was gradually increased from a low value of 0.001 s^{-1} to a high value of 100 s^{-1}. The storage modulus G' and loss modulus G'' were calculated as a function of strain.

Figure 4.7 represents a typical linear viscoelastic range for 10% gelatine solution at 30°C. At low strains, G' and G'' increased with strain with slight fluctuations in G'

due to low torque. As the strain was increased, a range of points was observed where both G' and G'' vary insignificantly, indicating linear viscoelastic behaviour (denoted by two red parallel lines below). Beyond this range, both G' and G'' start to drop indicating the shear thinning behaviour. The behaviour of aqueous gelatine solution is changing from mostly solid-like to fluid-like as the shear strain is increased.

The maximum strain up to which G' remains constant is called the critical strain which indicates the minimum energy required to disrupt the ink structure. In dynamic tests, a sinusoidal shear strain smaller than the critical value is imposed on the ink. The trend observed for the 1%, 3%, 5% and 7% gelatine solutions during the strain sweeps were consistent with those observed for the 10% gelatine solution. The linear viscoelastic range was determined to fall within the shear rate region of 0.05 s^{-1} to 0.7 s^{-1}. A strain shear rate of 0.1 s^{-1} was therefore used in performing all dynamic tests such as time sweep, temperature ramp, and fourier transform mechanical spectrometry (FTMS) tests.

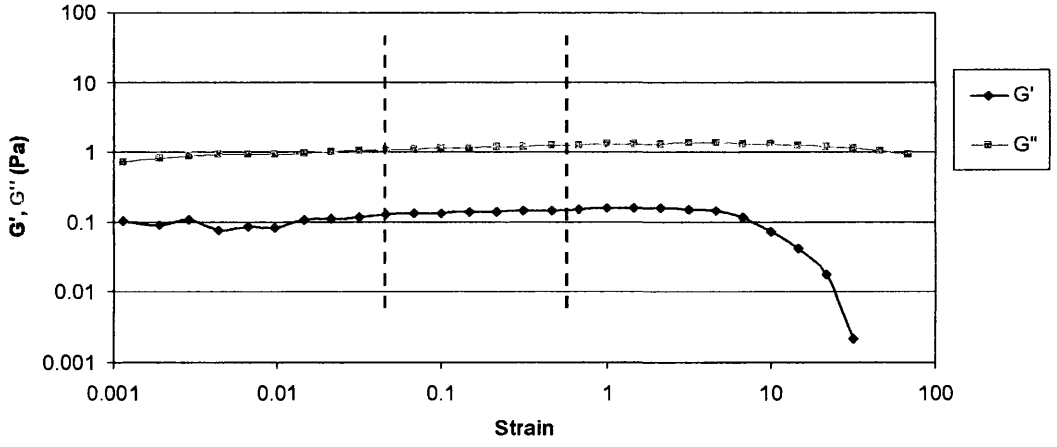

Figure 4.7: Typical LVR of 10% gelatine solutions at a temperature of 30°C

4.4.3 Time sweep test

Dynamic time sweep test was performed to monitor the buildup or breakdown of the structure of gelatine in aqueous solution (5%, 7% and 10% w/v). The sample was subjected to a sinusoidal oscillation at a fixed low frequency of 1Hz and strain level of 0.1 s^{-1} (as determined in the dynamic strain sweep test) to ensure linear viscoelastic behaviour for a given amount of time (about 1000 s). A constant operating temperature of 30°C was maintained throughout the tests. The storage modulus G' and loss modulus G'' were continuously recorded during the time sweep. G' and G'' were calculated as a function of time, representing the elastic and viscous behaviour of the biopolymer inks.

The kinetics of hydrogel formation of gelatine has been studied using rheology. Figure 4.8 shows the development of G' and G'' modulus for 5% and 7% gelatine solutions. G' was found to be always smaller than G''. This indicates that the viscous property of gelatine is stronger than the elastic property where the gelatine has more fluid like behaviour. The structure build-up in gelatine is reflected by the increase in G', corresponding to an increase in the amount of energy dissipated as heat, representing by the viscous portion G''. Figure 4.9 shows the development of G' and G'' over time for the 10% gelatine solution. Phase displacement angle can also be used to define the dynamic properties of viscoelastic materials. A phase angle of 0° means purely elastic behaviour and an angle of 90° shows only viscous behaviour. As the gelatine in the ink began to aggregate, the G' versus time curve became concave and the average slopes increased during 500 s then remained straight. The G'' versus time curve remained straight. Both G' and G'' increase over time due to the triple helix formations. The transition from sol-to-gel is also reflected in a reduction in a phase angle. At the beginning the G'' is greater than G' indicating that the ink displays more fluid-like viscoelastic behaviour. After approximately 720 s, a crossover point of G' and G'' was observed with a phase angle of about 45°, indicating the occurrence of phase transition from sol-to-gel [11]. At this instant the

triple helix formation starts and the development of a 3D network effectively extends throughout the entire sample. Beyond this point, G' is greater than G'' indicating that the ink displays more solid-like viscoelastic behaviour.

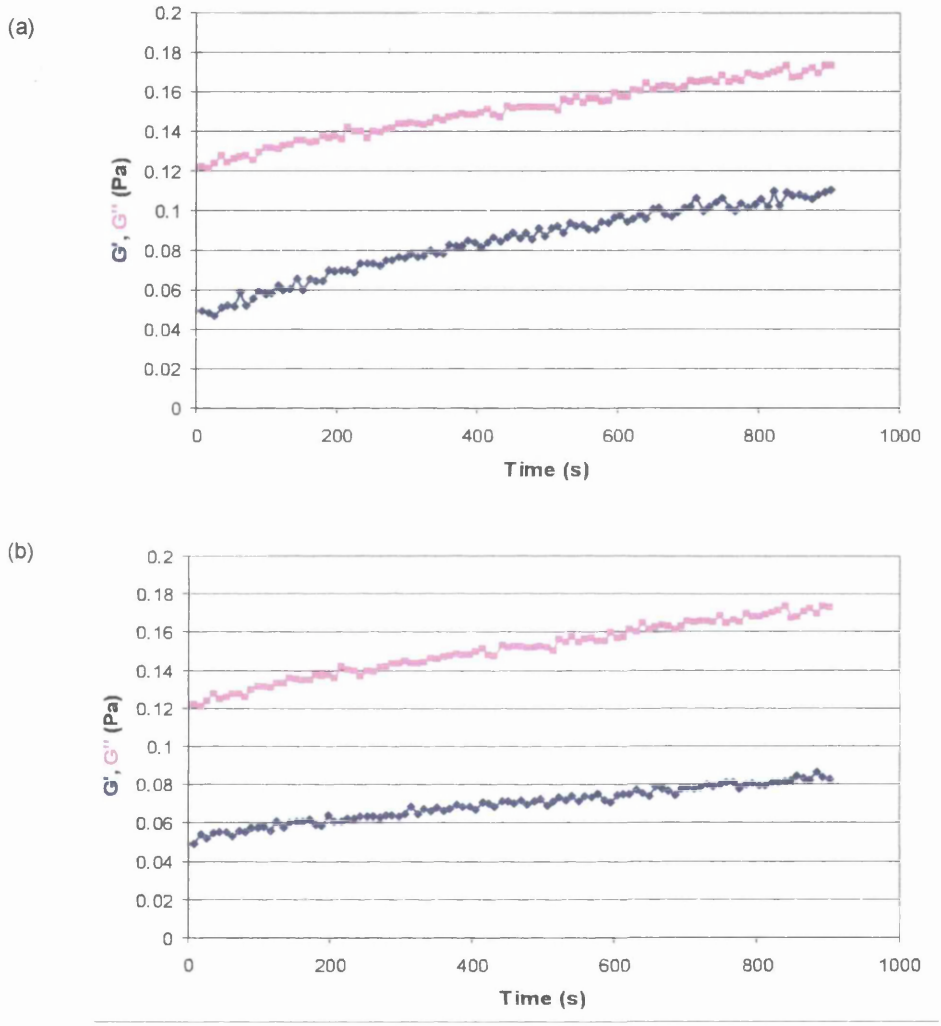

Figure 4.8: Typical development of G' and G'' modulus for (a) 5% (b) 7% gelatine solution at 30°C at constant frequency of 1 Hz at a fixed strain level of 0.1 s^{-1}

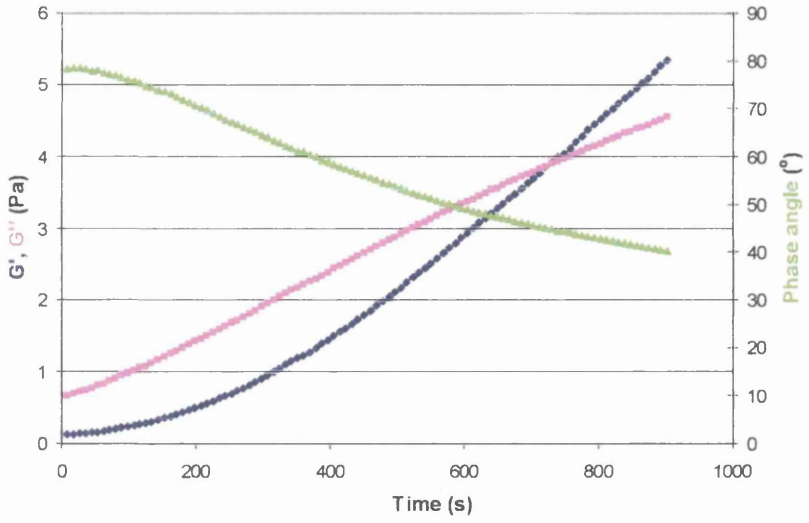

Figure 4.9: Typical development of G' and G'' modulus for 10% gelatine solution at 30°C at constant frequency of 1 Hz at a fixed strain level of 0.1 s^{-1}

The effect of gelatine concentrations on G' and G'' is shown in Figure 4.10. Both elastic and viscous modulus of biopolymer inks increase with an increase in gelatine concentration. The rate of triple helix formation and development of a 3D network is significantly higher for 10% gelatine solution as opposed to 5% and 7% gelatine solutions. G' and G'' increase with time which indicates structure build-up in all gelatine solutions. Thus, all inks display time dependency.

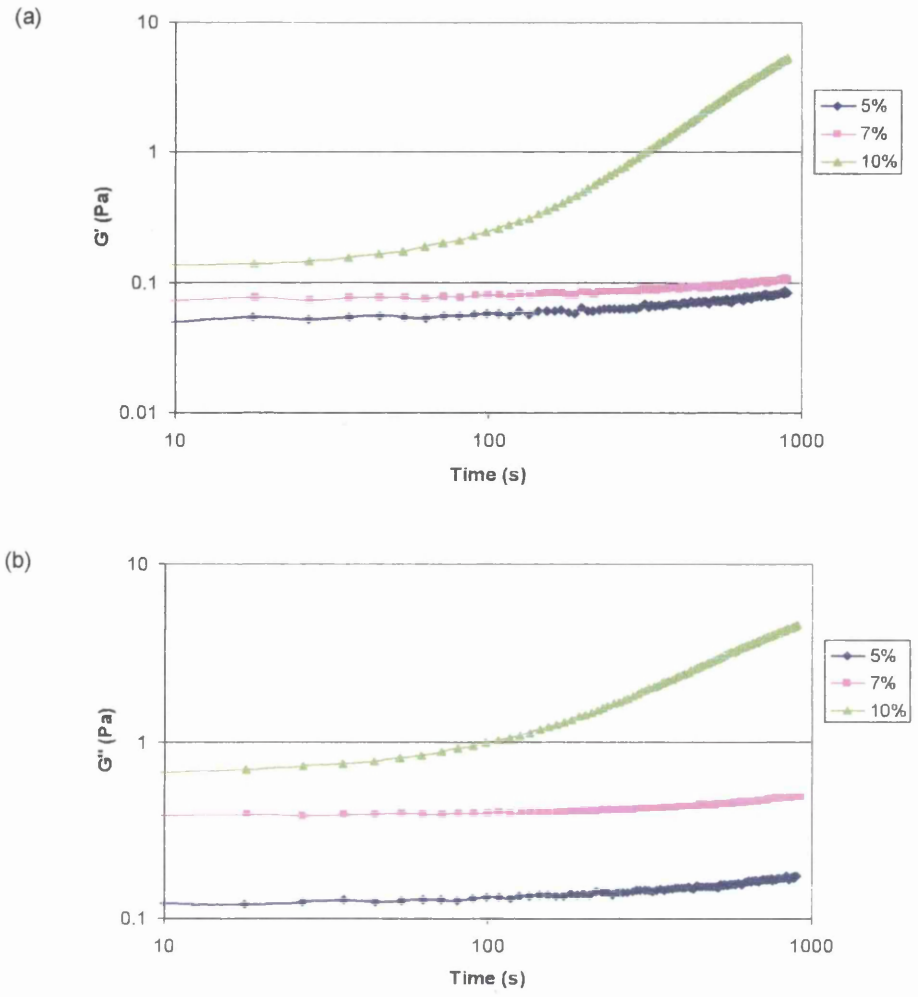

Figure 4.10: (a) Storage modulus G' and (b) loss modulus G'' of 5%, 7% and 10% aqueous gelatine solutions at 30°C

4.4.4 Temperature ramp

According to Tung and Dynes [11], the gel point can be identified and located by monitoring the dynamic viscoelastic parameters throughout the reaction. They pointed out that the crossover of the storage modulus G' and loss modulus G'' occurs in the vicinity of the gel point. Hence, the temperature range where both G' and G'' intersect can be taken as an indication for the gelation temperature.

In this case, temperature ramp was carried out on aqueous gelatine solutions of different concentrations: 3, 5, 7 and 10% w/v. The gelatine solutions were cooled from 40°C to 10°C, at a rate of 2°C/min in order to determine the temperature range that gelation starts. The oscillating applied strain was 0.1 at 1 Hz frequency. The change in G' and G'' was recorded. The gelling temperature range was determined from there G' and G'' crossover during the cooling period using a similar method as described by Gudmundsson M. [12] and Michon and et al. [13]. The results are presented below.

4.4.5 Results

Hydrogel formation is characterised by development of a 3D network, an increase in the molecular weight and a reduction in the mobility of the system. This reduction in mobility will finally trap the system. The proceeding of the hydrogel formation can be characterised by the T_{gel}, which is the temperature where the 3D gel network starts to percolate the whole system. Therefore, the T_{gel} is an important criterion for the development of the hydrogel microstructure. Several methods are currently in use to measure T_{gel} [14]. In this study the storage modulus, G' and the loss modulus, G'' during cooling were studied in order to determine the T_{gel} of the inks. The T_{gel} was determined by the G'- G'' crossover temperature method [11][15].

Figure 4.11 displays G' and G'' values as a function of temperature in 3%, 5%, 7% and 10% gelatine solutions. Inks were cooled slowly, while G', G'' and phase angle, δ were continuously measured. The temperature at which tan δ = 1 (G'= G'') is defined as T_{gel}. The crossover point of G' and G'' indicates the phase transition from sol-to-gel. Beyond the crossover point, all inks display more solid-like property with G' greater than G''. For 3% gelatine solution, the gelation temperature range was between (17.5 ± 0.5)°C where G' and G'' crossover at a gelation time of

approximately 11 min, Figure 4.11(a). The gelation temperature of 5% gelatine solution was found to be in the range of (21 ± 1) °C, Figure 4.11(b). 7% gelatine solution started to gel between (24 ± 1) °C which is shown in Figure 4.11(c). 10% gelatine solution gelled in shortest time out of all which was about 7 min, in a temperature range of (26 ± 0.5) °C, Figure 4.11(d).

The T_{gel} increases with an increase in gelatine concentration. The opposite is observed for the gelation time. It decreases with an increase in concentration from 660 s down to 420 s. Thus, inks with higher gelatine concentration gelled within shorter time at higher temperature in comparison to those of lower concentration. It has to be noted that T_{gel} obtained by this method would underestimate T_{gel} for low concentration inks more than for high concentration inks [14]. Thus, the rate of ordering and gel formation of biopolymer inks is concentration-, temperature- and time-dependent. The trends observed during the temperature ramps were consistent with those observed by other researchers [16]. The onset of ordering and helix formation in gelatine hydrogel is close to 40°C [17]. The T_{gel} and gelation time can be used to optimise the process parameters during printing trials.

(a)

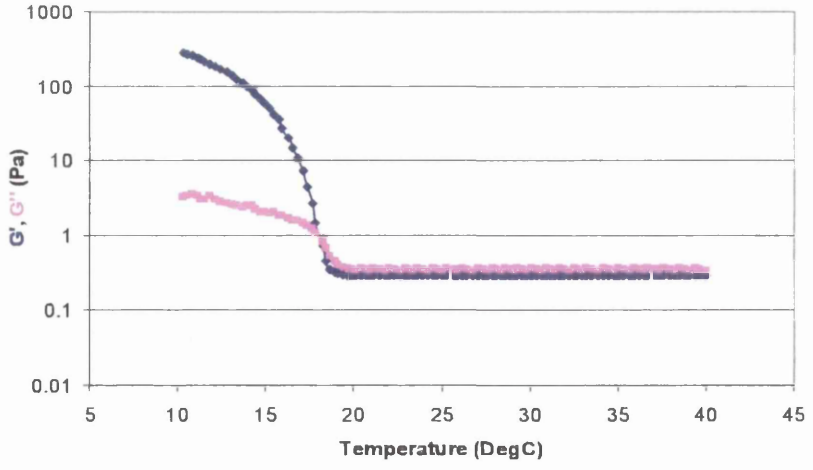

(b)

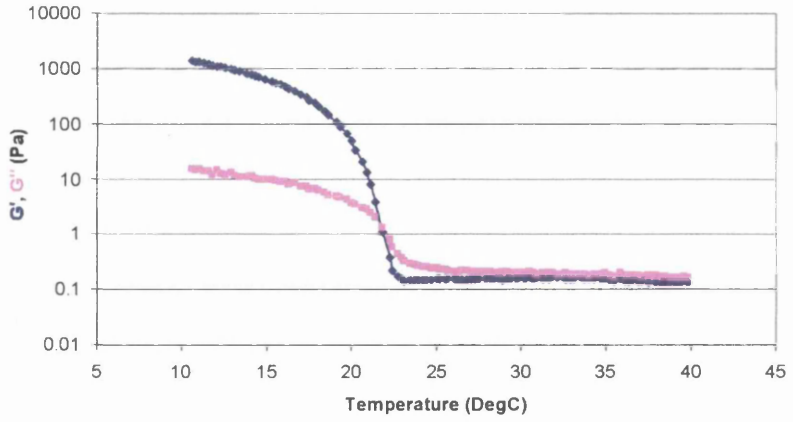

(c)

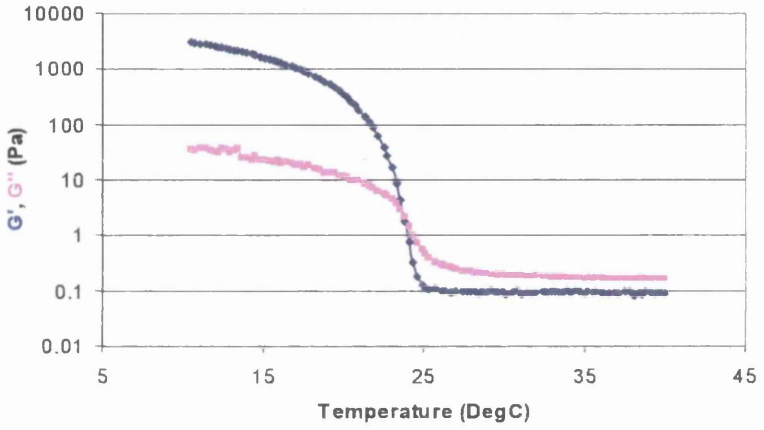

(d)

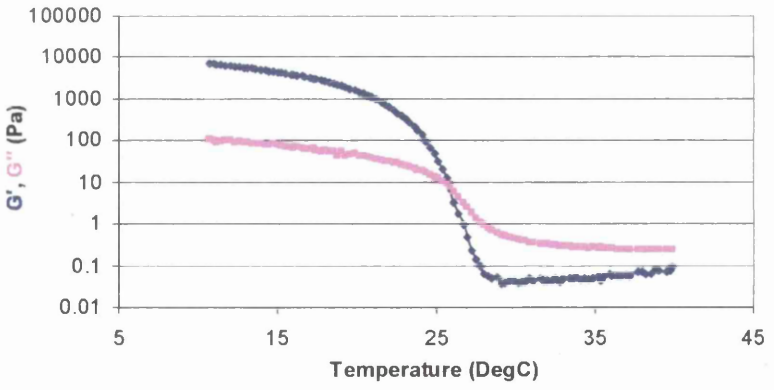

Figure 4.11: Cooling profiles of G' and G'' moduli for (a) 3%, (b) 5%, (c) 7% and (d) 10% (w/v) gelatine solutions

4.4.6 Discussion

Gelatine powder dissolves in warm water and exists as flexible random coils in aqueous solution [18]. These random coils move freely among the water molecules. Gelatine solutions can be diluted or concentrated. The difference is that there is only intramolecular interaction between the dissolved coils in dilute solution, Figure 4.12(a). In semi-dilute or concentrated solutions, intermolecular interactions are formed when the chains are forced to approach each other due to the increase of gelatine molecules as shown in Figure 4.12(b). By cooling the gelatine solution, the envelope of water of hydration surrounding adjacent gelatine chains becomes too sparse to prevent interchain attractions. The formation of single helices from the random coils segments of gelatine chains begins, and eventually leads to triple helix formation. Gelation is motivated by the formation of a continuous three dimensional network of chains attached to one another via physical cross-linking.

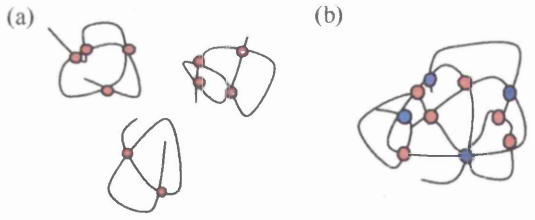

Figure 4.12: Schematic diagram of random coils with (a) intramolecular interactions (red circles) in dilute solutions and (b) both intra- and intermolecular interactions in concentrated solutions [18]

Tung and Dynes [11] suggested that the crossover of the storage modulus and loss modulus marked the transition from liquid to gel. However, the point at which the storage modulus exceeds the loss modulus can be a function of frequency and is

readily observable in the liquid phase of many polymer fluids not containing an extended network [19]. The crossover of G' and G'' can be observed in uncrosslinked polymers at the onset of the plateau zone due to the presence of entanglements [20]. Thus, the crossover point of G' and G'' cannot be universally assigned as the gel point. In this case, the temperature ramp tests were used only for a simple indication of the temperature range where gelation occurs. This is useful in implying that the temperature should be applied in FTMS test in section 4.5 for different concentrations. It can also be used as a reference to the operational temperature of the printing trials later in the following chapters 5 and 6.

Figure 4.13 shows that the gelation time decreased exponentially while the gelling temperature increased, when the concentration of gelatine solutions was increased. This is because of gelatine solutions of higher concentrations having greater amount of amino acids per volume which bring the molecules closer to each other. Hence, the polypeptides chain can be formed more quickly within the solution during the process of cooling, reducing the gelation time. Gelatine solutions of low concentrations are less viscous with more water molecules than amino acids, so it takes a longer time for polypeptides chain to form.

The storage modulus G' is used to evaluate the gel strength of gelatine formed and to make comparisons of the gel strength as a result of changing the concentration of the gelation solutions. The strength of gel is directly related to the concentration of the amino acids available to form peptide bonds that constitutes the gel structure. The higher the concentration of the gelatine solutions, the greater in strength of gelatine formed, indicated by the increase in G' values of gelatine solutions at the crossover region, Figure 4.14.

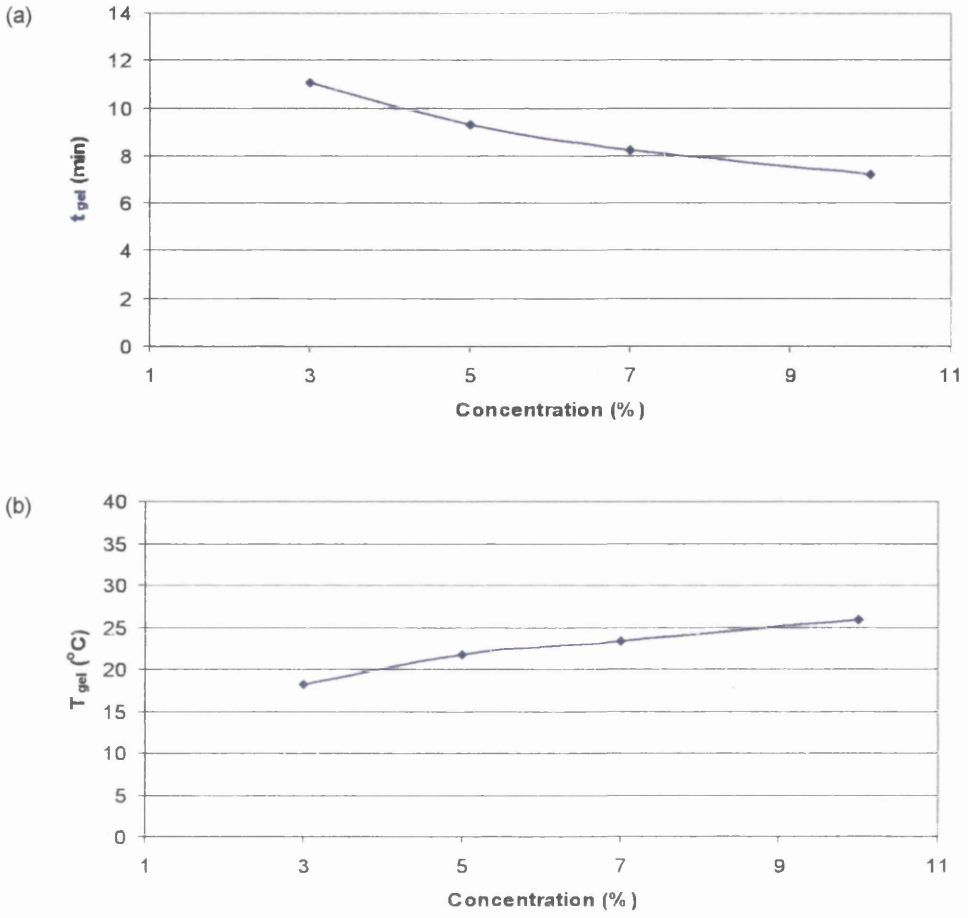

Figure 4.13: The effect of concentration on (a) gelation time (min) (b) gelation temperature

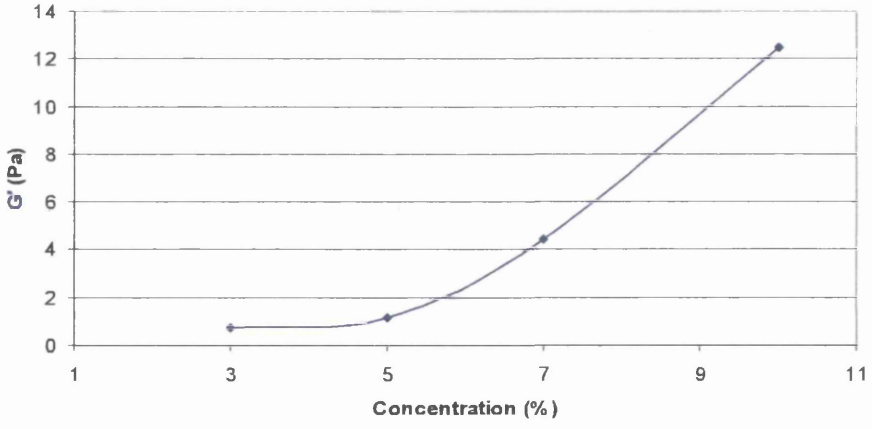

Figure 4.14: Variations in G' values during gelation with concentration

4.4.7 Summary

This section investigated the effect of concentration of gelatine on gelation time and gelation temperature. The increase in concentration from 3% up to 10% reduced the gelation time required from 11 minutes to 7 minutes and the gelation temperature was increased from approximately 17°C to 26°C. This is due to the amount of gelatine molecules being increased with increasing concentration.

It is important to determine the temperature range that the gelation of aqueous gelatine solutions occurred. However, it will be more accurate if the gel point of gelatine solutions can be identified. Multi-Waves' test is a more reliable method to more clearly and precisely locate the gel point as described in the next section.

4.5 Gel Point Determination

4.5.1 Introduction

The determination of the precise gelation point at which a material passes from bulk behaviour from that of a liquid to a gel is not a simple procedure [21]. This section describes the rheological methods developed by Winter and Chambon [22] in order to detect gel points from oscillatory shear measurements. It is based on the observation that gel point is conveniently located by identifying the occurrence of a frequency independent loss tangent tan δ according to Winter-Chambon Gel Equation. The material changes from one which exhibits viscoelastic liquid-like beaviour, through gel point, to one which exhibits viscoelastic solid-like behaviour. It is given by

$$\tan\delta(\omega) = \frac{G'(\omega)}{G''(\omega)} \qquad (4.4)$$

The phase angle δ can be represented by equation below

$$\delta = \frac{\alpha\pi}{2} \tag{4.5}$$

where α is defined as the relaxation exponent, $0 \leq \alpha \leq 1$.

This method gives a single value for the relaxation exponent α from the tan δ relationship at the transition point. The values of α approaching 0 indicate a rigid or strongly elastic gel while α values close to 1 indicate a more viscous gel.

4.5.2 Fourier transform mechanical spectrometry (FTMS)

The Bohlin Gemini HR nano Rheometer was used to perform oscillatory shear measurements in a Multi-Waves' or a frequency-multiplexed mode known as Fourier transform mechanical spectrometry (FTMS)[23][24]. The FTMS test has an advantage that a response can be measured instantaneously as a function of the frequency, and thus the response is not influenced by the timescale of test as in the ordinary dynamic frequency sweeps. It is also advantageous for testing a gel transition material that requires speedy testing because its structure may change during the test. Besides, this oscillatory shear technique satisfies the requirement of negligible mutation number, N_{mu} where the rheological properties of the sample are assumed to be stable throughout the whole period of imposed oscillatory deformation[25].

Three concentrations of 5, 7 and 10% aqueous gelatine solutions were investigated at a constant operating temperature of 26°C which was determined by temperature ramp tests in previous section. The tests were repeated for 7 and 10% solutions at slightly higher temperature of 28°C to investigate the effect of temperature on gel point. The FTMS tests consist of a total of five harmonics frequencies, a fundamental frequency of 0.2 Hz and four additional harmonics of 0.4, 0.8, 1.6 and 3.2 Hz were employed,

with reference to previous works done by Hawkins K. et al. [25]. They were designed to operate in a time sweep mode so that the entire gelation process of aqueous gelatine solutions was monitored. The sample was tested in the linear viscoelastic response regime by applying a strain level of 0.1 which was previously determined in strain sweep test.

A 55 mm diameter acrylic parallel geometry with a gap of 150 microns was chosen due to its high sensitivity. The sample was carefully loaded onto the lower plate of the rheometer and being sealed by low viscosity silicone oil to prevent evaporation of the sample. Prior to each test, the sample loaded was cooled rapidly from 40°C to desired test temperature. The rheological measurement was then started once reaching the test temperature which was kept constant throughout the test.

4.5.3 Results and Discussions

The resulting plots of phase angle δ versus time are presented in Figure 4.15. The results of FTMS tests are summarised in Table 4.3, in terms of the time taken to achieve gel point, t_g, and the frequency independent phase angle δ registered at gel point. The corresponding values of relaxation exponent α were calculated and the range of storage modulus, G' and loss modulus, G'' at gel point was also recorded over the frequency range.

Inks (w/v %)	Temperature	Gel time		Phase angle at gel point		Storage modulus at the Gel Point	Alpha
	T (± 0.1°C)	t_g (s)		δ_{av} (± 0.5°)		G'_{av} (± 0.06 Pa)	α_{av}
		Mean	S.D	Mean	S.D		
5	26	199	61	65.6	0.4	0.02 – 0.6	0.72
7	26	83	8.3	63.7	0.8	0.05 – 0.8	0.71
7	28	544	15	66.0	1.3	0.06 – 0.6	0.73
10	26	37	8.0	60.1	0.6	0.40 – 2.4	0.67
10	28	119	7.5	62.2	0.4	0.29 – 2.4	0.69

Table 4.3: FTMS for gelatine solutions of 5%, 7% and 10% for five frequencies: 0.2, 0.4, 0.8, 1.6 and 3.2 Hz

For 5% solution, the gel point is located in the FTMS test, Figure 4.15(a) after 199 s with a phase angle δ of (73 ± 0.5) ° which corresponds to a relaxation exponent α of 0.72. A gelation time of 83 s was determined for 7% solution with δ = (63.7 ± 0.5) ° which corresponds to α = 0.71, Figure 4.15(b). The gel point of 10% solution was identified in a gelation time of only 37 s with a lower value of δ = (60.1 ± 0.5) °, corresponding to α = 0.67. As expected, when the concentration of solution increased, the gelation time was reduced significantly at constant temperature. At higher temperature of 28°C, the gel point of 10% solution is indicated in Figure 4.15(c) after 119 s with a higher value of δ = (62.2 ± 0.5) °, corresponding to α = 0.69. At higher temperature, the gelation occurs much more slowly due to the difference in the hydrolysis and condensation rates of sol-gel reaction. Figure 4.16 illustrates the corresponding values of the storage and loss modulus, G' and G'' respectively, over time during the gelation of 10% solution at 28°C. Both values of G' and G'' increased

over time implying the build-up of gel structure which is gradually solidified beyond the gel point.

In these experiments, the corresponding values of α were found to be close to 0.69. These findings are in agreement with an earlier study [26], which reported that under conditions of appropriately low sample mutation number, the relaxation exponent α falls between 0.64 and 0.72, a range consistent with theoretical treatments reported in previous studies done by Michon et al. [13].

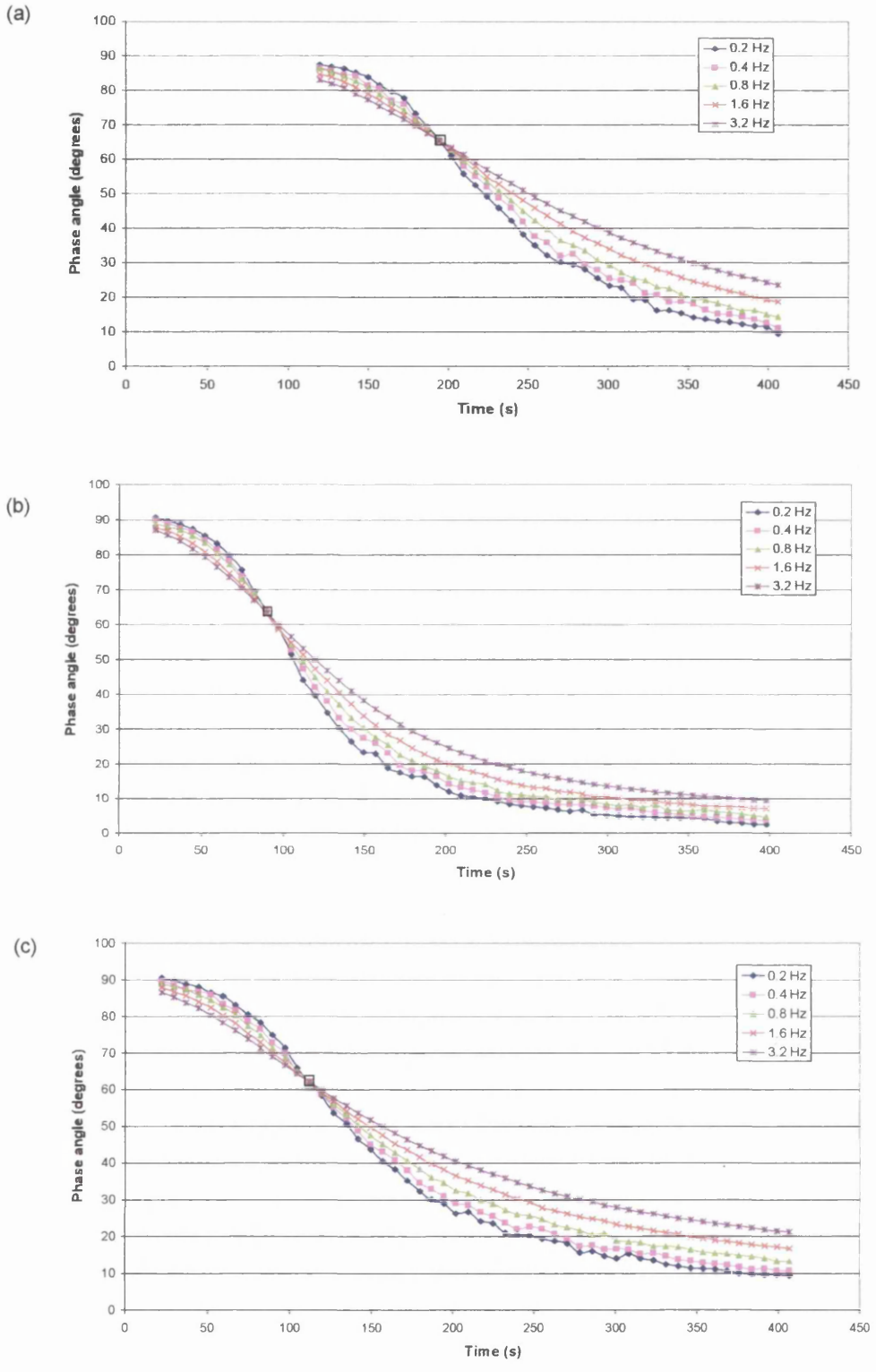

Figure 4.15: Results of FTMS tests for gelatine solutions. (a) 5% gelatine solution at 26°C; (b) 7% gelatine solution at 26°C; (c) 10% gelatine solution at 28°C

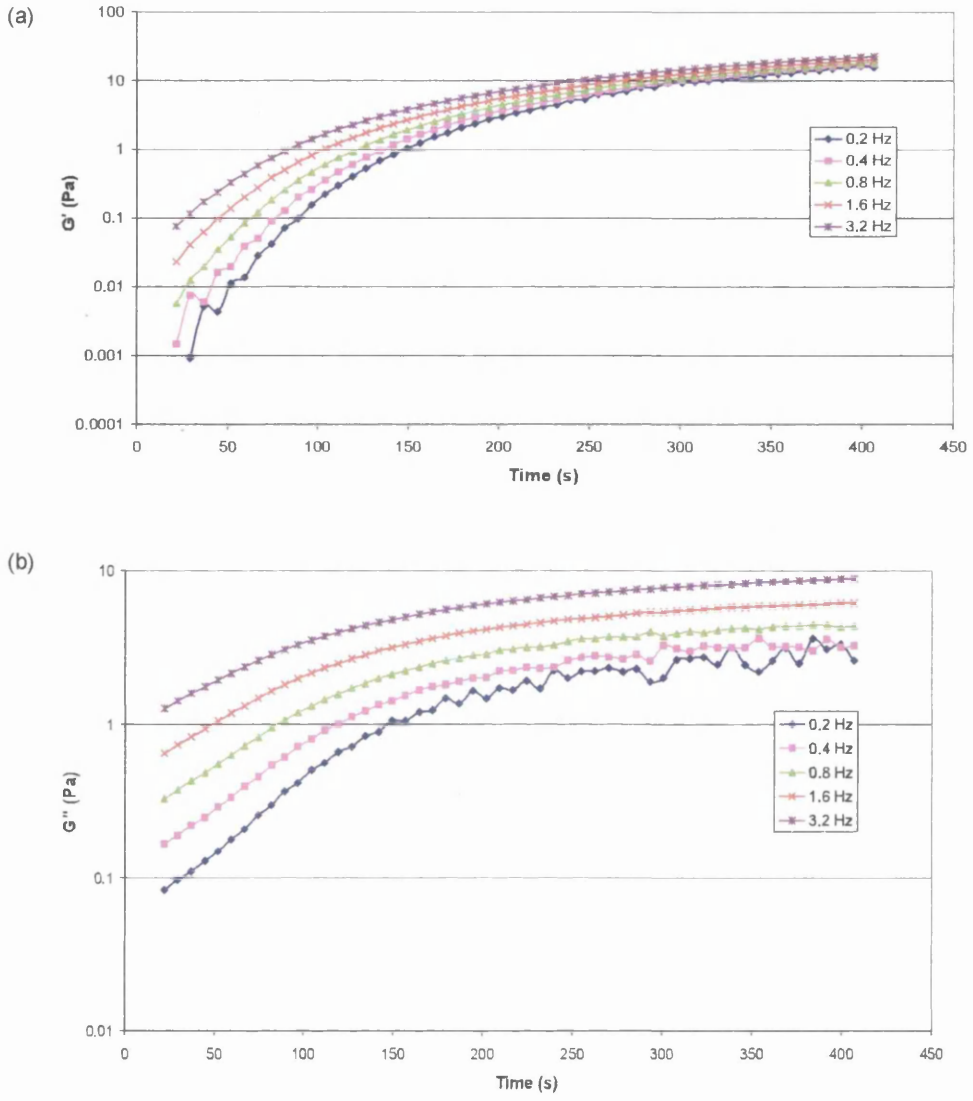

Figure 4.16: (a) Evolution of the storage modulus G' during the gelation of 10% gelation solution at 28°C (b) Evolution of the loss modulus G'' during the gelation of 10% gelation solution at 28°C

4.5.4 Closure

The experiments reported in this section, which were performed over a range of gelatine concentrations and an elevated temperature, give gelation times as low as 37 s up to 544 s. The gel points were identified and corresponded to the values of relaxation exponent α within the range of 0.67 and 0.72. The α values are temperature and concentration independent. In addition, the influence of the gelatine concentrations and temperature on gelation time has been studied. An increase in gelatine concentration and lower temperature will reduce the gelation time significantly. Thus, the gelation time was strongly dependent on gelatine concentrations and operating temperature.

4.6 Dynamic surface tension measurement

4.6.1 Introduction

Surface tension is an effect within the surface layer of a liquid that causes that layer to behave as an elastic sheet. It is caused by the attraction between the molecules of the liquid by various intermolecular forces. In printing, surface tension is an important parameter where its effect is crucial to the behaviour of an ink on both the microscopic and macroscopic scale.

4.6.2 Surface tension of aqueous gelatine solutions

The dynamic surface tension measurements were performed using a tensiometer (Fibro System DAT 1100) with an accuracy of 1 mNm^{-1}. The apparatus allows the dynamic surface tension to be measured continuously drop by drop, while keeping the drop volume constant. The dynamic surface tension was obtained from the shape of a pendant drop by fitting the Laplace equation to the drop profile (see Chapter 3). The

measurements were performed at room temperature (26°C) with a relative humidity of about 45% to minimise the solvent evaporation. The gelatine concentrations tested were 1%, 2% and 3% (w/v). It was difficult to measure the surface tension of higher concentration of gelatine solution at room temperature (high viscosity) due to the formation of gel [27] and also limitation of FibroDAT. A total of 40 measurements were taken for each ink to ensure the consistency of the results. These results were averaged and are presented in Figure 4.17; error bars show the featured standard deviation.

The average surface tension of 1% gelatine solution was about 65.3 mN/m, 62.3 mN/m for 2% gelatine solution and 58.7 mN/m for 3% gelatine solution, Figure 4.17. Increasing the percentage of gelatine resulted in an appreciable decrease in the ink surface tension. This observation is in agreement with the previous works of Davis et al. who showed that an addition of 0.5 to 0.8 gram gelatine to 100 ml water caused a significant decrease in the surface tension of water, while further addition would reach an equilibrium state eventually [27]. Water has extremely high surface tension of 72.62 mNm^{-1} at 20°C. The addition of gelatine to water (increased the amount of sol form in the solution) would disrupt the network of hydrogen bonds in water by forming hydrogen bonds with water molecules, thus lowering the surface tension. The surface tension of gelatine solutions would also decrease at elevated temperature and addition of electrolytes [27]. This indicates that an increase in the solubility or peptide bond formation of the gelatine would cause a lowering in surface tension. Errors of the measurements were calculated in terms of standard deviation which were quite low, ranging from 0.4 (1%) to 0.6 mN/m (3%). The scattering of data might be corresponding to the natural fluctuations of the measurements. Hence, the results obtained could be considered reliable.

In printing application, the surface tension of the gelatine solutions is considered reasonable for printing on substrates such as polystyrene. However, a small amount of surfactant will be added to the sample to reduce the surface tension, thus favouring

the printing by increasing its wettability. Hence, the wetting of the sample depends on its surface tension and that of the substrates used. In fact, the lower the surface tension of the sample, the better is its wettability on the substrates.

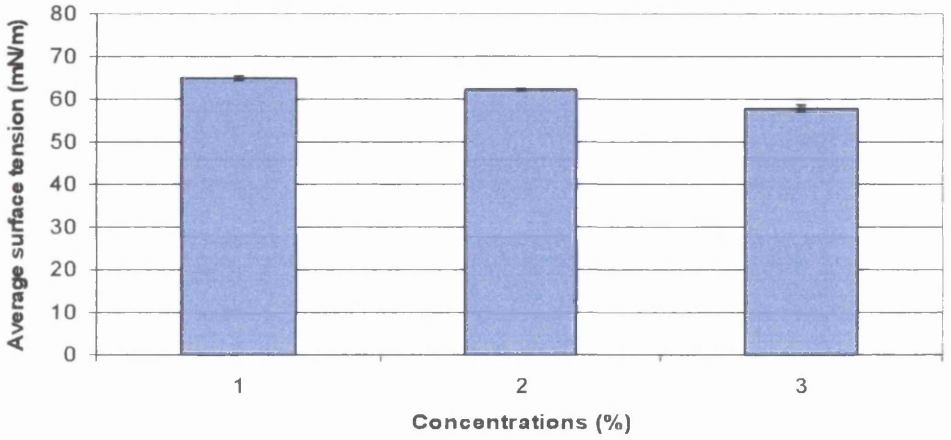

Figure 4.17: Variations of surface tension with concentration of gelatine solutions

4.6.3 Surface Tension Measurements of Gelatine with Surfactants

Surfactants were added to the biopolymer inks (1%, 2% and 3% w/v) to reduce the surface tension. Surfynol surfactants, PSA 336 and 104E, were chosen because they are effective in reducing dynamic surface tension and also have low foaming characteristics, providing good dynamic wetting without coating defects. The measurements of the surface tension of aqueous gelatine solutions with addition of 0.5% surfactants were performed and compared to those without surfactants. The samples were prepared (as described previously) and warmed for 10 min to ensure the surfactants mix well with gelatine solution.

With an addition of 0.5% surfynol 104E, the surface tension of 2% gelatine solution was decreased to 31.0 mN/m, about 50% of the original surface tension. It could be decreased to 25.4 mN/m which was lower than that of surfynol 104E by adding 0.5%

surfynol PSA 336, indicating that surfynol PSA 336 reacts with gelatine more efficient in decreasing its surface tension, Table 4.4. By adding 0.5% surfynol PSA 336, the surface tension of 1% and 3% gelatine solutions was reduced to 25.9 mN/m and 25.0 mN/m respectively, Table 4.4. This will ensure good flow and adhesion properties of the inks during ink transfer using printing processes such as flexographic. Also, this allows the jetting of ink using inkjet printing process which in general requires relatively low surface tension, less than 30 mN/m.

Inks (w/v %)	Surfynol PSA 336 Concentration (%)	Surface Tension (mN/m)
1	0	65.3
	0.01	51.1
	0.05	37.7
	0.10	33.1
	0.50	25.9
2	0	62.3
	0.50	25.4
3	0	58.7
	0.50	25.0

Table 4.4: Effect of surfactant on ink surface tension

For an aqueous gelatine solution without surfactant, some gelatine molecules would form inter- and intra- chain aggregates, while some would adsorb at the water-air interface. Surfynol PSA 336 is an acetylenic diol-based non-ionic surfactant which has no electrical charged head group. Since the electrostatic interactions, attractive or repulsive or both are not present, the surfynol molecules can only interact hydrophobically with gelatine molecules when surfynol PSA 336 is added to the

system. Figure 4.18 displays the model of interaction between surfynol surfactant and gelatine solution. The surfynol molecules adsorb at the interface and cause the gelatine molecules at the interface to move into the bulk. In other words, the specific binding of surfynol molecules to the hydrophobic groups of gelatine chain which forms gelatine-surfactant complex would shield the hydrophobic regions from contact with water, thus lowering the surface tension. With increasing surfactant concentrations, more surfynol molecules would adsorb at the interface and eventually the surface of solution is mainly occupied by surfynol molecules. Therefore, the surface tension of the mixed system would become the same as pure surfynol solution.

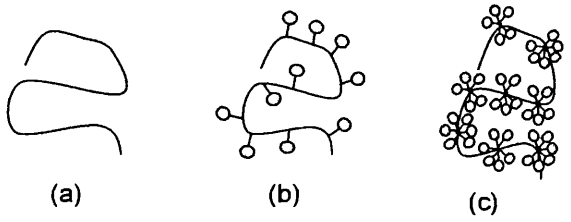

Figure 4.18: Model of gelatine-surfynol surfactant interactions. (a) Free gelatine chain (b) Binding of surfactant molecules to gelatine chain and (c) formation of gelatine-surfactant complex

4.7 Discussion

Many parameters influence printing process, mainly dependent on the flow properties of printing inks such as viscosity, thixotropy and surface tension. The key characteristics for biopolymer inks are printability and gelation temperature. Gelatine forms thermoreversible gels through the formation of hydrogen bond stabilised triple helixes as gelatine solutions are cooled [28]. Gels form when a gelatine solution is

cooled and melt when gels are reheated. This phenomenon is a result of the low energy interactions that stabilise the gel network. Therefore, the biopolymer inks have to be printed at temperatures above gelation temperature and cured at temperatures below gelation temperature.

The main requirements for printing inks are: shear thinning or Newtonian behaviour, low to medium viscosity at high shear rates, good adhesion and sufficient curing rate. An appropriate printing process has been identified for each biopolymer ink based on its viscosity under high shear at 30°C as shown in Table 4.5.

Inks (w/v %)	Viscosity at 30°C (high shear) Pa.s	Printing process
1	0.004	Inkjet
3	0.01	Inkjet /Gravure
5	0.03	Gravure /Flexo
7	0.07	Flexo
10	0.17	Flexo /Screen

Table 4.5: Printing process for inks

The key ink property is viscosity, which normally has to be lower than the threshold for each printing process. Inkjet printing is only possible for inks within a defined range of rheological and surface tension properties [29][30] with typical viscosity threshold being around 30 mPas. For example, a commercial laboratory scale inkjet printing system such as DMP 2800 (Fujifilm Dimatix, Santa Clara, CA, USA) has an optimum viscosity of about 10 mPas and surface tension of about 30 mN/m. This relatively low viscosity threshold limits the choice of inks severely. Only 1% ink satisfies this viscosity requirement. The surface tension of 1% ink was measured using a dynamic absorption tester FibroDAT 1100 and was about 65.3 mN/m. This

exceeds the optimum surface tension for inkjet printer. In order to reduce the ink surface tension surfynol surfactant PSA 336 was used (as described in previous section). Addition of 0.5% w/v of surfactant reduced the ink surface tension below the threshold limit. In order to print structures that contain cells, the printed material in both its liquid and solid forms (after phase transition during curing) cannot be cytotoxic. However, the surfynol surfactant was determined to be toxic to algae (seaweeds) in a 72 hour acute toxicity test[31]. This surfactant might also be cytotoxic to cells. Thus, an alternative non-cytotoxic surfactant has to be used to replace current one.

The ink characteristics determined have shown that conventional printing technologies can be used to pattern surfaces with biopolymer inks in order to fabricate scaffold structures on or in which the cells can attach. In principle this is relatively straightforward to achieve by the sequential printing of layers. Printing delivers inks in liquid form which form a solid structure through some form of phase transition. The phase transition of the biopolymer inks (1%, 3%, 5%, 7% and 10% w/v) from sol-to-gel is well suited to solidify scaffold structures after printing. Printing conditions that are compatible with printing biopolymer inks for each printing technology are being optimised in terms of operation temperature interval for accommodating phase transition in the printing trials.

4.8 Conclusion

Conventional printing technology is a powerful technique with many potential applications in tissue engineering and guided tissue repair. To assess the feasibility of using printing technology for the printing of fine features for tissue engineering scaffolds two types of biopolymer inks have been compared to identify their limits. In order to be able to volume manufacture the bioscaffolds, the properties of the

scaffolding material has to be consistent and reproducible. Thus, gelatine, which can be prepared in higher concentration in solution, appeared to be more favourable than collagen for volume manufacture of scaffolds by printing technologies due to the consistency of the properties of gelatine while collagen suffers from inconsistency according to the different source of material. Collagen is only available in low concentrations where higher concentration of material is required in this investigation. Also, collagen carries animal diseases such as CJD which would transmit to human causing deaths. Unlike collagen, gelatine does not exhibit any antigenicity in physiological conditions and much easier to obtained for industrial production.

Rheological measurements were used to investigate their flow and gelation properties. It was found that all inks display shear-thinning (pseudoplastic) behaviour which is important for good printing. Higher ink concentrations resulted in an increase in both pseudoplasticity and viscosity. The viscosity of biopolymer inks is strongly dependent on temperature. Therefore, great care must be taken to control the operating temperature in order to ensure the print consistency. Dynamic tests have been used to determine gelation properties. An increase in gelatine concentration or reduction in temperature will reduce the t_g significantly. The rate of ordering and gel formation of biopolymer inks was found to be concentration-, temperature- and time-dependent. An appropriate printing technology has been identified for each ink.

There are some challenges on the bioink:

- Phase transition occurs in gelling process where the gelatine changes from its liquid state to solid state. Its properties change along the process.
- It is thermoreversible. A slight change in temperature will change its properties.
- It is a thixotropic liquid which shows time dependent behaviours.
- Also, it exhibits shear history dependent.
- Higher concentration of gelatine gives stronger gel but the viscosity of the gelatine solution might be too high to be printed.

4.9 References

[1] Van Wazer, J. R., Lyons, J. W., Kim, K. Y., Colwell, R. E. (1963), Viscosity and Flow Measurement: a Handbook of Rheology, Interscience, New York.

[2] Deyl Z., Miksik I., Eckhardt A. (2003) Preparative procedures and purity assessment of collagen proteins. J. Chromatogr. B Analyt. Technol. Biomed. Life Sci. 790: 245-75.

[3] Troy D. B., Beringer P. (2005) Remington: The Science and Practice of Pharmacy, Edition 21, Lippincott Williams & Wilkins.

[4] Wulansari R., Mitchell J. R., Blanshard J. M. V., Paterson J. L. (1998) Why are gelatine solutions Newtonian? Food Hydrocolloids 12: 245-249.

[5] Barnes, H.A., Hutton J. F. and et al. (1989) Viscosity. In: An introduction to rheology. Elsevier Applied Science, New York, pp. 11-35.

[6] Marcotte M., Taherian Hoshahili A. R. and et al. (2001) Rheological properties of selected hydrocolloids as a function of concentration and temperature, Food Research International, 34 (8): 695-703.

[7] Djabourov M., Papon M. (1983) Influence of thermal treatment on the structure and stability of gelatine gels. Polymer 24(5): 537-542.

[8] Eldridge J. E., Ferry J.D. (1954) Studies of the cross-linking process in gelatine gels. III. Dependence of melting point on concentration and molecular weight. J. Phys. Chem. 58(11): 992-995.

[9] NakaJima N., Okuno S. (1998) Time- and strain-history-dependent dynamic moduli of semidilute solutions of nitrile rubber containing multiple-branched molecules. Journal of macromolecular science. Physics ISSN 0022-2348, 37 (3): 375-385.

[10] Barnes H. A. (1997) Thixotropy – a review. J. Non-Newtonian Fluid Mech. 70: 1-33.

[11] Tung C. Y. M., Dynes P. J. (1982) Relationship between viscoelastic properties and gelation in thermosetting systems. J. Appl. Polym. Sci. 27: 569-574.

[12] Gudmundsson M., (2002) Rheological properties of fish gelatines, J. Food Sci. 67 (6): 2172-2176.

[13] Michon C., Cuveiier G., Launay B. (1993) Concentration dependence of the critical viscoelastic properties of gelatine at the gel point. Rheol Acta 32: 94-103.

[14] Tosh S. M., Marangoni A. G. (2004) Determination of the maximum gelation temperature in gelatine gels. Applied Physics Letters 84(21): 4242-4244.

[15] Loren N., Hermansson A. M. (2000) Phase separation and gel formation in kinetically trapped gelatine/maltodextrin gels. Int. J. Biol. Macromol. 27:249-262.

[16] Djabourov M. (1988) Architecture of gelatine gels. Contemp. Phys. 29(3): 273–297.

[17] Michon C., Cuvelier G., Relkin P., Launay B. (1997) Influence of thermal history on the stability of gelatine gels. Int J Biol. Macromol. 20(4): 259-264.

[18] Osada Y., Khokhlov A. R. (2002) Polymer gels and networks. New York: Marcel Dekker, Inc.

[19] Winter H. H., Morganelli P., Chambon F. (1988) Stoichiometry effects on rheology of model polyurethanes at the Gel Point, Macromolecules 21: 535-537.

[20] Muller R., Gerald E., Dugand P., Rempp P., Gnanou Y. (1991) Rheological characterisation of the gel point: A new interpretation, Macromolecules 21: 1321-1326.

[21] Ross-Murphy S. B. (1991) Incipient behaviour of gelatine gels, Rheol. Acta 30: 401-411.

[22] Chambon F., Winter H. H. (1987) Linear viscoelasticity at the gel-point of a cross-linking PDMS with imbalanced stoichiometry. J. Rheol. Acta 33: 683-697.

[23] Holly E. E., Venkataraman S. K., Chambon F., Winter H. H. (1988) Fourier-transform mechanical spectroscopy of viscoelastic materials with transient structure. J. Non-Newtonian Fluid Mech. 27: 17-26.

[24] Arridge R. G. C., Barham P. J. (1986) Fourier transform mechanical spectroscopy. J. Phys. D: Appl. Phy. 19: L89-L96.

[25] Hawkins K., Lawrence M., Williams P. R., Williams R. L. (2007) A study of gelatine gelation by Fourier transform mechanical spectroscopy. J. Non-Newtonian Fluid Mech, doi:10.1016/j.jnnfm.2007.05.016.

[26] Hsu S., Jamieson A. M. (1993) Viscoelastic behaviour at the thermal sol-gel transition of gelatine, Polymer 34: 2602-2608.

[27] Davies C. K. E., Salisbury H. M., Harvey M. T. (1924) Surface tension of gelatine solutions. Industrial and Engineering Chemistry 16 (2): 161-163.

[28] Nijenhuis K. te. (1997) Gelatine thermoreversible networks. Viscoelastic properties and structure of gels. Adv. Pol, Sci. 130: 1.

[29] Seerden K. A. M., Reis N., Evans J. R. G., Grant P. S., Halloran J. W., Derby B. (2001) Ink-jet printing of wax-based alumina suspensions. J. Am. Ceram. Soc. 84: 2514-2520.

[30] Reis N., Ainsley C., Derby B. (2005) Ink-jet delivery of particle suspension by piezoelectric droplet ejectors. J. Appl. Phys. 97: 094903-1-094903-6.

[31] Material Safety Data Sheet of Surfynol PSA 336, Version 1.14 (2006) Air Products and Chemicals Inc., Allentown, USA.

5.0 Preliminary Investigation in Printing Biopolymer Inks

5.1 Introduction

Although conventional printing technologies are mainly used for graphic arts and packaging applications, recently there have been significant developments in the use of conventional printing for applications in biomaterials and biosensors to directly print proteins, enzymes and living cells [1]. Printing is a powerful tool for precision patterning and volume manufacture. These developments offer promising possibilities for tissue engineering. Layers of biomaterials can be printed on top of each other to build scaffolds in desired size and shape. Understanding the printing of a thin layer with fine lines onto the substrate is the first fundamental step building a scaffold.

The rheological behaviour of aqueous gelatine solution was presented in the previous chapter. This chapter sets out a preliminary investigation that aims to establish the best printing method for gelatine by comparing the results observed from inkjet printing, flexographic printing and screen printing. The next section describes the materials, which is followed by three sections presenting the results of printing fine features (solids or lines) of gelatine by those three printing processes. Inkjet printing was chosen due to its inherent flexibility and ability to control the formation of ink

droplets and positions of droplets on target substrate digitally. The temperature of the platen and the nozzles could also be controlled above room temperature. It is possible to deposit small amounts of material (picolitre). However, it is restricted to ink of low viscosity from 0.05 Pa.s to 0.1 Pa.s. Flexographic printing deals with medium ink viscosity from 0.1 Pa.s to 10 Pa.s. The flexibility of screen printing enable it to print a wide range of ink viscosity, ranging from 0.1Pa.s to 40 Pa.s, and ink film thickness from 5 microns up to 50 microns. The work focuses on identifying a suitable printing technology, out of three, with which it is feasible to print quality gelatine fine lines.

5.2 Materials

5.2.1 Bioink

In this investigation, a new biopolymer ink was formulated for the printing trials. The details of the components, gelatine in the biopolymer ink and the preparation method were the same as described in the previous chapter.

5.2.2 Black food colouring

SuperCook black food colouring is non-toxic and gluten free. Due to the transparency of the ink, 5% black food colouring in liquid form was added to the inks so that the inks were visible after printed on substrates, which also enables image analysis. The resulting ink was kept in the water bath at 60°C for 10 min to ensure it was well-mixed and homogeneous temperature.

5.2.3 Surfactant

For inkjet printing process, surfynol PSA 336 was used to reduce the ink surface tension to the allowable level for jetting, about 30mN/m. The surface tension measurement of ink with and without surfactant was presented in the previous chapter.

5.2.4 Substrate

Pretreated white glossy polystyrene sheet was used in all trials due to the good compatibility and adhesion to gelatine (bioink) [2] which was observed during previous print trials on different substrates. This is non-permeable, so the amount of ink measured is the amount transferred after the solvent had evaporated. The thickness of the polystyrene substrate is 610 microns. Its smooth and flat reference surface with a Ra value of 37.6 nm provides a more accurate measurement of the line profile. Samples of the substrates were cut to the required size prior to undertaking the trials.

5.3 Drop-on-demand (DOD) piezoelectric inkjet printing

5.3.1 Introduction

This trial was performed by using the inkjet (Dimatix materials printer DMP-2800) to print the biopolymer ink onto substrate. The gelatine concentrations used were 1%, 2% and 3% (w/v) with and without addition of surfactant, ranging from 0.1 to 0.5% (w/v). The process parameters were optimised for ink deposition by jetting.

The temperature and ink rheology such as surface tension and viscosity were key factors in successfully firing the ink for printing. The ink was kept in water bath at 60°C prior injecting into the cartridge which was then wrapped tightly by two layers

of insulator to prevent the ink from gelling. The ink film thickness of the printed solid patches were measured and analysed.

5.3.2 Jetting trial

The DMP was used in a controlled temperature and humidity environment to aid in uniform test results. Atmospheric conditions can have a great effect on the gelatine solutions used in jetting trials. The jetting trial was carried out in a constant temperature room with the temperature set to 28°C (maximum possible) and relative humidity of 40%. Although the room temperature was set at 28°C, it reached 29°C due to the additional heat generated by the equipment. Higher room temperature prevented the ink from gelling so that it can be jetted in liquid form. Also, the nozzle and substrate platen temperature was increased over time from 30°C to 32°C and further to 34°C as the temperature of the DMP parts increased due to the additional heat generated by equipment. This allowed the DMP to start jetting without waiting for a long time while the temperature control system was trying to lower the nozzle and platen temperature.

Table 5.1 indicates that the outcome of the jetting of ink at different concentrations with different amount of surfactants. Only 1% gelatine solution with 0.5% of surfynol PSA 336 was successfully jetted on substrate via nozzles, Figure 5.1. The cartridge settings applied for the trial were 40 V for each nozzle (highest possible) and 5 inches H_2O meniscus set point (4 for black model ink). The gelatine concentration influenced the inkjet printability through viscosity. At gelatine concentrations above 1% (w/v), all nozzles did not eject ink droplets although a few cleaning cycles were carried out. This might be due to the bouncing back of the droplet and finally withdrawal of the droplet caused by elastic stresses. Also, the presence of gelatine in the ink caused the formation of a long tail connecting drop and nozzle. Due to the lack of temperature

control of the cartridge, the ink of higher concentration might have started to gel prior firing, increasing the ink viscosity. For this DOD inkjet printer, the ink viscosity has to be suitably low due to its limited power produced.

Ink (% w/v)	Viscosity (Pa s)	Surfynol PSA 336 (% w/v)	Surface tension (mN/m)	Jet	Notes
3	0.004848	0	58.7	No	High surface tension
3	0.004848	0.5	25.0	No	High viscosity
2	0.002862	0	62.3	No	High surface tension
2	0.002862	0.5	25.4	No	High viscosity
1	0.002373	0	65.3	No	High surface tension
1	0.002373	0.5	25.9	Yes	Low concentration

Table 5.1: The laboratory DOD inkjet printing trial

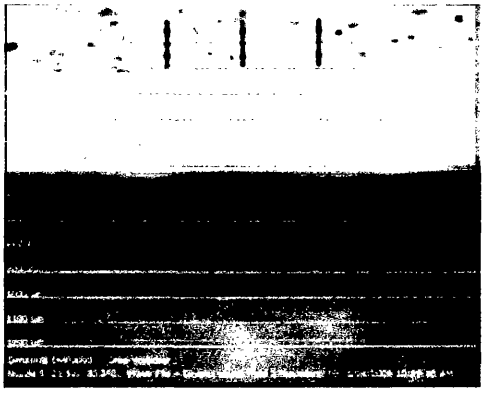

Figure 5.1: Typical image of firing of biopolymer ink

Solid patches and fine lines of 1% ink were printed and the ink film thickness was measured (Figure 5.2). The average ink film thickness obtained by inkjet printing solid patches of 5x5 mm and 10x10 mm was about (1.90 ± 0.04) μm and (1.20 ± 0.05) μm respectively. However, the film thickness was even thinner for printed 200 μm fine lines, which was only 0.1 μm with width of 198 μm, slightly under 200 μm. Similar thin line films were also observed by Yun et al. where the width and the height of the line were 160 – 200 μm and 0.25 – 0.30 μm [3], slightly thicker than that of lines here. This might be due to the higher firing voltage of 40 V instead of 22 V was applied that decreased the printability. When the loosely bound water evaporates from the biopolymer ink, the subsequent increase in the hydrostatic tension draws the matrix together that resulted in contraction of the printed gelatine fine features. Thus, the printed fine features were observed to be below the target width.

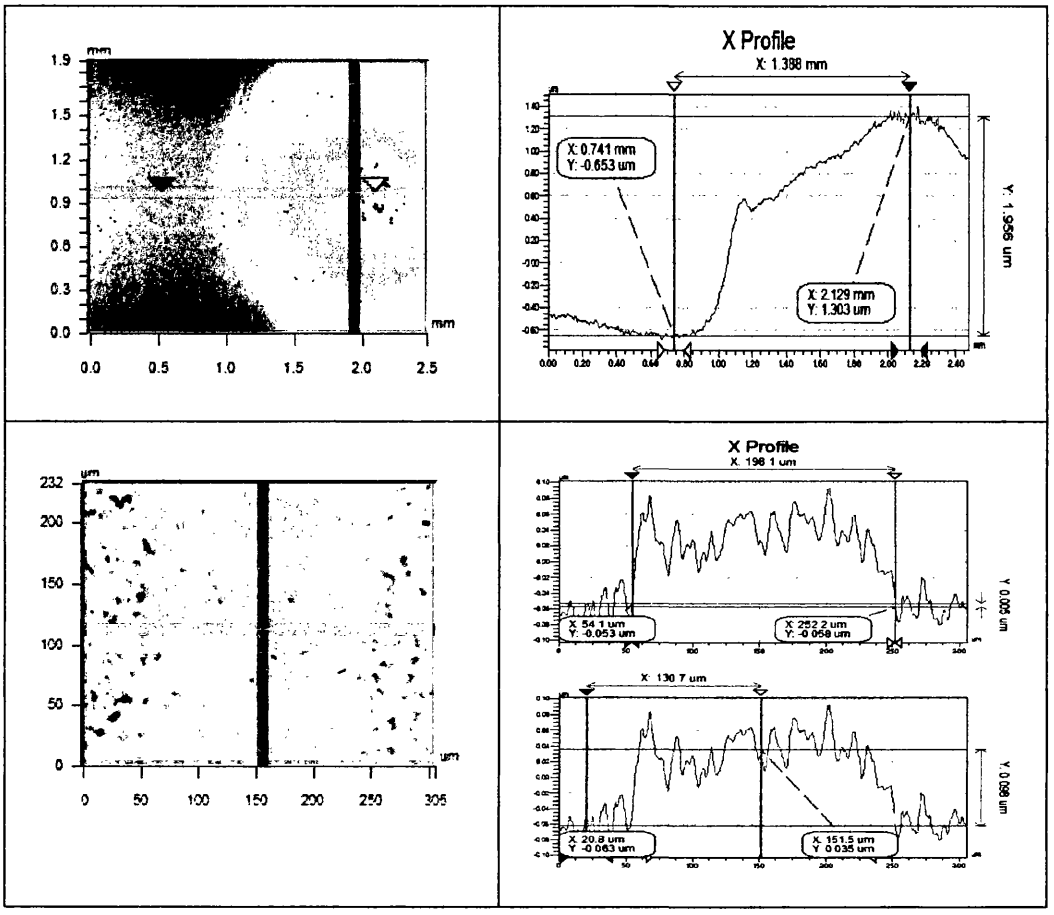

Figure 5.2: Example of printed solid patch of 5x5 mm (above) and 200 micron fine line (bottom)

5.3.3 Discussion

DOD inkjet printing is an efficient approach for depositing picolitre drops on various substrates. It is a non-contact printing method that is compatible with various liquids. DOD inkjet technology has been successfully used in a variety of applications which include inkjet printing DNA microarrays, printing of organic transistors, printing of light-emitting diodes, and ceramics and biopolymer arrays [4][5]. However, the fundamental dynamics of DOD inkjet drop formation and impact on substrate are not yet fully understood. This is mainly because the key stages during drop formation and

impact last less than 100 μs for a micron-size drop (of the order of 40 – 50 μm in diameter). General rules relating optimal operating conditions with driving signal, liquid properties and printhead geometry are not available [6].

Flow in inkjet microchannels is largely dominated by the interfacial effects (interfacial forces over bulk forces at microscales). The flows in microchannels contain a moving boundary of liquids. Such flows are described by a large number of parameters that describe the surface phenomena, bulk phenomena, as well as the variations in density and viscosity across the liquid. Fortunately, the small scale reduces the number of parameters, since viscosity or surface tension often dominate other effects that can be present. Several parameters are naturally small in this case. For instance, inertial effects are small compared to viscous effects, yielding small Reynolds numbers. Gravitational effects will also generally be small compared to surface tension, yielding a small Bond number. In contrast, some effects can be strong or weak depending on the details of the flow.

Inkjet printing requires the formation of drops from small nozzles (30 – 60 μm in diameter) involving predominantly extensional deformations of liquid filaments. The capillary number, which describes the relative importance of viscosity and surface tension, is small when droplets of liquids of high surface tension (water-like) are formed in such process. It is defined as

$$Ca = \mu u/\gamma \qquad (5.1)$$

where μ is the dynamic viscosity, u is a typical velocity, and γ is the surface tension coefficient. The coherence or breakup of the interface will depend strongly on Ca, hence on the velocity of the moving interface [7]. The capillary number of inks (1%, 2% and 3%) was determined and showed relatively small values which were 0.005, 0.006 and 0.012 respectively. Figure 5.3 displays that the values of Ca increased with increasing gelatine concentration.

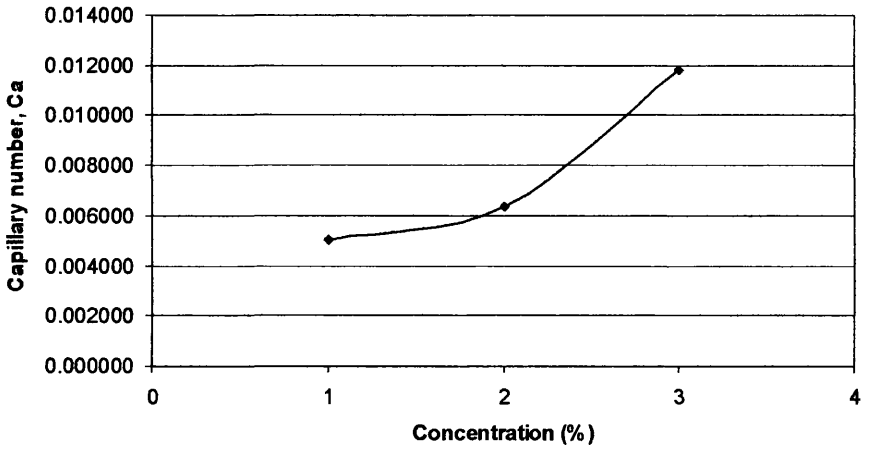

Figure 5.3: The variations of capillary number on gelatine concentration

Variations in surface tension due to temperature or surfactant concentration can be used to actuate motion in microscale flows. The surface tension of the ink with and without surfactants has been studied and the results were presented in the previous chapter. The greater the gelatine concentration, the lower the ink surface tension. However, due to the ink still having a very high surface tension, surfactant had to be used to lower the ink surface tension to the allowable level for inkjet printing. Thus the ink surface tension was further reduced to about 25 mN/m by adding 0.5% surfynol PSA 336.

Saunders et al. [8] carried out printing experiments using a stationary single piezoelectric printhead (Microfab Inc., Plano TX, USA). The cells were printed into growth media in a well plate or directly onto a well plate surface. Printing voltages used were in the range of 30 to 80 V. The nozzle orifice used for fibroblasts was 30 μm in diameter while 60 μm for both osteoblasts and chondrocytes. Despite the very high shear rates applied during inkjet printing, the mammalian cells showed cellular viability to attach, spread and proliferate over time after printing. The cells were able to survive the harsh conditions of drop formation and impact without harm. The influence of voltage on cell survival was observed to show a decreasing trend in

cell survival and proliferation rates with increasing voltage. Proteins have complex tertiary structure that controls activity and are sensitive to shear. When the printing voltage was increased, the droplet mass, velocity and momentum increased [8]. Thus, cells printed at higher voltages will then be subjected to a higher impact forces which might kill the cells after printing. Similar decreasing trend in the enzymatic activity of glucose oxidase with increasing printing voltage after inkjet printed on functionalised silicon oxide was observed in previous works of Arrabito et al. [9].

5.3.4 Closure

It is vital in optimising the temperature of biopolymer ink as the ink can gel in cartridge prior to jetting. The gelation temperature of the ink at different concentrations were found and presented in Chapter 4. Therefore, the room temperature for printing trial was set to maximum (28°C) to ensure that the ink was in liquid form before and during printing. In this print trial, 1% ink has very low gelatine concentration which will be cured at low temperature (<16°C). After the water evaporation, the ink left on substrate would contain very small quantity of gelatine. It was expected that with such low gelatine concentration and without any chemical cross-linker, the construct fabricated will have insufficient rigidity and mechanical properties to sustain the shape for cell attachment and growth. However, the work of others on the printing of mammalian cells and enzymes, suggest that inkjet may be a way in which to locally inject cells, growth media or enzymes into a foam scaffolding structure. This would require further study once a full scaffolding structure had been successfully printed.

5.4 IGT F1 laboratory printing trial

5.4.1 Introduction

To investigate the printability of gelatine solutions by means of flexographic printing process, a laboratory investigation was performed on a printability tester IGT F1. This simulates the flexographic printing process and was designed to evaluate ink-substrate compatibility. The aim of the experiment was to optimise process parameters for printing fine lines in the range of 50 to 150 micron line width. The printed line quality was examined in terms of width and film thickness.

Print quality of 10% ink with 5% black food dye on the polystyrene substrates by flexographic printing was examined initially using a microscope. However the printed images have insufficient contrast to be viewable under microscope and image analysis could not be carried out. Therefore, EPSON Perfection Photo Scanner 4990 was used to gather the images of the trial for line width analysis. The quality of the prints was determined by using image analysis software package. The line film thickness was measured using white light interferometer. The analysis of printed line quality was focused on 150 μm lines with 150 μm spacing. The lines on plate were also measured for comparison to printed lines.

5.4.2 Materials

The photopolymer plate used was given by Welsh Centre of Printing and Coating, Swansea University as shown in Figure 5.4. The thickness of the plate used during the investigation was 1.70 mm. This was produced using photopolymers, which harden when exposed to ultra-violet radiation. A double-sided tape of 0.61 mm thickness was used to attach the plate to the plate cylinder. The plate was attached firmly to the plate without any air bubbles being trapped between the plate and the tape.

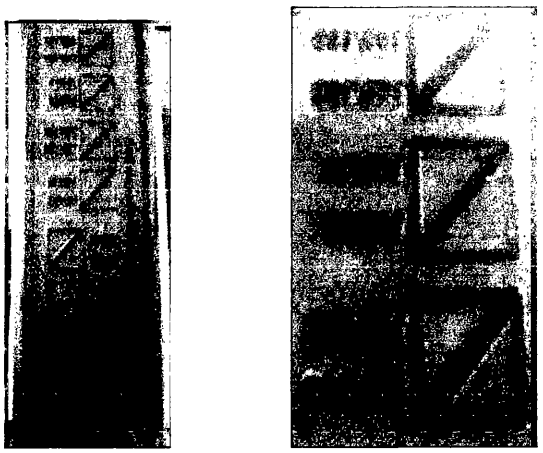

Figure 5.4: Photopolymer printing plate

The test image used for the trial is shown in Figure 5.5, containing three line directions: vertical, horizontal and diagonal lines with 16 different line width (μm) / line gap (μm) combinations, 150/150, 150/100, 150/75, 150/50, 100/150, 100/100, 100/75, 100/50, 75/150, 75/100, 75/75, 75/50, 50/150, 50/100, 50/75 and 50/50. The surface topography and line width of 3 sections within each combination at each line direction were measured using WYKO NT2000 white light interferometer [10].

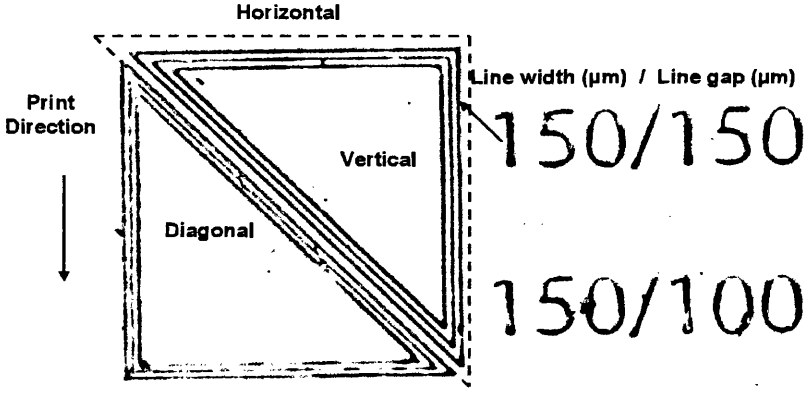

Figure 5.5: Test image scanned and used in image analysis

5.4.3 Experimental Procedure

During a print run on a full scale press, the anilox continuously rotates within a chamber or bath filled with ink and the plate is in continuous contact with the anilox. Therefore a fresh supply of ink is constantly being transferred to the plate. This prevents the ink from drying on the plate, and within the cells of the anilox due to the evaporation of the solvent. However, the IGT F1 has no provision for this and therefore the procedure when using an IGT F1 is to clean the anilox roll, doctor blade and plate surface on the completion of each print with a suitable solvent. Here, the gelatine solution was kept in the water bath at 60°C prior printing to prevent gelling. Warm water was used to clean the anilox roll, doctor blade and plate surface immediately after each print cycle. IPA solvent was also used for further cleaning which evaporates within one minute.

Unlike the majority of full-scale presses where the contact between the anilox and the plate, and the plate and the substrate are controlled by a linear engagement, on the IGT F1 nip contact is controlled by setting the engagement forces. These can be set between 10 N to 500 N. In order to examine how the lines on the plate were affected by changes in the printing nip engagement, different forces were used. Four printing forces of 75 N, 100 N, 150 N and 200 N were selected with two anilox forces of 75 N and 100N. The 75N force was chosen with reference to the observations in previous results of printed images of Black carbon inks on polystyrene substrate. The higher forces were selected to cover a range over which a measurable difference in ink transfer would be observed.

The conditions (constant parameters) used for the experiments are tabulated in Table 5.2 and the parameter settings (variables) of each run are shown in Table 5.3. These parameters were chosen based on the data obtained from the preliminary investigation which was performed prior to printing trials. The substrate was positioned on the substrate holder which was rotated to ensure the substrate was

that it would not creep to one side during printing. The impression cylinder was then rotated back so that the substrate was in its starting position. The anilox and the plate were engaged and ink applied to the anilox behind the doctor blade using a pipette. The plate then completed one revolution with the anilox, which pre inked the plate prior to printing. The impression cylinder was then engaged with the plate. Rotation of the plate and impression cylinder pulled the substrate through the printing nip, producing the print, while the anilox continued to ink the plate. After each sample was printed, it was labelled and dried in ambient air. The cleaning work and changeover of substrate sample took about 20 minutes.

Parameter	**Settings**
Anilox cell volume	8.0 cm^3/m^2
Anilox ruling	137.8 lpcm
Printing speed	0.2 m/s
Ink	10% gelatine solution with 5% black food colouring
Substrate	Polystyrene
Ambient temperature	19°C

Table 5.2: Parameters maintained constant for printing trial

Runs	Anilox Force	Printing Force	Notes
1	75	100	Analysed
2	75	75	Analysed
3	75	150	Broken lines
4	75	200	Analysed
5	100	100	Broken lines
6	100	75	Broken lines
7	100	150	Broken lines
8	100	200	Broken lines

Table 5.3: Parameter settings used for each run during printing trial

5.4.4 Analysis method

The lines on plate were measured and compared to the printed lines. All surfaces have profile, the surface topography roughness and waviness can be defined by the magnitude and spacing of the peaks and valleys that may be observed on the surface. Surface topography is known to affect print quality. For example ink may only transfer to the high points on the plate surface, or conversely may be held in valleys. Thus an evaluation of topography becomes an important consideration in printing process. Surface topography can be measured by using contact and non-contact techniques. The latter is particularly suitable for flexographic plate as it is appropriate for soft surfaces.

The printing plate was measured using the WYKO NT2000 white light interferometer (WLI) in vertical scanning mode [10]. The plate was measured using 5.0x objective lens combined with an internal magnification of 1.0x, providing a measurement area of approximately 1220 μm by 930 μm, sufficient to cover all three horizontal lines. The same settings were used for all measurements so that the results can be directly

compared. The resolution of the instrument at this magnification is tabulated in Table 5.4. Prior to measurement, the instrument was focused onto the top of the plates and the measurement table was adjusted to minimise the tilt of the plate surface. The scan length used for the measurements was 300 μm to encompass the depth of the lines. A 2% modulation threshold was used throughout the measurements. The modulation threshold determines the sensitivity of the instrument in detecting the fringes and hence sets the signal-to-noise level for which a given pixel is considered "valid". Any measured pixel that has amplitude below 2% of the maximum fringes intensity, which does not meet the modulation threshold, are identified as invalid data by the software and are excluded from the analysis. Initial measurements showed a 2% modulation threshold was the optimum for plate measurement providing the maximum amount of data with minimum noise. A modulation threshold above 2% reduced the data on image area, while below 2% a lot of noise appears particularly on the top surface of the lines.

Parameter	**Resolution**
Measurement area	1220 x 930 μm
Lateral (X)	1.6576 μm
Lateral (Y)	1.9375 μm
Vertical (Z)	< 0.0010μm
Surface area function	0.01 μm2

Table 5.4: White light interferometry measurement resolution

The interferometer provides a 3D topographical measurement of the lines, which includes the top surface (image area), line shoulder and depth mark. Surfaces perpendicular to the illumination reflected more light than those that were not. As a

result, a very high percentage of data was collected from the perpendicular surfaces such as the top surface, while comparatively very little data was collected on the shoulders.

A typical image of the vertical lines is shown in Figure 5.6. Colours are used to depict the surface heights within the measurement. The image area of the plate is shown in red, while areas where no data has been collected are shown in white. Due to the transparent nature of the plates, the surfaces are not reflective which allow the light to penetrate through, resulting in insufficient data collected. Thus the data was averaged by the software using 100% cursor width so that the line width of the lines could be determined. It is also important that any tilt remaining on the top surface of the lines was being removed prior to analysis, so that the surface appeared flat, which in fact, the top surface of the image area on the plate is flat.

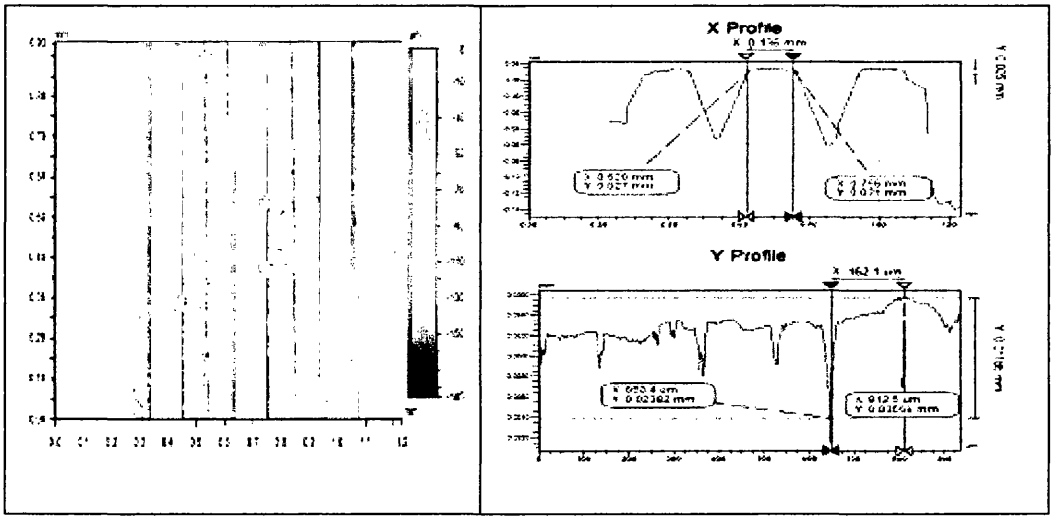

Figure 5.6: Typical contour plot of vertical lines on printing plate

For the printed samples, EPSON Perfection Photo Scanner 4990 was used to scan and gather the 48 bit colour images of printed samples. The images were obtained by scanning at 9600 dpi resolution to ensure the best quality. The parameter settings of the scanner are tabulated in Table 5.5. The work focused on the printed lines of the run 1, 2 and 4 which were scanned and analysed. The image was then cropped for image analysis. All lines were rotated to be at vertical position as the image analysis software used to determine the line quality only recognizes vertical lines. Figure 5.7 illustrates the typical binary image used in the analysis. During image analysis, the contrast and brightness of the scanned images were enhanced in order to obtain enough contrast for line analysis.

Parameter	**Settings**
Image type	48 bit colour
Best quality scanning	9600 resolution dpi
Document size	17.6 mm x 32.7 mm
Scale	100 %

Table 5.5: Parameter settings used for scanning printed images

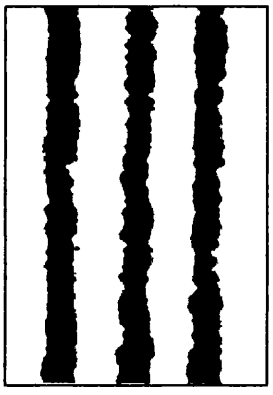

Figure 5.7: Typical binary image of printed lines

Image analysis software package developed in the WCPC allows quantitative measurement of a number of parameters including line width, line edge quality, printed line quality, dot quality, physical dot area and registration. It was utilised to provide quantitative assessment of the printed lines to enable reliable comparison [11]. In this investigation, line width has been measured. Only the quality of lines of 150 μm width with 150 μm spacing at three different line directions were examined and compared with the same lines. This was because other lines of narrower width were observed to be broken and have rough edges. This might be due to the occurrence of dewetting phenomenon which will be further discussed in the next section. The system was calibrated by measuring circles of known physical size, and relating the number of pixels to the measured size. One pixel equated to 2.77 μm. The film thickness of the printed lines was measured using white light interferometer.

5.4.5 Results and discussions

The test image was analysed and compared in terms of line width and line profile on both the plate and the prints. The work focused on the 150/150 lines on the plate and printed images of run 1, run 2, and run 4. The measurement of the lines on plate is presented first followed by the measurements of printed lines on polystyrene.

5.4.5.1 Lines on plate

150/150 lines on the flexographic plate were measured using white light interferometer. The average line width of these lines as well as line profiles are compared. Three measurements were made on each of three lines for vertical, horizontal and diagonal line directions.

Figure 5.8 illustrates the typical line profile of 150/150 lines on plate. These images include non-image and image areas. The top surface of the image areas on plate is not smooth along the lines, see Y profile. A number of peaks and valleys are present. Hence, the roughness along the top surface of the lines (peak to trough along the surface) was measured. The line surface is quite rough with a Ra value of about 1 μm. This might affect the uniformity of the ink film thickness obtained where large errors may arise.

In order to determine the line width of the lines on plate, the 2-D line profile plot data was analysed. The line widths for each line direction were taken by measuring the top flat surface of the lines and are tabulated in Table 5.6. It shows that the line width of the lines on plate was quite uniform from line to line, about (135 ± 4) μm which were less than the nominal value.

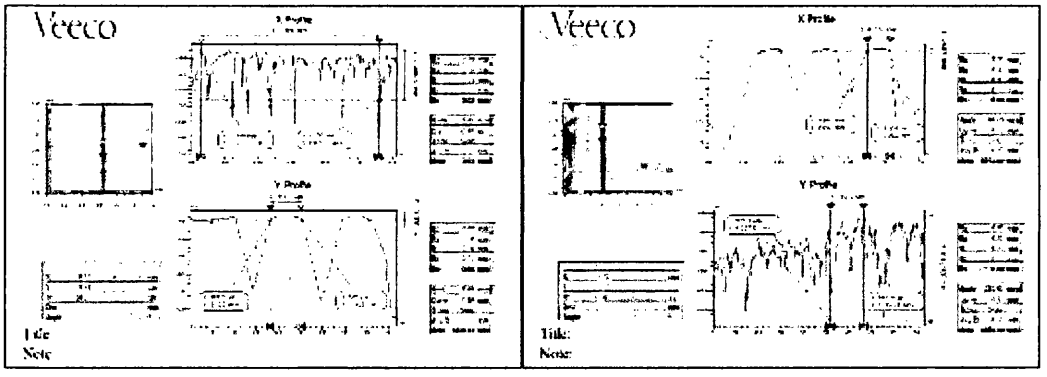

(a) Vertical lines (b) Horizontal lines

Figure 5.8: Line width of 150/150 lines on plate by taking the top flat surface of image area

Line	Line Direction	Line Width (μm)			Average line width (μm)	Standard deviation (μm)
		1	2	3		
150/150	Vertical	131.33	136.33	129.66	132.44	3.93
	Horizontal	132.83	139.33	135.43	135.86	4.23
	Diagonal	133.00	133.66	134.33	133.66	0.78

Table 5.6: Summary of line width measurements and standard deviation for flexographic plate

5.4.5.2 Printed lines on polystyrene

In this trial, two anilox forces of 75N and 100N were chosen. All printed lines were continuous with no sharp edges. Also those images printed at 75N anilox force appeared to be better visually and three out of four runs at this anilox force in this trial could be analysed due to sufficient contrast. Thus, lower anilox force of 75N enables sufficient ink transferred to the substrate.

There were three printed lines available for each line direction for each run. All of them were measured and the data was averaged and used to represent the quality of the line for each printing force used in the printing trial with constant anilox force of 75N. The standard deviation σ of these measurements was also calculated using the mean range of samples, $\overline{R}$ and Hartley's conversion constant, d_n due to small sample size, $n < 12$, $n < 12$ [12]. It is given by

$$\overline{R} = \sum_{i=1}^{k} \frac{\overline{R}_i}{k} \tag{5.2}$$

where k is a number of samples of size n

$$\sigma = \frac{\overline{R}}{d_n} \tag{5.3}$$

where d_n is the Hartley's Constant

Table 5.7 shows the average line width and standard deviation of different line directions for runs 1, 2, and 4 respectively. The line width lies in the range of 110 to 134 microns. The best line quality in terms of standard deviation was obtained for run 1, followed by run 4 and the poorest line quality was observed for run 2. By comparing these measurements to Table 5.6, the printed vertical lines have the greatest gain in width of about 15% greater than the original line width on plate, followed by horizontal and diagonal lines respectively. These scanned images appeared to be mottled and blur, resulting in large errors in measuring the line width.

Run	Printing force (N)	Line direction	Line width (μm)			Average line width	Standard deviation
			1	2	3		
1	100 N	Vertical	131.35	130.30	140.23	133.96	5.87
		Horizontal	126.93	103.61	108.11	112.88	13.78
		Diagonal	102.50	118.29	114.45	111.74	9.33
2	75 N	Vertical	125.21	116.76	146.61	129.53	17.63
		Horizontal	142.30	111.10	83.65	112.35	24.64
		Diagonal	79.47	124.99	122.09	108.85	26.89
4	200 N	Vertical	150.96	131.52	120.22	134.23	10.48
		Horizontal	128.18	107.01	109.44	114.88	11.70
		Diagonal	105.94	118.74	116.57	113.75	12.99

Table 5.7: Summary of line measurements and featured standard deviation

Also, in order to evaluate the effect of IGT printing force on print quality, biopolymer ink was printed with printing force of 75 N, 100 N and 200 N. The result is presented

in Figure 5.9. The line width is important because if a large gain in line width occurs then connections between two parallel lines may occur. The line width increased by about 3% when the printing force was increased from 75 N to 100 N, due to the plate deformation and ink spreading when greater force was engaged. At 200 N printing force, the line width of printed lines was observed to be comparable to those at 100 N, giving similar volume of ink transfer onto substrate. However, all printed lines were still narrower than target line width of 150 μm. The line film thickness was also measured and found that the film thickness of fine lines printed by flexographic printing was only about 0.2 μm which was considered quite thin. Thus low image contrast was observed on the printed gelatine lines.

In comparison to the line width on plate, most printed lines showed narrower width than that of lines on plate as shown in Figure 5.9. This might be due to dewetting occurred at the solid-liquid interface. Generally, dewetting describes the rupture of a thin liquid film on the substrate (either a liquid or a solid) and formation of droplets [13]. The key factor determining this phenomenon is the spreading coefficient S. Consider a droplet of oil placed on a liquid substrate (say water), the work of adhesion (a measure of the force of attraction between oil and water) is greater than the work of cohesion. The term ($W_a - W_c$) is called the spreading coefficient S [13].

$$S = W_a - W_c = (\gamma_L + \gamma_S - \gamma_{SL}) - 2\gamma_L \tag{5.4}$$

$$S = \gamma_S - \gamma_L - \gamma_{SL} \tag{5.5}$$

where γ_L is the liquid surface tension, γ_S is the surface tension of liquid substrate and γ_{SL} is the interfacial tension between two liquids.

At equilibrium, Young's equation resolves the surface and interfacial tensions into

$$\gamma_S = \gamma_{SL} + \gamma_L \cos\theta \tag{5.6}$$

where θ is the contact angle between the liquid droplet and substrate.

By substituting equation 5.6 into equation 5.5, this gives

$$S = \gamma_L(\cos\theta - 1) \qquad (5.7)$$

The spreading coefficient of gelatine solution on polystyrene substrate was determined to be negative and the value was considered quite high where S= -23.4. This value was slightly higher than that calculated by Sinko et al. [13], S= -19.7 with tablet as substrate. This is because polystyrene surface has greater contact angle than that of a tablet surface, thus increasing the value of S. As the printed gelatine line films obtained were very thin (≈ 0.2 μm), the films were not stable on polystyrene substrate and droplets were formed. This may result in the waviness on the edge of printed gelatine lines (as shown in Figure 5.7) which had significantly reduced the average printed line width below the line width on plate. The curing of gelatine line film via phase transition (gelation) and water evaporation might cause the shrinkage of line film which in turn, decreased the printed line widths. Besides, holes were randomly formed in the line films which led to high standard deviations in film thickness of about 0.05 μm. The dewetting phenomenon can be used to explain the broken lines obtained when the anilox force was increased to 100N. The ink volume transferred from anilox roll to plate was reduced when the anilox force increased, which resulted in even thinner line film thickness (< 0.2 μm). This increased the instability of gelatine films on the substrate, causing the printed fine lines to break.

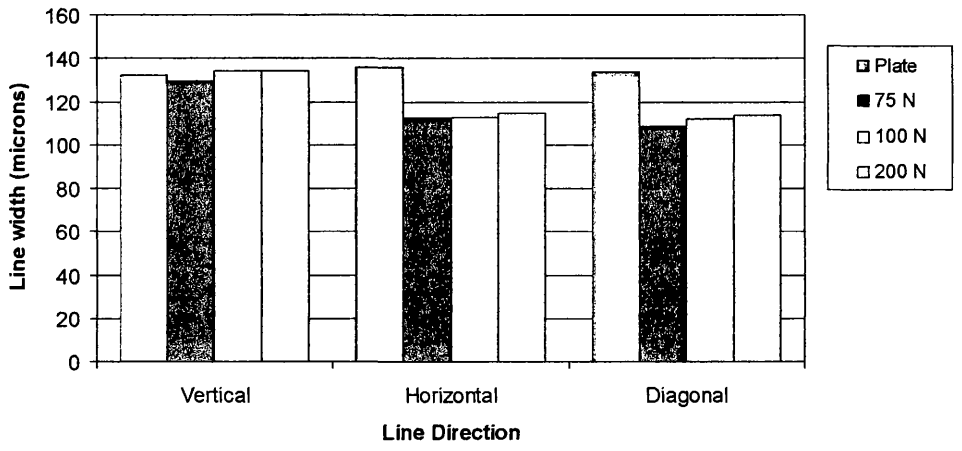

Figure 5.9: Measured line width at different printing forces

5.4.6 Closure

The 10% ink with 5% black food dye could be printed on the polystyrene substrates by flexographic printing technology. The widths of lines on plate were quite consistent from line to line, resulting in small error in averaging the data. During analysis, the contrast and brightness of the image were increased slightly so that measurements can be carried out, but introducing high measurement errors, especially in printed images at 75N printing force which was unreliable. Alternatively, the amount of black food dye can be increased to obtain enough contrast for the ink to be printed in future printing trial. The width of printed lines increased with increasing printing force from 75 N to 100 N due to greater engagement between the plate and substrate. However, all printed line widths were narrower than that of line width on plates which might be due to the dewetting phenomenon and the shrinkage of line film caused by gelation and water evaporation.

A few control issues arose in this printing trial. The temperature is an important factor in processing gelatine. The ink was kept in bath at 60°C and used for printing at room temperature. The temperature of the ink decreased once it has been taken out of bath.

Unfortunately, the ink temperature could not be controlled precisely in this printing trial. The impression force has to be optimised to obtain better print quality.

The temperature of the printing process has to be optimised as well as the curing after printing. In this investigation, only width and film thickness of 150/150 lines have been examined. In this preliminary printing trial, the measured width and film thickness of printed gelatine fine lines were interested rather than the parameter effects, in order to determine the feasibility of this printing process for scaffold fabrication. Therefore, not all process parameters were investigated. A full analysis of this phenomenon may lead to a further understanding of the physics of the flexographic printing process. It would appear that there is a strong interaction between the plate surface properties including both roughness and surface energy, the surface energy of the substrate and the surface tension properties of the bioink. This could be addressed by modifying the properties of the plate. However, development of new plate materials for this application is beyond the scope of this study.

5.5 Analysis of laboratory screen printing trial

5.5.1 Introduction

The printability of biopolymer solutions on screen printing process was investigated by performing a laboratory print trial. The objective of the experiment was to examine the quality of fine lines printed in terms of width and film thickness.

5.5.2 Choice of parameters

The screen is made up of three parts: the frame, the mesh and the stencil. In this study, a polyester mesh was used (Figure 5.10) due to its greater elasticity comparing to stainless steel mesh. Its quality characteristics as shown in Table 5.8 were chosen

based on the results obtained from previous tests in printing fine lines (100 – 200μm) of water-based inks.

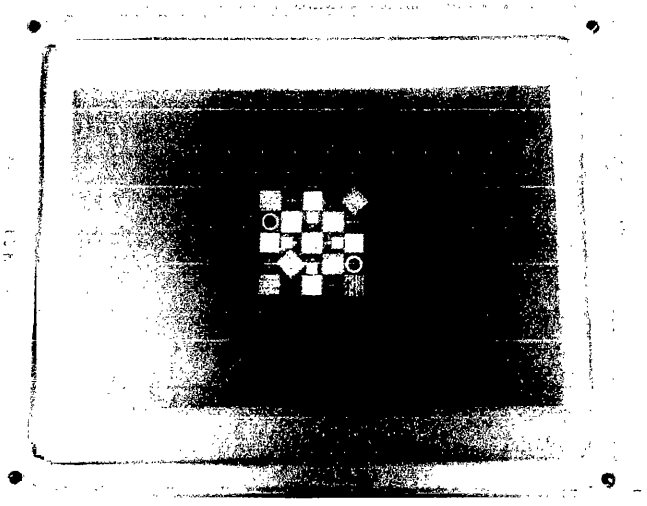

Figure 5.10: Typical screen used in screen printing trial

Mesh	90 – 48
Mesh Count	90 threads per cm
Thread Diameter	48 μm
Mesh Opening	55 μm
Open Area	24.6 %
Fabric Type	Polyester
Fabric Thickness	65 μm
Tension	22 N/cm
Emulsion Type	EC4
Emulsion Thickness	13 μm

Table 5.8: The properties of the screen used for printing trial

The test image used for the trial is shown in Figure 5.11. This was designed to give a range of line widths at different orientations, containing three different line width (μm) / line gap (μm) combinations: 100/100 vertical lines only, 200/200 and 300/300 at three line orientations (print directions: vertical, horizontal and diagonal). Solid patches of different cross sections: 81mm^2, 25 mm^2, 1 mm^2 and 2.5 mm^2. Two circles of 200 μm and 400 μm are also included. The surface topography and ink film thickness of printed lines were examined by using Wyko NT2000 white light interferometry [10][11] while the line width was characterised using image analysis [11].

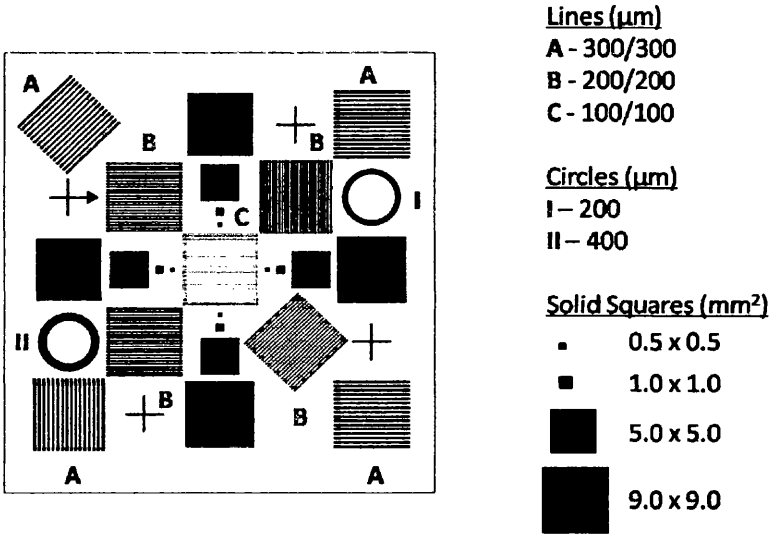

Figure 5.11: The image used for the studies in fine line reproduction

5.5.3 Experimental Procedure

The screen printing trial was performed on a small format Presco SP1 screen printing press (as described previously in Chapter 3). The samples of polystyrene substrate were cut to the required size of 83 mm by 83 mm prior to undertaking the printing experiments. The conditions used for the experiments are summarised in Table 5.9.

The parameters were set with reference to previous work [14]. Both squeegee speed and squeegee pressure were the gauge values taken from the system on the press. These gauge values were quantified in standard pressure unit using a force sensor (see Chapter 6). The substrate was positioned on the platen which was vacuumed to ensure the substrate was held firmly during printing. The ink was kept in water bath at 35°C throughout the trial to prevent it from gelling. Six samples were printed for each run at same parameter settings. The cleaning work was carried out after each run which took about 15 minutes.

Parameter	**Settings**
Screen	90 - 48
Ink	10% gelatine solution with 5% black food colouring
Substrate	Polystyrene (83 x 83 mm)
Ambient temperature	20°C
Squeegee type	Soft
Snap off (mm)	2.0
Squeegee speed (rev)	1.0
Squeegee Pressure (mm gauge)	6.4

Table 5.9: Experimental conditions for printing trial

5.5.4 Analysis method

Two methods were considered for the measurement of the profile of the lines; image analysis and white light interferometer (see descriptions in Chapter 3). Image analysis was used during an initial optical examination of the line quality and measurement of line widths. The images of printed lines were captured, Figure 5.12(a) and segmented

to obtain binary images, Figure 5.12(b). The raw data collected was analysed to gain some information on the measurements performed. However, it is not possible to measure the three dimensional characteristics of the lines using image analysis. White light interferometer was used to investigate the screen characteristics and the ink film thickness of printed line.

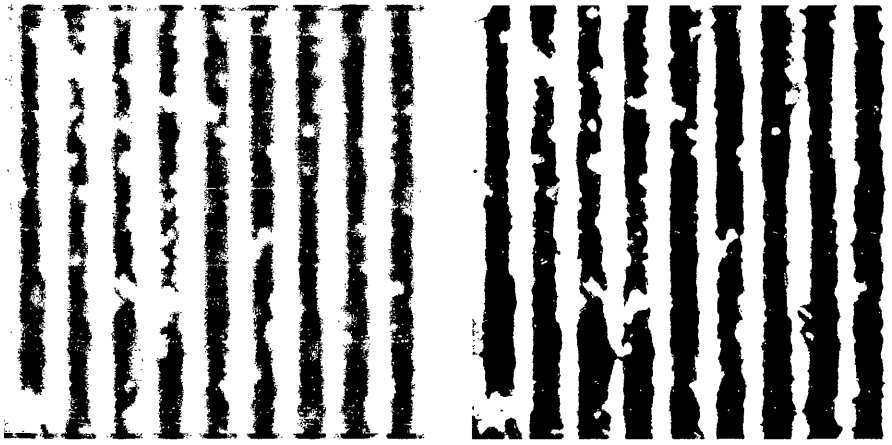

(a) Original image (b) Binary image

Figure 5.12: The original image and segmented image when the correct greyscale threshold value is applied

Images of every patch of pattern were taken for printed sample of run 1 which were observed visually to be better prints. Figure 5.13 shows the typical actual printed image. This investigation only focused on line width of 300/300 parallel lines which were measured for analysis as other lines were broken and could not be recognised by the software as "lines". The system was calibrated by measuring circles of known physical size, and relating the number of pixels to the measured size. It was then established that one pixel is equal to 7.32 μm.

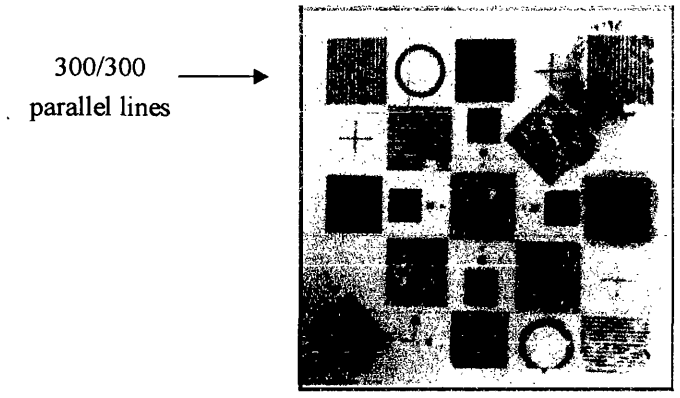

Figure 5.13: The typical actual printed image: 300/300 parallel lines being analysed

White light interferometer was used in vertical scanning mode to generate a three dimensional map of a surface over a two dimensional area. The screen was measured using 5.0x objective lens combined with an internal magnification of 0.5x, providing a measurement area of approximately 2460 μm by 1870 μm, largest possible area to cover most lines. The same settings were used for all measurements so that the results can be compared. The resolution of the instrument at this magnification is shown in Table 5.10. The scan length used for the measurements was 100 μm in order to encompass the depth of the image area and 2% modulation threshold was used throughout the measurements.

Parameter	Resolution
Measurement area	2460 x 1870 μm
Lateral (X)	3.342 μm
Lateral (Y)	3.895 μm
Vertical (Z)	< 0.001μm
Surface area function	0.01 μm^2

Table 5.10: White light interferometry measurement resolution

5.5.5 Results

The results from the experimental investigations are presented for the screen and the printed line and then discussed in the next section. The line width of the printed lines was compared to the mesh opening width of screen. The ink film thickness was also determined. The work focused on the 300/300 parallel lines on the screen and printed image of run 1 – 5 due to broken lines obtained on other narrower lines. The result from the 3D profile of the screen is presented first followed by the measurements of printed lines on polystyrene.

Figure 5.14(a) shows the contour plot of the mesh structure of the screen and the 3D image of 300/300 lines on the screen was taken, Figure 5.14(b). The width of the 300/300 parallel lines on screen was determined using the 2-D line profile plot data, positioning the X and Y cursors at the desired location on 2D profile plots, Figure **5.15**. The line width of the lines on screen is very constant from line to line (± 6% error), Table 5.11. The 300/300 parallel lines have an average line width of 299 μm with a small standard deviation of 2.76 μm. These measurements were compared to those printed lines.

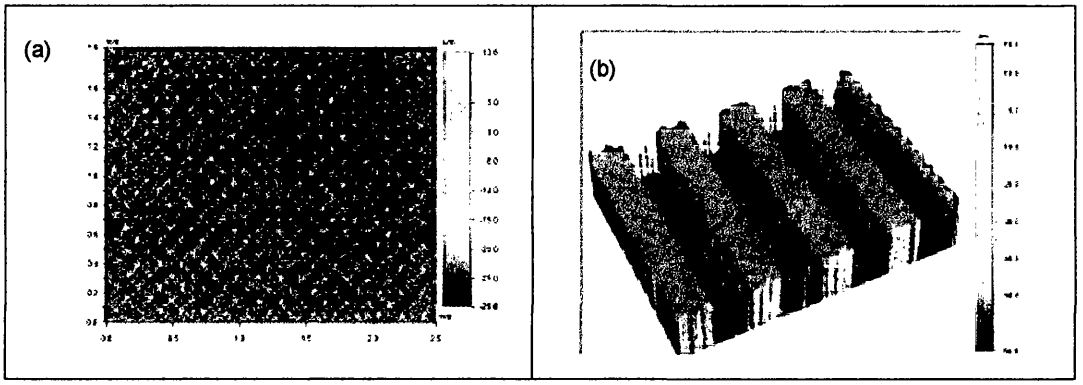

Figure 5.14: Typical (a) contour plot of the non image area of screen and (b) 3D plot of 300/300 parallel lines on screen

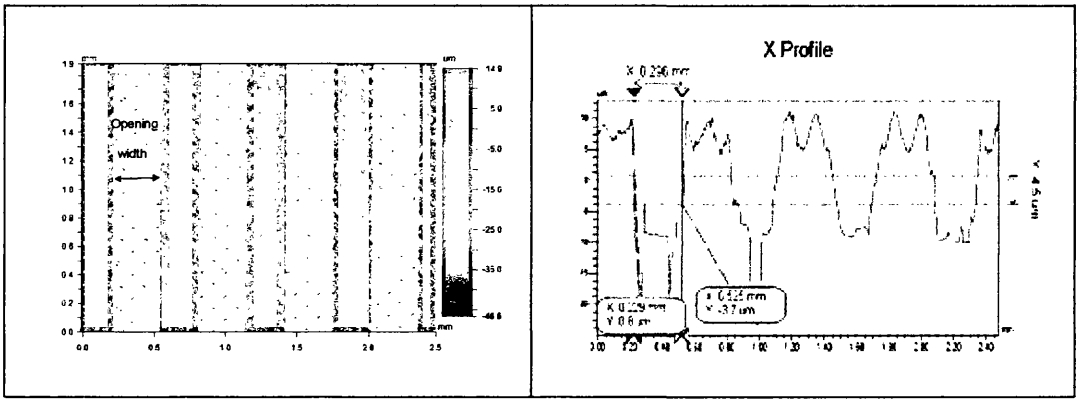

Figure 5.15: The 300/300 parallel lines on screen

Line	Line Width (μm)				Average Line width (μm)	Standard Deviation (μm)
	1	2	3	4		
300/300 parallel	293	296	300	300	297.25	3.40
	300	296	300	300	299.00	2.00
	303	300	300	300	300.75	1.50
Average	299	297	300	300	299.00	2.76

Table 5.11: Summary of line width measurements and standard deviation for screen

For image analysis, threshold value is a critical parameter which can have a significant effect on any geometrical measurement, so it is important to use the same threshold value for all measurements. Figure 5.16 shows typical image printed on first run and second run. Two runs were performed where the first run gave better prints than the second run. This might be due to the temperature of ink of first run is 60°C before printing which is higher than that of the second run of 35°C. The ink might already be gelled before printing for the second run as it took shorter time for gelation to occur, thus giving bad quality prints. The low room temperature of about 20°C caused even quicker gelation of ink. Figure 5.17 shows the comparison of measurement of line width on screen, on printed sample, and at both ends. The printed line widths were found to be 237.65 μm with a standard deviation of 9 μm. By comparing to Table 5.11, the measured line width is lower than the width of mesh openings on screen. The printed lines at both ends were observed to have greater line width of about 44 μm than those in the middle, with sharper edge definition.

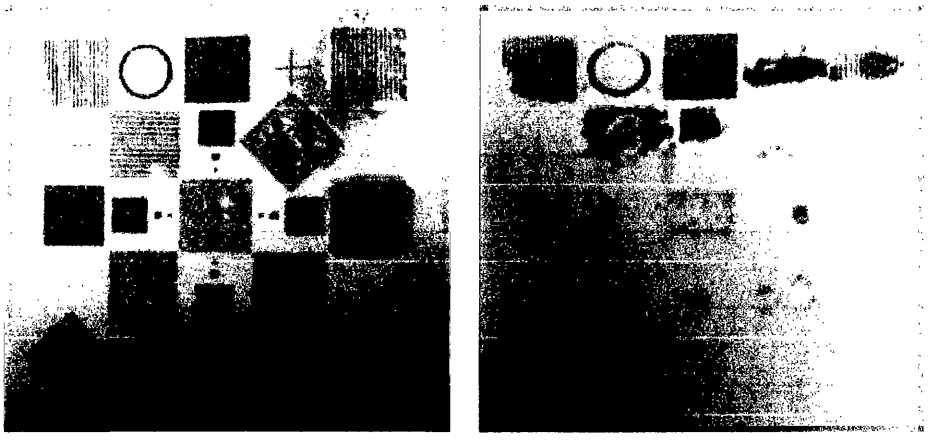

(a) Printed image of first run (b) Printed image of second run

Figure 5.16: Typical image printed

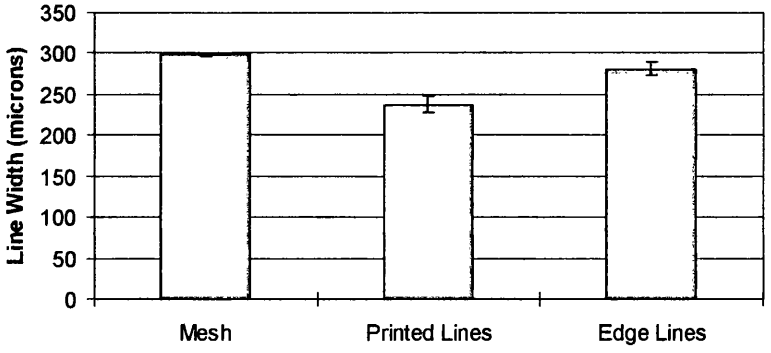

Figure 5.17: Comparison of line width of 300/300 parallel lines

Also, the measurements of the ink film thickness were taken at the top of the negative fine line area. Three measurements were taken for four lines each and are averaged over 2.5 x 1.9 measurement area. Typical measurement result is shown in Figure 5.18 where the primary features of the experimental measurement are presented. Besides, a feature which was evident in many of the measurements was a raised area at the edge of the ink film. This feature of 'crowning' will be discussed in the next section. The average ink film thickness was found to be around (7.8 ± 2) μm.

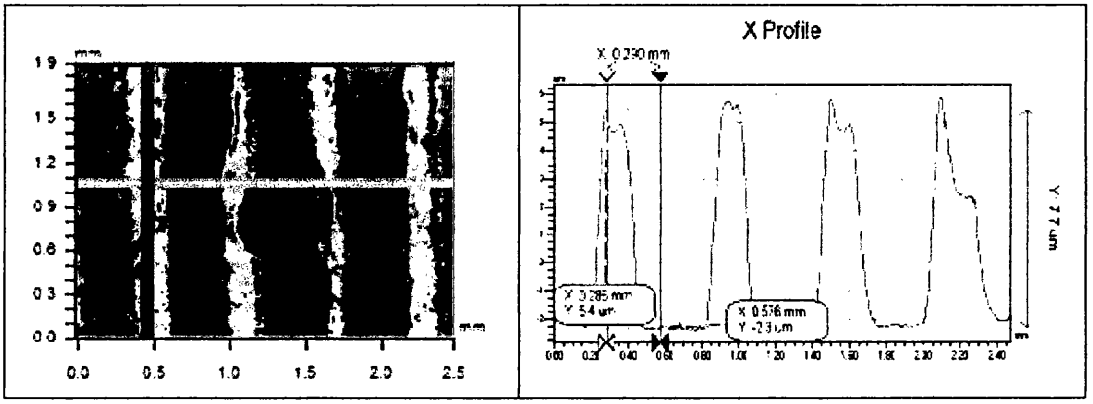

Figure 5.18: Measurement of the ink film thickness, illustrating 'crowning' at the edge of the ink film

5.5.6 Discussion

The study has found that better quality of lines was obtained when the ink started to gel (with reference to sample run 1 – 5). This might be due to: when the gelatine solution started to gel, its viscosity would increase and the surface tension would decrease. As a result, the ink adheres better to the substrate giving better line quality, comparing to others which have unclear pattern of lines. Also, when the tension of the screen pulls the stencil off the substrate behind the squeegee, the substrate tends to stick to the screen, due to gelling of ink. The force applied to detach the sample from the stencil was not uniform thus might be causing the printed lines in the middle have no sharp edge definition and far below the desired line width.

The "crowning" observed on the edge of the solid ink film results in a small lip on the edge of the solid ink film is most likely the effect of the ink release mechanism from the screen [15]. In a review by Fox [16], the ink transfer theory postulated by Messerschmitt stated that the tension in the screen tears the ink film from the substrate after the passage of the squeegee. This feature at the edge of the solid ink film would tend to support this theory.

5.5.7 Closure

10% ink with 5% black food dye could be printed on the polystyrene substrates by screen printing technology. The mesh opening widths on screen were fairly consistent from line to line. The printed lines at both ends have greater line width with sharper edges, comparing to those in the middle. The ink film thickness was about 8 microns.

Temperature is an important factor in dealing with gelatine based biopolymer inks. Thus, the ink temperature has to be controlled precisely before and during printing. The press parameters have to be optimised. The minimum printable line width and

line thickness were also interested to be cost effective. Different stencil can also be used to perform the same printing trial to study the effect of stencil parameters on the line profiles.

5.6 Conclusions

Inkjet printing process was found not to be suitable for printing gelatine. There are too many alterations in the printer itself to keep the ink (gelatine solution) in liquid form prior jetting; and the ink formulation (addition of surfactants to reduce the ink surface tension), allowing it to be jetted on substrate. It is also difficult to make low viscosity gelatine solution to gel. After evaporation of water, only very small amount of gelatine was left on substrate. This ink film thickness obtained was ranging from 0.1 to 2.0 microns which was considered thin. The dimensions of gelatine lines produced by inkjet printing would not have sufficient strength and rigidity to sustain the construction of a scaffold. However, inkjet may have a role in adding cells and locally modifying the scaffold, e.g. by adding growth agents in a controlled manner.

The printed images of flexographic printing have low image contrast, possibly due to its very thin ink film thickness and insufficient dye. The manipulation of the printed images might introduce large errors in measurement. The amount of ink transfer would appear to be dependent on the relative surface energies of the plate, the ink and the substrate. Thus, if flexography were to be considered in future for scaffold production because of its higher production speeds, then this would require development of new plate technology. However, the thin ink film thickness would negate the increase in speed as it would require multiple passes to obtain the same ink film thickness as screen printing.

The results of the screen printing and flexographic printing trials indicate that screen printing process looks more promising in printing gelatine solutions. It gives better

quality fine lines of gelatine in terms of larger line width and much thicker line film comparing to those printed by inkjet printing and flexographic printing. The complex nature of gelatine makes the printing work more complicated. The process parameters have to be optimised to obtain better quality of fine line. Thus, a full investigation in fine gelatine lines reproduction by screen printing was carried out to study the effect of various process parameters on the line quality in Chapter 6.

5.7 References

[1] Derby B. (2008) Bioprinting: inkjet printing proteins and hybrid cell-containing materials and structures. J. Mater. Chem. 18 (47): 5717-5721.

[2] Sagvolden G., Giaever I., Feder J. (1998) Characteristic protein adhesion forces on glass and polystyrene substrates by Atomic Force Microscopy. Langmuir 14 (21): 5984-5987.

[3] Yun Y. H., Kim J. D., Lee B. K., Cho Y. W. (2009) Polymer inkjet printing: Construction of three-dimensional structures at micro-scale by repeated lamination. Macromolecular Res. 17 (3): 197-202.

[4] Calvert P. (2001) Electroactive polymer gels. Chem. Mater. 13: 3299-3305.

[5] Percin G, Khuri-Yakub B. T. (2003) Piezoelectric droplet ejector for ink-jet printing of fluids and solid particles. Rev. Sci. Instrum. 74 (2): 1120-1127.

[6] Sirringhaus H., Shimoda T. (2003) Inkjet printing of functional materials. MRS Bull. 28: 802-806.

[7] Olbricht W. (1996) Pore-scale prototypes of multiphase flow in porous media. Annu. Rev. Fluid Mech. 28: 187-213.

[8] Saunders R., Gough J., Derby B. (2005) Inkjet printing of mammalian primary cells for tissue engineering applications. Mater. Res. Soc. Symp. Proc. 845: 57-62.

[9] Arrabito G., Musumeci C., Aiello V., Libertino S., Compagnini G., Pignataro B. (2009) On the relationship between jetted inks and printed biopatterns: Molecular-thin functional microarrays of glucose oxidase. Langmuir 25 (11): 6312-6318.

[10] Lamb C., Zecchino M. (1999) WYKO Surface Profilers Technical Reference Manual. Veeco Metrology Group, Version 2.2.1.

[11] Jewell E. H. (2004) Image analysis Version 3 Instruction Manual, WCPC, Swansea University.

[12] Oakland J. S. (2003) Statisical process control. Oxford: Butterworth-Heinemann Fifth edition.

[13] Sinko P. J., Martin A. N. (2005) Martin's physical pharmacy and pharmaceutical sciences. Lippincott Willians and Wilkins, fifth edition.

[14] Jewell E. H., Barden T., Claypole T. (2000) The effect of flat bed screen printing parameters on ink film thickness. Report no: 00-01-SPTG, WCPC, University of Wales, Swansea.

[15] Barden T. (2005) The application of three-dimensional profiling to the measurement and characterisation of screen printed fine lines. Phd. Thesis University of Wales Swansea.

[16] Fox I. (1999) A review of ink flow through screens, published by the Screen Printing Technology Group, WCPC, University of Wales, Swansea.

6.0 The Effect of Variables on Screen Printed Gelatine Fine Lines

6.1 Introduction

The previous chapter described the preliminary trials of three printing processes considered for producing gelatine fine lines. Screen printing process was found to produce the best quality fine lines in terms of width and ink film thickness. This has led to the design of this laboratory screen printing trials using an orthogonal array experimental design to increase the understanding of the process. Work is also conducted to further investigate the factors affecting the quality of gelatine fine lines. This chapter starts with a description of the orthogonal array approach used to perform the experiment trial. The characteristics of the materials used are shown in Section 6.2. The methods applied to measure and analyse the printed images are also described. The results are presented in Section 6.3, investigating the effects of parameters on the printed line width and ink film thickness. The effect of line orientation on line width is also investigated. These are further discussed in Section 6.4.

6.2 Methodology

An experiment was performed to investigate the effect of the process parameters on printed gelatine fine lines. A full description of choice of experimental procedure, along with details of the different parameters, press settings and process variables is given in this section. The printing press, test image and the substrate type were maintained constant for all the experiments.

6.2.1 The ink

New bioink (aqueous gelatine solution with black food dye) developed at WCPC was used for all experiments. The details of the components in bioink and the preparation method were described in the previous chapter. The bioink was freshly prepared every time on the day of trial. Once the bioink was well-mixed, the temperature of the water bath was reduced to 35°C and the solution was left for 15 minutes to attain equilibrium prior printing.

The ink was printed in ambient environment maintained at (25 ± 1) °C with a relative humidity of 40% to 55%. The drop in temperature from 35°C to 25°C triggered the gelation of the solution, increasing the ink viscosity significantly which brought it to the level required for screen printing. The room temperature and relative humidity were monitored to reduce the discrepancies between successive experiments because both are key factors in gelling process of solution.

6.2.2 The substrate

White gloss pre-treated polystyrene sheet was used in this investigation due to the good compatibility and adhesion to gelatine (bioink) which was observed during preliminary print trials. The properties of polystyrene substrate have been detailed in the previous chapter.

6.2.3 Parameter studied

The previous work suggests that the ink type is the dominant parameter in determining the ink film thickness [1]. There are two characteristics of the ink that affect the screen printing process, viscosity and surface tension which were discussed in Chapter 4. Thus two identical orthogonal arrays (16 experiments each) were conducted for 10% and 15% aqueous gelatine solutions in this study. It is expected that 15% ink would give narrower lines than those of 10% ink due to its higher viscosity.

In order to determine the settings of process parameters, preliminary trials were performed prior actual trial to study the level of process parameters that produced better prints which were then used in this print trial. Two mesh types were selected which are polyester and stainless steel for comparison in line quality. Table 6.1 shows the properties of both meshes. The mesh tensions in warp and weft directions were measured before and after each print run. This was found to be (21 ± 1) N/cm for polyester screen and (20 ± 1) N/cm for stainless steel screen respectively which was within the quoted accuracy of the tension measurement instrument. Stainless steel mesh is commonly used in printing fine features due to its greater mesh count. It was expected that the stainless steel mesh produced wider lines with lower film thickness due to its greater open area and lower mesh thickness.

Mesh properties	Polyester	Stainless steel
Mesh tension (N/cm)	22	20
Mesh count (threads/cm)	90	97
Thread diameter (μm)	48	30
Opening (μm)	55	50
Open area (%)	25	39
Mesh Thickness (μm)	65	47

Table 6.1: Summary of mesh properties

The effect of squeegee type was investigated at two levels, 65 – 70 (soft) and 70 – 75 (medium) Shore A hardness. Commercially available standard ULON HP squeegees of diamond profile 9.5 mm x 9.5 mm were used. The squeegees were cut into 135 mm length to accommodate the squeegee carrier of the press. The angle of the squeegee was fixed at 45° for all experiments.

The snap-off gap was set at 2 mm (normal operating condition, level 1) and 3 mm (level 2). These values were measured by placing copy paper sheets of 0.11 mm thickness each, between the screen and substrate, then the thickness of the total number of copy papers were measured by using a calliper. These measurements were repeated several times, and proved to be reliable.

Two levels of squeegee pressure were used, 6.4 mm as level 1 and 6.7 mm as level 2. These are the gauge values taken from the system on the press. In order to quantify the gauge values in standard pressure unit, a force sensor was positioned on the substrate carrier to determine the force applied on the screen, onto the sensor for each pressure setting and each squeegee type. The applied squeegee pressure was then calculated (Figure 6.1) in bars. Squeegee of 75 – 80 (hard) Shore A hardness was tested with the same settings to determine the trend of the measurements. By changing the soft squeegee to medium squeegee, the pressure increases greatly by 81%, while only a small increase

of 12% from medium to hard squeegee. For the pressure settings, the pressure of soft and medium squeegees has risen by about 0.15 bar from level 1 to level 2, while only 0.05 bar for that of hard squeegee. This confirms the interaction between squeegee pressure and squeegee type.

Squeegee speed was set at two levels, 1 revolution (normal operating condition) and 1.5 revolutions, which are also the gauge values taken from the system. Similarly, the squeegee speed was calculated and shown in Figure 6.2. The movement of squeegee is slowed down by increasing the shore A hardness of squeegee. From level 1 to level 2 speed setting, the squeegee speed was increased by approximately 0.03 m/s. This confirms there is interaction between squeegee speed and squeegee type.

The summary of the process parameters chosen for this laboratory printing trial is shown in Table 6.2.

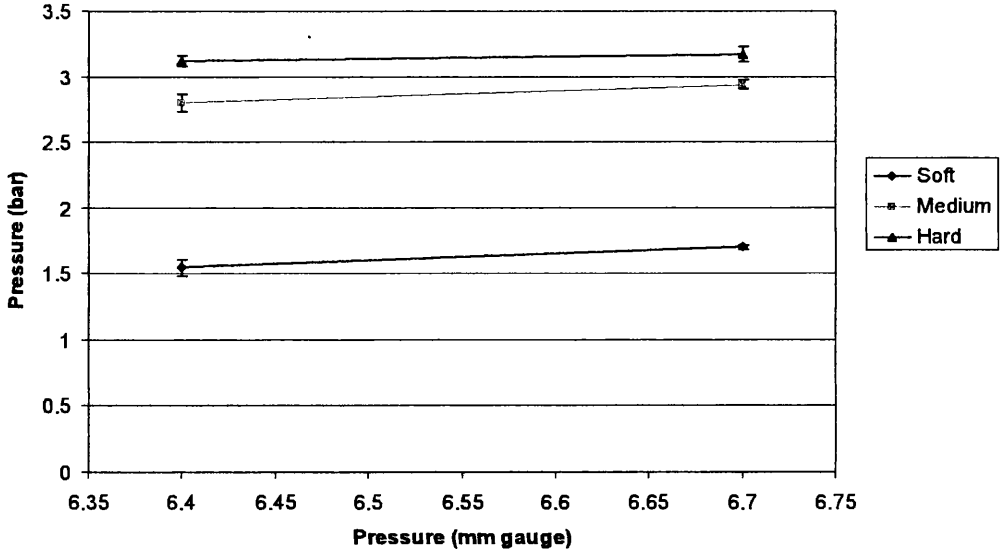

Figure 6.1: Squeegee pressure applied on press in standard unit

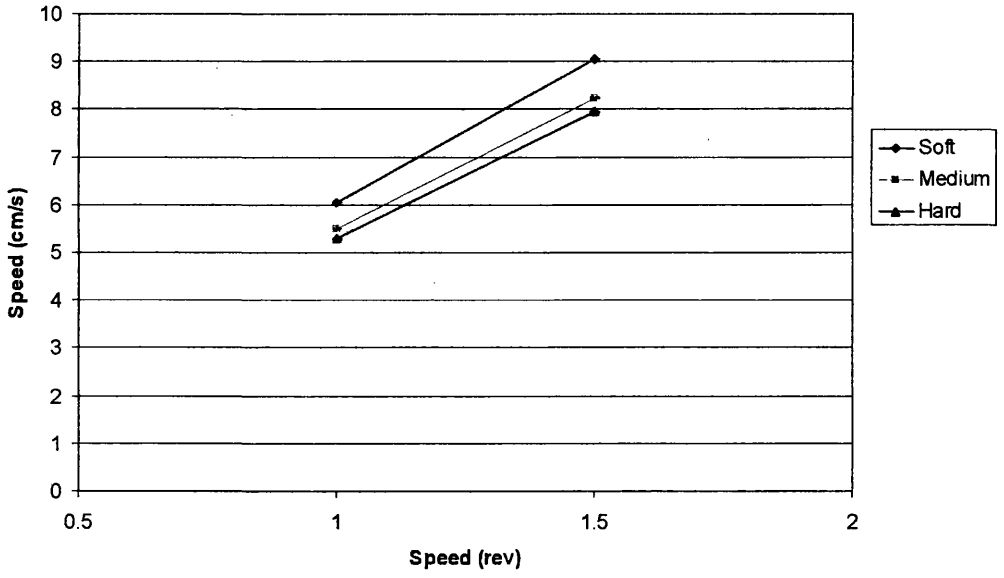

Figure 6.2: Squeegee speed applied on press in standard unit

Process Parameters	Level 1	Level 2
Mesh type	Polyester	Stainless Steel
Squeegee type	Soft	Medium
Snap off (mm)	2.0	3.0
Squeegee speed (rev)	1.0	1.5
Squeegee Pressure (mm gauge)	6.4	6.7

Table 6.2: Summary of process parameters used in trial

6.2.4 Orthogonal Array Approach

An orthogonal array experiment was designed. L_{16} orthogonal array was selected as it was able to examine the five variables interested, and their interactions. This experimental technique also reduces the number of experiments which need to be carried out [2], sixteen experiments were performed, compared with conducting a full factorial experiment which would require thirty two experiments. A description of orthogonal array was presented in Chapter 3.

Two levels were selected for each process parameter (referred to as 1 and 2). In each case, the normal setting of the parameter was level 1 and a different higher level setting as level 2. The design of the L16 orthogonal array is shown in Table 6.3.

The linear graph of the orthogonal array used is shown in Figure 6.3 for the L_{16} array where each dot indicates a variable, and each line indicates the interaction between these two variables.

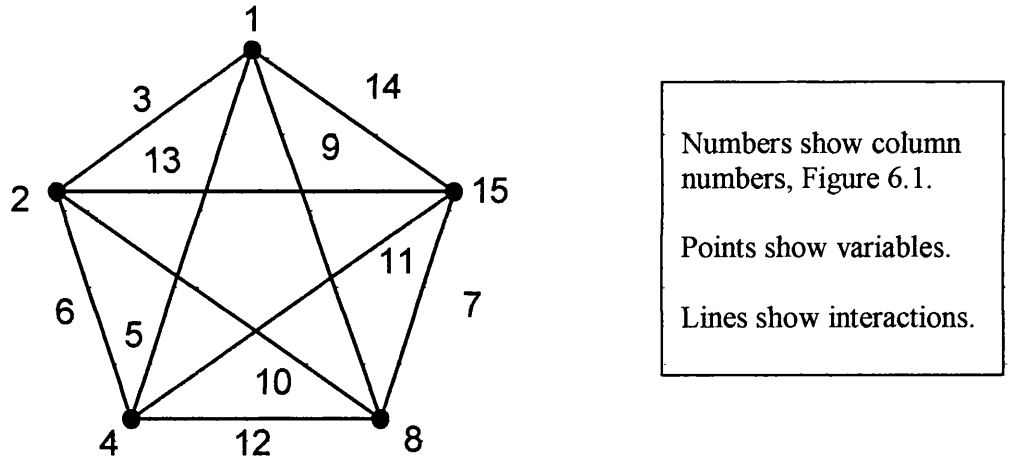

Figure 6.3: Linear graph selected for L_{16} array

Exp. no.	Mesh type	Sq type	Mesh type / Sq type	Snap off	Mesh type / Snap off	Sq type / Snap off	Sq speed / Sq pressure	Sq speed	Mesh type / Sq speed	Sq type / Sq speed	Snap off / Sq pressure	Snap off / Sq speed	Sq type / Sq pressure	Mesh type / Sq pressure	Sq pressure	Quanti-tative result
	1	**2**	**3**	**4**	**5**	**6**	**7**	**8**	**9**	**10**	**11**	**12**	**13**	**14**	**15**	
1	1	1	1	1	1	1	1	1	1	1	1	1	1	1	1	
2	1	1	1	1	1	1	1	2	2	2	2	2	2	2	2	
3	1	1	1	2	2	2	2	1	1	1	1	2	2	2	2	
4	1	1	1	2	2	2	2	2	2	2	2	1	1	1	1	
5	1	2	2	1	1	2	2	1	1	2	2	1	1	2	2	
6	1	2	2	1	1	2	2	2	2	1	1	2	2	1	1	
7	1	2	2	2	2	1	1	1	1	2	2	2	2	1	1	
8	1	2	2	2	2	1	1	2	2	1	1	1	1	2	2	
9	2	1	2	1	2	1	2	1	2	1	2	1	2	1	2	
10	2	1	2	1	2	1	2	2	1	2	1	2	1	2	1	
11	2	1	2	2	1	2	1	1	2	1	2	2	1	2	1	
12	2	1	2	2	1	2	1	2	1	2	1	1	2	1	2	
13	2	2	1	1	2	2	1	1	2	2	1	1	2	2	1	
14	2	2	1	1	2	2	1	2	1	1	2	2	1	1	2	
15	2	2	1	2	1	1	2	1	2	2	1	2	1	1	2	
16	2	2	1	2	1	1	2	2	1	1	2	1	2	2	1	
Lev1																
Lev2																

Variable Interaction Results

Table 6.3: L_{16} Orthogonal array used in the investigation

6.2.5 Test image

The same test image (85 x 85 mm) was used for the investigation as was used in the preliminary investigation (Figure 6.4). The image included groups of parallel lines of width and separation 100μm, 200μm and 300μm at 0° (horizontal), 45° (diagonal) and 90° (vertical) to the print direction as well as various size solid patches (81mm^2, 25 mm^2, 2.5 mm^2 and 1 mm^2) and two circles of 200 μm and 400 μm line width. It was designed to investigate several line widths and the orientation of lines to the print direction. This investigation focused on the widest lines of 300 μm.

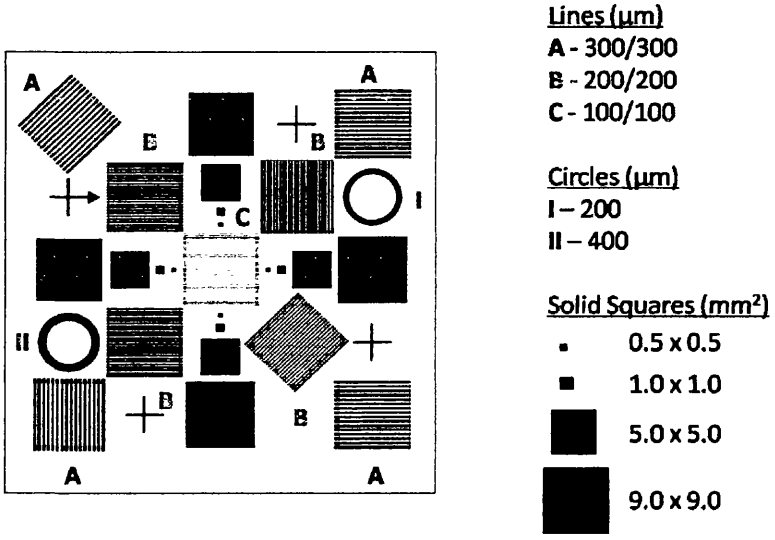

Figure 6.4: The image used for the investigation into screen printed gelatine fine lines

6.2.6 Experimental procedure

Before starting an experiment trial, the ink was freshly prepared and held in the water bath at 35°C. IPA solution was used to clean the substrates to remove dust and any contamination. All samples were labelled and placed on top of a clean surface. The press settings were set as required for the particular experiment.

The screen press was then run for approximately 8 minutes to produce six prints with two acceptable prints which were visually accessed to have the better print quality for measurement and analysis, Figure 6.6. The chosen prints were the second and third printed images for each run. The print run was repeated twice in order to obtain six acceptable prints required for analysis. After each run, the ink was returned to the water bath to prevent gelation; the screen was also cleaned gently with warm water and dried for about 5 minutes. All printed images were air-dried for 24 hours prior to measurements. Once the experiment was completed, the parameter settings were adjusted to those needed for the next experiment.

6.3 Results

6.3.1 Lines on screen

The 300 micron stencil lines on polyester and stainless steel screen were measured using white light interferometer. The measured line width was presented in Figure 6.5 for three line directions. Standard deviation is displayed as an indication of line consistency. The width of stencil lines on stainless steel screen was approximately 310 microns, while polyester screen has stencil lines of 298 micron width, regardless of line directions. The stencil lines produced on both screens have good consistency in width due to its low standard deviation, within 4 microns. The width of stencil lines were compared to the width of lines printed.

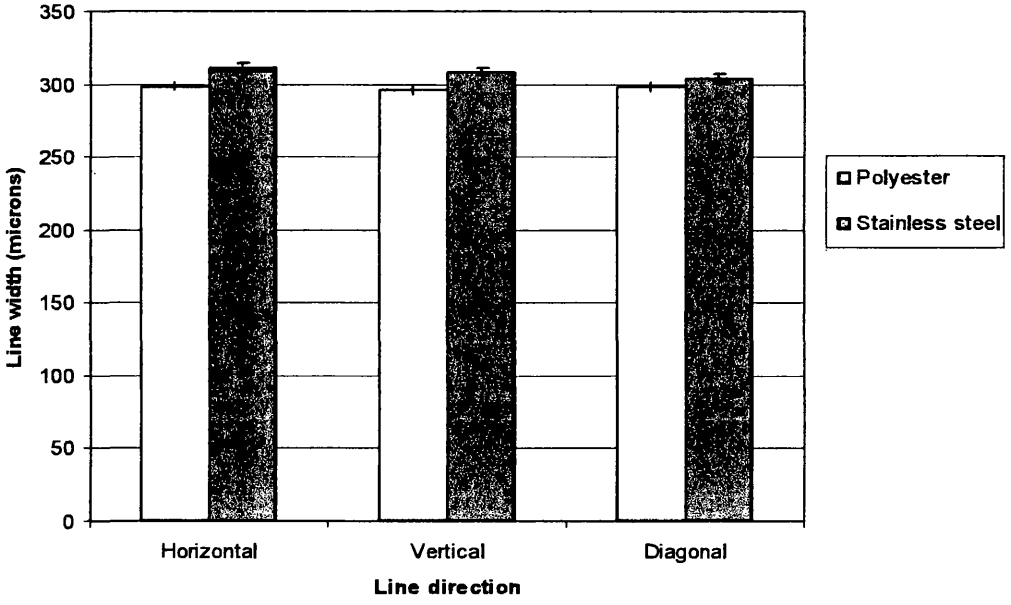

Figure 6.5: Stencil lines on polyester and stainless steel screen

6.3.2 Lines on printed image

The quality of printed lines of 10% ink on polystyrene substrates was examined. The work focused on the 300 micron lines with 300 micron gap at 0° (horizontal), 45° (diagonal) and 90° (vertical) to show the trends due to process parameters. The interactions are also presented. In this study, only 300 micron printed lines were investigated. This was because the printed lines of narrower width, 100 and 200 μm were observed to be broken. There were also connections between parallel lines due to ink spreading.

Figure 6.6 shows six typical images printed using parameter settings for experiment no.7 which produced the best line quality in terms of width and film thickness with lowest standard deviation, out of sixteen experiments. The printed lines are better defined from print (a) to (c), but started to fade from forth print and getting worse till the last print (f). During printing, the gelling process of ink was triggered when the ink temperature

dropped from 35°C (water bath) to about (25 ± 1) °C (room temperature), increasing the viscosity of ink over time. When the ink was first deposited onto the screen straight from the water bath, the ink was still in diluted liquid form. The ink was spread by the flowcoater and forced through the mesh by the squeegee and transferred onto the substrate. During printing stroke, the originally low viscosity of ink was further reduced due to high shear applied; causing the ink to flow. This resulted in massive ink spread that connected the parallel lines. Then, the increase in ink viscosity over time due to gelling, reaches an optimum level which gives good quality second and third print. From print to print, the combined effect of gelling and evaporation of water content in ink occurs significantly every time when the flow coater scraps the ink back to original position after the print stroke. The print quality therefore starts to become worse and blurry from fourth print onwards as less ink was transferred to the substrate. The ink gels completely after the sixth print.

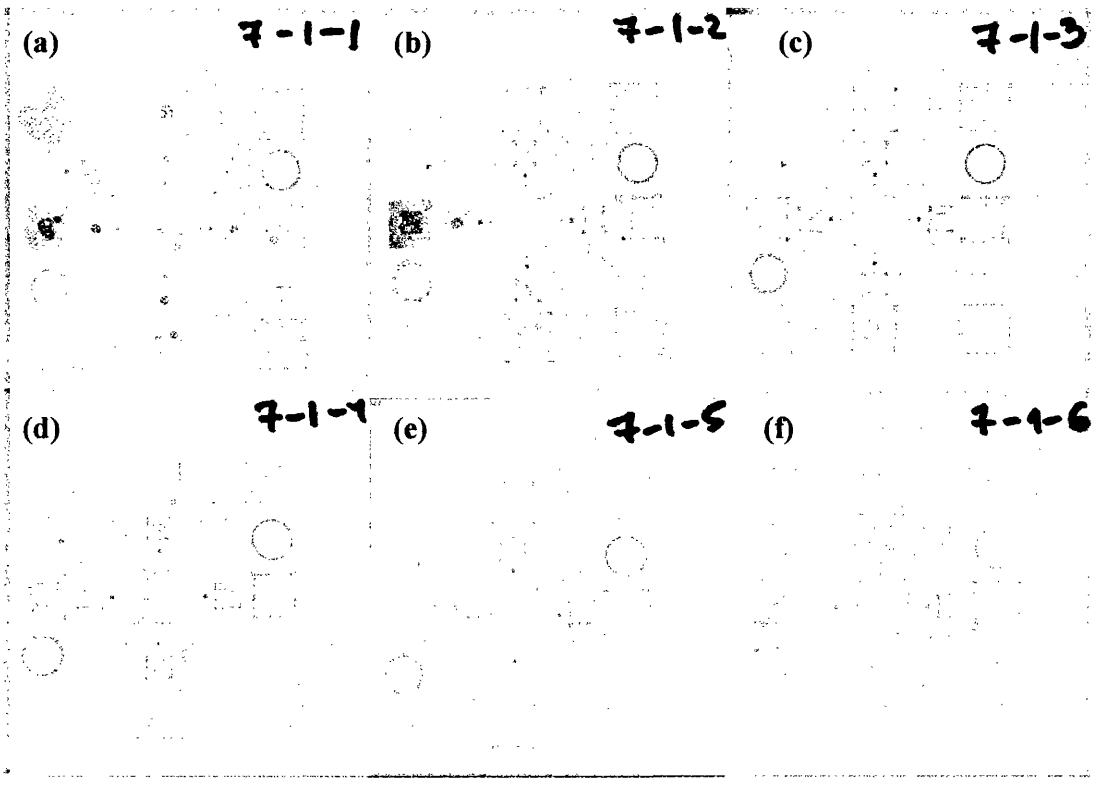

Figure 6.6: Six typical printed images per run of each experiment

6.3.2.1 Line width

Standard deviation is an indication of line consistency. For width of printed gelatine lines, the effect of squeegee type on standard deviation is the most significant, decreasing about 8.8 μm to 4.7 μm when soft squeegee was changed to medium squeegee. This is followed by mesh type and snap off gap. When stainless steel mesh was used, the standard deviation increased about 7.5 μm. An increase in standard deviation of line widths was observed, ranging from 6.9 μm to 1.4 μm when snap off gap was increased from 2 – 3 mm. Both squeegee pressure and squeegee speed have the least effect on the width variability. Slightly better width consistency was obtained when higher squeegee speed and lower squeegee pressure were used.

The effect of five process parameters on line width is illustrated in Figure 6.7. The snap off gap has the greatest effect on the line width. It was expected that the line width would increase when the snap off gap was increased. However, this was not the case. The increase in snap off gap from 2 mm to 3 mm decreased the width of printed lines by approximately 20%, bringing it closer to the nominal line width. The width of diagonal lines decreased the most from 367 μm to 285 μm, followed by horizontal lines and the least for vertical lines. This is further discussed in section 6.4.

The effect of mesh type is also significant, where the stainless steel screen produced wider lines than those of polyester screen. With the compensation of 12 μm difference between the width of stencil lines on both screens, the greatest increase of about 21 μm in width was observed for vertical lines, 39 μm for horizontal lines and the least of about 20 μm for diagonal lines.

All three squeegee parameters: squeegee pressure, squeegee type and squeegee speed, have much smaller effect on the printed line width. The increase in squeegee pressure increased the width of printed lines by 6 μm, but only produced an increase of 2 μm for vertical lines. The squeegee speed and squeegee type have least effect on line width where greater squeegee pressure and lower squeegee speed produce greater line width. For a given squeegee angle and pressure, there is a reduction in the solid density with increasing hardness of the squeegee [3]. The line width between the soft and medium squeegee followed this trend where softer squeegee gave similar wider lines than that of medium hardness squeegee.

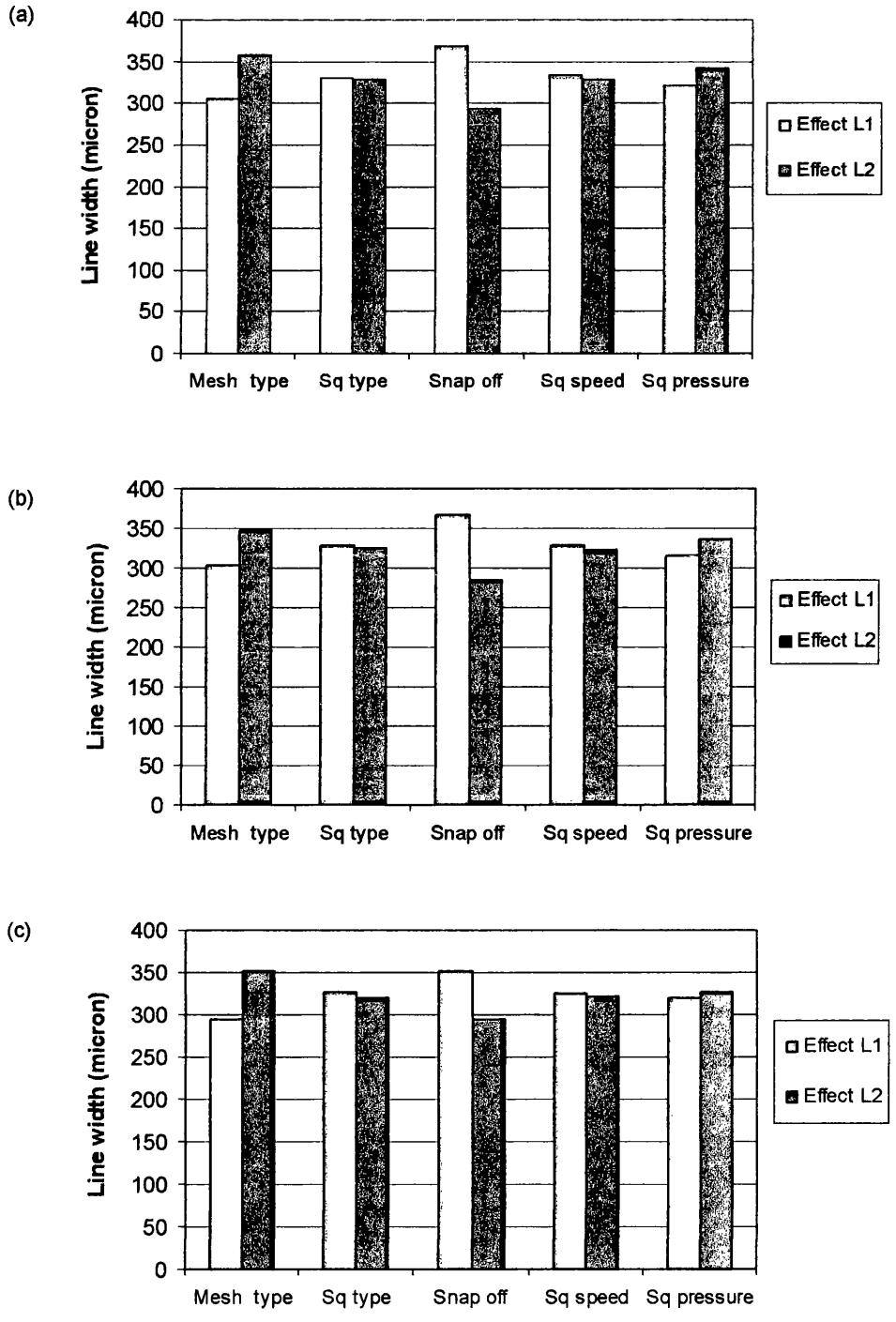

Figure 6.7: The effect of 5 parameters on line width of (a) horizontal (b) diagonal and (c) vertical lines

It is possible to examine the net effect of each parameter on line width by taking the difference between the mean line width produced at level 1 and level 2, Figure 6.8.

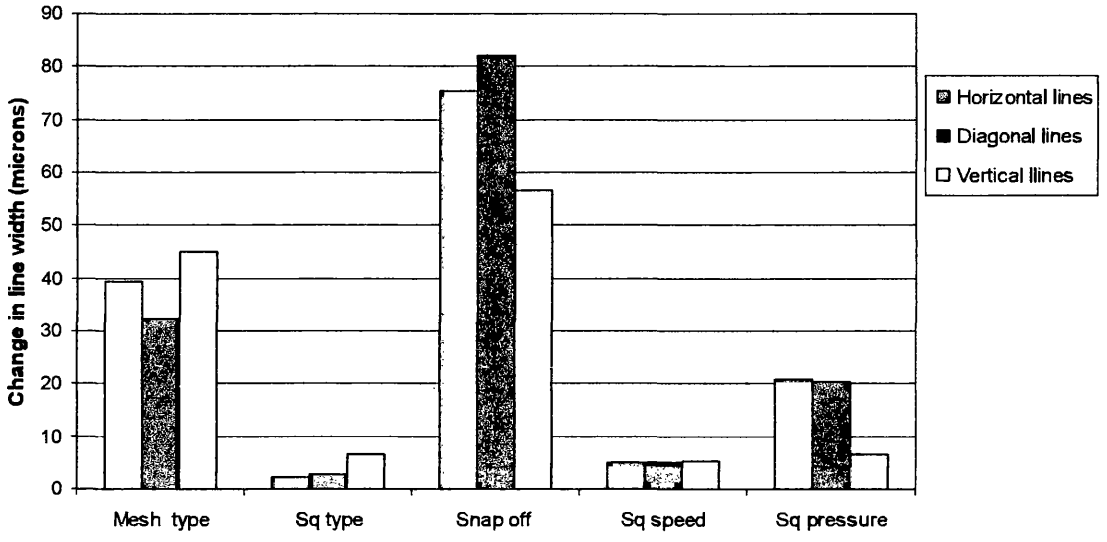

Figure 6.8: The net effect of each of the parameters on line width

6.3.2.2 Interactions between process parameters for line width

Interactions are often assumed to be negligible because results are generally easier to explain and implement if there are no interaction effect. However, this might lead to erroneous conclusions. Therefore interaction plays an important role in the analysis and interpretation of results from experimental and observational studies [4]. When the effect of a parameter on the process changes when another parameter setting is changed, an interaction occurs [2].

By virtue of the design of the L_{16} array, the interactions between each of the parameter settings can be examined, Figure 6.9 to Figure 6.14. The results suggested that interactions exist between mesh type and squeegee hardness; the change in mesh type

from polyester to stainless steel increased the line width significantly when medium squeegee was used, Figure 6.9. Mesh type also interacted with squeegee pressure, Figure 6.10. The line width remained the same, independent of squeegee pressure when polyester screen was used. When the stainless steel screen was used, the line width increased significantly at higher squeegee pressure, about 53 μm while only 3 μm at squeegee pressure of 6.4 mm gauge. Thus, the system was observed to be more sensitive at greater squeegee pressure of 6.7 mm gauge. For conversion of squeegee pressure and squeegee speed, refer to Figure 6.1 and Figure 6.2.

There were also interactions between snap off gap and squeegee pressure, Figure 6.11. Snap off gap has slightly greater effect at greater squeegee pressure (6.7 mm gauge). When the snap off gap increases, more of the pressure applied to the squeegee is used to deflect the screen and bring it in contact with the substrate. Thus, applying a large screen gap has similar effect on print thickness as the use of low squeegee pressure.

As expected, there were interactions between squeegee type and both squeegee speed and squeegee pressure, Figure 6.12 and Figure 6.13. At lower squeegee speed, the line width decreased by about 10 μm when medium squeegee was used. An opposite effect was shown when higher squeegee speed was applied where wider lines were observed by changing the squeegee type from soft to medium. The interaction between squeegee type and squeegee pressure showed similar trend. At lower squeegee pressure of 6.4 mm gauge, the line width increased 10 μm when medium squeegee was used, whilst a decrease of 18 μm occurred at higher squeegee pressure of 6.7 mm gauge. The printing system had greater effect on line width at higher squeegee pressure of 6.7 mm gauge and lower squeegee speed of 1.0 rev. There was also interaction between squeegee speed and squeegee pressure, Figure 6.14. The squeegee pressure had insignificant effect on the printed lines at lower squeegee speed where similar width was shown. When the squeegee speed was changed to a higher level of 1.5 rev, there was a reduction in the line width, about 20 μm at lower squeegee pressure, but an increase of about 12 μm was observed at squeegee pressure of 6.7 mm gauge.

There were either insignificant or no interactions at all between the parameters as given below. These graphs are included in Appendix B.

(a) mesh type and snap off gap
(b) mesh type and squeegee speed
(c) snap off gap and squeegee speed
(d) squeegee type and snap off gap

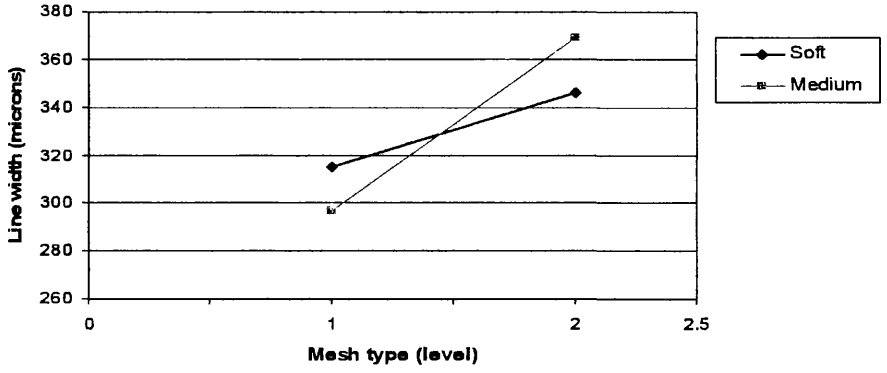

(a) Horizontal lines

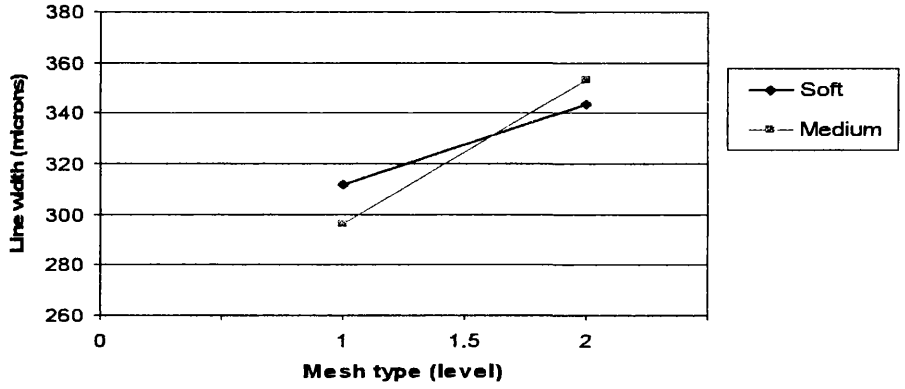

(b) Diagonal lines

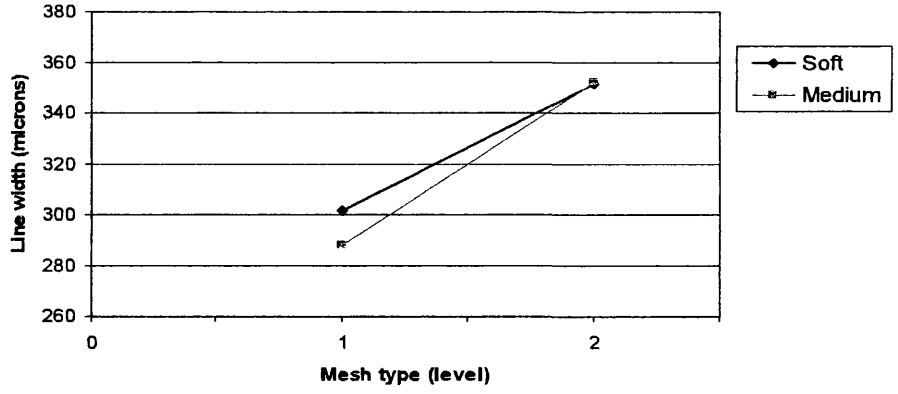

(c) Vertical lines

Figure 6.9: The effect of interaction between mesh type and squeegee type on line width

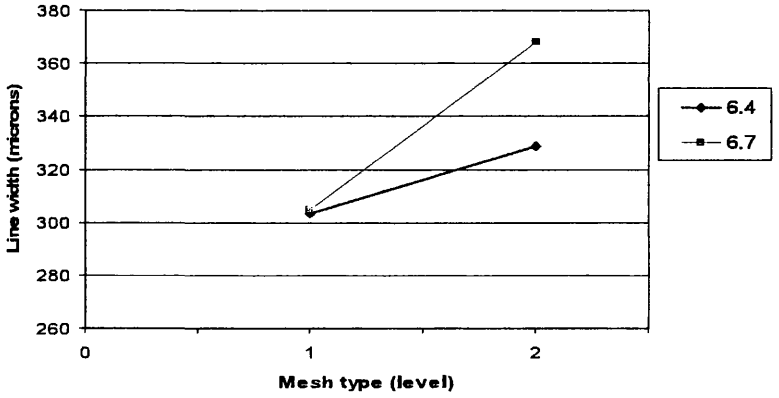

(a) Horizontal lines

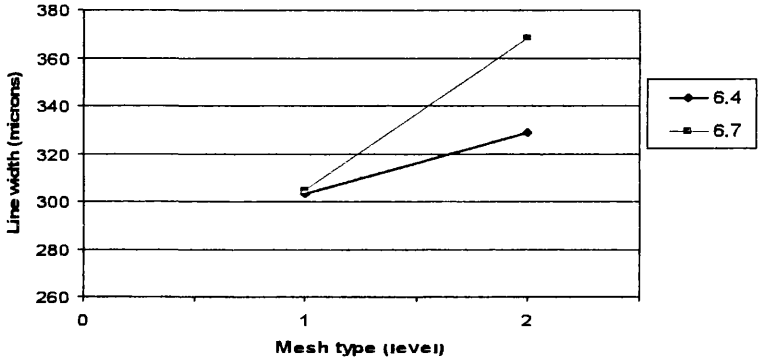

(b) Diagonal lines

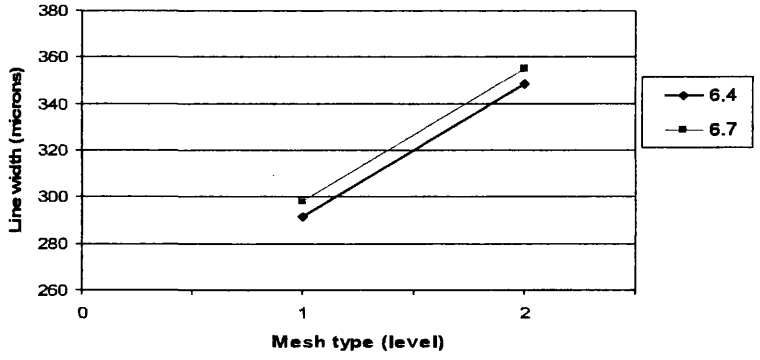

(c) Vertical lines

Figure 6.10: The effect of interaction between mesh type and squeegee pressure on line width

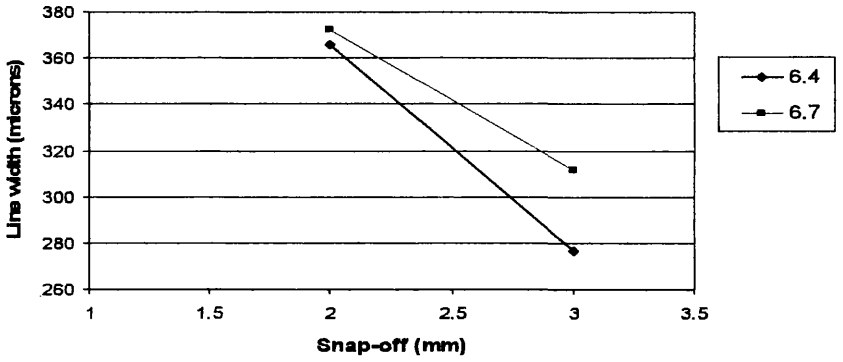

(a) Horizontal lines

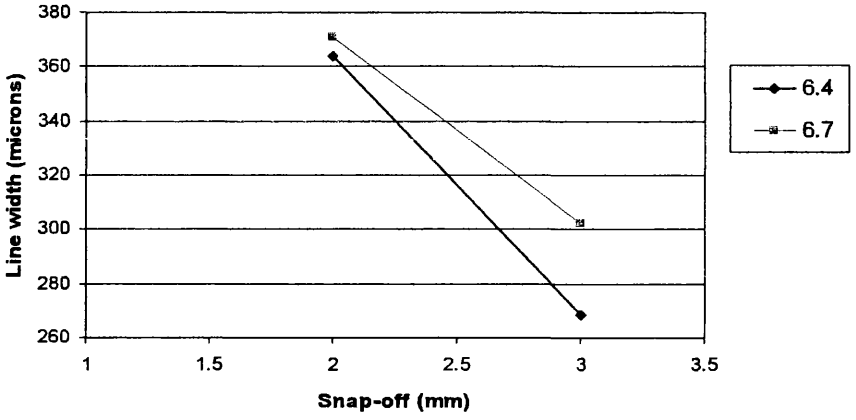

(b) Diagonal lines

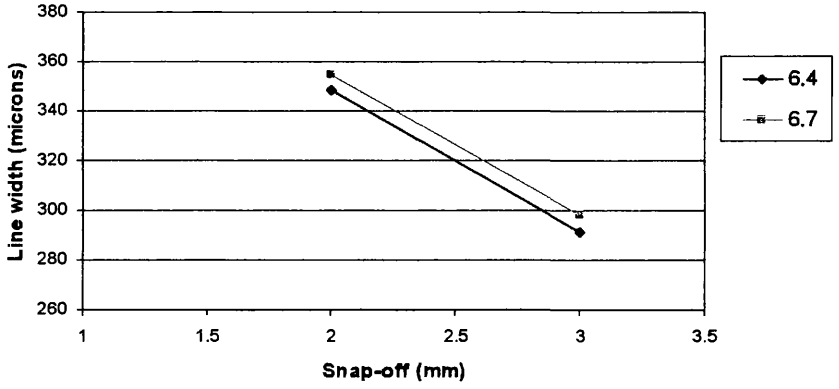

(c) Vertical lines

Figure 6.11: The effect of interaction between snap off gap and squeegee pressure on line width

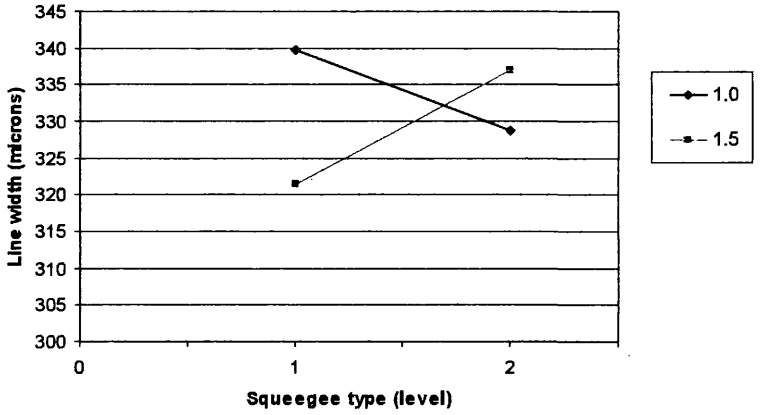

(a) Horizontal lines

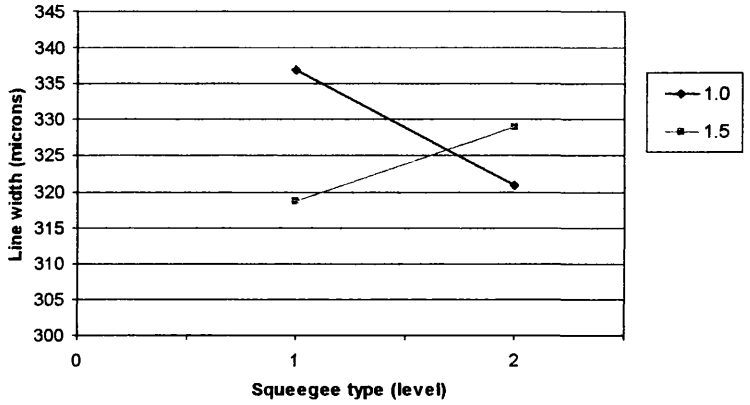

(b) Diagonal lines

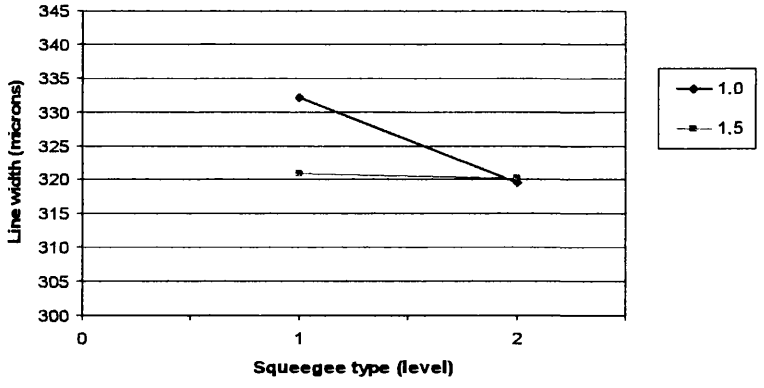

(c) Vertical lines

Figure 6.12: The effect of interaction between squeegee type and squeegee speed on line width

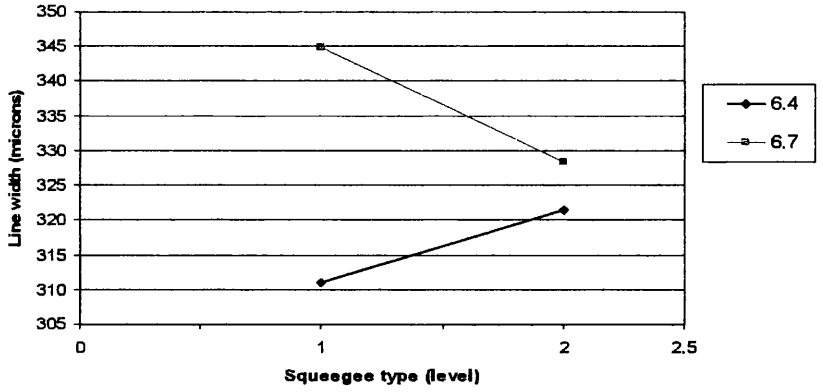

(a) Horizontal lines

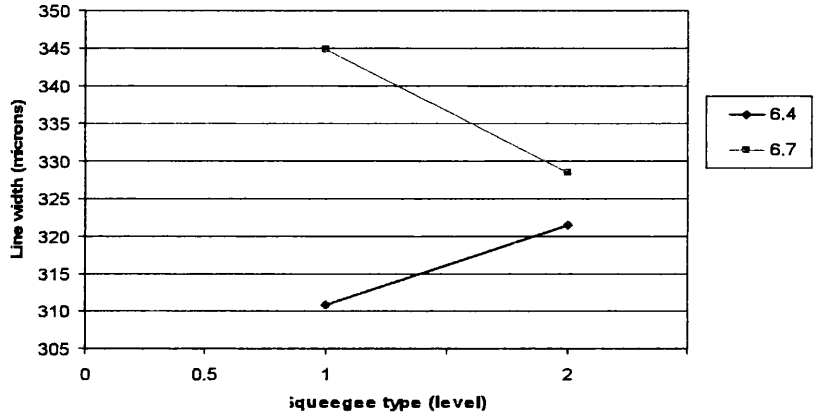

(b) Diagonal lines

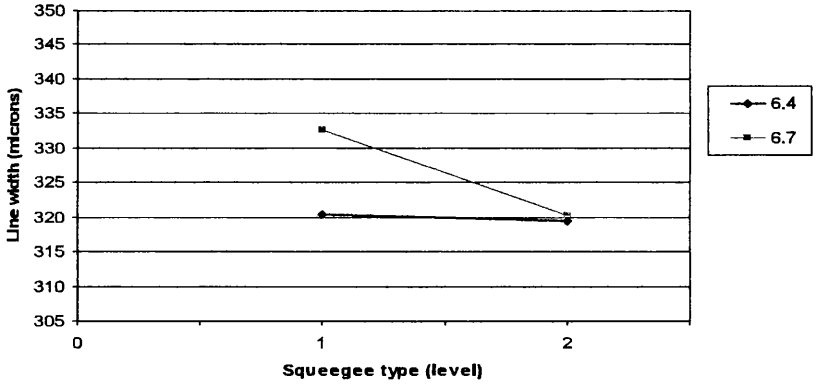

(c) Vertical lines

Figure 6.13: The effect of interaction between squeegee type and squeegee pressure on line width

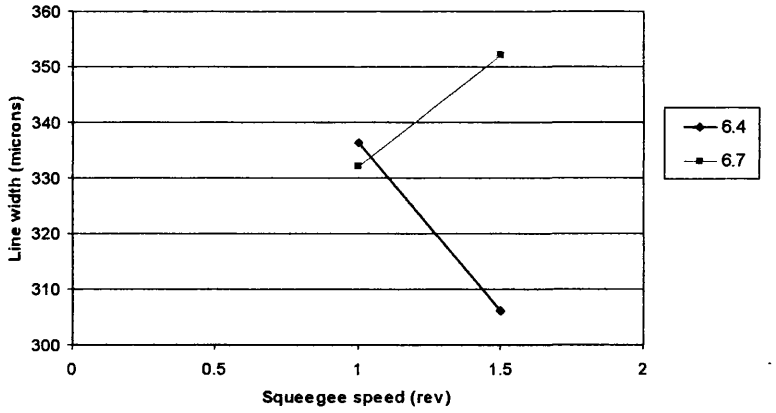

(a) Horizontal lines

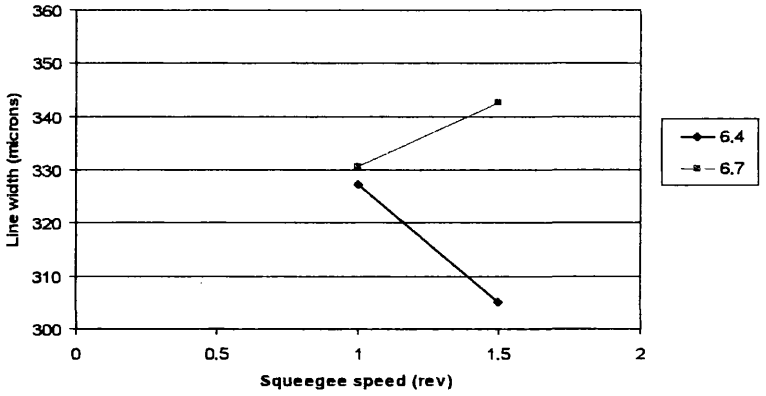

(b) Diagonal lines

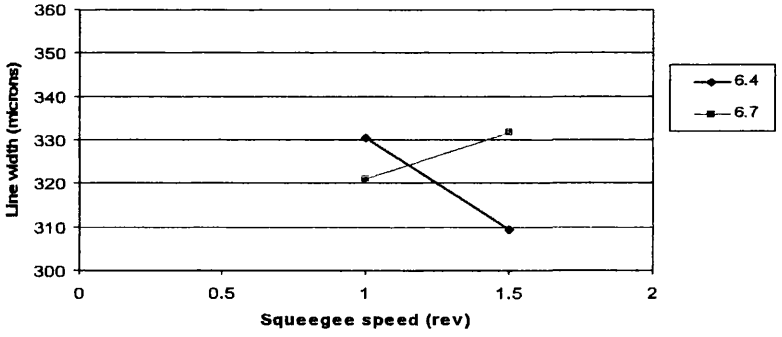

(c) Vertical lines

Figure 6.14: The effect of interaction between squeegee speed and squeegee pressure on line width

6.3.2.3 Ink film thickness

In determining the line quality, the line width analysis has focused on the fluctuations in the line in 2-dimentional plane as perceived when the print is visually examined. In many instances, for example bio-applications and electronics industries, the variation in line film thickness is also very important as it plays a key role in defining the cross sectional area of the line. Dry ink film thickness was measured instead of the wet one because the line height of wet samples changed with solvent evaporation and therefore was time dependent, whilst dry sample was time independent and can be stored for re-measurement if necessary. The dry line film thickness has been averaged for each experiment for all three line orientations. The line consistency is reflected in standard deviation.

The film thickness for 300 micron nominal line width displays a large variation in results depending on the combination of parameter settings. The line film thickness varied from 1.4 μm to 7.0 μm, with standard deviation ranging from 6 μm to 0.2 μm. Similarly, the effect of each parameter on the standard deviation of line film thickness was studied. Snap off gap was found to have the greatest effect on the standard deviation with a significant reduction of 1.5 μm when 3 mm snap off gap was used. This is followed by squeegee type and mesh type. The standard deviation of line film thickness increased about 0.98 μm when medium squeegee was used whereas decreased about 0.91 μm when stainless steel mesh was used. This trend is similar to the results obtained for line width. Both squeegee speed and squeegee pressure have the least effect on the line film thickness variability. Slightly better line consistency was obtained when greater squeegee speed and squeegee pressure were used with a variation of about 0.15 μm.

The effect of each parameter is presented in the bar charts, Figure 6.15. The heights of the bars indicate the effect of each setting on the line film thickness. The effect of most process parameters on line film thickness was similar to those on line width. Snap off gap was found to have the most significant effect on line film thickness, same as its effect on line width. When the snap off gap was increased from 2 mm to 3 mm, the line film

thickness was reduced by about 1.4 μm for diagonal and vertical lines, while only 0.4 μm for horizontal lines.

The next most significant parameter was mesh type. By changing the mesh type, the polyester screen produced thicker lines than that of stainless steel mesh for diagonal lines. Mesh type was shown to have only a little effect on printed horizontal and vertical lines. Squeegee type also affects the thickness of diagonal lines, and a small effect on vertical lines obtained where softer squeegee gave thinner lines, Figure 6.15. The greatest difference in line film thickness was approximately 0.8 μm thinner when soft squeegee was used. This was probably because the extra ink transferred during printing caused more ink spreading which resulted in wider lines printed, rather than increasing the line film thickness.

The squeegee speed had a small effect on the line film thickness showing a small reduction in the ink deposit with increasing speed. By increasing the squeegee pressure the ink deposit was increased, giving thicker lines. Overall, the effect of both squeegee parameters was relatively small on line film thickness.

The net effect of the process parameters on line film thickness were also determined and shown in Figure 6.16. The film thickness of both diagonal and vertical lines was affected significantly by changing the parameter settings, whereas there was a smaller effect on horizontal lines.

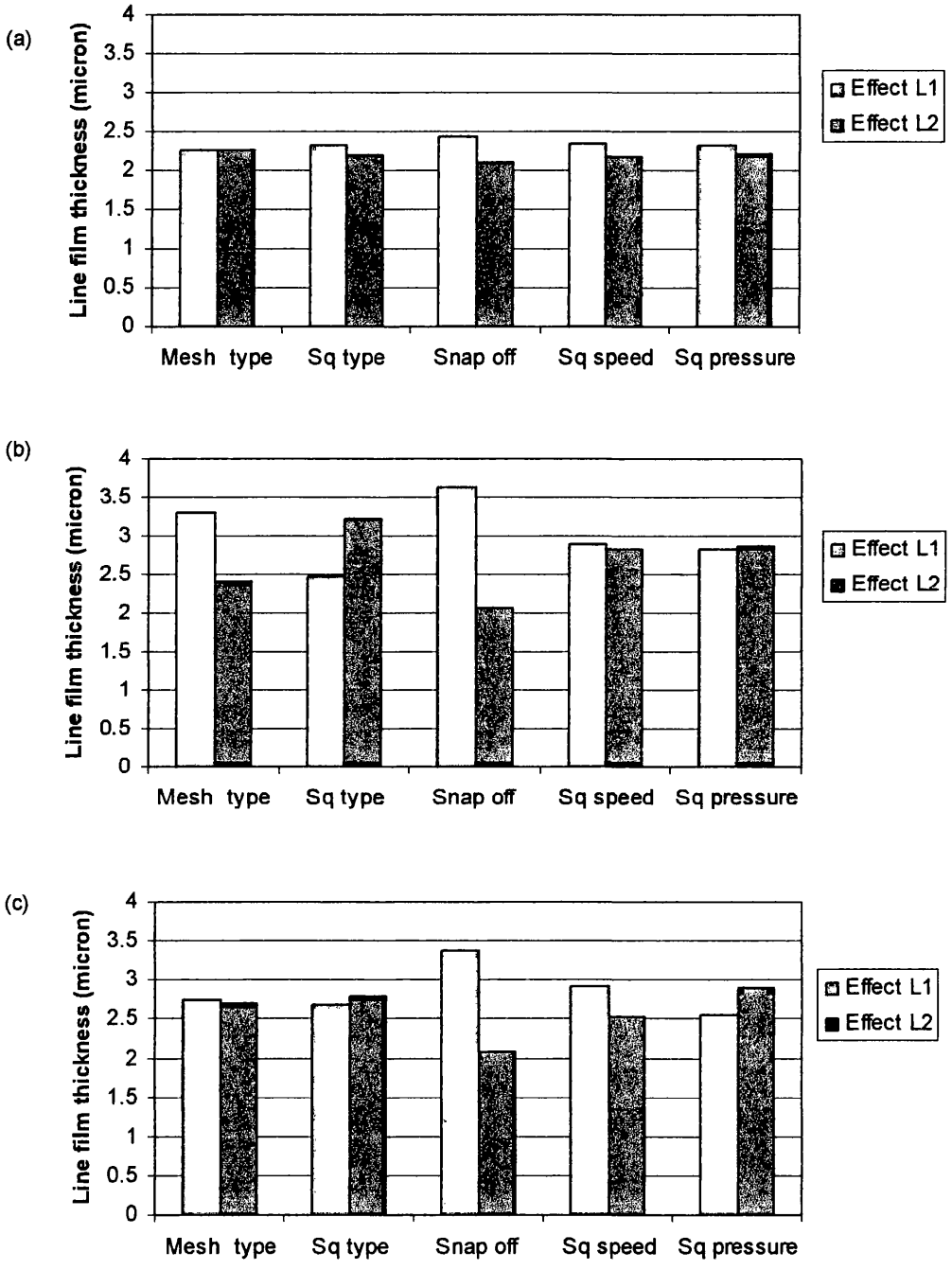

Figure 6.15: The effect of 5 parameters on line film thickness of (a) horizontal (b) diagonal and (c) vertical lines

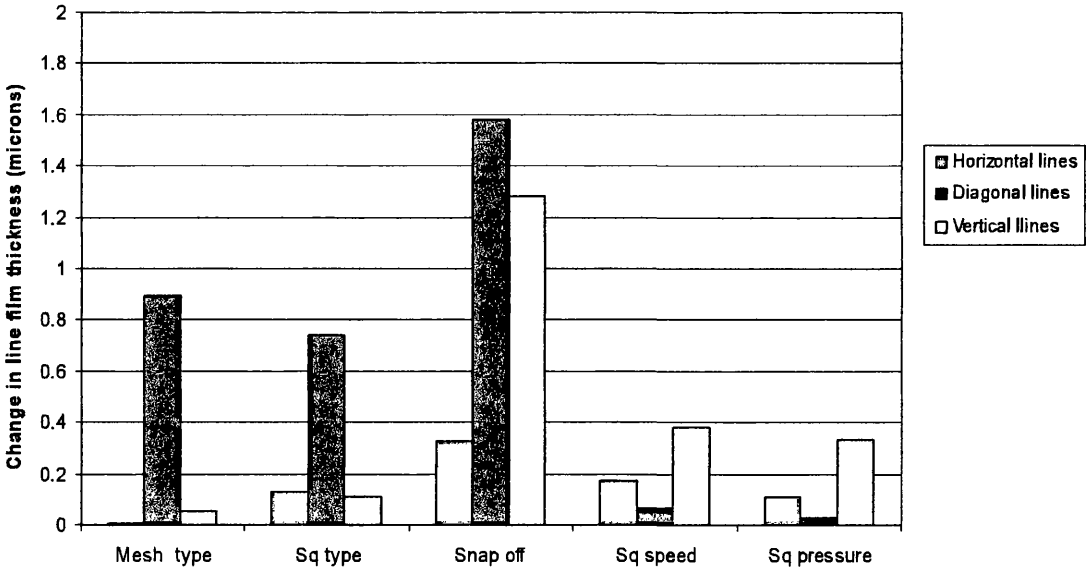

Figure 6.16: The net effect of 5 parameters on line film thickness

6.3.2.4 Interactions between process parameters for line film thickness

The interactions between the squeegee parameters for line film thickness of 300 micron printed lines of three line directions are shown in Figure 6.17 to Figure 6.20. The mesh type interacted with squeegee type on film thickness of diagonal lines. There was no effect of squeegee type on the film thickness when stainless steel screen was used. The polyester screen was more sensitive where thicker lines (about 1.5 μm) were obtained when medium squeegee was used compared to soft squeegee, Figure 6.17. An anti-directional interaction was observed between mesh type and snap off gap, Figure 6.18. When polyester screen was used, small snap off gap produced higher line film thickness of 3.5 μm than that of larger snap of gap. Snap off gap had no effect on line film thickness when stainless steel screen was used. The line film thickness remained the same at 2.4 μm.

There was interaction between squeegee type and snap off gap, Figure 6.19. The thickness of printed lines increased at 2 mm snap off gap whilst remained almost the same at 3 mm snap off gap, when changing the squeegee type from soft to medium. Thicker lines were obtained by using medium squeegee at smaller snap off gap. Besides, squeegee speed and squeegee pressure did interact with each other (Figure 6.20) where higher line film thickness was observed when higher squeegee pressure and lower squeegee speed were applied and vice versa.

No interaction was found between other combinations of process parameters as the follows (see Appendix B for these graphs):

(a) Mesh type and squeegee speed
(b) Mesh type and squeegee pressure
(c) Snap off gap and squeegee speed
(d) Snap off gap and squeegee pressure
(e) squeegee type and squeegee speed
(f) squeegee type and squeegee pressure

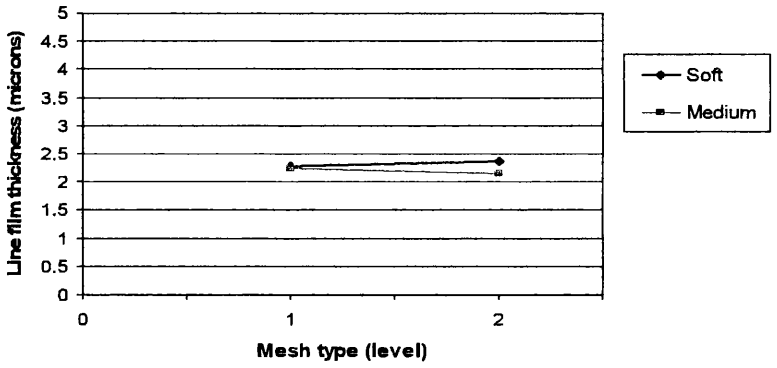

(a) Horizontal lines

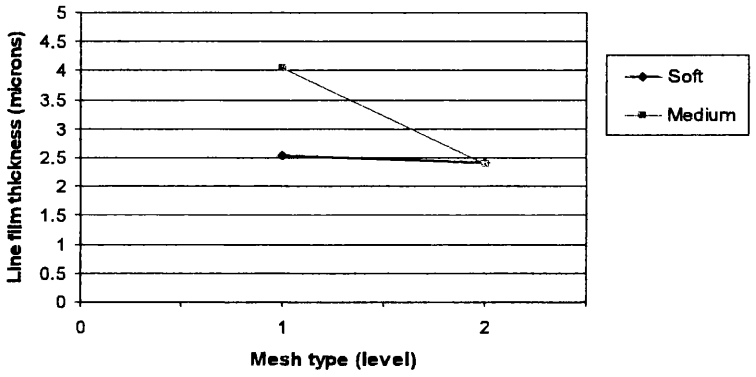

(b) Diagonal lines

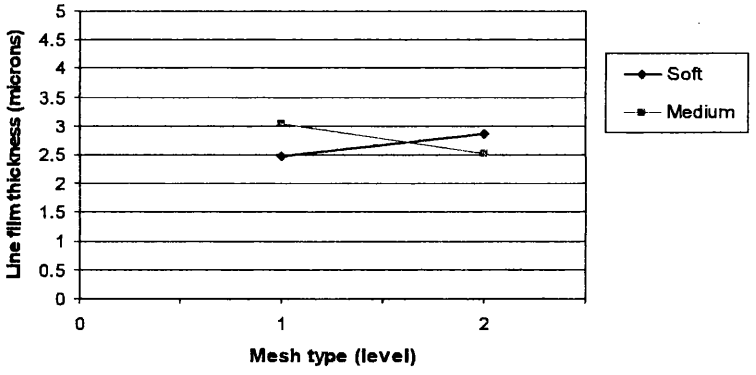

(c) Vertical lines

Figure 6.17: Interaction between mesh type and squeegee type on line film thickness

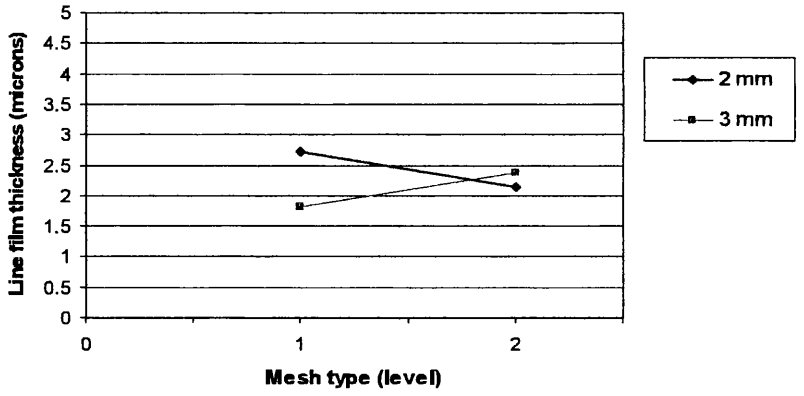

(a) Horizontal lines

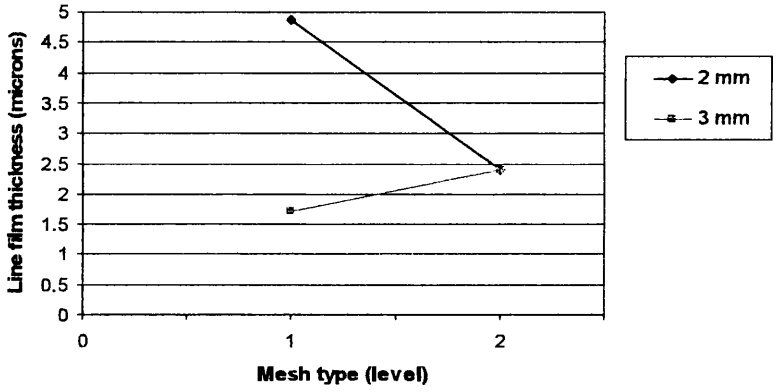

(b) Diagonal lines

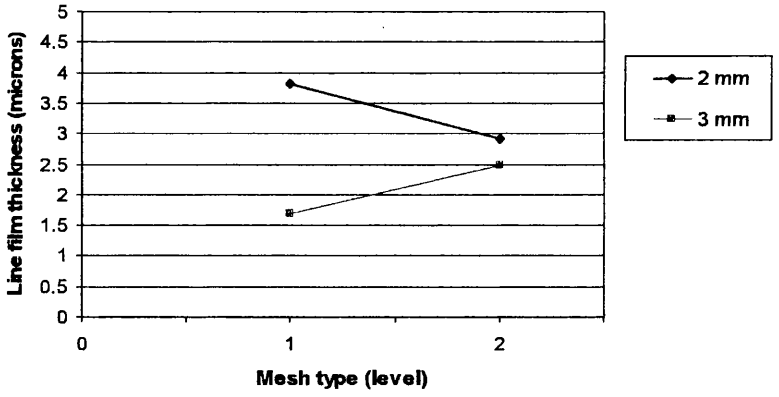

(c) Vertical lines

Figure 6.18: Interaction between mesh type and snap off gap on line film thickness

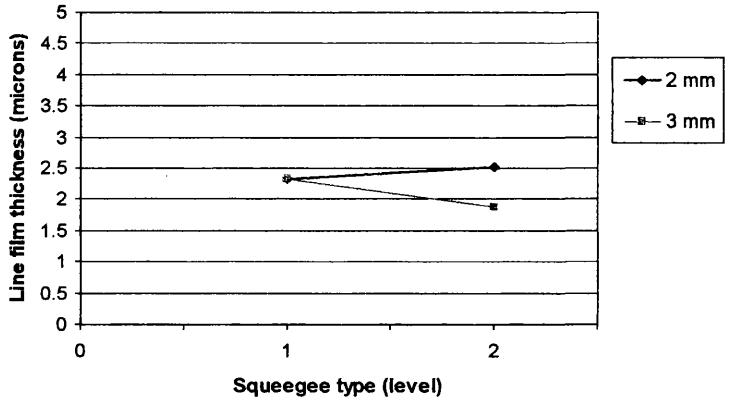

(a) Horizontal lines

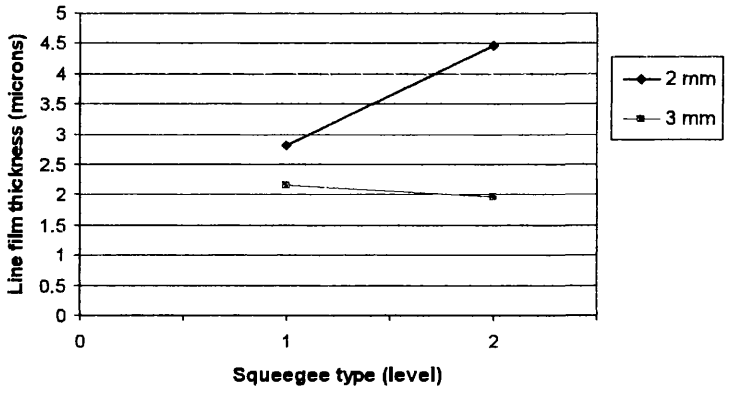

(b) Diagonal lines

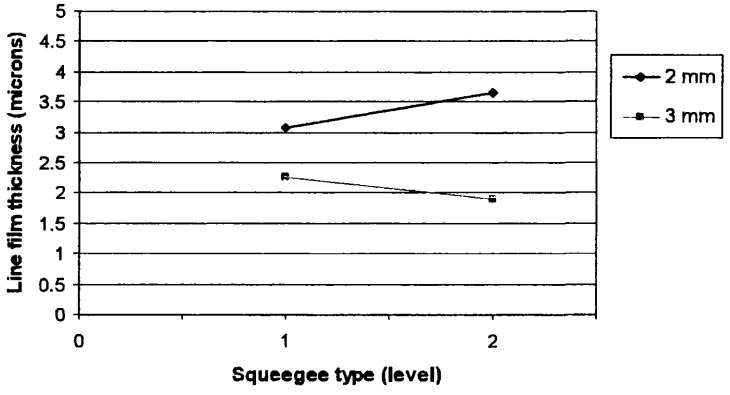

(c) Vertical lines

Figure 6.19: Interaction between squeegee type and snap off gap on line film thickness

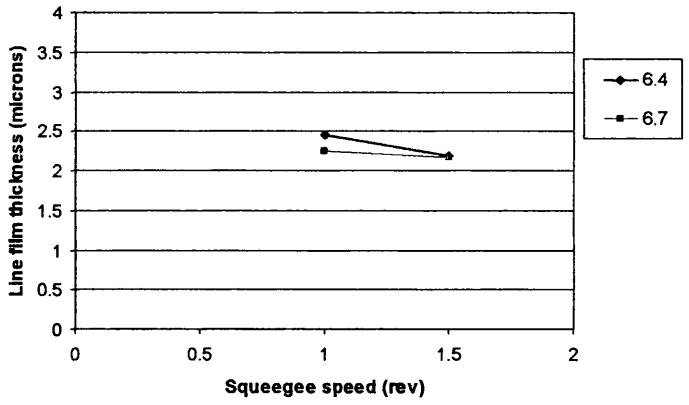

(a) Horizontal lines

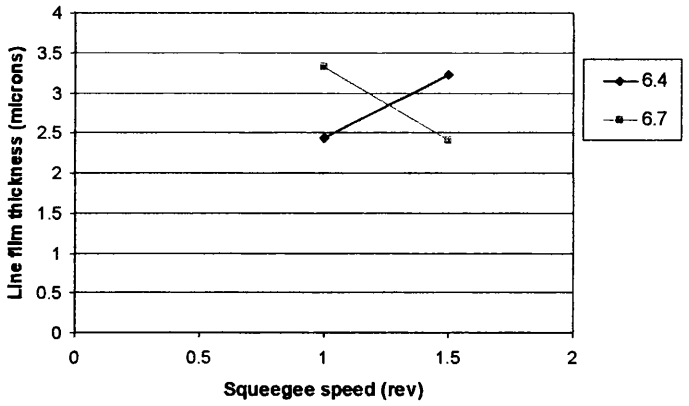

(b) Diagonal lines

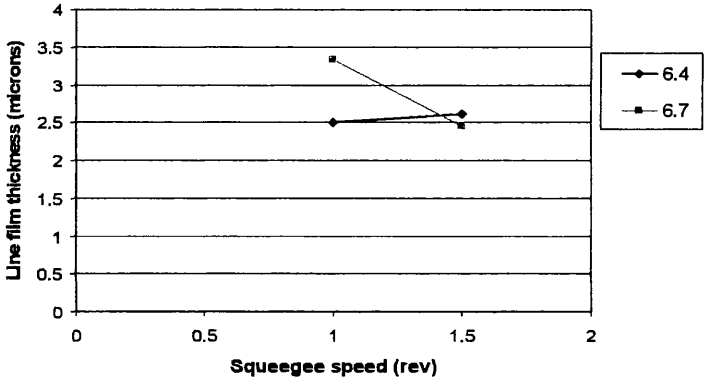

(c) Vertical lines

Figure 6.20: Interaction between squeegee speed and squeegee pressure on line film thickness

6.3.2.5 The effect of ink type on line width

In order to determine the effect of ink type on the line quality of printed gelatine fine lines, the printing trial was repeated for a higher concentration of 15% aqueous gelatine solution.

Overall, the effect of parameters on featured standard deviation of printed 15% line widths was considerably lower than those of 10% lines. Similarly to 10% ink, the squeegee type has the greatest effect on line widths with a decrease of about 5.1 μm when medium squeegee was used, followed by snap off gap. When the snap off gap was changed from 2 mm to 3 mm, the standard deviation decreased about 4.3 μm. The remaining parameters: squeegee pressure, mesh type and squeegee speed have insignificant effect on width consistency which are 1.0 μm, 0.9 μm and 0.2 μm respectively. Better width consistency of printed gelatine fine lines was achieved when polyester mesh and 3 mm snap off gap were applied on the press. Overall, all lines printed of 15% had better quality in terms of consistency, with smaller variations in standard deviation of line widths.

By averaging the widths of printed fine lines for all three line directions, 10% ink was found to give slightly greater line width compared to those of 15%. The difference in line width gain was within (10 ± 3) μm, Figure 6.21. This suggests that for 300 micron lines, higher viscosity inks produced lower line width but with higher ink film thickness. Inks of higher viscosity tend to gel faster and thus most of the ink transferred was used to build up the ink film thickness instead of line expansion. The amount of ink transferred was calculated and showed that the volume of 15% ink transferred on substrate was 990 μm^2 which was 123 μm^2 more than that of 10% ink, about 867 μm^2. This proves that the width reduction observed in 15% printed lines was not due to less ink transferred, but the ink nature of gelling. The printed lines of 15% ink were also considered better in line consistency with lower standard deviation. The line orientation seems to have no significant effect on average line width of 15% ink, remaining the same for all three line directions.

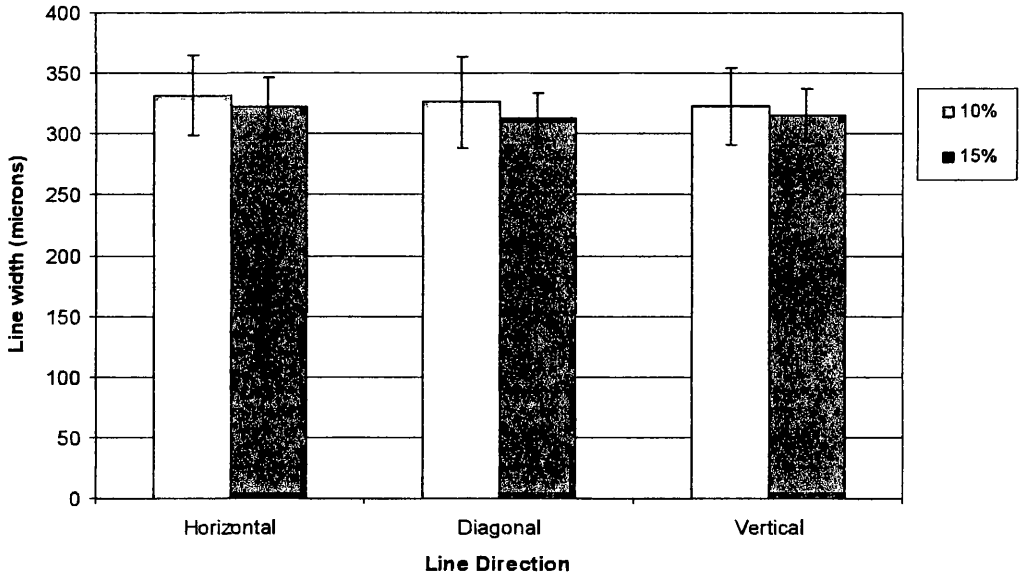

Figure 6.21: The effect of ink type on line width

The interaction between ink type and process parameters was also studied. These interactions between ink type and each process parameter followed similar trend for all three line directions. The results are presented in Figure 6.22 to Figure 6.24. An anti-directional interaction was observed between ink type and mesh type for all line directions where the system was more sensitive with the 10% ink when mesh type was changed from polyester to stainless steel screen, Figure 6.22. The printed line width of 10% ink increased significantly by about 40 μm; whereas the line width of 15% ink remained almost the same. Moreover, the ink type showed no effect on line width when stainless steel screen was used.

There was also an interaction between ink type and squeegee type, Figure 6.23. Apart from vertical lines, the line width increased greatly by 20 μm for 15% ink while the line width of 10% ink remained constant, when the squeegee was changed from soft to hard Shore A hardness. The interaction between ink type and snap-off gap was found to be directional, Figure 6.24. Both types of ink affected the printed line width to the same

extent where the line width decreased with increasing snap-off gap from 2 mm to 3 mm. No interaction was found between ink type and both squeegee speed and pressure (see Appendix B for full results of these interactions).

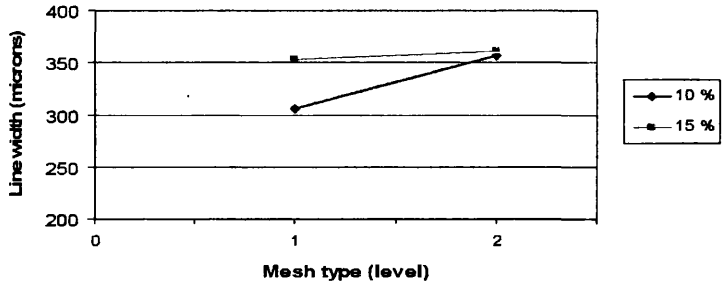

(a) Horizontal lines

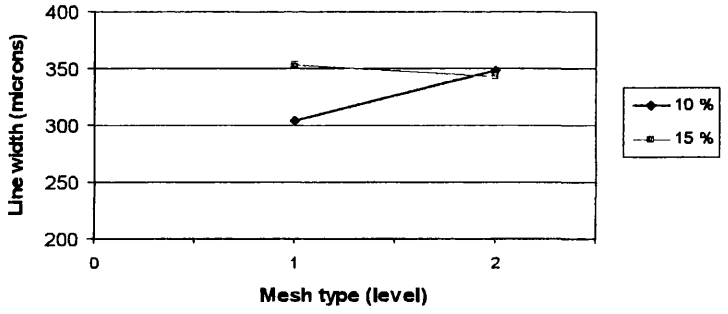

(b) Diagonal lines

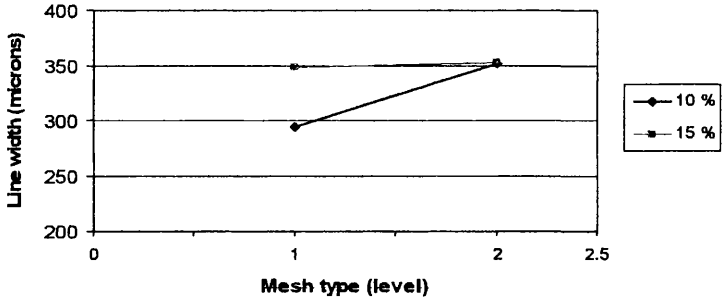

(c) Vertical lines

Figure 6.22: Interaction between ink type and mesh type on line width

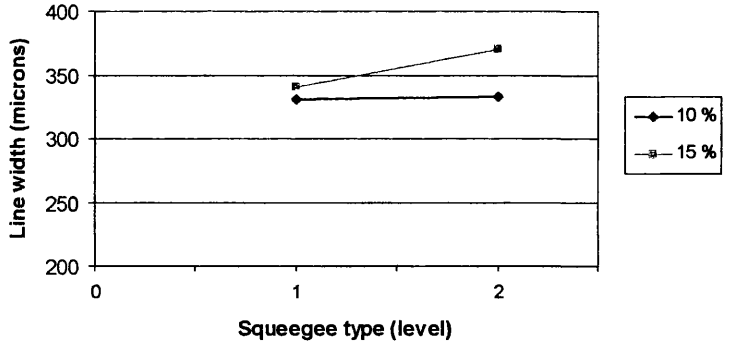

(a) Horizontal lines

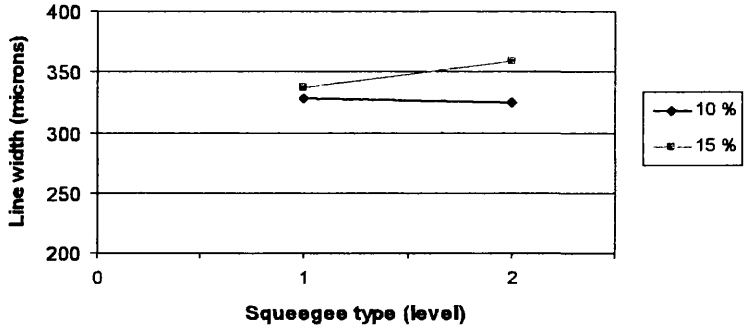

(b) Diagonal lines

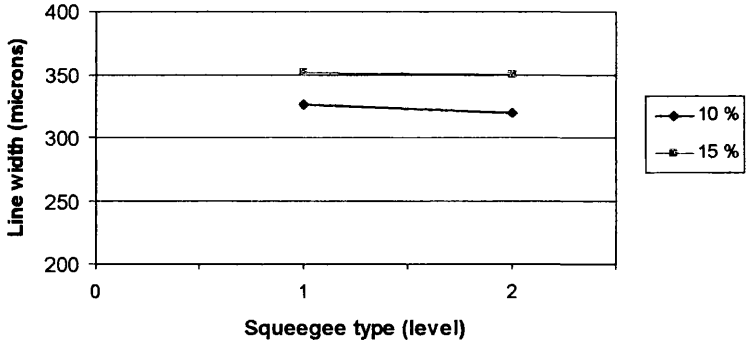

(c) Vertical lines

Figure 6.23: Interaction between ink type and squeegee type on line width

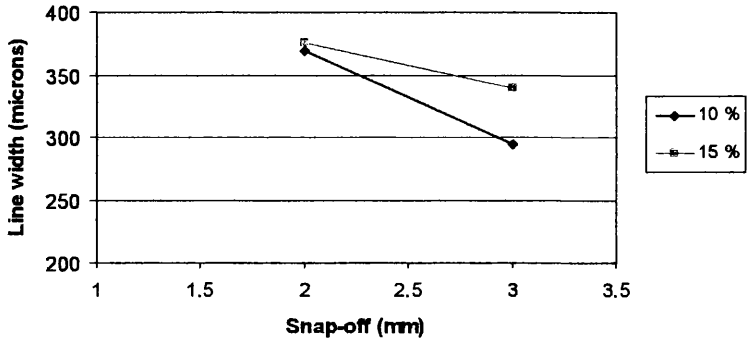

(a) Horizontal lines

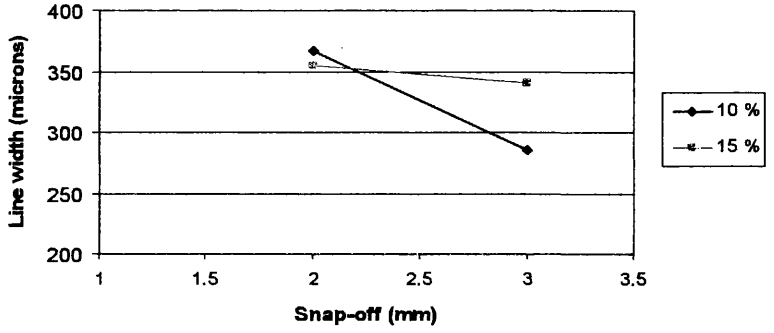

(b) Diagonal lines

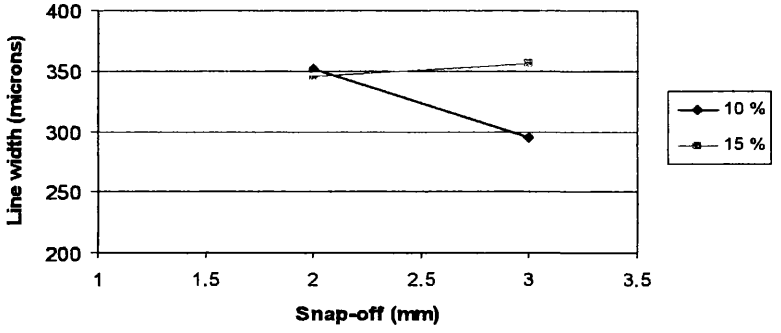

(c) Vertical lines

Figure 6.24: Interaction between ink type and snap-off gap on line width

6.3.2.6 The effect of ink type on line film thickness

Previous experimental works [6] found that the dominant parameter in determining line film thickness was the ink type. The results for consistency in line film thickness are measured in terms of standard deviation for all three line directions. For diagonal lines, the line film thickness was considered quite consistent with standard deviation ranging from as low as 0.1 μm to 4 μm. Similarly, the standard deviation of horizontal line film thickness was slightly lower, ranging from 0.1 μm to 3 μm, whereas the line film thickness of vertical lines were shown to have the greatest range of standard deviation, between 0.1 μm to 5 μm.

The best quality printed gelatine fine lines were produced by experiment 11 in terms of line consistency. The featured standard deviation was the lowest amongst all lines. For line film thickness, the effect of mesh type on the standard deviation is the most significant with an increase of about 1.8 μm when the mesh was changed from polyester to stainless steel one. A reduction of 1.1 μm was obtained when higher snap off gap of 3 mm was used. All squeegee parameters had must smaller effect on the line film thickness standard deviation, ranging from 0.25 μm to 0.04 μm. Although the effect of parameters is slightly lower than those of 10% lines, the range of featured standard deviation in each experiment was wider, ranging within 5.01 μm to 0.08 μm. This was probably due to the printed lines were full of air bubbles of different diameters, resulted in very inconsistent line profile. Human errors might also occur during printing which affected the results. 15% ink is 50% greater in concentration comparing to 10% ink, leading to faster gelling of ink. As the printing process was performed manually, a small difference in speed of loading ink on screen; speed of changing substrate from print to print in each run for each experiment might cause a big difference in the quality of printed lines.

With the application of averaging technique on the film thickness of printed fine lines for all experiments in the three line directions, a clearer view on the effect of line orientation on line film thickness is illustrated in Figure 6.25. The result shows that 15% ink

produced slightly thicker lines compared to those of 10%. For horizontal lines, the ink type had slightly greater effect on film thickness with an increase of about 0.5 μm with increased ink viscosity, others remain similar.

It can be concluded that orientation has insignificant effect on the line film thickness of printed 300 micron gelatine fine lines, similarly to its effect on line width. Overall, the lines printed by 15% ink were considered to have better quality with greater film thickness and lower standard deviation.

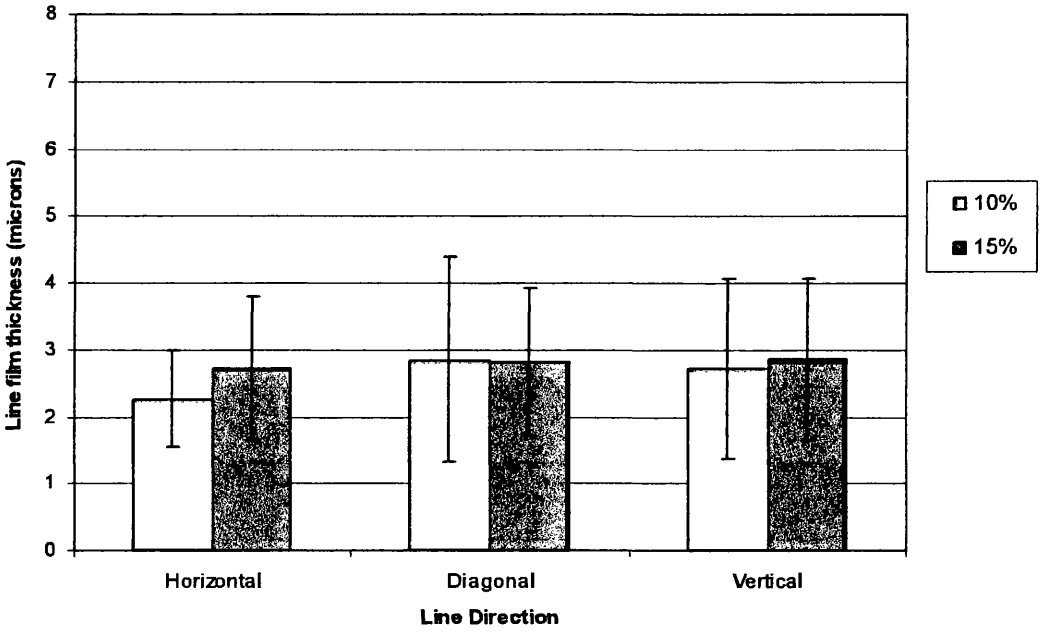

Figure 6.25: The effect of ink type on line film thickness

The interaction between ink type and process parameters on line film thickness was also investigated. The results are shown in Figure 6.26 to Figure 6.27. The interactions between ink type and each process parameter on line film thickness followed similar trend for all three line directions. There was an anti-directional interaction between ink type and mesh type for all line directions, Figure 6.26. The printed line film thickness of 15 % ink increased; whereas the line film thickness of 10% ink decreased when the mesh type was changed from polyester to stainless steel screen. In other words, thicker lines were produced by 10% ink when polyester screen was used whilst 15% ink gave thicker lines when stainless steel screen was used. Figure 6.27 illustrates that there was a directional interaction between ink type and snap off gap. Lower line film thickness was observed at greater snap off gap of 3 mm for both inks. 10% ink had greater effect on line film thickness which showed a reduction of 1.5 μm for diagonal lines, followed by 1.3 μm for vertical lines, whereas the film thickness of horizontal lines remained the same, when the snap-off gap was increased from 2 mm to 3 mm.

There was no significant interaction observed between ink type and all three squeegee parameters: squeegee type, squeegee speed and squeegee pressure (see Appendix B).

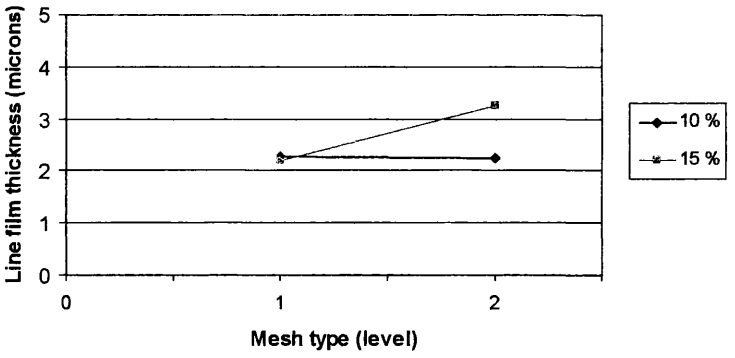

(a) Horizontal lines

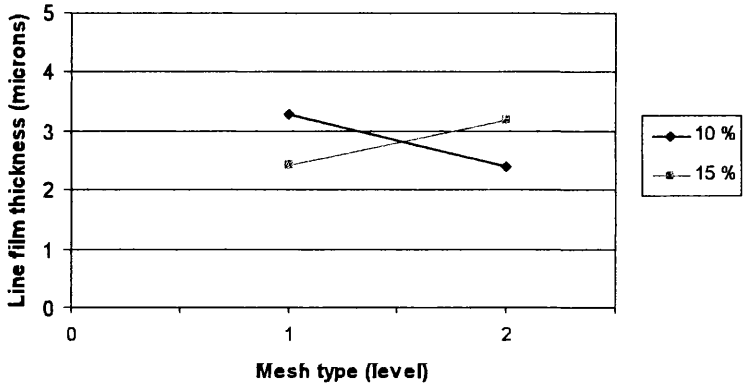

(b) Diagonal lines

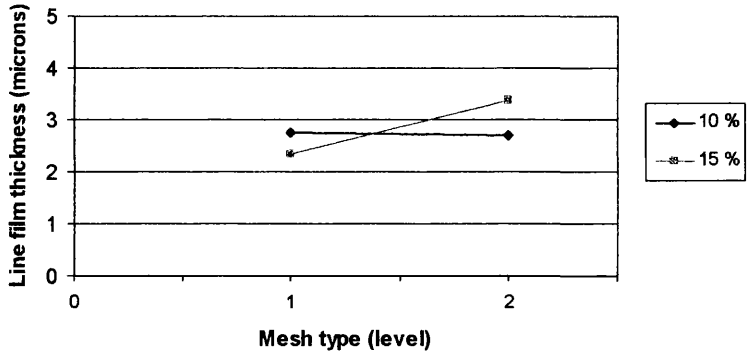

(c) Vertical lines

Figure 6.26: Interaction between ink type and mesh type on line film thickness

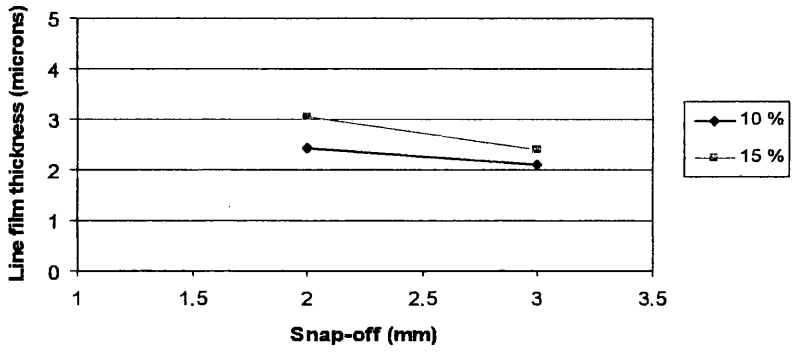

(a) Horizontal lines

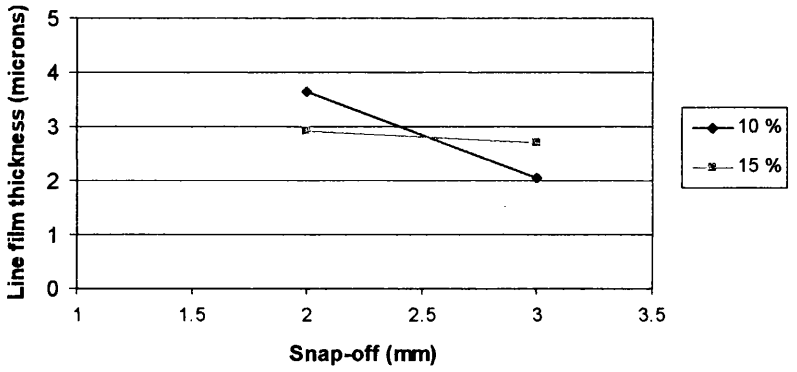

(b) Diagonal lines

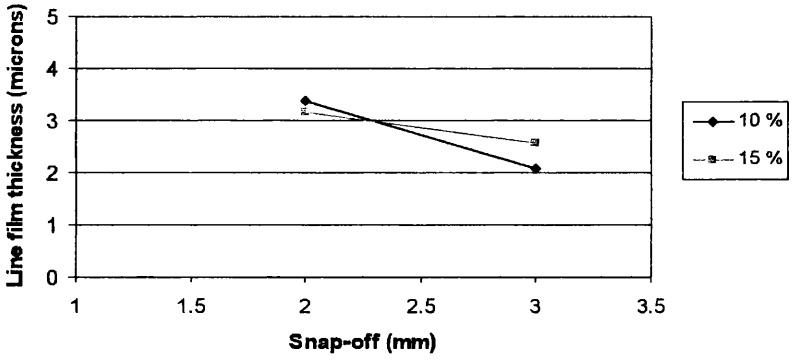

(c) Vertical lines

Figure 6.27: Interaction between ink type and snap-off gap on line film thickness

6.4 Discussions

6.4.1 The effect of printing press parameters on printed line width

It is important to characterise parameter effects on line width because line width affects how close the lines can be placed together, as connections will be formed between two parallel lines if the ink spreads too much. The results for the net effect of the process parameters on line width are shown in Figure 6.8.

The study has found that the dominant parameter in determining the line width is the snap-off gap. The snap off gap should be set just big enough so that the screen peels away immediately behind the squeegee as it travels over the screen surface. As the increase in mesh tension increased the ink deposit, it would be expected that the increase in snap off gap increases the ink transfer. However, the width of printed lines decreases with increasing snap off gap from 2 mm to 3 mm. The snap-off speed was reduced at smaller snap-off gap and thus increasing the contact duration between the screen and substrate. The combined effect led to an increase in ink transfer which increases the ink spreading. This has been found in previous studies on precision screen-printing with a roller squeegee [7]. When the snap-off gap was small, some prints stuck to the screen after the print stroke. The printed images had to be peeled manually, causing even longer contact duration. In terms of line quality, printed lines at increased snap-off gap had better quality with fairly straight edges and better line consistency with much lower standard deviation as shown in Figure 6.28. There was more air bubbles trapped on printed lines at 2 mm snap-off gap, affecting the line width as well as line film thickness which is presented in section 6.3.2.3.

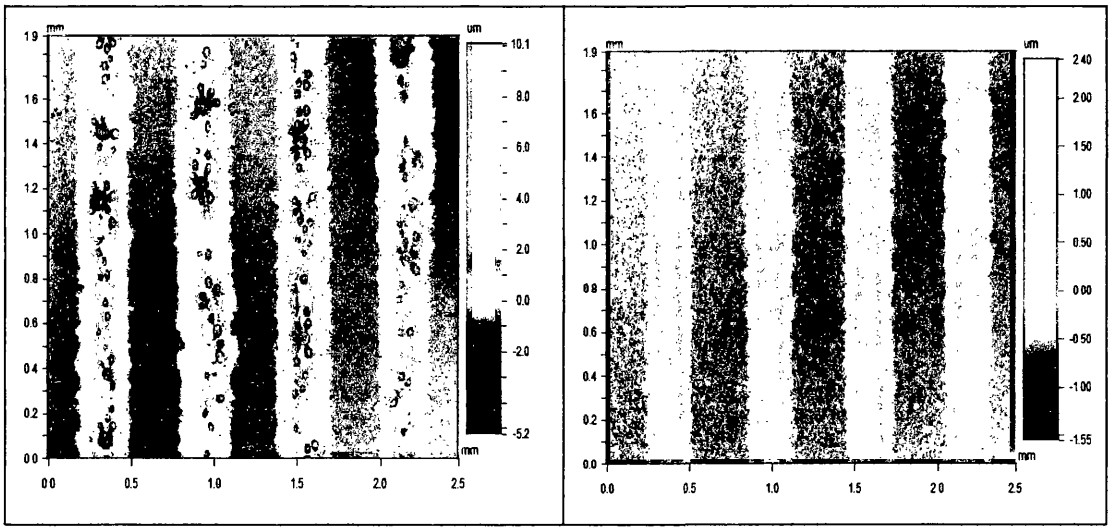

Figure 6.28: Two-dimensional images of printed lines at 2 mm snap-off gap (left) and 3 mm snap-off gap (right)

The next most significant parameter was the mesh type. In this study, the printed lines produced by using stainless steel screen were about 38 μm wider than those of polyester which was expected. As the ink deposit increases with decreasing mesh tension [5], more ink was transferred by using stainless steel mesh with lower mesh tension. Also, the opening area of stainless steel mesh is 39%, which is greater than that of polyester mesh (see Table 6.1) so more ink could flow through the mesh easily and transferred onto the substrate, comparing to polyester mesh with 24.6% opening area. The width of stencil lines on both screens was compared in Figure 6.5. The 300 micron stencil lines on stainless steel screen were wider than those on polyester screen. The difference was approximately 12 μm which was taken into account during analysis.

The phenomenon of 'drying in' was observed during the printing process. As the ink tends to gel with time, it was expected that some ink would stick to the wall of holes in mesh, leading to a reduction in ink transfer onto the substrate. This is generally true, as the measured width of printed lines decreased from print to print, Figure 6.29. The fine lines produced in third printed image were about 8 μm narrower than those in second

print. This demonstrates how drying in effected the results, leading to large standard deviation.

Prior to printing trial, a wooden box was built to cover up the whole screen press so that the printing process could be performed at constant elevated temperature of 28°C to slow down the gelling process of ink. This method was also expected to reduce the 'drying in' effect to minimum. However, the ink viscosity reduced significantly when the temperature was increased. This resulted in poor quality prints due to excessive ink spreading where connections between parallel lines were observed. Other methods to minimise the effect of drying in require further investigation.

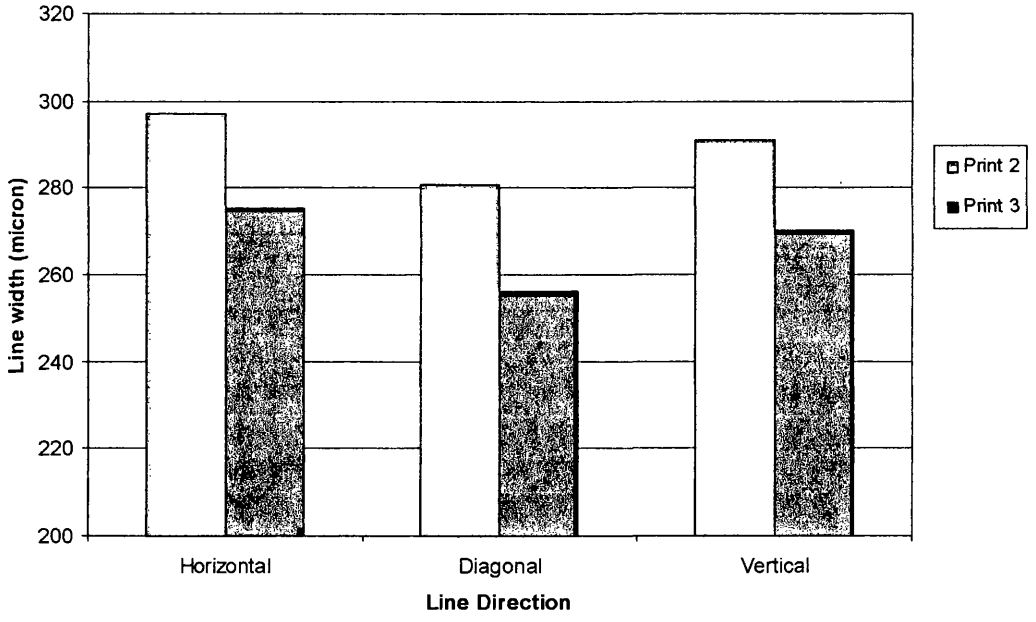

Figure 6.29: Average line width measured for second and third printed images in experiment 7

6.4.2 The effect of printing press parameters on printed line film thickness

Line film thickness affects the cross-sectional area of the printed line, which determines the layers of gelatine required to build a bio-scaffold for application. The effect of screen printing process parameters on the reproduction of the screen printed fine lines has previously been investigated [6]. The results are mainly for the squeegee and screen parameters. The relationship between ink transfer and line cross-sectional size and spreading has also been investigated. Theories have been put forward on the effect of the ink characteristics and these are compared to the results found by this study. The line width has been shown in the previous section to have an effect on the release of the ink from the screen over time because of the gelling process of the bio-ink.

For different combination of parameter settings, a large variation was found in the line film thickness obtained for 300 micron nominal line width. This is most likely due to the air being trapped during the ink transfer, some air bubbles were stuck inside the air dried gelatine line prints, affecting the line profile. This resulted in uneven top surface along the lines, leading to high standard deviation. Generally, the presence of air bubbles increases the line film thickness significantly. There were less air bubbles on printed images of experiment 7 which were reflected in film thickness reduction, Figure 6.30.

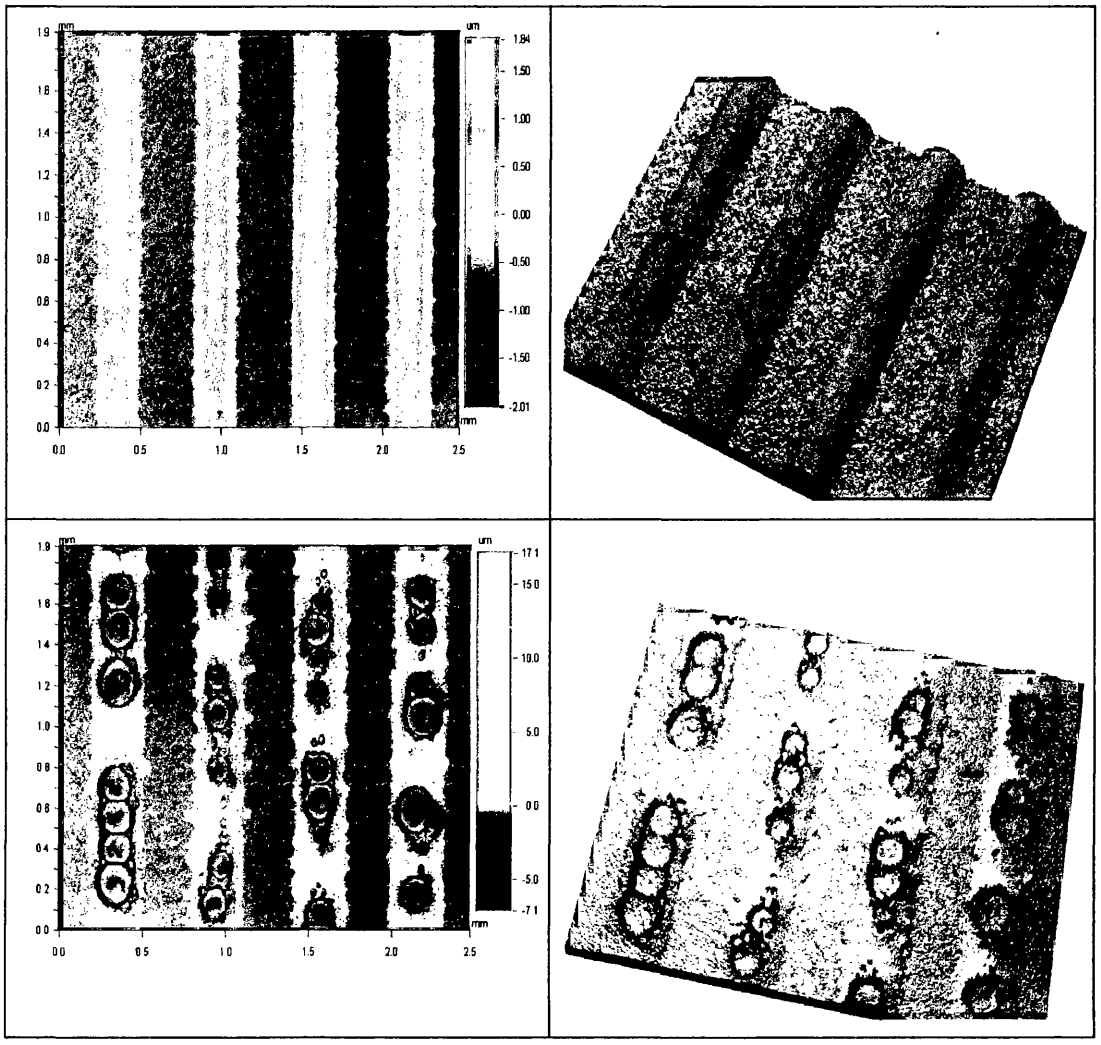

Figure 6.30: Example of horizontal printed lines: Experiment 7 (top); Experiment 5 (bottom)

Snap off gap has the greatest effect of the process parameters on ink transfer; it also has the greatest effect on line film thickness, similar to its effect on line width. In this investigation, mesh type affects the ink transfer where polyester screen produced thicker line film thickness than stainless steel screen. This might be due to the polyester screen used that has a greater mesh thickness, 65 μm, which is 18 μm thicker than that of stainless steel screen, Table 6.1. The mesh thickness has an effect on line height but

smaller effect on line width. This means that mesh thickness affects ink transfer. During printing, the additional ink deposit was achieved by either using a thicker mesh or by increasing the stencil thickness. The extra ink transferred increases the thickness of the line film, instead of causing line spreading.

Previous experimental results [7] have shown that for a given angle and pressure there is a reduction in the solid density as the hardness of the squeegee increases [7]. However, the highest ink deposit was achieved with the medium squeegee. This trend was also found in this study, Figure 6.15 where soft squeegee produced thinner film thickness than that of medium squeegee.

A reasonable correlation between the results in this study and those from previous studies was found for the relationship between line film thickness and process parameters. Screen printing process parameters had a similar effect on the line film thickness, as on the ink transfer. There were also some exceptional cases where the presence of air bubbles trapped on the printed gelatine lines affected the film thickness significantly. More work is required to optimise the parameter settings in order to minimise or even better to eliminate the occurrence of the air bubbles which was inevitable in this investigation.

6.4.3 The effect of line orientation on printed lines

Previous studies [6] have shown that orientation relative to the print direction affects the line width [6]. Five line orientations were investigated from 15° to 75° in steps of 15°. It was found that lines printed at 15° to the print direction were narrower than lines at 75° to the print direction. This difference varied from 5 microns to 20 microns. This was due to the non-uniformity of the stretching of the screen.

Figure 6.31 displays the orientation relative to the print direction for lines printed in this investigation. The vertical lines which are perpendicular to print direction were slightly narrower than horizontal lines. This might be due to the mesh marking observed on vertical lines, Figure 6.32. Mesh marking produced large regularly spaced thinning of the lines where the difference of maximum and minimum width measured was about 40 μm. As the line width was averaged along the line, the mesh marking occurred on vertical lines reduced the width significantly, resulting in narrower lines than horizontal lines. Barden [6] also found that the distance between the thinning of the line was affected by the orientation to the print direction. This is evidently true when the diagonal lines had a shorter wavelength compared to vertical lines. Representative images are shown in Figure 6.33, which were obtained by white light interferometer.

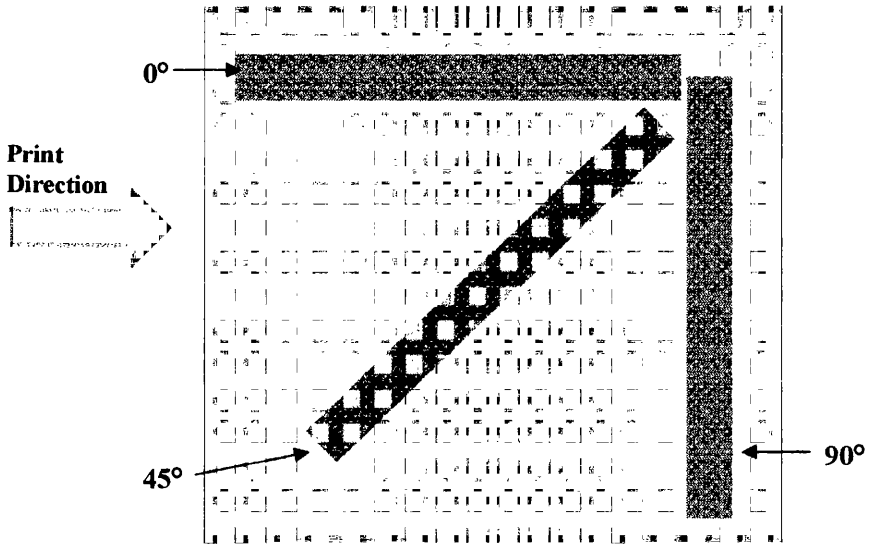

Figure 6.31: Orientation of the lines examined in this investigation

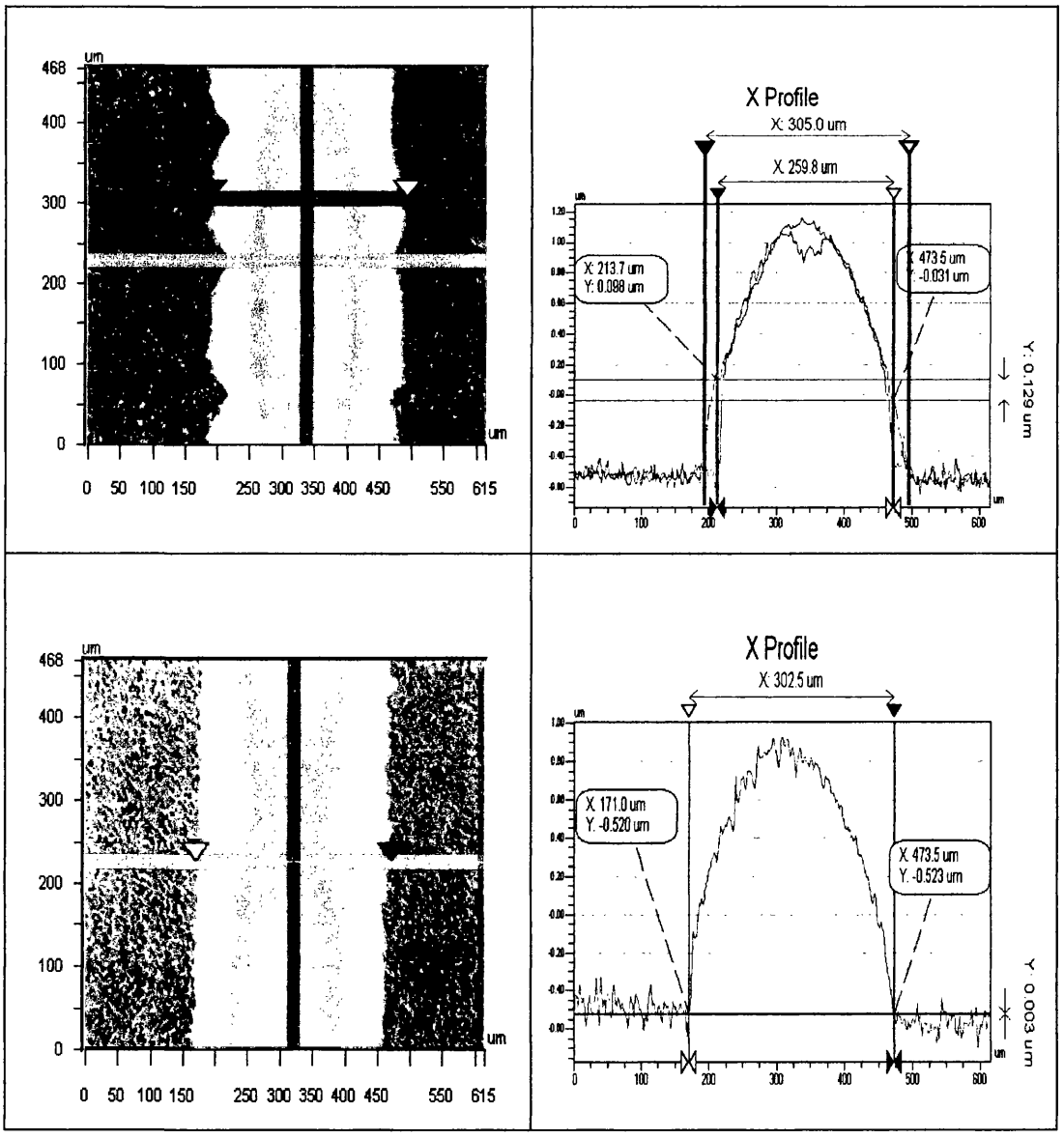

Figure 6.32: Example of Experiment 7 printed lines: vertical lines with visible mesh marking (top); horizontal lines (bottom)

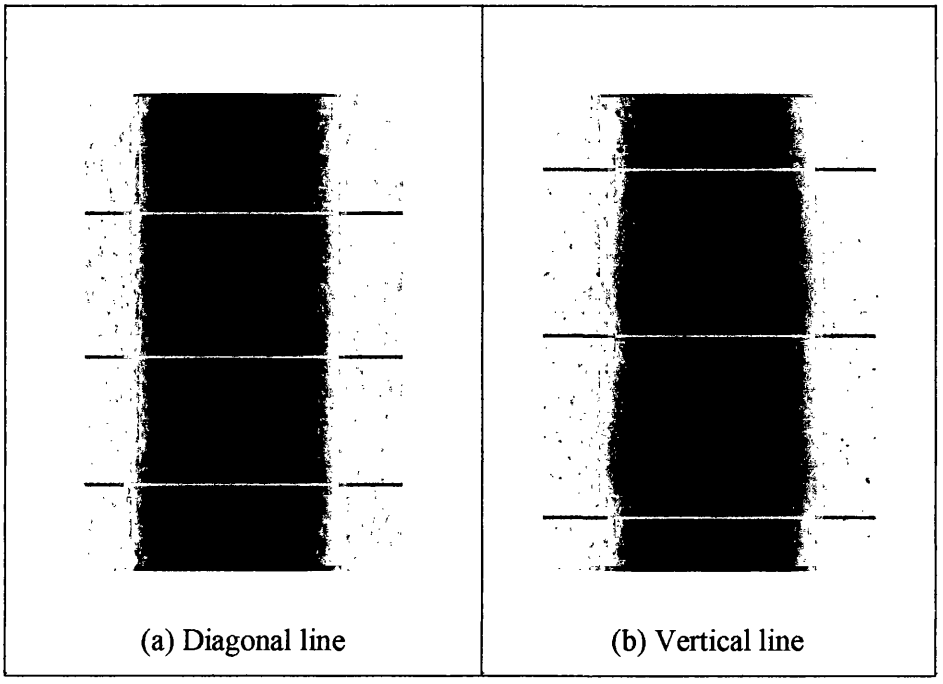

Figure 6.33: Examples of mesh marked lines at two orientations to the print direction: (a) diagonal and (b) vertical. They have been binarised to illustrate the difference in wavelength more clearly.

6.4.4 The effect of ink type on printed lines

Ink type was found to be the most significant parameter in determining film thickness. For narrower lines such as 90 μm and 120 μm, the line width was shown to be affected by the surface tension where inks with a lower surface tension spread more. At higher line widths, ink transfer and the viscosity affected the line width [6]. Since it was difficult to determine the surface tension of the gelatine solutions at high concentration due to the phase transition, it was assumed that for wider lines, 300 μm, the viscosity is more significant than the surface tension for line width. Thus, the effect of surface tension on line width was negligible.

Previous rheological characterisation experiments in Chapter 4 showed that the ink viscosity increased with concentration of the solutions. Ink with higher concentration reduced the gelation time at constant temperature. 15% ink is greater in concentration, so it gelled faster than that of 10% ink. Hence, first and second prints were selected for measurements, instead of second and third prints as of 10% ink. This might lead to a slight increase in line gain measured for 15% ink as the width of printed lines was reduced from print to print. It is reasonable to assume that 15% ink might produce lines with even narrower width than those obtained in this investigation. As a result, there was less line gain in width when the ink viscosity increased which was a good correlation with previous studies [6].

6.5 Conclusion

The effect of the screen printing process parameters on line width and line film thickness has been presented. The most significant parameter was the snap-off gap, followed by mesh type. The printed line width increased when the snap-off gap decreased due to lower snap-off speed which resulted in longer contact duration between the screen and substrate. Stainless steel mesh produced wider lines because of its properties of greater opening area and actual stencil line width. Inks with lower viscosity produced wider lines. Screen with higher fabric heights produced more ink transfer, increasing the line film thickness. The orientation has an effect on line width but insignificant effect on line film thickness. Most process parameters had interactions with one another which complicated the optimisation of the process parameters.

Ink type has effect on line width and line film thickness. Higher viscosity inks produced narrower but thicker lines. There were also interactions between ink type and process parameters.

6.6 References

[1] Barden T. J. (2000) The effect of process parameters on ink film thickness and fine line reproduction in the flat bed screen printing process. WCPC, University of Wales Swansea.

[2] Phadke M. S. (1989) Quality engineering using robust design. Prentice Hall Int. 1989.

[3] Jewell E. H., Claypole T. C., Barden. T. J. (1998) A comprehensive study of the effect of squeegee parameters on flat bed screen printing, SPTG report, WCPC, University of Wales Swansea.

[4] Hinkelmann K. (2004) Evaluating and interpreting interactions. Technical Report Number 04-5. Department of Statistics, Virginia Polytechnic Institute and State University, Blacksburg, Virginia.

[5] Jewell E. H. (2000) The screen printer's press-side companion. First edition, University of Wales Swansea, WCPC Reports no. 008-01-01.

[6] Barden T. J. (2007) The application of the three-dimensional profiling to the measurement and characterisation of screen printed fine lines. Phd Thesis University of Wales Swansea 2007.

[7] Fox I. J., Claypole T. C., Gethin D. T. (2003) An experimental investigation into ink transfer using a roller squeegee in high-speed screen printing. Proceedings of the IMECHE Part E, Journal of Process Mechanical Engineering 217 (4): 307-321.

[8] Jewell E. H., Barden T. J., Claypole T. C. (2000) The effect of flat bed screen printing parameters on ink film thickness. Report no: 00-01-SPTG, WCPC, University of Wales Swansea.

7.0 Conclusions and Recommendations

7.1 Summary of completed work

This thesis reports an experimental investigation into the potential for using volume printing technologies to manufacture scaffolds from biopolymers. This has focused on printing of a single layer as a necessary precursor for the creation of scaffolds. This aimed to understand and assess the feasibility of printing fine features for tissue engineering scaffolds using conventional printing technology.

The biopolymer inks, which were diluted collagen solutions and aqueous gelatine solutions, were characterised in terms of rheological behaviour and surface tension. The rheological tests focused on ink viscosity, viscoelastic and gelation properties. In addition, the dynamic surface tension of the inks has been measured. Appropriate printing technologies were identified for each ink. As a result, it was identified that gelatine was the most appropriate biopolymer for manufacture of such scaffold because of its more consistent nature, ease of gelation, low biohazard and high availability for volume manufacture.

Measurement and analysis methods have been developed and used to analyse results from the printed images obtained by the experimental programme. The three-dimensional profile of the lines was measured, and thus obtaining the profiles for line width and line film thickness.

A preliminary print trial was carried out that aimed to establish the best printing method for gelatine fine lines by comparing the results observed from inkjet printing, flexographic printing and screen printing. The printed lines were examined in terms of line width and line film thickness. The surface roughness of printed lines is not that important as cell likes to adhere to rough surfaces. Screen printing process was determined as the more appropriate method in printing gelatine solutions as the printed fine lines obtained showed the best quality. The line width and line film thickness measured were more consistent and closer to the desired dimensions.

A laboratory screen printing trial was conducted using L_{16} orthogonal array technique to investigate the most significant process parameters affecting the quality of printed gelatine fine lines. Six parameters studied were ink type (inks of different concentrations), mesh type, squeegee hardness, snap-off gap, squeegee speed and squeegee pressure. Each parameter was set at two levels. The lines with equal width and spacing of 300 μm were examined in terms of line width and line film thickness. The investigation into orientation examined at three line orientations of 0, 45 and 90 degrees to print direction. Repeat readings were taken to ensure the results were representative of the line printed and a total of over 1200 measurements were made.

The overall conclusion is that screen printing of gelatine has the greatest potential for the volume manufacture of scaffolds for biomedical applications. Ink jet has the potential to add localised amounts of growth agents and cells if required.

A summary is given below of the conclusions obtained by this study.

7.2 Conclusion from the work completed within this study

A study of the rheological characteristics of model biopolymer inks was made to investigate their flow and gelation behaviour and identify their limits. The surface tension was measured to study the ink wettability on substrates. The following conclusions were found during the investigation.

- Gelatine appeared to be more favourable than collagen for scaffolds fabrication by printing technologies because it has more consistent rheological properties, comparing to collagen. Gelation gels more easily and quicker by lowering the temperature comparing to collagen solutions which has to maintain at 37°C for a period of time. Moreover, as described in the literature review, gelatine does not exhibit any antigenicity in physiological conditions and much easier to obtained for industrial production. Unlike collagen, gelatine also does not carry animal diseases which might cause death to human.
- All inks display shear-thinning or pseudoplastic behaviour which is important for a good printing ink. Inks of higher concentrations resulted in an increase in both pseudoplasticity and viscosity.
- The viscosity of biopolymer inks is strongly dependent on shear and temperature.
- All inks are thixotropic liquids which exhibited time dependent behaviours.
- The biopolymer inks would gel when the temperature was lowered to below gelation temperature. The gelation time decreased dramatically when the gelatine concentration was increased or the temperature was reduced. The rate of ordering and gel formation of biopolymer inks was found to be concentration-, temperature- and time-dependent.
- The surface tension of biopolymer inks was determined to decrease with increasing gelatine concentrations, 1%, 2% and 3% (w/v), ranging between 58 – 65 mN/m. The surface tension of inks above 3% (w/v) could not be measured at room temperature (high viscosity) due to the formation of gel and limitation of FibroDAT.
- An appropriate printing technology was identified for each ink best on the rheological characteristics. Printing conditions that are compatible with printing

biopolymer inks were being optimised in terms of operation temperature interval to accommodate phase transition.

Preliminary printing trials were conducted to print fine features of biopolymer inks using inkjet, flexographic and screen printing processes. The best printing method in terms of producing good quality fine lines was identified. The following conclusions were found.

- Inkjet printing process was not suitable for printing gelatine. Only 1% ink was jettable which gave relatively thin ink film ranging from 0.1 to 2.0 μm, for fine lines and solid patches respectively. This would not have sufficient strength and rigidity to sustain the construct.
- Flexographic printing produced printed images of low image contrast, might be due to its very thin ink film thickness (about 0.2 μm) and insufficient dye. The manipulation of the printed images might introduce large errors in measurement.
- The results on the screen printing and flexographic printing trials indicated that screen printing process looks more promising in printing gelatine solutions. It gave better quality fine gelatine lines in terms of greater width and film thickness. The process parameters have to be optimised to obtain better quality of fine line.

A full investigation was made into the effect of process parameters on the reproduction of the screen printed fine gelatine lines. The parameters chosen were those had been shown to have an effect on screen printing from previous work conducted in the graphic screen printing.

- Mesh marking was observed on the printed fine lines which largely reduced the average line width obtained. This was possibly due to the insufficient ink transfer onto the substrates because of the interaction between the mesh and the stencil at the edge of the line. Thus, this problem can be reduced by increasing the ink transfer. In addition, the line orientation was found to affect the distance between the thinning of lines.

- The screen printing process parameters had a similar effect on line width and line film thickness, as on ink transfer, unless otherwise discussed. The most significant parameter was the snap-off gap, followed by mesh type. In comparison to those two parameters, the effect of squeegee parameters (squeegee type, speed and pressure) was considered insignificant. The orientation has an effect on line width but insignificant effect on line film thickness. Most process parameters had interactions with one another which complicated the optimisation of the process parameters.
- Of all the parameters examined, ink type influenced the line quality dramatically where higher viscosity inks produced narrower but thicker lines. There were also interactions between ink type and process parameters.

7.3 Recommendations for future work

There are some challenges encountered during printing biopolymer ink:

- During printing, the phase transition that occurred in gelling process complicated the printing work. It is also difficult to control the gelation process.
- Temperature is a crucial factor in making the printing of biopolymer ink successful. A heater which includes a thermostat can be connected to the ink cartridge or ink chamber (e.g. a metal double jacket cartridge connected with a thermostat) to heat and keep the ink at high temperature above the gelation temperature, preventing the ink from gelling prior printing.
- Not all process parameters were investigated. However, most of the parameters not examined in this study had been studied previously for line width. Further understanding could be obtained by examining the squeegee angle, screen tension and substrate. The squeegee angle and screen tension are expected to have an effect on the line width due to orientation. The relative free surface energies of the ink and substrate were shown previously to have an effect on ink transfer and ink spreading, causing a change in the printable line resolution.
- Only line width and spacing of 300 μm has been examined. This was shown in previous work as appropriate dimensions (line widths and pore sizes of

7.4 References

[1] Boyan B. D., Hummert T. W., Dean D. D., Schwartz Z. (1996) Role of material surface in regulating bone and cartilage cell response. Biomaterials 17 (2): 1370146.

[2] Kim J. Y., Cho D. W. (2009) The optimization of hybrid scaffold fabrication processs in precision deposition system using design of experiments. J. Microsystem Technologies 15 (6): 843-851.

[3] Kim J. Y., Yoon J. J., Park E. K., Kim D. S., Kim S. Y., Cho D. W. (2009) Cell adhesion and proliferation evaluation of SFF-based biodegradable scaffolds fabricated using a multi-head deposition system. Biofabrication 1(015002): 7 pp.

[4] Roth E. A., Xu T., Das M., Gregory C. Hickman J. J., Boland T. (2004) Inkjet printing for high-throughput cell patterning. Biomaterials 25: 3707-3715.

Appendix A

Calibration circles used for the image processing

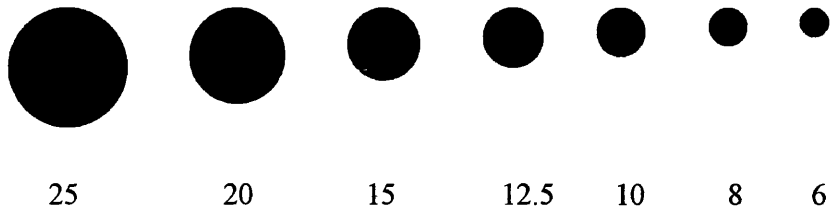

Figure A.1: Circles used for the calibration

These are calibrated black circles on a glass slide that can be placed under the microscope to calibrate the image processing system, converting pixels into microns.

Circle Number	Diameter (μm)
6	0.1110
8	0.1460
10	0.1830
12.5	0.2280
15	0.2730
20	0.3630
25	0.4540

Table A.1: Diameters of circles used for the calibration

Appendix B

Results from the investigation into the interactions between parameters

B.1 Introduction

The results are shown here for the interactions between the process parameters which are insignificant. They are not presented in the main thesis. The line width data is presented first (Figures B1), followed by the line film thickness (Figures B2). Then the insignificant interactions between ink type and other process parameters are presented where the line width data is shown first (Figures B3), followed by the line film thickness (Figures B4).

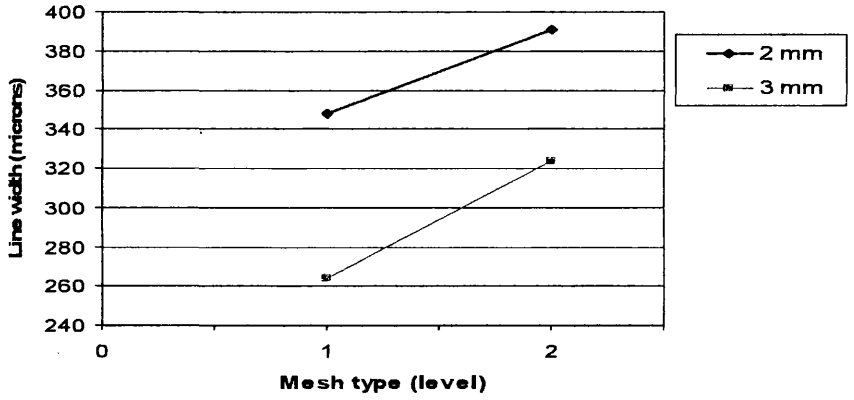

(a) Horizontal lines

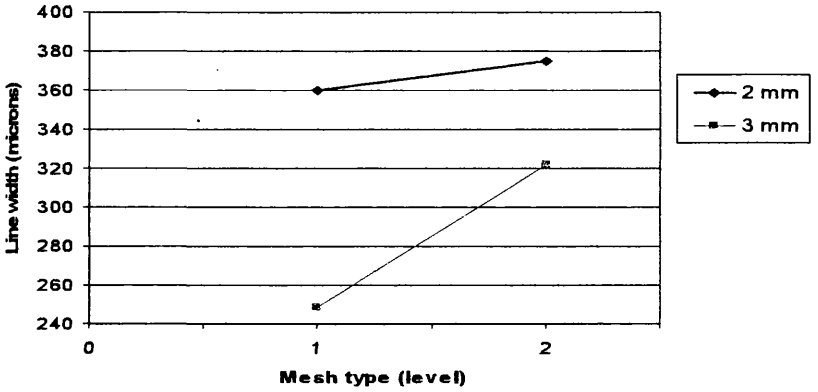

(b) Diagonal lines

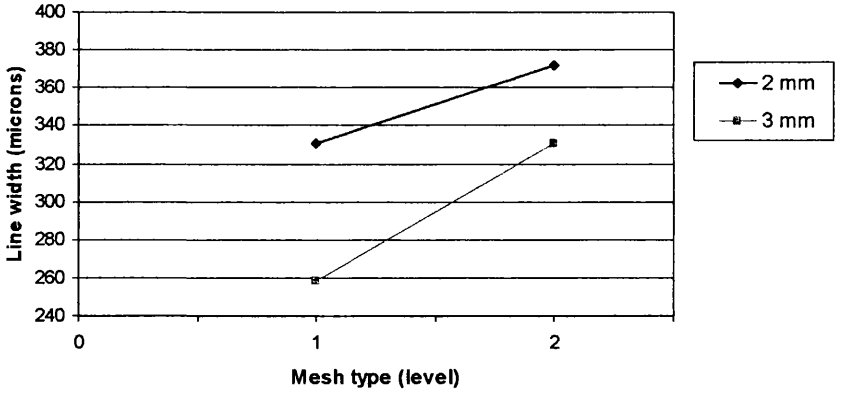

(c) Vertical lines

Figure B1.1: The effect of interaction between mesh type and snap off gap on line width

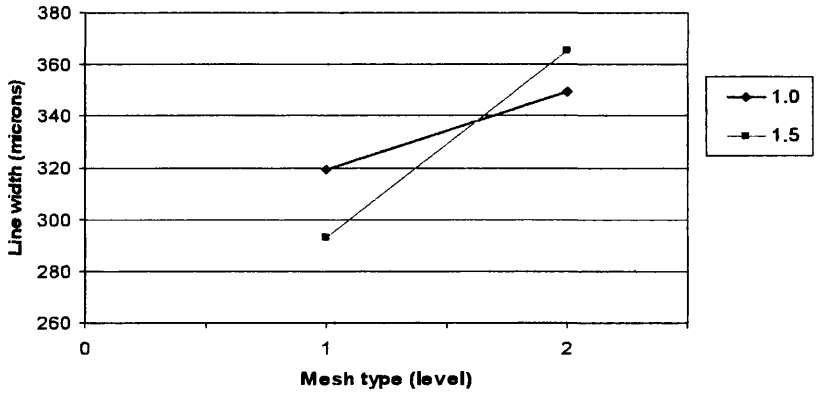

(a) Horizontal lines

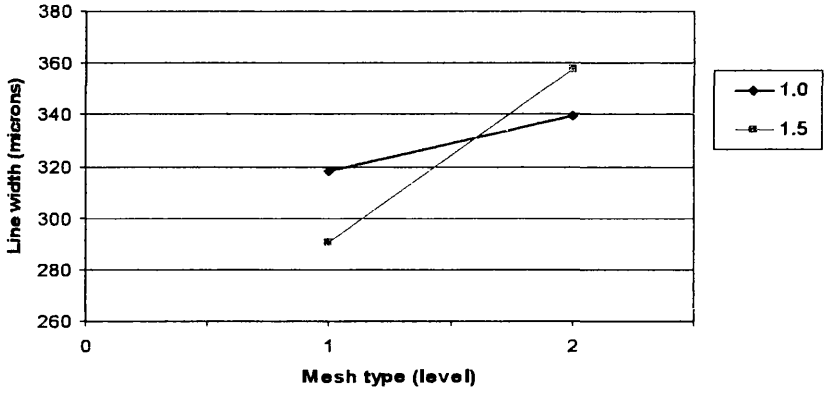

(b) Diagonal lines

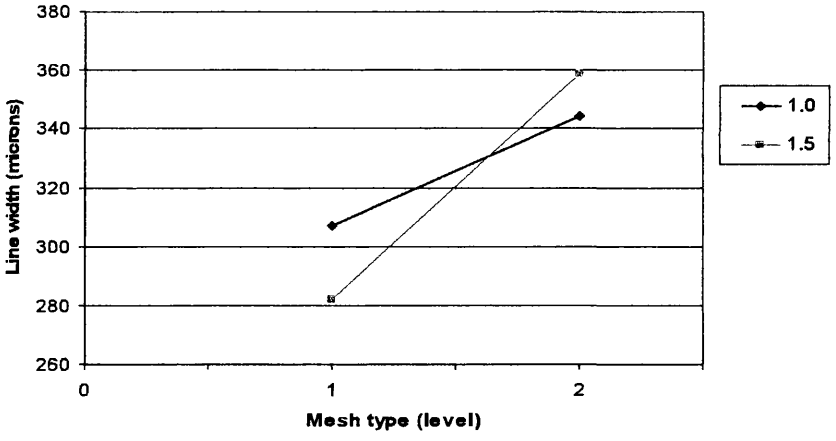

(c) Vertical lines

Figure B1.2: The effect of interaction between mesh type and squeegee speed on line width

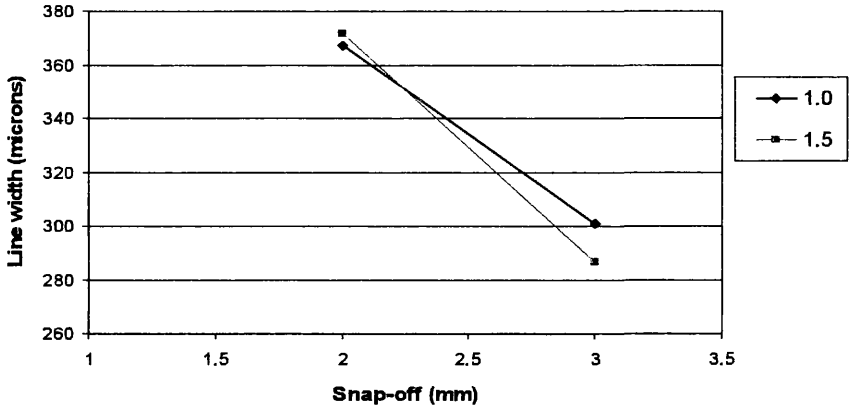

(a) Horizontal lines

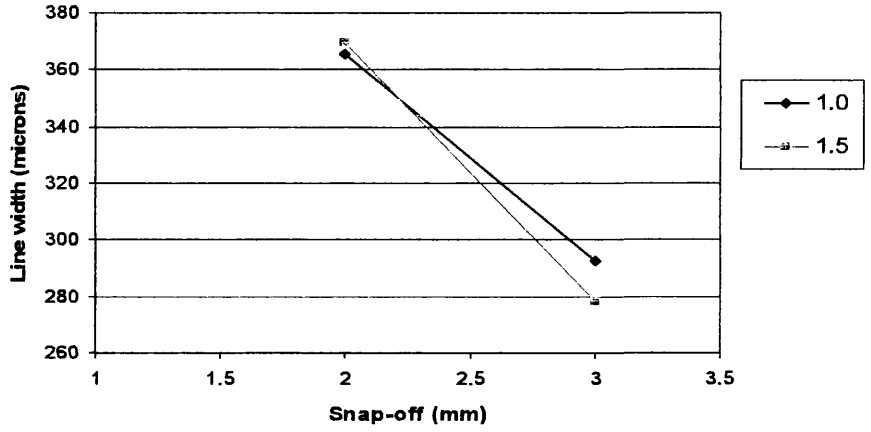

(b) Diagonal lines

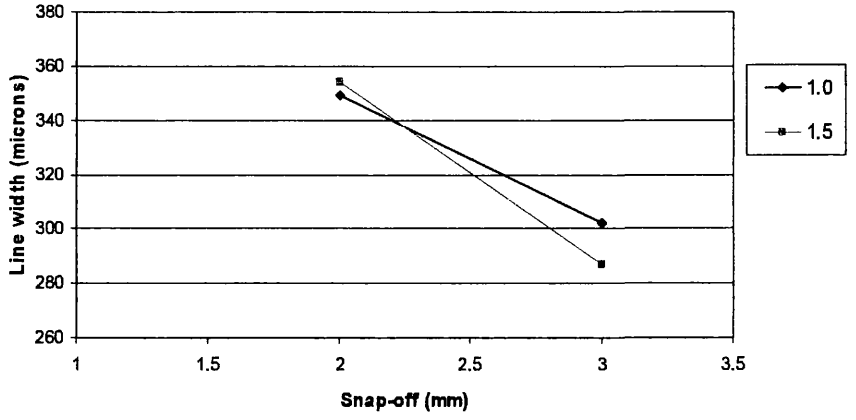

(c) Vertical lines

Figure B1.3: The effect of interaction between snap off gap and squeegee speed on line width.

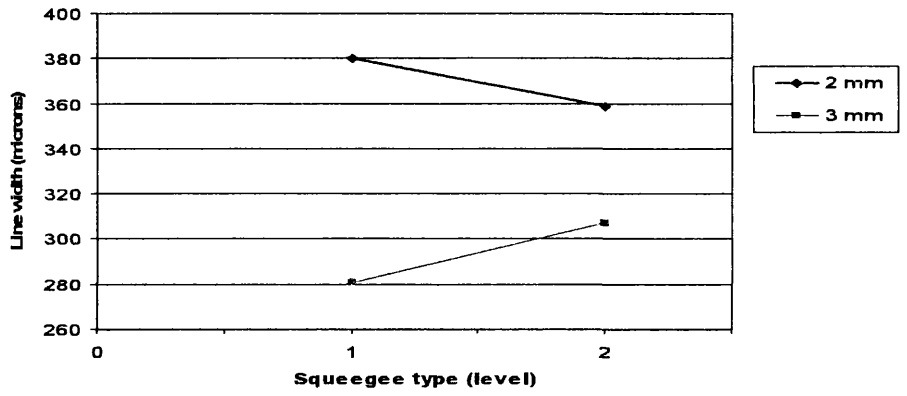

(a) Horizontal lines

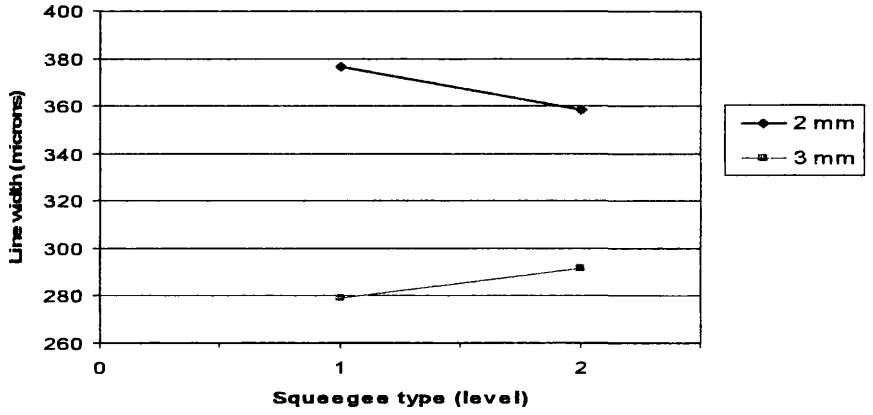

(b) Diagonal lines

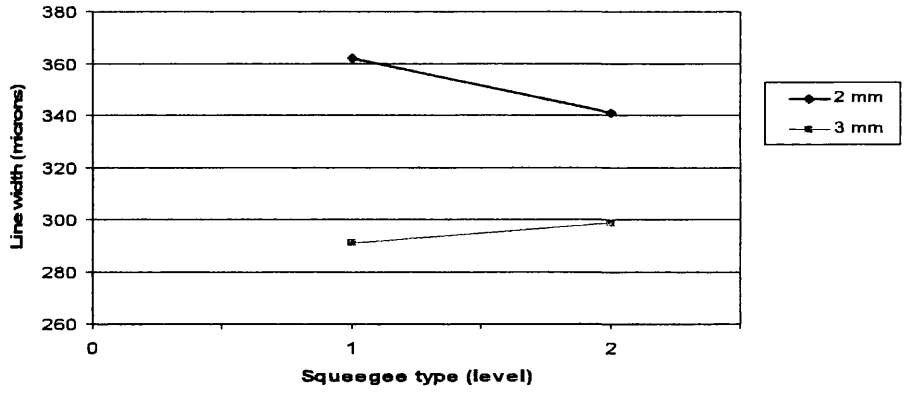

(c) Vertical lines

Figure B1.4: The effect of interaction between squeegee type and snap off gap on line width

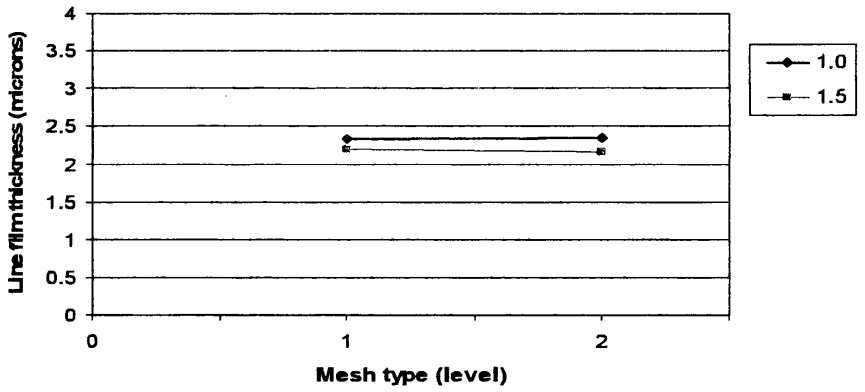

(a) Horizontal lines

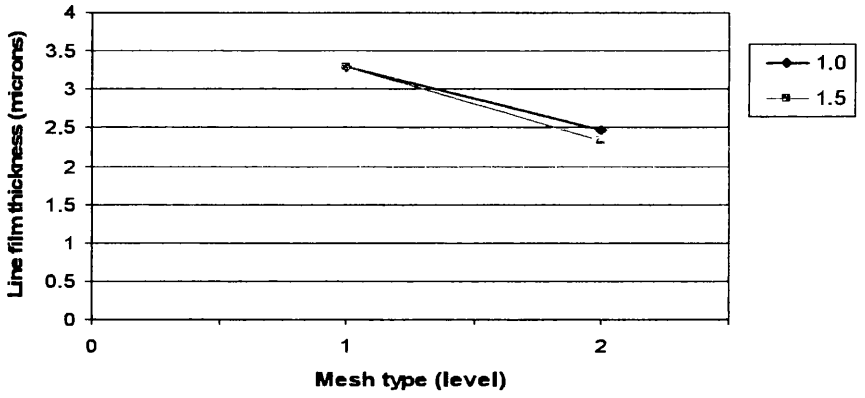

(b) Diagonal lines

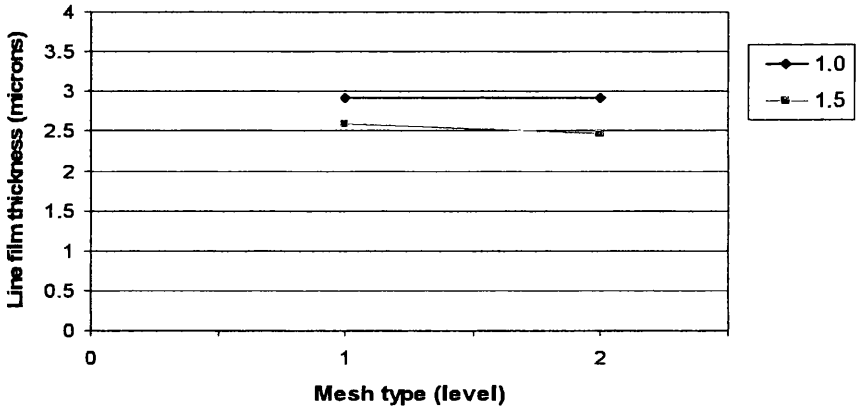

(c) Vertical lines

Figure B2.1: Interaction between mesh type and squeegee speed on line film thickness

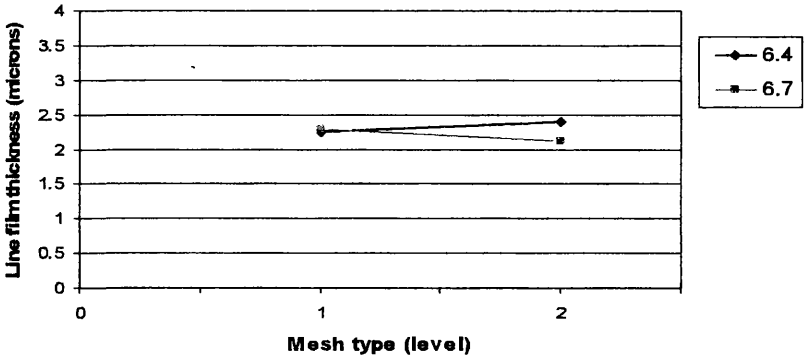

(a) Horizontal lines

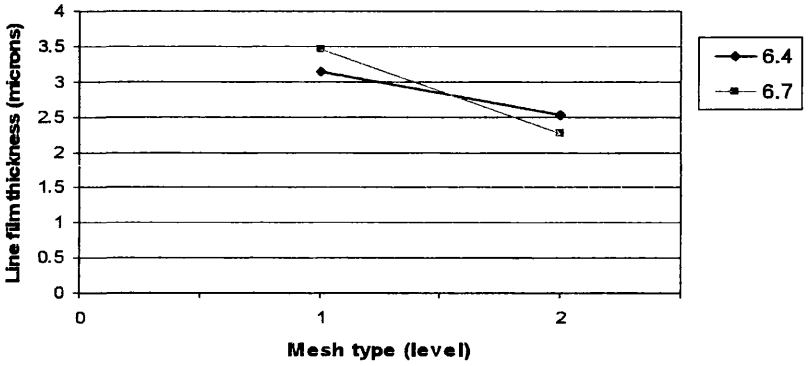

(b) Diagonal lines

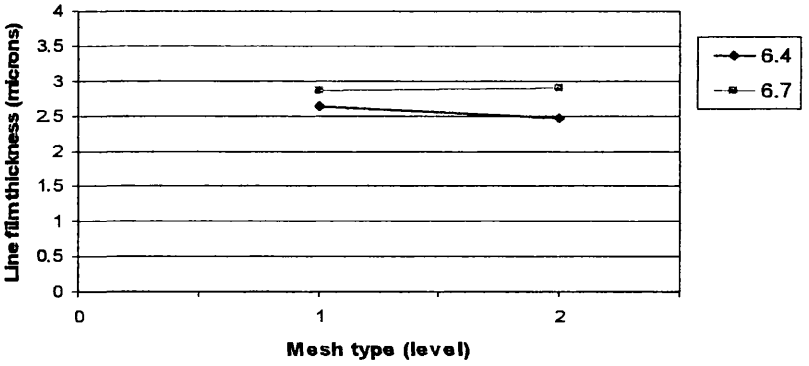

(c) Vertical lines

Figure B2.2: Interaction between mesh type and squeegee pressure on line film thickness

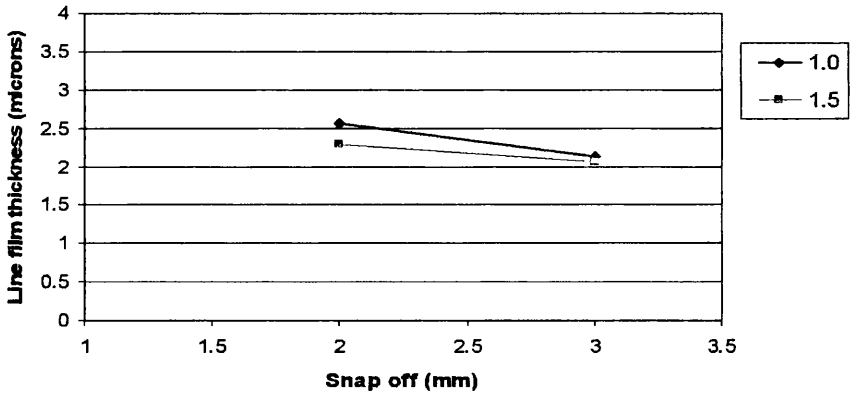

(a) Horizontal lines

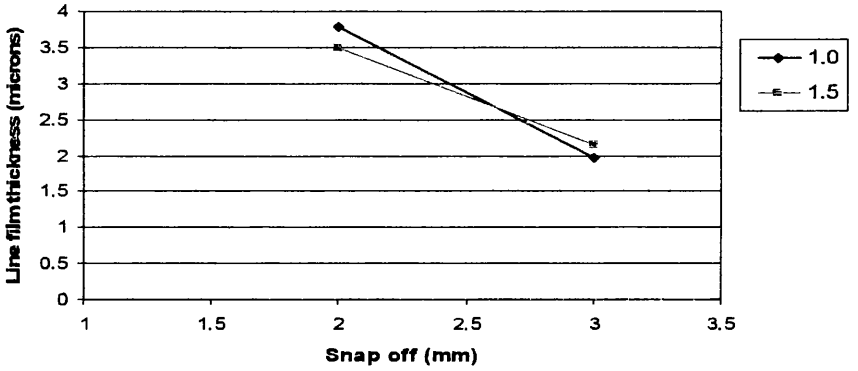

(b) Diagonal lines

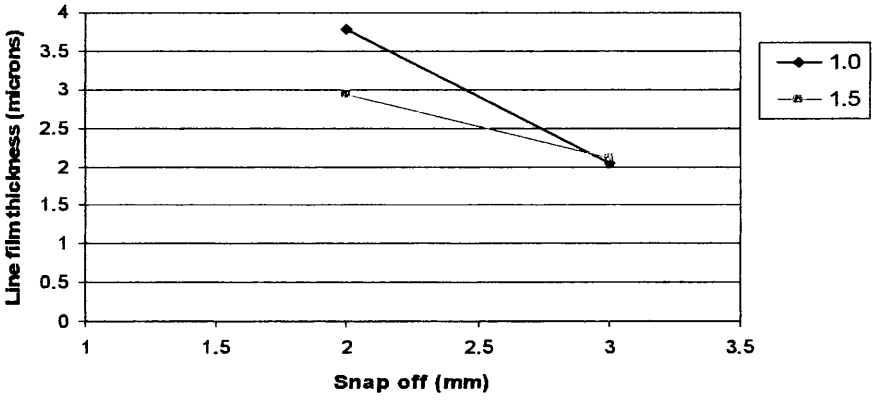

(c) Vertical lines

Figure B2.3: Interaction between snap off gap and squeegee speed on line film thickness

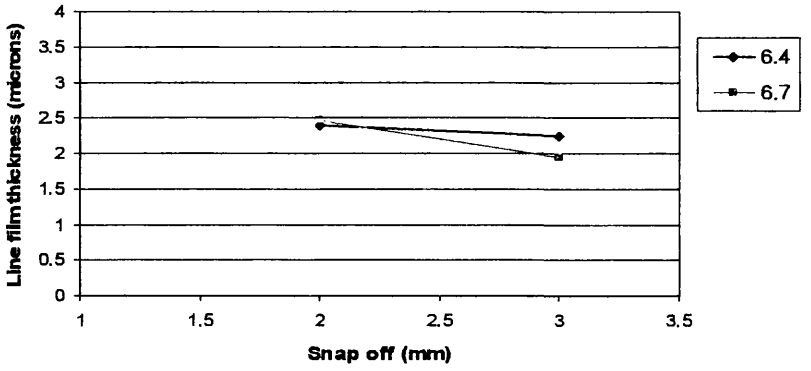

(a) Horizontal lines

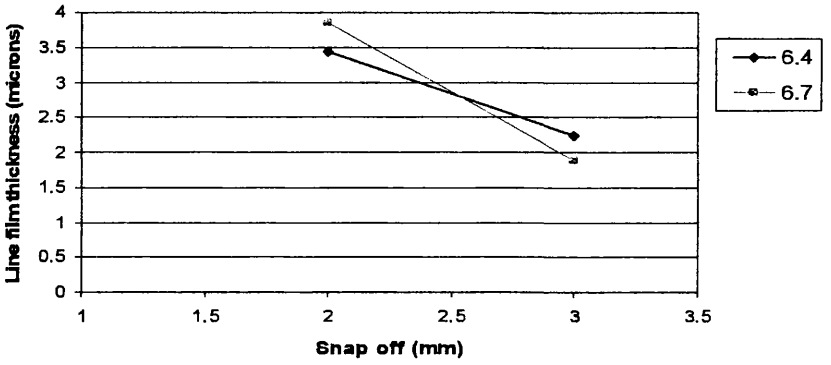

(b) Diagonal lines

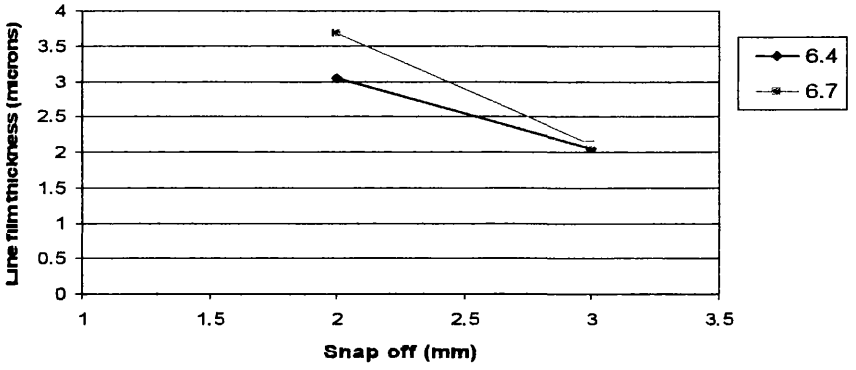

(c) Vertical lines

Figure B2.4: Interaction between snap off gap and squeegee pressure on line film thickness

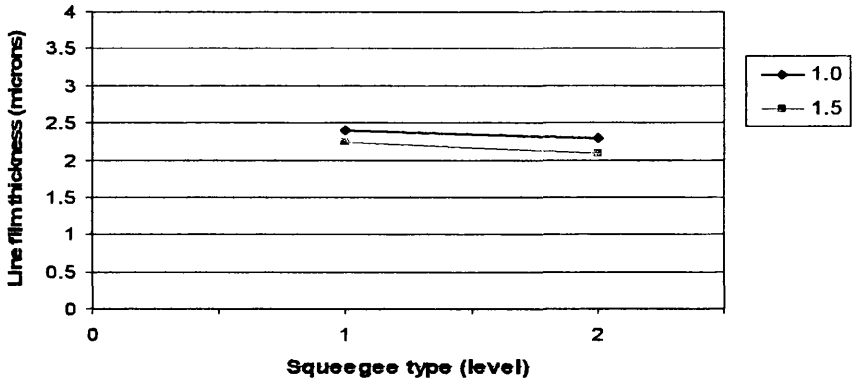

(a) Horizontal lines

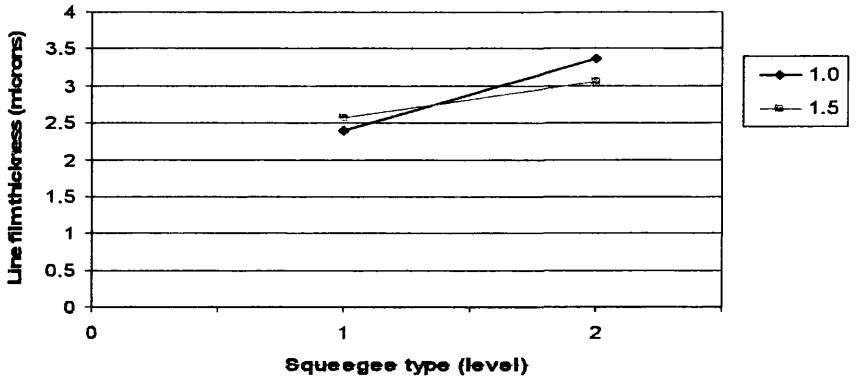

(b) Diagonal lines

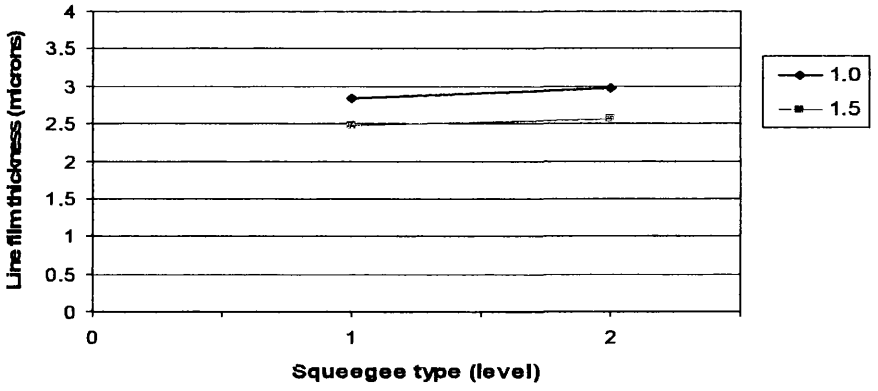

(c) Vertical lines

Figure B2.5: Interaction between squeegee type and squeegee speed on line film thickness

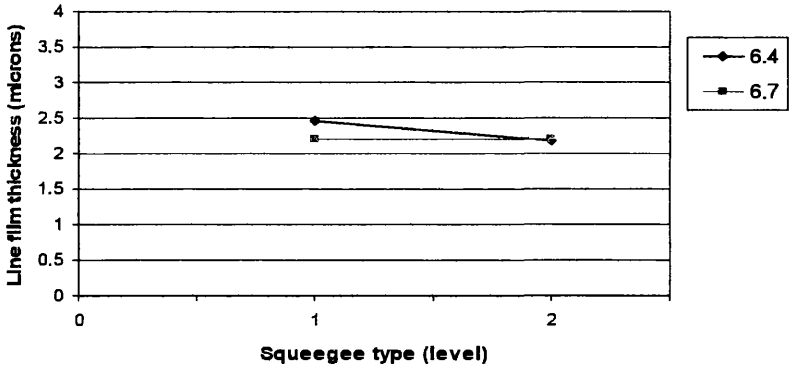

(a) Horizontal lines

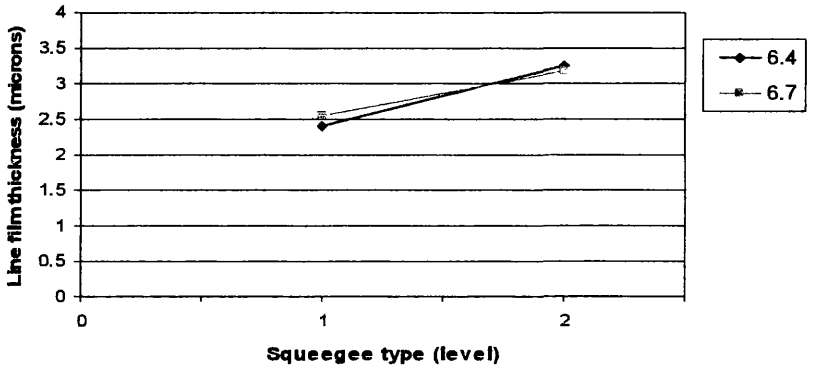

(b) Diagonal lines

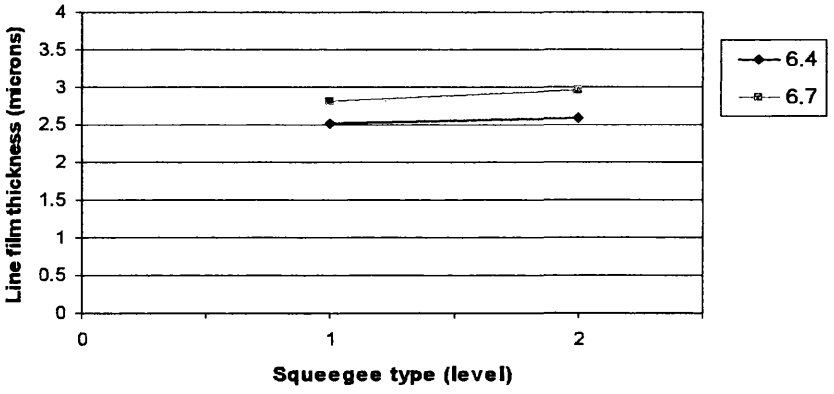

(c) Vertical lines

Figure B2.6: Interaction between squeegee type and squeegee pressure on line film thickness

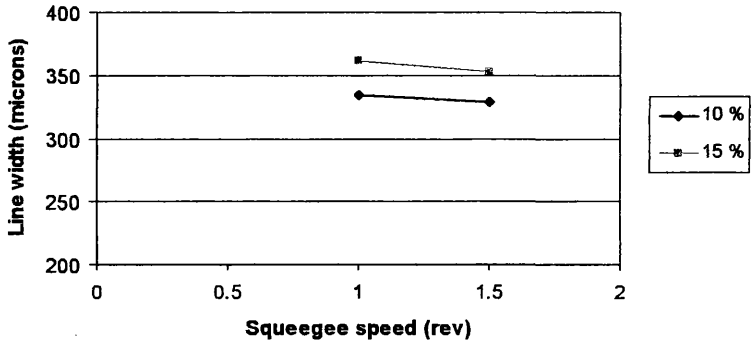

(a) Horizontal lines

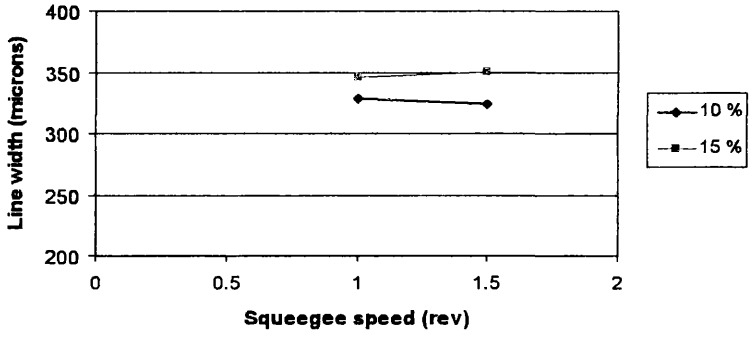

(b) Diagonal lines

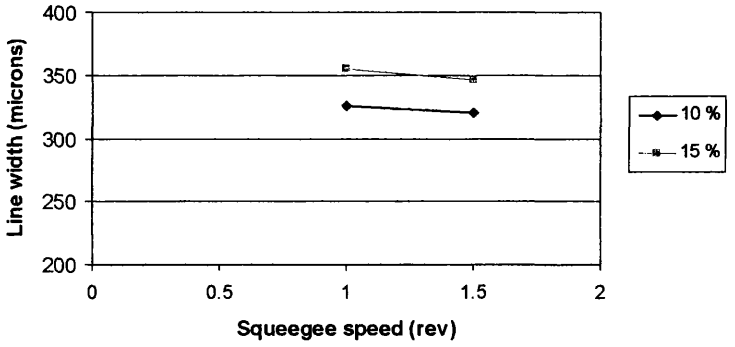

(c) Vertical lines

Figure B3.1: Interaction between ink type and squeegee speed on line width.

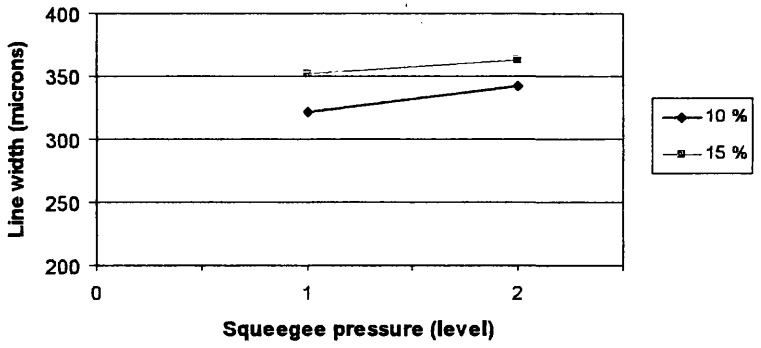

(a) Horizontal lines

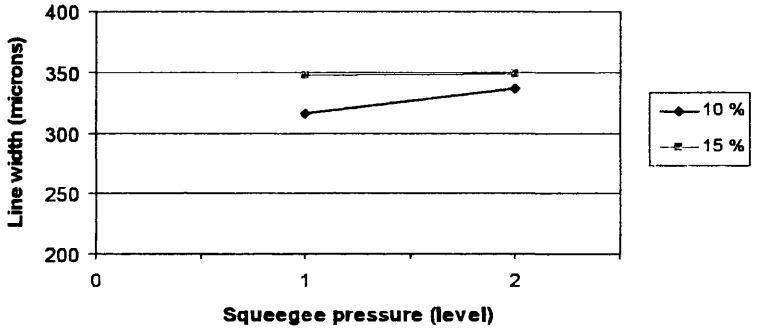

(b) Diagonal lines

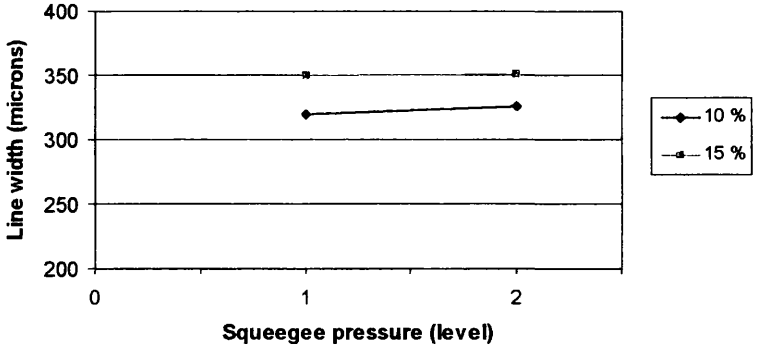

(c) Vertical lines

Figure B3.2: Interaction between ink type and squeegee pressure on line width

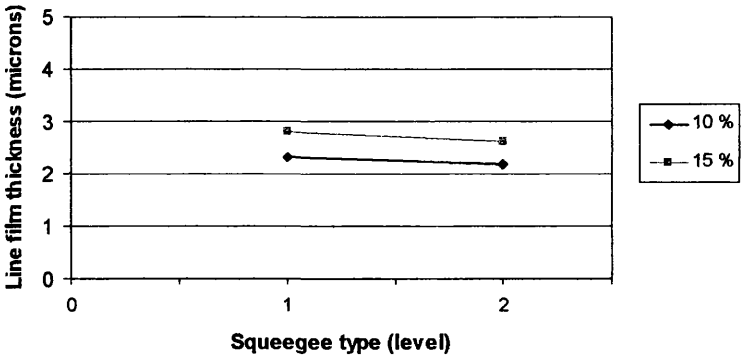

(a) Horizontal lines

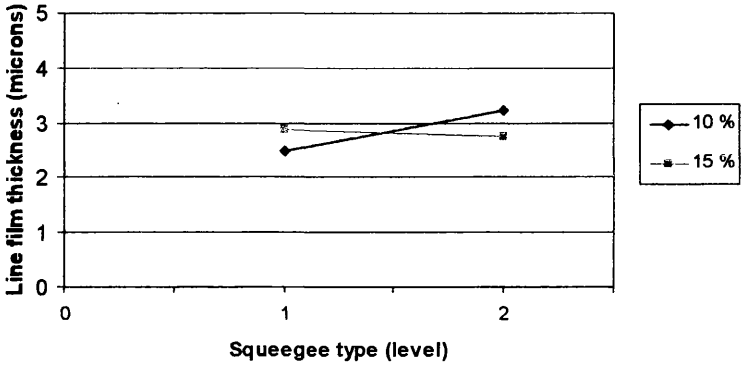

(b) Diagonal lines

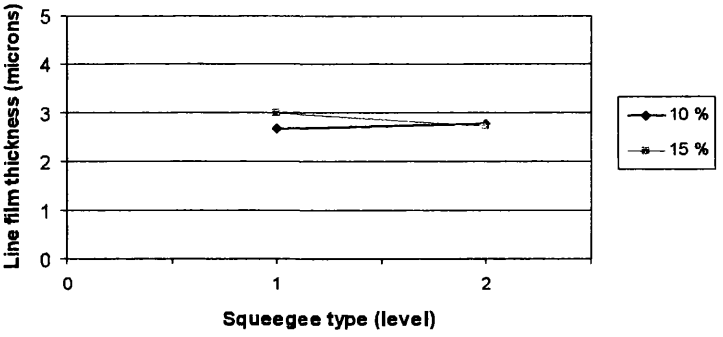

(c) Vertical lines

Figure B4.1: Interaction between ink type and squeegee type on line film thickness

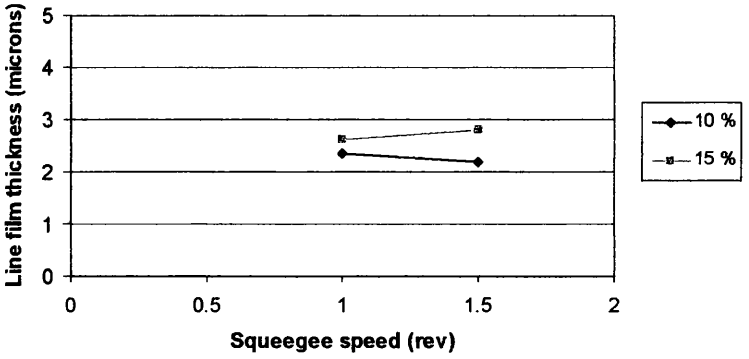

(a) Horizontal lines

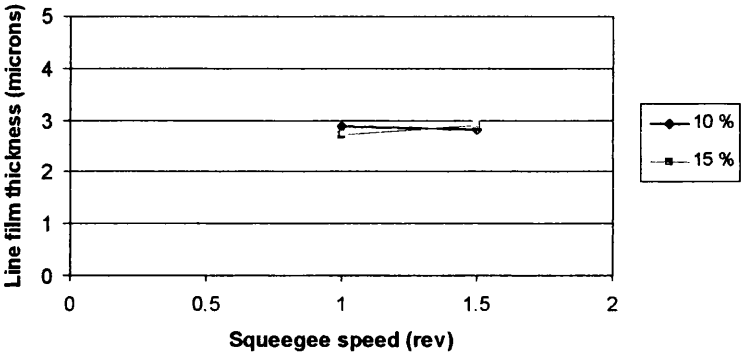

(b) Diagonal lines

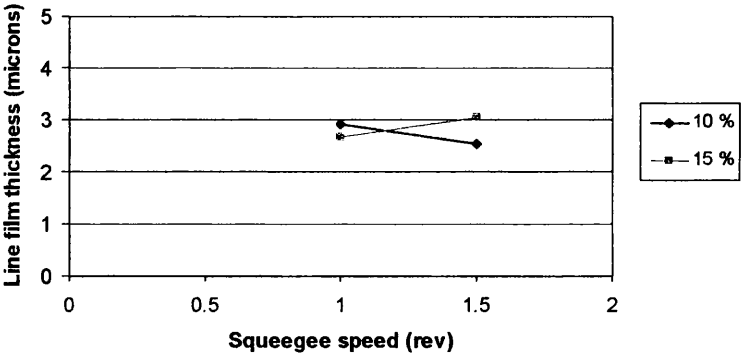

(c) Vertical lines

Figure B4.2: Interaction between ink type and squeegee speed on line film thickness

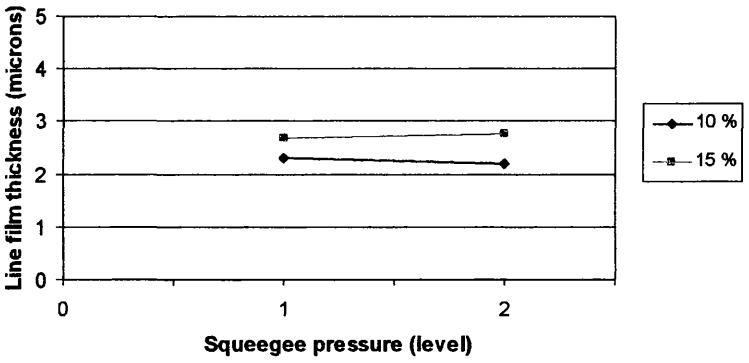

(a) Horizontal lines

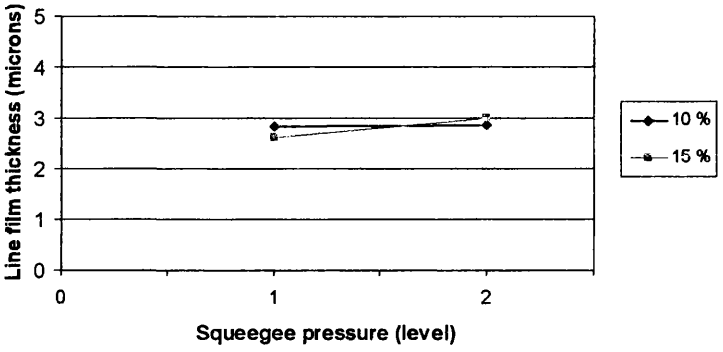

(b) Diagonal lines

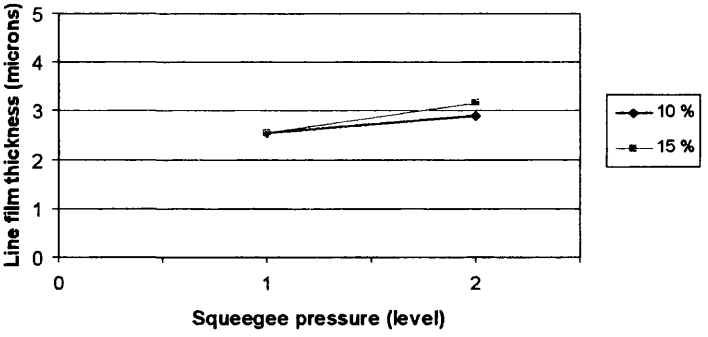

(c) Vertical lines

Figure B4.3: Interaction between ink type and squeegee pressure on line film thickness